Structure-Function Analysis of a Multifunctional Enzyme using the Atomic Force Microscope

By

Aneta E. Sikora

MSc

A thesis submitted in partial fulfilment of the requirements for the degree of

DOCTOR OF PHILOSOPHY

of the

University of Portsmouth

School of Biological Sciences
University of Portsmouth
King Henry Building
King Henry I Street
Portsmouth PO1 2DY
United Kingdom

November 2010

ABSTRACT

The type I R-M enzyme EcoR124I is a multifunctional, multisubunit molecular motor with the ability to self-assemble. In the presence of hydrophobic compounds, subunit disassembly has been observed leading to the possibility of using the enzyme as a nanoactuator in toxicity biosensors.

A better understanding of single molecule interactions between the subunits has been investigated using atomic force microscopy (AFM), a powerful tool for measuring forces and dynamics between single molecules with a picoNewton sensitivity.

AFM imaging of DNA fragments with a single recognition binding site for EcoR124I positioned in the middle or at 1/3 of the length of DNA, was used to study the assembled holoenzyme. Reproducible DNA imaging was investigated using divalent cations (Mg^{2+}, Ca^{2+}, Ni^{2+}). The presence of only one EcoR124I holoenzyme bound to DNA was observed, confirming the specificity of binding. Molecular volume (V_m) measurements were used to identify subunits and complexes. The effect of ATP analogues (ATP-γ-S and AMP-pnp) on enzyme stability was also investigated. The addition of ATP, although not novel, confirmed the enzyme activity by showing the ability of the enzyme to translocate.

Biotin-avidin interactions were studied using AFM force curves as a model to probe the novel HsdR-MTase system. AFM tips were functionalised using both glutaraldehyde and a PEG linker. In the former, many multiple event force curves were seen, although the final "pull-off" event yielded information on single-molecule or near single-molecule interactions: a single biotin-avidin interaction at 56 ± 13 pN was measured,

with further periodic force maxima at 98 ± 15 and 161 ± 3 pN (two and three interactions, respectively). The use of a PEG linker allowed more sensitive measurements to be made, with a single biotin-avidin interaction at 47 ± 9.5 pN and, again, periodic maxima were seen at 93 ± 7 and 143 ± 4 pN. The PEG linker method allowed more single molecules interactions to be measured (*ca.* 70% of analysed force-distance curves).

Forces between a GST-HsdR(PrrI) motor subunit attached to an AFM tip using a PEG linker and MTase on poly-L-lysine pre-treated mica were studied using dynamic force spectroscopy (DFS). A single barrier in the energy landscape of the complex was found in the dissociation pathway (x_{diss}) to be located 13.5 Å from the bound state. The value k_{diss} for the GST-HsdR(PrrI)-MTase complex was calculated to be 0.16 s^{-1} and the lifetime $\tau(0)$ of the GST-HsdR(PrrI)-MTase bond was found to be 6.25 s.

GST – anti GST antibody interactions and HsdR – anti-GST antibody interactions suggest that forces measured between HsdR and MTase were realistic for the GST-HsdR(PrrI)-MTase complex.

.

"If I know all mysteries and if I have all knowledge, but do not have love, I am nothing"

I dedicate this work to my family

TABLE OF CONTENTS

CHAPTER FOUR:

AFM imaging of the EcoR124I-DNA complex

CHAPTER FIVE:

Force-distance measurements of a model system: biotin-avidin

ACKNOWLEDGEMENTS

I would like to pass my greatest thanks to my supervisors Dr Keith Firman (Director of Studies), Dr James R. Smith and Dr Sheelagh A. Campbell, for providing me with the opportunity to embark on this research and their generous support, help, encouragement, inspiration and patience throughout my studies.

Dr Campbell was a great person, as a woman and mother she understood my concerns, gave me a lot of motivation and life gaudiness; she will stay in my memory forever. Thanks to Dr James R. Smith for constant support, patience, professional and friendly advice and Dr Firman for guidance throughout the project, useful suggestions and discussions.

I would like to extend my thanks to Dr Iwona Beech and Dr Anna Swiderska for their advice and support, Dr Gerald Kada at Agilent Technologies for his advice and Dr Dimitrios Lamprou for help with SEM.

Additionally I would like to thank to PhD students and Post-Docs in Biophysics lab, especially Dr Sabrina Amar and Miss Emily Newman for their friendship, encouragement and "writing dance", Mr Neil Ball for his advice, Mr Dan Fordham for help with proteins preparation, Dr Jim Youell for primers design and advice, Mrs Yanhong Li from the School of Pharmacy and Biomedical Sciences for sharing not only the office space but emotions and experience.

Last but by no means least, thanks to all my family. In particular, thanks to my Mum for looking after Maja, without her help finishing writing would not have been possible. Thanks also to my dearest husband for his love, friendship, support and for continuing to believe in me and Maja for bringing real sense to my life.

AUTHOR'S DECLARATION

I declare that while registered as a candidate for the degree of Doctor of Philosophy of the University of Portsmouth, I have not been a registered candidate for any other award.

Aneta E. Sikora

LIST OF ABBREVIATIONS

AA	Acrylamide
Aa	Amino acid
AdoMet	S-adenosyl methionine
AFM	Atomic force microscopy
AMP-pnp	Adenosine 5'-(β,γ-imido)triphosphate
APS	Ammonium persulfate
A 260	Absorbance at 260 nm wavelength
APTES	3-aminopropyltriethoxysilane
ATP	Adenosine tri phosphate
ATP-γS	Adenosine tri phosphate-γ-S
BAA	Bisacrylamide
Bp	Base pairs
BSA	Bovine serum albumin
Da (kDa)	Dalton(s) (kiloDalton(s))
DFS	Dynamic force spectroscopy
DMSO	Dimethyl sulphoxide
DNA	Deoxyribonucleic acid
DTT	Dithiothreitol
EDTA	Ethylenediaminetetra-acetic acid
EMSA	Electrophoretic Mobility Shift Assay
ESEM	Environmental scanning electron microscopy
EtBr	Ethidium bromide
GST	Glutathione-S-transferase
HEPES	(4-(2-hydroxyethyl)-1-piperazineethanesulfonic acid)
H	Hour(s)
hsd	Host specificity determinant
IPTG	Isopropyl-β-thiogalactoside
Kb	Kilobase(s)
MAC	Magnetic AC mode
Min	Minutes

MOPS	3-(N-morpholino)propanesulfonic acid
NHS	N-hydroxysuccinimide
Nm	Nanometre(s) (10^{-9} m)
L	Litre
OD	Optical density
PAGE	Polyacrylamide gel electrophoresis
PBS	Phosphate buffered saline
PCR	Polymerase Chain Reaction
PDP	3-(2-pyridyldithio)-propionyl
PEG	Poly (ethylene glycol)
pI	Isoelectric point
PLL	Poly-L-lysine
PMSF	Phenylmethylsulphonyl fluoride
pN	Pico Newtons (10^{-12} N)
QCM	Quartz crystal microbalance
R-M	Restriction-Modification
SD	Standard deviation
SDS	Sodium dodecyl sulphate
SDS-PAGE	Sodium dodecyl sulphate polyacrylamide
SPM	Scanning probe microscopy
STM	Scanning tunnelling microscopy
TAE	Tris-acetate-EDTA
TEMED	N,N,N′,N′-Tetramethyl-1,2-diamino-ethane
TRD	Target Recognition Domain
Tris	2-amino-2-(hydroxymethyl) -1,3-propanediol
Tm	Melting temperature of a DNA oligonucleotyde
UV	Ultraviolet
v/v	Volume for volume
w/v	Weight for volume

SYMBOLS

Å	Ånström(s) (10^{-10} m)
$A_{final,total}$ $A_{final,sep}$	Work done associated with the final rupture event / pN nm
B	V-shape probe base width / μm
D	Cantilever deflection / nm
E	Young's modulii / GPa
f^*	The most probable binding force required to rupture a molecular complex bond / pN
F_{final}	Force rupture (avidin-biotin) / pN
G	Grams
K	Spring constant / N m^{-1}
k_B	Boltzmann constant (1.38×10^{-23}) /J K^{-1}
K_d	Dissociation constant / M
k_{diss},	Dissociation rate of the bond/ s^{-1}
L	Cantilever length / μm
l_r	Rupture length / nm
l^*	the most probable rupture length
M_e	Normalised effective mass (0.163) / kg
M_o	Molecular mass of protein / g mol^{-1}
N_o	Avogadro's number (6.02×10^{23}) / mol^{-1}
E	Extinction coefficient / cm^{-1} M^{-1}
R_a	Surface roughness / nm
R_f	Loading rate / pN s^{-1}
T	Cantilever thickness / μm
υ	Velocity / nm s^{-1}
V_c	Molecular volume based on molecular weight / nm^3
V_M	Molecular volume derived from AFM images / nm^3
w	Cantilever width / μm

x_{diss}	Position of energy barrier / nm
µm	Micrometre(s) (10^{-6} m)
µL	Microlitre(s)
λ	Wavelength / nm
ρ	Density / kg m^{-3}
τ**(0)**	Lifetime of the bond / s

Chapter 1

Introduction

1.1 Restriction-Modification systems

The discovery of restriction enzymes in bacterial cells has become a "milestone" in the development of science and especially in gene technology. Molecular investigation carried out in *Escherichia coli* in the 1960s helped to understand the molecular mechanism of Restriction-Modification (R-M) systems; the phenomenon is a defence mechanism against invasion by foreign DNA, *i.e.*, viral attack. An R-M system (protein complex) is composed of the modification enzyme, a DNA methyltransferase, and its cognate endonuclease (ENase) and for some systems a control gene (Bickle and Kruger, 1993). Both endonuclease and methylase (MTase) recognise the same specific DNA sequence (usually comprised of four to eight nucleotides) and protection of the host DNA is based on modification (methylation) of specific bases in the ENase target sites on the DNA, which protect the DNA from restriction activity of the ENase. The modification enzymes (MTases) are capable of methylating unmethylated DNA, the preferred substrate usually being hemi-methylated DNA (Yuan *et al.*, 1975). Any foreign DNA is normally unmodified (unmethylated) and is a substrate for the endonuclease and degradation (Murray, 2000; 2002).

R-M systems are classified into four types based on their subunit composition, gene organisation, cofactor requirements, DNA target sequence and mechanism for cleavage of DNA (Table 1.1) (Wilson and Murray, 1991; Bickle and Kruger, 1993; Murray, 2000; Roberts *et al.*, 2003; Sistla and Rao, 2004).

Table 1.1. Types of restriction-modification systems and their functions (Sistla and Rao, 2004).

Function	Type I	Type II	Type III	Type IV
Subunits	Bifunctional, hetero-oligomeric, three different subunits: HsdS, HsdM, HsdR	Two, identical endonuclease subunits. Separate single subunit MTase	Two different, products of the Mod and Res genes	Two different subunits
Enzymatic activity	Endonuclease MTase ATPase	Endonuclease MTase (separate)	Endonuclease MTase ATPase	Endonuclease GTPase
Cofactor for DNA cleavage	ATP Ado-Met Mg^{2+}	 Mg^{2+}	ATP AdoMet Mg^{2+}	 GTP Mg^{2+}
Methylation	AdoMet, Mg^{2+}	AdoMet	AdoMet, Mg^{2+}	_
Recognition sequence	Asymmetric, bipartite	Symmetric, short, palindromic	Asymmetric require inverted orientation	Bipartite, methylated
Cleavage site	Random, remote from asymmetrical recognition site	Within or near recognition site	25-27 bp from recognition site	Between methylated bases at multiple positions
DNA translocation	Yes	No	Yes	Yes

1.1.1 Type I Restriction-Modification enzymes

Type I R-M enzymes are a group of multifunctional enzymes consisting of four families: Type IA is represented by EcoKI (the first to be identified and purified) (Meselson and Yuan, 1968; Bickle, 1987; Wilson and Murray, 1991), Type IB illustrated by EcoAI (Suri *et al.*, 1984), Type IC by EcoR124I, EcoR124II (Price *et al.*,

1987), EcoDXXI (Piekarowicz *et al.*, 1986), EcoprrI (Tyndall *et al.*, 1994) and Type ID by StySblI (Titheradge *et al.*,1996).

Type I R-M enzymes, having the MTase and endonuclease activity in the single enzyme, must undergo a genetic switch to control the opposing functions following recognition of the methylation status of the DNA (Yuan *et al*., 1975). Hemi-methylated DNA produced in the host bacterium, as a result of replication of fully methylated DNA is the most suitable substrate for methylation of the two adenines within the recognition sequence. The DNA recognition sequence of type I R-M enzymes is bipartite and asymmetric consisting of two parts (3 – 4 bp and 4 – 5 bp) separated by a spacer region (6 – 8 bp), *e.g.*, GAAnnnnnnRTCG - *Eco*R124I (Price *et al.*, 1987). In the presence of a fully methylated target sequence, the substrate is protected from restriction activity, and the endonuclease complex dissociates (Smith *et al.*, 1972). Unmethylated DNA at the specific target sequence recognised as "foreign" is a signal for an allosteric conformational change of the enzyme (switch from methyltransferase to an endonuclease) (Yuan and Meselson, 1970) resulting in cleavage of invading DNA accompanied by ATP hydrolysis and DNA translocation. It was shown that DNA modification (methylation) appears prior to restriction following conjugation of the R-M system into a new host bacterium, indicating a temporal control of the two functions (Prakash-Cheng and Junichi, 1993).

1.1.2 Type I restriction-modification enzymes as a multifunctional enzymes

Type I R-M enzymes are the most complex and were the first type to be discovered (Meselson and Yuan, 1968). They have several functionalities and provide catalysis for a number of processes. Type I R-M enzymes were found to be involved in: (a)

recognition of specific target sequences of DNA (DNA binding); (b) determination of the methylation status of the substrate; (c) methylation at the DNA binding site; (d) ATPase activity; (e) translocation of DNA; and (f) cleavage of unmodified DNA.

1.1.3 Structure and function of subunits

The multi-oligomeric Type I restriction enzymes are composed of three different subunits encoded by linked "host specificity determinant (*hsd*) genes":

hsdR - required for restriction activity;

hsdM - required for binding the methyl-group donor cofactor AdoMet;

hsdS - required for DNA recognition and binding.

Both HsdS and HsdM subunits (products of *hsdS* and *hsdM*, expressed from the same promoter P_{MOD}) are required for independent methyltransferase activity; whereas, the Enase holoenzyme is composed of two HsdR subunits (product of *hsdR* expressed from $P_{RES)}$, two HsdM subunits and one HsdS subunit (Dryden *et al.*, 2001). The HsdR subunit includes the active site for ATP hydrolysis, a cofactor necessary in translocation process while the HsdM subunit contains specific site for binding the AdoMet (Takasugava *et al.*, 1998), which acts as an allosteric effector (Yuan *et al.*, 1975), which is also essential for restriction activity of the enzyme (Meselson, and Yuan, 1968). Early experiments showed that AdoMet binds to the HsdM subunit of *Eco*KI (Buhler and Yuan, 1978) and is responsible for donation of the methyl group during DNA methylation.

1.1.4 DNA cleavage

DNA cleavage is the mechanism of restriction activity of the ENase in the presence of essential cofactors (ATP, Ado-Met, Mg^{2+}) (Table 1.2), and is preceded by DNA translocation. During this bi-directional process, each HsdR subunit acts as an individual molecular motor and moves the DNA past the DNA-bound complex, using hydrolysis of ATP as the energy source, with production of an expanding loop (Figure 1.1) (Janscak *et al.*, 1999). Translocation of DNA and subsequent cleavage occurs when two unmethylated bases are detected within the recognition sequence of the enzyme and after an ATP-dependent conformational change in the enzyme (Meselson and Yuan, 1968). The methylation status of a single base must be read and remembered by the enzyme reads the methylation status of the second base in the recognition sequence. DNA cleavage by Type I R-M enzymes has no turnover: one endonuclease molecule produces only a single cleavage event; fragments resulting from cleavage are random in size, from a few hundred base-pairs to thousands of base-pairs (Yuan *et al*., 1980; Studier and Banyopadhyay, 1988; Dryden *et al*., 1997; Szczelkun *et al*., 1996). Cleavage is a consequence of halted translocation commonly caused by collision of two moving enzymes; it was proposed that cleavage occurred exactly half way between both recognition sites on a two-site plasmid (Studier and Bandyopadhyay, 1988). Janscak *et al.* (1999) have shown that blockage of the translocation occurred in the presence of structural obstructions of DNA (Holliday junction), whereas inhibited translocation by DNA supercoiling was suggested by Szczelkun *et al.* (1996). Topological barriers to translocation with covalently closed circular DNA becomes another reason for blockage of the process resulting in DNA cleavage (DNA wound into the expanding loop, no more to translocate) (Szczelkun *et al.*, 1997).

Table 1.2. Functions of cofactors essential for modification-restriction activity (Sistla and Rao, 2004).

Function	S-AdoMet	ATP	Mg^{2+}
Complex conformation and activation	Allosteric effector for EcoKI (absolutely required for activation of enzyme by induction of specific DNA binding); Positive effector for EcoR124I.	Conformation of complex	Used as a Lewis acid for DNA cleavage.
Methylation	Determination of the methylation status of the target sequence (methyl donor group)	Inhibitor of methylation of un-modified DNA	Determination of optimal conditions for modification
Restriction	Stimulation of ATP hydrolysis and DNA cleavage	Substrate in ATP hydrolysis; ATP dependent formation of DNA loop; cofactor in the DNA cleavage	ATP hydrolysis; absolutely required; for restriction

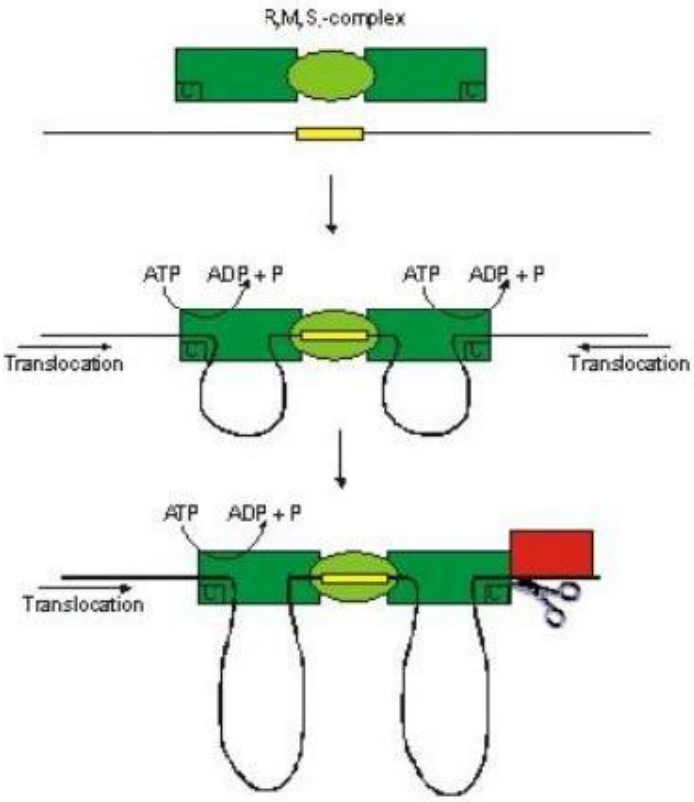

Figure 1.1. Mechanism of DNA cleavage (Janscak *et al.*, 1999). M_2S complex is represented as a green ellipse, HsdR subunit is shown as a green box, DNA with the recognition sequence (yellow box) represented by black line. Arrow shows direction of DNA translocation (Janscak and Bickle, 2000).

Berge *et al.* (2000) used information and images obtained with an AFM to propose a new model for the cleavage a linear DNA, containing two recognition sites by the Type I R-M enzyme EcoKI (a representative of IA family). In their model, the cleavage pathway involves the rapid dimerisation of the protein as a result of conformational changes during the binding of EcoKI to the two specific target sequences of DNA plasmid resulting in double strand cleavage preceded with translocation.

1.1.5 EcoR124I

Type IC R-M enzyme EcoR124I (originally found encoded by the conjugative plasmid R124) (Hedges and Datta, 1972), is a member of the family represented by

*Eco*R124II, *Eco*DXXI and the chromosomally encoded *Eco*prrI (Tyndall *et al.*, 1994; Murray, 2002). The recognition sequences of *Eco*R124I ($GAAn_6RTCG$) and *Eco*R124II ($GAAn_7RTCG$) differ by only one extra nucleotide in the non-specific spacer of *Eco*R124II (Price *et al.*, 1987), where R = purine and n = any nucleotide. The sequence analysis of the *hsdS* genes showed the only difference to be a 12 bp repeat existing as two copies in EcoR124I and three copies in EcoR124II.

1.1.5.1 HsdS subunit of EcoR124I enzyme

The HsdS subunit includes two Target Recognition Domains (TRDs) (separated by conserved regions) responsible for DNA recognition. The TRD1 domain nearest the NH_2-terminus recognises the 5´ component of the bipartite, specific sequence (GAA for EcoR124I). TRD2 nearest COOH terminus is involved in recognition of the RTCG (for EcoR124I) sequence (3´-end). (Figure 1.2) (Price *et al.*, 1987).

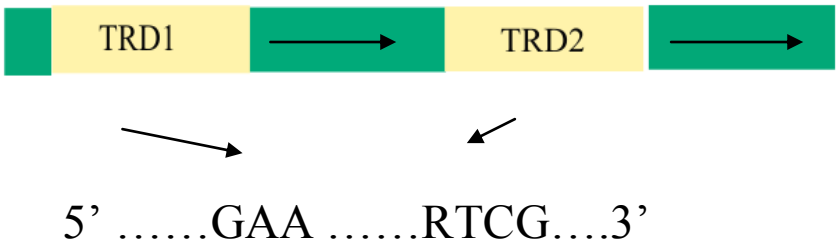

Figure 1.2. The domain structure of HsdS (DNA-binding) subunit EcoR124I (Type IC family member). Conserved regions shown by arrows.

Conserved domains (amino acids highly conserved within each family), one present midway between the C- and N- termini (central conserved region) and the second placed at the C-terminus (in type IC at the N-terminus of HsdS subunits), are thought to be responsible for protein-protein interactions (Cowan *et al.*, 1988; Kannan *et al.*,

1989). A changed ability to interact with the HsdM subunit and produce a functional MTase was observed for point mutations in the central conserved region of HsdS subunit of EcoR124I (Abadjieva *et al.*, 1994; Weiserova *et al.*, 1998, 2000). Based on this repeat structure, a “circular" organisation of the domains of HsdS subunit was proposed, providing the symmetry required for interaction with the two HsdM subunits and the recognition DNA sequence (Kneale, 1994).

HsdS subunit is insoluble on its own; solubility can be achieved only with the presence of HsdM subunit (Patel *et al.*, 1992), or as a GST fusion protein (Kusiak *et al.*, 1992). Two crystal structures, obtained for an HsdS subunit from the uncharacterised Type I R-M systems MjaXIP (Kim *et al.*, 2005) and MgeORF438 (Calisto *et al.*, 2005), confirmed the circular nature of the HsdS subunit and the close proximity of the N- and C-termini, also indicated by (Janscak and Bickle, 1998), however the DNA specificity of these uncharacterised systems and presence as the part of functional enzymes are still unknown. Based on MjaXIP and MgeORF438 crystal structures, a model for HsdS(EcoR124I) structure was proposed (Figure 1.3) (Obarska *et al.*, 2006).

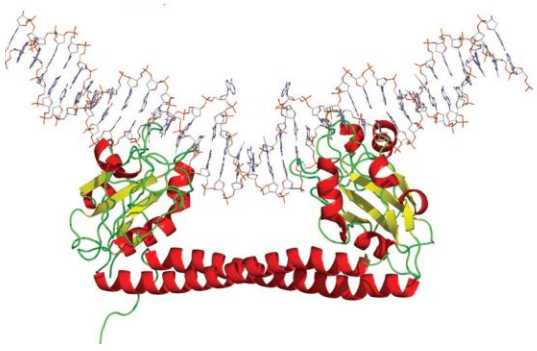

Figure 1.3. Structural model of HsdS(EcoR124I) (Obarska *et al.*, 2006).

1.1.5.2 EcoR124I MTase

The fully functional and independent MTase (162 kDa) of stoichiometry ($HsdM_2HsdS_1$) is composed of two HsdM (58 kDa) subunits and one HsdS subunit (46 kDa) (Taylor *et al.*, 1992; Dryden *et al.*, 1993). MTase in the presence of S-adenosyl methionine (AdoMet), catalyses DNA methylation through transfer of a methyl group, from the methyl donor AdoMet, to the N-6 position of the adenine residue on each part of the recognition site, one on the each strand of the DNA (Taylor *et al.*, 1993). A structural model for the DNA methylase of EcoR124I has been proposed by Obarska *et al.* (2006), Figure 1.4, based on the above HsdS modelled structure.

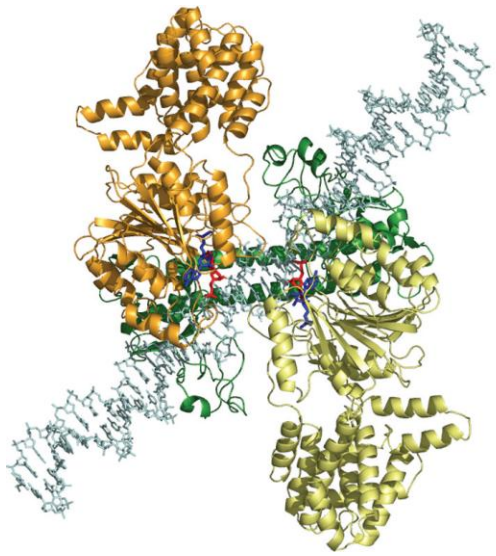

Figure 1.4. Model structure of the EcoR124I DNA methyltransferase (Obarska *et al.*, 2006). The HsdS subunit is shown in green, two HsdM subunits (yellow and orange) located on either side of the DNA in a symmetrical arrangement, two adenines of the recognition sequence (red) and the methyl donor (blue).

1.1.5.3 HsdR(motor) subunit

The largest individual subunit HsdR (120 kDa), transcribed from independent promoter P_{RES} (Zinkevich *et al.*, 1997) and necessary for restriction activity by the holoenzyme endonuclease (ENase). A detailed structural model of the EcoR124I HsdR subunit

obtained using protein-fold recognition and homology modelling techniques has been proposed (Figure 1.5) (Obarska-Kosinska *et al.*, 2008). In addition, progress towards a crystal structure for HsdR(EcoR124I) has been described (Lapkouski *et al.*, 2007, 2009).

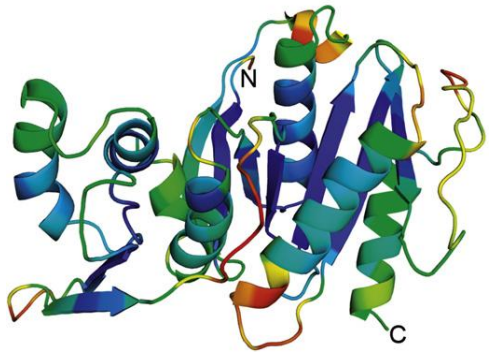

Figure 1.5. Model of the N-terminal domain of EcoR124I HsdR (Obarska-Kosinska *et al.*, 2008).

The HsdR (EcoR124I) is closely related to the chromosomally encoded member of Type IC R-M enzyme EcoPrrI (Tyndall *et al.*, 1994). The two subunits have a 74.46 % identity over 325 aa and further 10.46 % similarity. A hybrid protein HsdR(PrrI) has been constructed by replacing the first 200 aa of the EcoR124I with the equivalent region of EcoPrrI. The hybrid subunit was found to be functional, however the binding affinity for MTase was different when compared to wild-type HsdR (Dutta, C., Weiserova, M., Lisle, W., Firman,K., 2001, unpublished).

1.1.5.4 EcoR124I assembly pathway

The holoenzyme in stoichiometry $R_2M_2S_1$ (Figure 1.6) can be reconstituted *in vitro* from the purified MTase and HsdR (Janscak *et al.*, 1998).

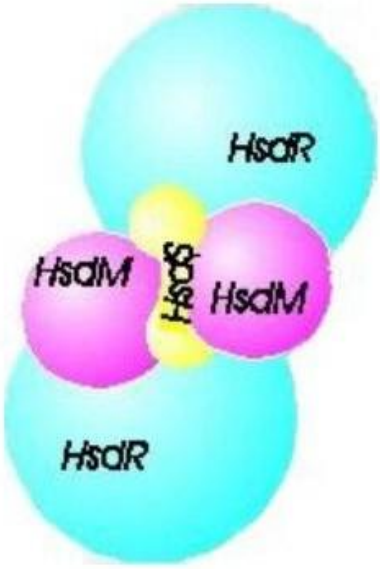

Figure 1.6. A cartoon illustrating the assembly of the EcoR124I holoenzyme $R_2M_2S_1$.

The Electrophoretic Mobility Shift Assay (EMSA) analysis of EcoR124I assembly *in vitro* indicates that $R_1M_2S_1$ complex is an intermediate stage in the assembly pathway (Figure 1.7), characterised as a stable complex that is modification-proficient, but without the capability for DNA cleavage, whereas the $R_2M_2S_1$ holoenzyme is capable of modification and restriction activities (much weaker complex). The equilibrium between $R_1M_2S_1$ and $R_2M_2S_1$ complexes was determined by Janscak *et al.* (1998) and the K_d was found to be 24 µM.

Binding of the final HsdR subunit provides temporal control of the restriction activity of ENase (Firman *et al.*, 2000). Limited concentration of HsdR *in vivo* guarantees that endonuclease activity will be preceded by methylation process (time for synthesis of HsdR) and the host DNA will be protected from restriction.

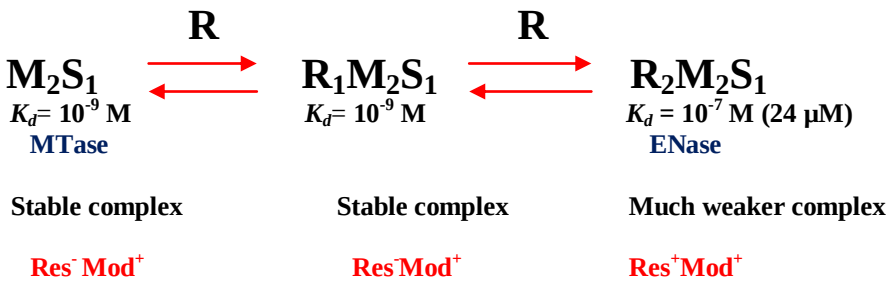

Figure 1.7. The assembly pathway of EcoR124I.

1.1.5.5 EcoR124I as a molecular motor (nanoactuator)

A unique feature of EcoR124I compared to other representatives of Type I Restriction-Modification enzymes is a lowered strength of HsdR binding (complex formation by MTase and formation of the ENase is dependent upon the MTase:HsdR ratio). The R_2-complex, with two motor units, is obtained at an 8:1 ratio of HsdR to MTase (Janscak, *et al.*, 1998), whereas, formation of the R_1-complex occurs at a ratio 1:1. The R_2-complex can be also formed by association of a free HsdR subunit to an already translocating R_1-complex. This is proof that binding and translocation initiation by the two motors are independent from each other (Seidel *et al.*, 2005). Single molecule analysis of EcoR124I was obtained with a Magnetic Tweezer Setup (Figure 1.8); the mechanics of the translocation process in real time was investigated. The height measurement of the magnetic bead was used to determine the decrease in DNA end-to-end distance as a result of translocation by EcoR124I. Seidel *et al.* (2004) demonstrated independent motor activity (uncoordinated translocation) for the two HsdR subunits of EcoR124I. Translocation of the R_2-complex (990 ± 30 bp s^{-1}) occurred with twice the velocity of the R_1-complex (510 ± 30 bp s^{-1}). Stalled translocation by EcoR124I results from dissociation of the HsdR motor subunit from the core MTase, which can load a new motor subunit from solution and initiate a new translocation event. Reinitiation of

translocation is concentration dependent of HsdR subunit and independent of MTase concentration in the solution.

The independent work by the HsdR subunits was confirmed by AFM imaging of translocating EcoR124I. It was shown that the R_2-complex forms two loops during DNA translocation (van Noort *et al.*, 2004). However, the rate of translocation was found to be much lower (10-fold) than observed in the bulk solution, probably due to problems with timing, surface immobilisation and effects of the surface on motor activity.

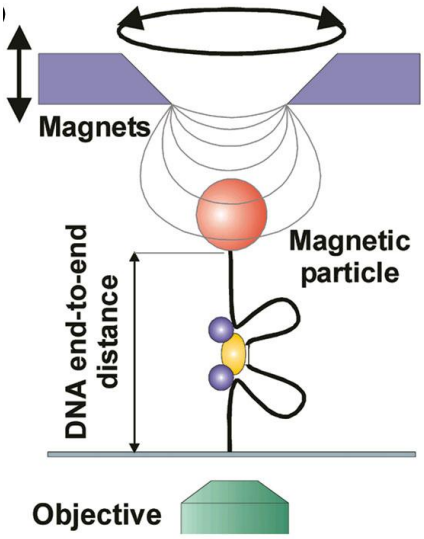

Figure 1.8. The magnetic tweezers setup. A DNA molecule is attached to the bottom of the flow cell and at the other end to a magnetic bead (5µm diameter), held by magnets used for DNA rotation resulting in supercoiling in the DNA. The change in DNA end-to-end distance (translocating EcoR124I shortens the DNA) was determined with video microscopy of the bead.

The possibility of pulling DNA through the complex and the system, thus acting as a nanoactuator, gives an opportunity for construction of a useful device where DNA can be attached to the surface instead of the motor – a much simpler situation than enzyme-

surface attachment. The study of the forces holding the multi-subunit complex together would be of interest to motor activity and use of the motor in any form of active device.

1.2 Scanning probe microscopy

1.2.1 Scanning tunnelling microscopy (STM)

Scanning Probe Microscopy (SPM) is a general name for a number of related microscopy techniques based on scanning a sample with a sharp probe which can provide three-dimensional topological information (Bining *et al.*, 1982). High-resolution imaging is a powerful tool in many disciplines, such as biology, material science, physics, chemistry and chemical engineering. The first SPM technique to be developed was Scanning Tunnelling Microscopy (STM), which allows imaging of conductive surfaces. The tunnelling current is measured between a sharp STM tip, made of a conductor, such as gold or platinum-iridium, and a surface after applying a bias potential across the gap (*ca.* 5 Å) (Binnig *et al.*, 1985; Dai *et al.*, 1993). STM studies are limited to conducting substrates although tunnelling through DNA and other biomolecules *via* an uncertain mechanism, have been reported (Miles *et al.*, 1990; Ohshiro and Maeda, 2010). The energetic and charge transport properties of semiconductor-protein junctions have been examined using reverse transcriptase (Campbell *et al.*, 2007).

1.2.2 Atomic force microscopy

Atomic force microscopy (AFM), also known as the scanning force microscopy (SFM), was invented in 1986 by Binnig, Quate and Gerber, later laureates of the Nobel Prize for Physics (Binnig *et al.*, 1986; Czajkowsky *et al.*, 2000). AFM is able to provide topography images at the nanometre-scale, in either air or liquid (water or physiological

buffer) environments (Bowen *et al.*, 2001). In addition to imaging, AFM can be used to probe forces of interaction between the AFM tip and a surface. It is now common to chemically or biologically functionalise the AFM tip with proteins, nucleic acids and cells (Muller *et al.*, 2000), which enables information concerning interactions between molecules, dynamics and structure to be obtained (Engel *et al.*, 1999). Images can be obtained in either contact or tapping modes; details of these are summarised in Table 1.3.

1.2.2.1 Contact mode

Contact mode is the most basic mode of operation, where the tip and sample remain in contact during scanning. The bending of the cantilever, controlled by a feedback system, is kept constant by moving the sample away from or towards the AFM probe (Gaboriaud and Dufrene., 2007). Contact operation mode is not suitable for imaging isolated biological samples, which can be easily damaged by this process. The need to bring the surface in contact with the probe, however, is important for force spectroscopy measurements.

1.2.2.2 Tapping mode

One of the main operating modes in AFM imaging is tapping mode. Here, the tip is not in contact with the surface, but a high amplitude (typically > 20 nm) cantilever oscillation is induced by z-piezo motion and the sample is moved towards the oscillating tip until it begins to softly touch (tap). The frequency of vibration is typically 5% less than the resonant frequency of the cantilever. During scanning, the cantilever oscillation amplitude is maintained constant by a feedback loop. The normal resonant frequency of the cantilever can be damped during imaging in liquids, however, the best

results are usually obtained using very soft cantilevers (spring constants, *k*, typically *ca.* 0.1 N m^{-1}) compared to tapping mode in air (*k ca.* 1 – 100 N m^{-1}).

Table 1.3. Differences between main AFM operating modes (Wiesendanger, 1994).

Contact mode (for topography, elasticity, adhesion and friction measurements)	Tapping mode (Intermittent) (for topography and adhesion force measurements)
The tip and the sample are in constant contact; Simple technique; Constant bending of the cantilever is caused by the feedback system (moves away and toward the cantilever from the surface). 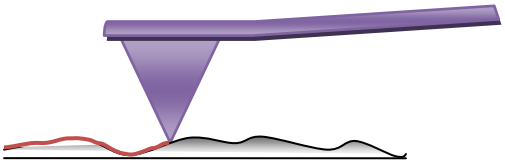	The tip is oscillated near resonant frequency using piezoelectric actuator. During the imaging the tip briefly touches the surface decreasing the oscillation amplitude becomes the feedback control signal used for surface topography measurement; Can reduce lateral forces during imaging (necessary for soft biological samples); The disruption of the soft samples is reduced by imaging in liquid. 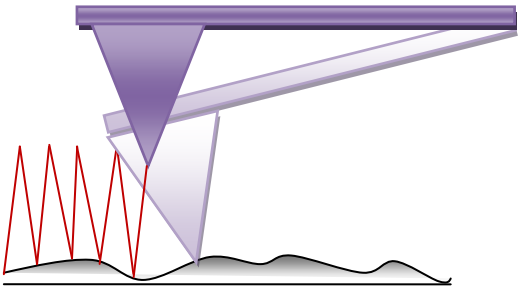

1.2.2.3 Principles of AFM

The essential features of AFM are the tip-mounted cantilever, the optical deflection system (laser diode and four quadrant photodetector) (Hinterdorfer and Dufrene, 2006),

piezoelectric scanner and a feedback control loop (maintains constant oscillation amplitude). The laser beam is reflected off the back of the cantilever onto the photodetector which provides information about the normal bending (AB-CD) and torsion (AC-BD) of the cantilever, corresponding to normal and lateral forces (Figure 1.9) (Colton *et al.*, 1997).

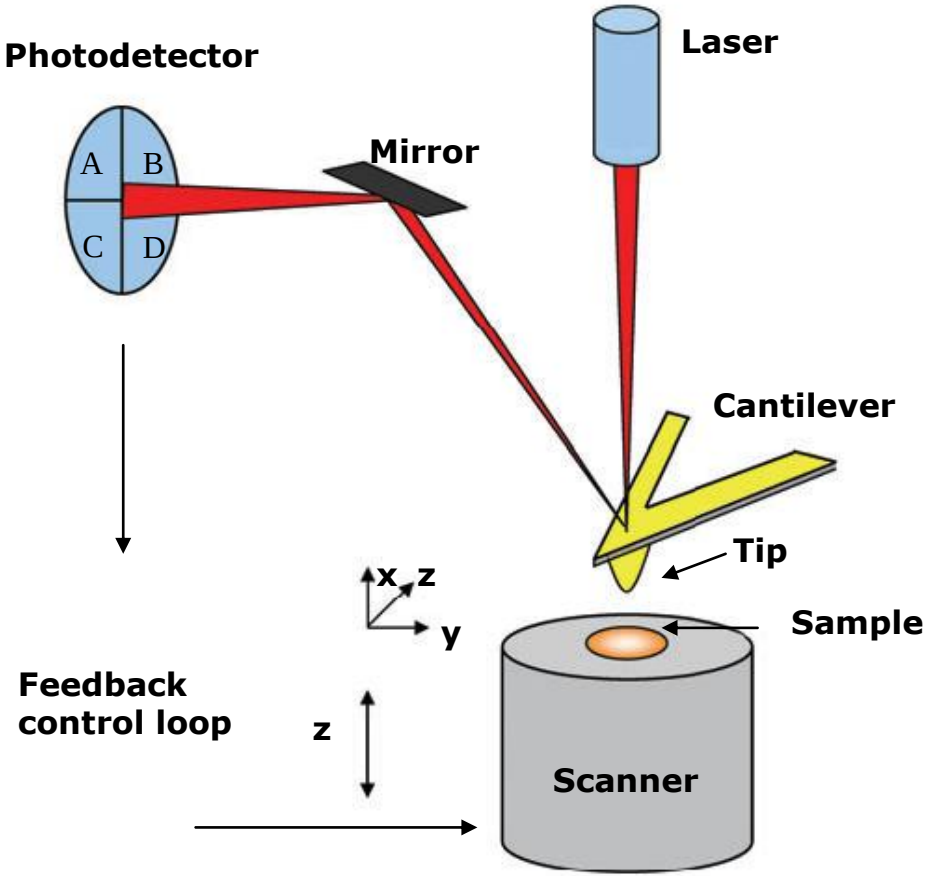

Figure 1.9. Schematic showing the essential features in AFM (Hinterdorfer and Dufrene, 2006).

The AFM cantilever, with integrated tip, is usually made of silicon or silicon nitride with typical dimensions: 100 – 300 µm in length, 10 – 30 µm in width and 0.5 – 3 µm in thickness (Colton *et al.*, 1997). The sample is placed on top of a piezoelectric scanner and moved close to the AFM tip using an automated approach. Piezoelectric ceramics

(able to change dimensions as a function of an applied electric field) control the position of the sample by moving it in three dimensions relative to the cantilever. The sample can then be raster-scanned against the tip, or moved vertically to maintain a constant force on the tip. A three-dimensional topographic image of the surface can thus be obtained. Alternatively, the forces acting between the tip and sample can be measured as the sample approaches, is pushed onto and then is withdrawn from the AFM tip; a force *versus* distance curve is thus acquired (Zhong *et al.*, 1993; Jaschke *et al.*, 1996).

1.2.2.4 Force curves

Force spectroscopy refers to the acquisition of AFM force-distance curves (Heintz *et al.*, 1999). For single proteins, measured forces are usually of the order of pico-Newtons (pN) to a few nano-Newtons (nN) (Lee *et al.*, 1994; Moy *et al.*, 1994a). In force spectroscopy, the sample is pushed towards the tip and then retracted at a constant velocity and the deflection of the cantilever (d) is recorded as a function of the vertical displacement of the piezoelectric scanner (z) (Figure 1.10). This can be monitored at x and y locations to obtain an array of force curves. Two conversions have to be implemented to obtain the force (F, measured in nN) (Hinterdorfer and Dufrene., 2006): (i) photodetector voltage conversion into cantilever deflection (nm) and (ii) cantilever deflection conversion to force (F, nN) using Hooke's Law (Equation 1.1) (Figure 1.10),

$$F = kd \qquad \text{(Equation 1.1)}$$

where k = cantilever spring constant (N m^{-1}).

Determination of *k* for each cantilever is essential for accurate force distance experiments, as the values quoted by manufacturers often vary by a factor of two or even more (Sader, 1995) and can introduce serious experimental error.

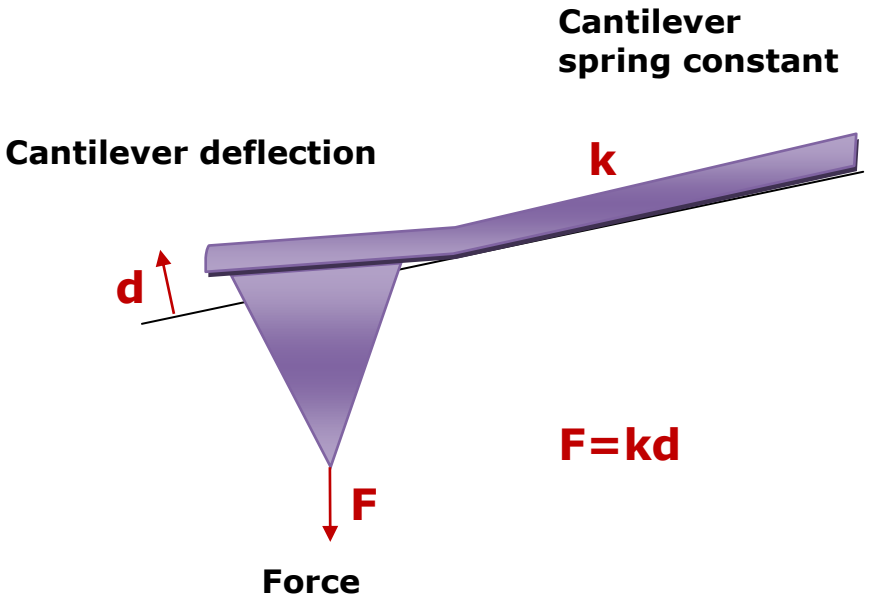

Figure 1.10. Calculation of force from cantilever deflection and spring constant.

Various methods of determining *k* have been described. The simplest method relies of the geometry of the cantilevers (Sader and White, 1993; Sader, 1995). Alternately, *k* may be measured from the deflection of cantilever in response to a known force (Senden and Ducker, 1994; Torii *et al.*, 1996), or changes in dynamical properties of vibrating cantilevers (Cleveland *et al.*, 1993; Hutter and Bechhoefer, 1993).

Initially, the sample is positioned at a relatively long distance away from the tip (point A, Figure 1.11). As the sample is moved closer to the tip, atoms in the sample surface interact with those on the surface of tip resulting in a bending of the cantilever away from the sample caused by the repulsive (electrostatic) forces, or towards the sample (in

the presence of attractive, van der Waals and electrostatic forces) resulting in a "jump to contact" (B-C, Figure 1.11). In this contact region, some elastic deformations of the sample and/or tip can be observed and provide the information about mechanical properties (stiffness) of the sample (C-D) (Engel *et al.*, 1999). At a certain distance, sometimes known as the trigger threshold, the sample is pulled away from the tip and forces associated with adhesion, solvation and the hydrophobicity of the sample can be observed (F-G, Figure 1.11; Table 1.4) (Zlatanova *et al.*, 2000). During retraction, separation of the tip and the surface may be delayed due to the contact adhesion forces. "Jump from contact" appears when the adhesive interactions (between tip and surface) have been overcome by the elastic constant of the cantilever.

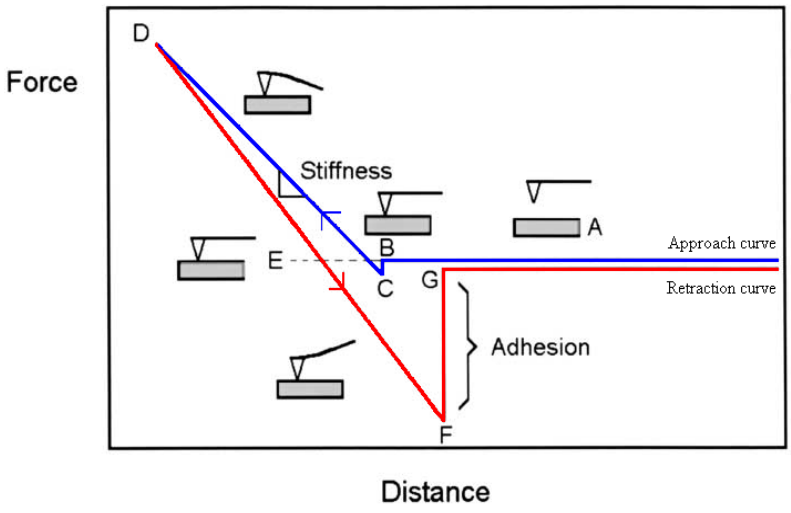

Figure 1.11. Schematic diagram of an ideal AFM force-distance curve. Approach curve (blue) (A-B): sample approaches AFM tip; (B-C): sample contacts tip ("jump to contact"); (C-D): cantilever flexes and/or tip indents into surface; (D-F): sample is withdrawn from tip (retraction curve, red); (E): no net forces (attractive or repulsive) between the tip and sample; (E-F): sample is adhered to the tip; (F): surface is removed from tip ("jump-off"); (F-G): adhesion event; (G-A): surface moves away from tip (Beech *et al.*, 2002).

Table 1.4. Types of interaction forces during the approach and retraction. Adapted from Zlatanova *et al.* (2000).

Force	Description	Shape of curve
From approach curve		
Attractive van der Waals force	Creates jump-to-contact peak; depends on force between tip and sample and the system geometry; meniscus forces must be eliminated by working in a low humidity environment or in liquid.	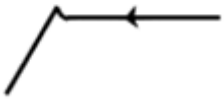
Repulsive double-layer electrostatic force	Due to charging both sample and tip surfaces with like charges (adsorption of ions from solution and dissociation of functional groups on surfaces).	
Repulsive hydration force	Comes from repellent interactions between hydrated ions bound to tip and sample surfaces; apparent at high salt concentration.	
Solvation force	When tip and sample are within a few molecular diameters from each other, oscillation between attraction and repulsion may be observed; caused by ordering of non-polar liquid molecules between the two liquid-solid interfaces; force follows density of solvent.	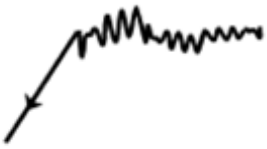
From retraction curve		
Adhesion	Due to van der Waals forces and indentation of sample by tip (which increases contact area); meniscus force must be eliminated.	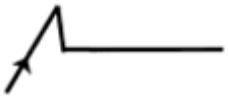

1.2.3 Forces acting in biological systems

Interactions between biomolecules are essential in many important processes, such as antigen-antibody recognition, DNA replication and enzymatic reactions. According to the Derjaguin Landau, Verwey and Overbeek (DLVO) theory developed in the 1940s, two charged surfaces interacting through a liquid medium do so as a result of the combined effect of the attractive van der Waals and the electrostatic repulsion forces (Israelachvili, 1992). The theory fails at very small distances (of a few nm), where hydration, hydrophobic and steric forces are present. Different forces may be observed between interacting molecules, *e.g.*, attractive or repulsive van der Waals forces appear as a result of interaction of dipole moments of the particles, or between the parts of the same molecule (Israelachvill., 1992). In the presence of two identical molecules, van der Waals forces are always attractive, whereas, those between two different molecules can be attractive or repulsive (Leckband and Israelachvili, 2001).

Electrostatic "double layer" repulsive forces are created as a result of the presence of two identically charged surfaces at a close distance. In an electrolyte solution, the charge on the layer of the molecule is compensated by the double layer of ions. The energy of electrostatic interaction between two equal charged molecules, or surfaces, is always negative(Leckband and Israelachvili, 2001).

Hydration forces exist between hydrophilic molecules (DNA, proteins) interacting with water molecules. These kind of forces act over short distances (< 3 nm) and are dependent on the energy necessary to disrupt hydrogen bonds, or the dehydration of two approaching surfaces (Israelachvilli, 1992).

Information concerning weak van der Waals, hydration and electrostatic forces between surfaces can be obtained by specific AFM tip modifications. During the AFM operation in air, a thin layer of water can be present on the tip and the sample surface producing capillary forces, which may obscure weak van der Waals forces (Burnham *et al.*, 1993)

1.2.4 Surface binding strategies

It is important to immobilise biomolecules on surfaces prior to AFM observation and force measurements. This can be achieved on glass, mica and gold using a variety of methods (Rief *et al.*, 1997). The simplest method is non-specific adsorption, although data interpretation can be difficult due to uncertainty in the location of the attachment points on the molecule.

Mica is the most frequently used substrate for imaging biological specimens, including double-stranded DNA, proteins and DNA-protein complexes. Muscovite mica, $KAl_2(OH)_2AlSi_3O_{10}$, is a non-conducting layered mineral composed of multiple 1 nm thick layers (Bailey, 1984). It can be cleaved easily, using adhesive tape, to produce clean, atomically flat surfaces that are negatively charged.

Interestingly, the modified mica surface promotes the adsorption or covalent binding of the biomolecules (Lyubchenko *et al.*, 1992). Immobilisation of negatively charged samples onto negatively charged mica surface can be obtained by surface modification to avoid the AFM tip sweeping away poorly attached molecules (Thundat *et al.*, 1992). Negatively charged DNA, proteins, or membrane fragments, can be immobilised on mica using a buffer solution with divalent cations, *e.g.*, Mg^{2+}, Ca^{2+}, Ni^{2+} (Vesenka *et al.*,

1992; Hansma *et al.*, 1995; Klein *et al.*, 2003), or by coating mica with a thin layer of poly-L-lysine (PLL), which provides a positively charged surface (Müller *et al.*, 1997).

Similar methods for derivatisation of mica can be used for silicon or silicon nitride probes, since all these materials have silanol (Si-OH) groups presented at their surfaces. For example, covalent attachment of proteins can be achieved following five separate steps (Hinterdorfer *et al.*, 2001; Friedsam *et al.*, 2004):

(i) Amination of surfaces. A low density of amino groups on the tip surface is desired for single molecule studies; several methods have been developed: gas-phase silanisation with 3-aminopropyltriethoxysilane (APTES) and aqueous phase adsorption of APTES dissolved in toluene (in the presence of water molecules will hydrolyse and produce ethanol and trisilanol), spontaneous esterification between silanol groups (Si-OH) presented on mica and ethanolamine (suitable for stretching experiments) and aminophenyltrimethoxysilane (APhS) treatment in toluene solution. These strategies suitably functionalise AFM tips, although Ebner *et al.* (2007a) noticed that a slightly lower surface density of amino groups resulted after APTES treatment. Liu *et al.* (2005) investigated two methods (evaporation and water solution) for DNA immobilisation on mica surfaces for imaging using APTES.

(ii) PEGylation of tips and/or mica surfaces allows molecular linkers to be attached to both reactive amino groups on the surface and biomolecules of interest, *e.g.*, hydroxysuccinimide (NHS) ester-maleimide heterofunctional crosslinkers (Roberts *et al.*, 2002).

(iii) Blocking un-reacted surface amines (to be certain that further reaction steps will not occur with PEG linkers).

(iv) Tethering molecules of interest to the PEG linkers.

(v) Blocking PEG (to remove reactivity from PEG linkers; this step can be avoided, depending on the nature of PEG reactivity).

1.2.4.1 Non-covalent and covalent attachment using cross-linkers (tip modifications)

The precision and quality of experiments based on single molecule interactions are mostly dependent on the coupling method. Successful tip functionalisation with the protein of interest may be difficult to achieve and, therefore, several important issues need to be considered: the attached protein should be able to freely react with complementary molecules; the same orientation of the molecules is required in site-directed coupling; the surface density of the attached molecules should be low to allow the chance of single molecule interactions; measured forces between the pairs of molecules should be weaker than forces involved in immobilising the molecules on the tip (Dupres *et al.*, 2007).

Protein attachment to AFM tips can be achieved covalently through chemical modification of the tip using crosslinkers (Hinterdorfer *et al.*, 1996; 1998) or non-covalently by physiosorption of proteins using bovine serum albumin (BSA) (Figure 1.12a). The BSA-coated tip may be adsorbed with streptavidin and then modified with

biotinylated proteins (Florin *et al.*, 1994; Lee *et al.*, 1994). Care should be taken in the former that chemical modification does not affect protein function.

The second approach involves the chemisorption of alkanethiols on gold (Figure 1.12b) (Berquand *et al.*, 2005; Dupres *et al.*, 2005). This type of chemical modification allows for the correct orientation of biomolecules, *e.g.*, the attachment of histidine-tagged proteins onto a gold-coated tip modified with nitrilotriacetate (NTA)-terminated alkanethiols (Kienberger *et al.*, 2000; Dupres *et al.*, 2005). An advantage of this strategy is the optimal exposure of the N- or C-terminal domains, however, the binding strength of the NTA-His bond is low. An alternative approach is the covalent coupling of silanes on silicon oxide method (Figure 1.12c) (Hinterdorfer *et al.*, 1996; 1998), where proteins are coupled to the tip *via* a heterobifunctional crosslinker PEG. The NHS end of the PEG reacts with amines on the silicon tip, yielding a stable amide bond, and the reactive PDP group forms a bond with free thiols presented by cysteines in the protein (stable disulfide bond).

Yoshimura *et al.* (2006) reported a method which allows the covalent coupling of glutathione, *via* a PEG spacer, on to an AFM tip to tether glutathione S-transferase(GST)-fusion proteins. GST-fusion is used for affinity protein purification; GST binds to glutathione with a high efficiency and GST-fusion proteins are purified by glutathione-coupled beads (Kaelin *et al.*, 1992). The three main strategies of covalent attachment based on chemical modifications are shown in Figure 1.12 (Hinterdorfer and Dufrene, 2006).

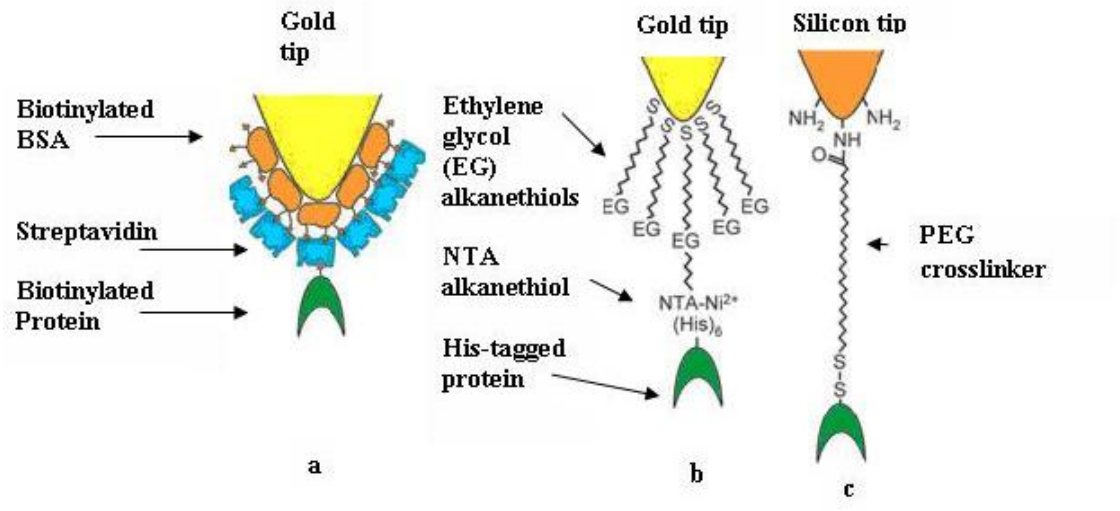

Figure 1.12. Chemical modification of AFM tips for single-molecule recognition studies: (a) physiosorption of proteins (BBSA), (b) chemisorption of alkanethiols on gold, and (c) covalent coupling of PEGs to amino-terminated silicon/silicon nitride (Hinterdorfer and Dufrene, 2006).

1.2.4.2 Crosslinkers

Many biological applications use PEGs as spacers or linkers (Hinterdorfer *et al*., 1996; Kamruzzahan *et al*., 2006). These molecules are commercially available and are synthesised by the nucleophilic attack of a hydroxide ion on an epoxide ring that effects ring-opening polymerisation, to form an ethylene glycol. The PEG spacer is usually in the form of a linear polyether terminated with hydroxyl groups with the general structure: $HO–(CH_2\ CHRO)_n –CH_2CHR–OH$ (Roberts *et al*., 2002).

The availability of a reactive group on the molecule of interest dictates the choice of the PEG linker type. Derivatisation of the end groups and chemical conjugation to biological molecules in their native environment can be obtained by solvation of PEG in organic solvents and aqueous solutions.

In successful coupling strategies using PEG crosslinkers, some important aspects should be considered, such as the structure, molecular weight and the number of PEG chains attached to the protein, localisation of PEG sites present on the molecule and the type of chemistry used for attachment (Roberts *et al.*, 2002). However, stable linkages to the protein may lead to a decrease in activity in the presence of PEG chains or steric crowding at the active site of the molecule.

Heterobifunctional crosslinkers

Heterobifunctional PEG linkers are important for the tethering of proteins to surfaces. Different types of PEG linkers can be used in biosensing, drug targeting, liposomes, viruses and many other studies. This flexible, hydrophilic and biocompatible spacer, with functional groups at either end, can be used for successful linkage. The amino and thiol groups are the most reactive in biomolecules and, therefore, the most commonly used. Desirable groups in PEG linkers are: maleimide, sulphone, and pyridyl disulfide, however many types of heterobifunctional linkers have been reported. Akiyama *et al.* (2000) synthesised heterobifunctional PEGs containing aldehyde and thiol end groups. Various functional groups have been reported: hydroxyl and amino groups (Yokoyama *et al.*, 1992), amino and hydroxyl or methoxy groups (Cammas *et al.*, 1995), formyl and hydroxyl groups (Nagasaki *et al.*, 1995). A variety of PEG lengths are available that allow tailoring of the distance between the two end groups, which is important when coupling reactions could be affected by steric hindrance.

In some force-distance experiments, PEG spacers can be used to prevent close approach of avidin binding sites with biotin, although the binding affinity is still strong (Finn *et al.*, 1984; Lim and Herron, 1992; Marek *et al.*, 1997; Hofmeier *et al.*, 2004). Many

researchers have noticed a significant role in the length of the linker on effectively blocking other binding sites of avidin (Kaasgaard *et al.*, 2001; Noppl-Simon and Needham, 1996).

PEG chemistry for cysteine modifications

N-hydroxysuccinimide (NHS) ester-maleimide heterofunctional crosslinkers, **s**uitable for protein attachment to silicon nitride tips, allow amide coupling to primary amines of chemically modified tips (Figure 1.13). The presence of the maleimide groups (PEG-maleimide (PEG-MAL)) on the other end of the linker gives an opportunity for PEGylation to available cysteine residues of desired protein and formation of a stable thioether bond (Figure 1.13). This site-specific modification allows reaction with thiols even at pH 6 – 7; although, the molecule is not very stable in water, leading to ring opening or addition of water across the double bond (Roberts *et al.*, 2002).

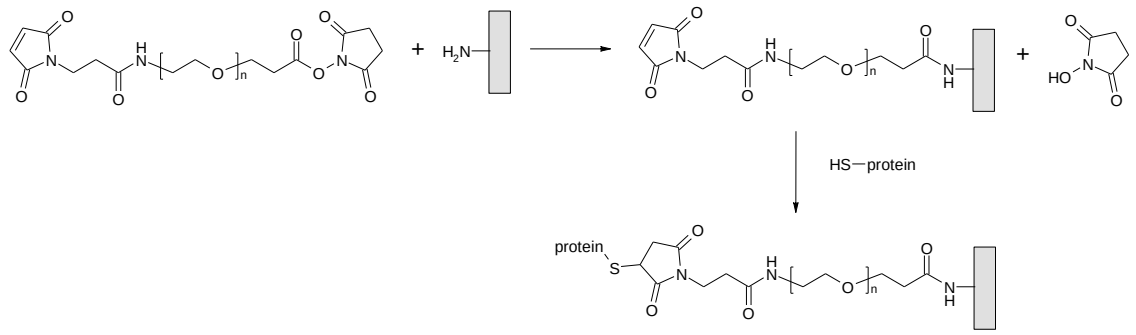

Figure 1.13. A typical protein coupling reaction to an amino terminated surface using a PEG linker molecule (MAL-dPEG$_{12}$-NHS ester; n = 12): NHS ester reacts with surface NH_2 group; maleimide group reacts with pendant thiol group in cysteine.

1.2.5 AFM studies of biomolecules

The AFM is a powerful tool for studying biological molecules at high-resolution, providing access to an incredible wealth of molecular information concerning biological complexes and biological systems (Hansma *et al.*, 1995). Molecular properties can be measured one molecule at a time in single-molecule experiments (Deniz *et al.*, 2007). In life sciences, many experiments are based on specific interactions that include molecular recognition, unbinding forces measurements (muscle protein titin) (Tskhovrebova *et al.*, 1997) and dynamics of the interaction between receptors and ligands (as a model system, the small ligand biotin interacts with the streptavidin or avidin and is a frequently used system) (Florin *et al.*, 1994; Lee *et al.*, 1994, Moy *et al.*, 1994b). Interaction forces between complementary strands of DNA, and a determination of forces needed to break bonds between double stranded DNA can be obtained (Lee *et al.*, 1994).

1.2.5.1 DNA-protein and protein-protein interactions

The use of AFM for high-resolution imaging has allowed observation of the structure of DNA and characterisation of the interactions between DNA and proteins (Hansma *et al.*, 1993).

The studies of processes between individual active proteins in their physiological environment with nanometre resolution is still extremely difficult and challenging (Lal and John, 1994; Hansma, 1995; Thomson *et al.*, 1996). One of the first direct measurements of molecular activity using the AFM was height variations of lysozyme corresponding to its conformational changes during hydrolysis (Radmacher *et al.*, 1994). Measurements and information about stoichiometry and the position of binding

sites of DNA-binding proteins or DNA bending induced by protein binding have been reported by Erie *et al.* (1994) and Wyman *et al.* (1995;1997).

Studies of biological macromolecules with the AFM impose several requirements on the way the sample is prepared and attached to the surface. Water, salt crystals, organic impurities and gases from the atmosphere can easily affect DNA imaging and force measurements and therefore extreme care should be taken, using solutions of the highest possible purity (Muller *et al.*, 1997; Siedlecki and Marchant, 1998; Engel *et al.*, 1999).

AFM imaging of immersed samples requires the presence of divalent or monovalent cations in the buffer, at an optimum concentration to promote adhesion between the specimen and the surface substrate, which for molecular biology applications is usually mica (Heuser, 1989). Mica can be also chemically modified to introduce cationic, anionic or hydrophobic groups to modify the adhesion characteristics (Lyubchenko *et al.*, 1993a).

The potential of AFM for directly visualising and quantitatively measuring in real time, dynamic conformational changes of DNA has been confirmed by characterisation of DNA bending induced by a ligand (MGT-6b), able to bind to DNA molecules with two linked parts: a polyamine (binds to the phosphate backbone) and a tripyrrole peptide (binds to the minor groove) (Hansma *et al.*, 1994). Remodelling activity of DnaD protein, involved in DNA replication, was suggested to be a result of oligomerisation and DNA binding activities of two linked N- and C-terminal domains (Carneiro *et al.*, 2006).

AFM has been used in the physical manipulation of individual strands of DNA where the tip was used as a surgical tool for cutting of DNA strands into pieces, necessary for further manipulation or imaging (Hansma *et al.*, 1992).

Yu *et al.* (2008) visualised alkali (NaOH)-denatured supercoiled plasmid DNA using AFM and compared it with untreated double-stranded super coiled DNA. Alkali-denatured DNA molecules were circular, had short contour lengths and variable diameters with kinks indicating alkali denaturation.

Several AFM methods of stretching DNA molecules on different substrates have been reported, where the strength of the forces needed to simultaneously break several hydrogen bonds have been measured (Li *et al.*, 1998; Ye *et al.*, 2000). In addition, pulling methods using multiple protein repeats, *e.g.*, the muscle protein titin, give knowledge of stability of different domains and behaviour under mechanical stress (Kellermayer *et al.*, 1997; Rief *et al.*, 1997; Tskhovrebova *et al.*, 1997).

1.2.6 Avidin-biotin as a model system

The interaction between avidin and biotin is the strongest known inter-molecular bond between a ligand and a protein (Green, 1975). High binding affinity and availability of the structural and thermodynamic data of the complex are desired for bio-recognition studies (Livnah *et al.*, 1993a). The homotetrameric structure of avidin has 222 point symmetry that provides specific orientation and immobilisation on the surface through binding sites to biotin present on one site of the molecule, leaving free biotin-binding

sites on the opposite side (Hendrickson *et al.*, 1989; Weber *et al.*, 1989; Livnah *et al.*, 1993a).

The glycoprotein avidin was originally isolated from chicken egg white (Heney and Orr, 1981); it is stable over wide pH and temperature ranges and soluble in aqueous solutions (Green *et al.*, 1975). The tetrameric structure of avidin consists of 512 amino acid residues and contains four binding sites for biotin, two each located at opposite sides of the protein (Figure 1.14) (Green *et al.*, 1971; Finn *et al.*, 1980). The four identical subunits of avidin, each of which contains a single biotin-binding site, enabled the study of subunit-subunit interactions. Biotin-avidin has strong binding affinities of 10^{15} M^{-1} for the avidin tetramer and 10^{7} M^{-1} for the monomer (Green, 1975). Different affinities of the single monomers of the tetrameric protein have been confirmed by Kurzban *et al.* (1991) and Eisenberg-Domovich *et al.* (2005).

Figure 1.14. Crystal structure of the avidin tetramer (monomers in magenta, blue, cyan and red) and interaction with four biotin molecules (shown in yellow) (Wilchek *et al.*, 2006).

Biotin may be covalently attached to substrates through the carboxyl group by facile attachment to linker molecules (Figure 1.15) (Wong *et al.*, 1999). PEGylated biotin has been widely used in force spectroscopy experiments, but has a lower affinity for avidin than biotin (Kaiser *et al.*, 1997).

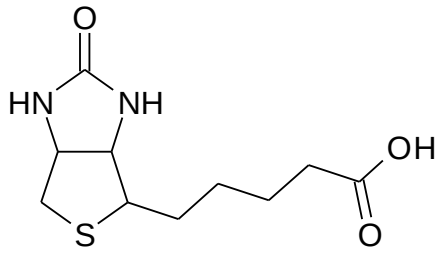

Figure 1.15. Structure of biotin (5-[(3a*S*,4*S*,6a*R*)-2-oxohexahydro-1*H*-thieno[3,4-*d*]imidazol-4-yl]pentanoic acid).

1.2.6.1 Specific interactions acting between receptor-ligand molecules

The attraction between molecules is based on strong or weak interactions. Strong covalent and ionic bonds are able to store chemical energy and have fixed lengths and angles. Interactions contributing to extremely tight binding between biotin and avidin are van der Waals forces, which act between biotin and the binding residues of the proteins (the aromatic side chains), hydrogen bonds between the protein pockets and the ligands, and the rearrangement of L 3,4 loops of the proteins upon biotin binding. The extent of these weak forces is dependent on the pH and ionic strength of the solution (Livnah *et al.*, 1993b; Grubmuller *et al.*, 1996; Freitag *et al.*, 1997).

1.2.6.2 Imaging of avidin

Many different attempts for direct visualisation of the structure, model complex formation and the nature of interaction of proteins with AFM have been reported. Neish *et al.* (2002) observed the presence of four binding pockets in strept(avidin) for biotin by imaging, in air, biotin modified by the addition of the short lengths of DNA to enable visualisation. Respective to orientations of the binding pockets of streptavidin (an avidin homologue), the two angles, acute and obtuse, between DNA-biotin were observed.

Shlyakhtenko *et al.* (2003) confirmed the capability of streptavidin to bind up to four biotinylated DNA molecules, by imaging in liquid following 1-(3-aminopropyl) silatrane (APS) modification of mica for surface attachment of DNA complexed with streptavidin. Most complexes were found to be dimers, however tetramers of streptavidin were also observed.

1.2.6.3 Force spectroscopy of avidin-biotin complex

An understanding of molecular recognition forces, which are usually non-covalent interactions, such as hydrogen-, ionic- or hydrophobic-bonding, is important in the study of biological processes. The goal for recognising an individual antibody-antigen binding event is the detection of the ligand (attached to the AFM probe) binding to the surface coated with antibody (Allen et al., 1997). Dissociation appears at a measurable unbinding force associated with reduction in the lifetime of the complex (Hinterdorfer *et al.*, 1996).

The biotin-avidin complex has been widely studied as a model system in force spectroscopy measurements (Florin *et al.*, 1994; Allen *et al.*, 1996; Dammer *et al.*, 1996; Wong *et al.*, 1999; Yuan *et al.*, 2000; Lo *et al.*, 2001; Kamruzzahan *et al.*, 2006). A full understanding of the high-affinity interactions between avidin and biotin is an extremely useful model to define and understand interactions between different pairs of proteins that will have lower affinity (Weber *et al.*, 1992; Livnah *et al.*, 1993a).

Some models of the interactions between proteins neglect many possibilities that may occur in the system. The tetrameric structure of avidin allows the interactions and binding of more than one biotin, increasing the probability of observing multiple events before a final separation in AFM force-distance measurements. The retract traces of force-distance curves may exhibit several transitions corresponding to multiple interactions (many molecules attached to the tip), where information concerning sequential unbinding of multiple avidin-biotin complexes can be extracted. The evidence in the literature suggests that for the curves showing multiple events, the last event is most probably the breakage of one single bond (Figure 1.16), since only a few connections between molecules remain at that stage. However, this peak may still correspond to rupture of two or more bonds concurrently, especially if the layer of avidin molecules on the apex of the AFM tip is greater than one monolayer thickness (Figure 1.17). Interpretation of these force-distance curves can be very difficult and time consuming and therefore very often only traces showing a single interaction peak are taken into account during the analysis.

The force curves that indicate multiple events can be interpreted as a breakage of different contact points corresponding to antibody/antigen bonds. In addition, the van

der Waals, or electrostatic interactions may give a non-specific background and the non-linear convolution of multiple unbinding processes (Dammer *et al.*, 1996).

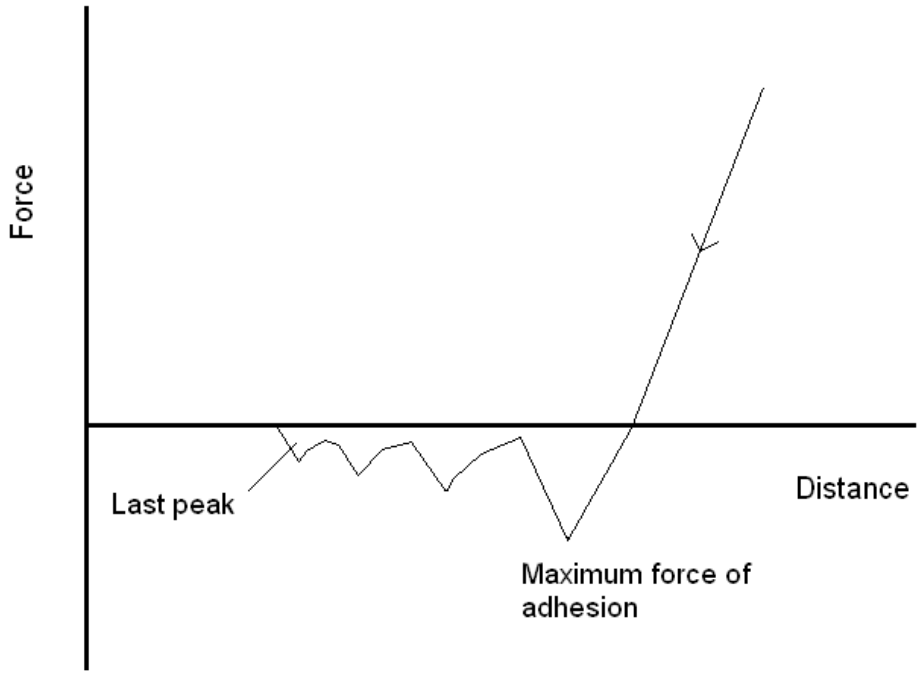

Figure 1.16. Retraction force curve showing maximum adhesion and last adhesion peak.

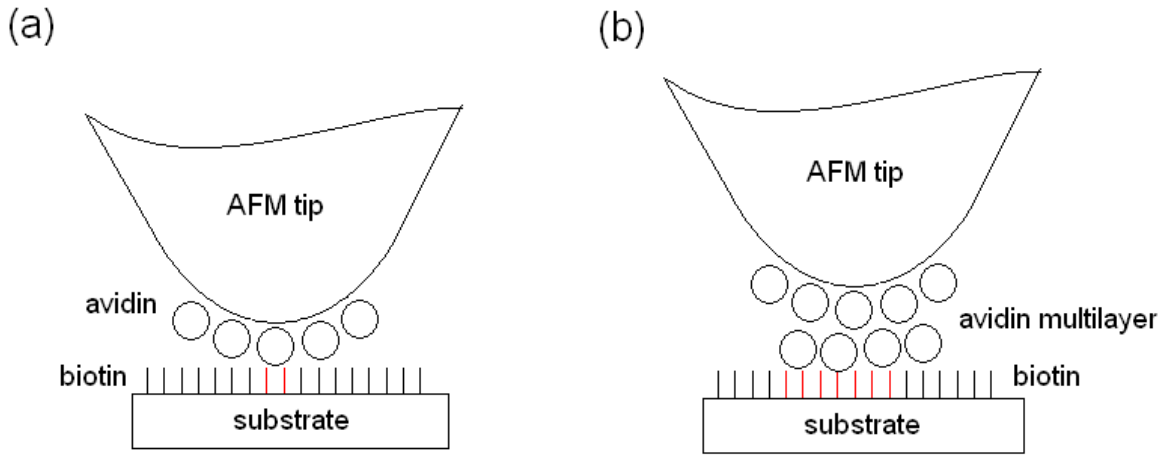

Figure 1.17. Schematic showing (a) single biotin-avidin interaction at the apex of an AFM tip; (b) multiple biotin-avidin interactions due to avidin (or biotin) multilayer; biotin-avidin interactions shown in red.

In experiments where proteins are not covalently attached to surfaces, the detection of single molecule interactions is very difficult, or in some cases not possible. The unbinding force peak presented can be due to simultaneous breakage of a few bonds at the same time, accounting for a wide-range of force reported in the literature (Table 1.5). These values are also dependent on external conditions such as immobilisation method, state and orientation of the complex, buffer, pH and temperature (Moy *et al.*, 1994b).

In some early force distance experiments, agarose beads functionalised with biotin have been used to obtain the forces acting between biotin and cantilevers derivatised with avidin. Florin *et al.* (1994) showed the forces needed to separate the tip and the bead was quantised in integer multiples of 160 ± 20 pN.

Table 1.5. Interaction forces between biotin and (strept)avidin.

Molecular partners	Experimental setup	Specificity control	Average forces / pN	Ref.
Avidin	Biotinylated bovine serum albumin (BSA) adsorbed on tip, with subsequent avidin adsorption; surface is biotinylated	Free avidin, free biotin, free BSA; biotin-coated tips	15000 ± 2000 (number of interacting molecular pairs estimated to be 100	Moy *et al.*, 1994a
Avidin/biotin Streptavidin/ biotin	Biotinylated BSA adsorbed on tip, with subsequent avidin or streptavidin adsorption; ligand (biotin or derivatives) immobilised on surface	Immobilised biotin derivatives; low or high pH	160 – 260	Moy *et al.*, 1994b
Avidin/biotin or derivatives	Biotinylated BSA adsorbed on tip, then incubated with avidin; biotinylated agarose beads as substrate	Free avidin or biotin in medium	160	Florin *et al.*, 1994
Streptavidin/ biotin	Biotinylated BSA adsorbed on glass microspheres (glued to cantilevers) and mica surface; surface further incubated with streptavidin	BBSA surface (no streptavidin); streptavidin surface blocked with biotin	340	Lee *et al.*, 1994a
Streptavidin/ biotin site-directed mutants	Biotinylated BSA adsorbed on tip and mica surface; surface further incubated with wild-type or mutant streptavidin	Free biotin in medium	100 – 450 for mutants	Chilkoti *et al.*, 1995
Antibody (Ab)/ antibiotin	Biotinylated BSA covalently bound to tip *via* linker; Ab covalently bound to surface *via* linker; also reverse configuration	Non-biotinylated BSA on tip; biotin and streptavidin in medium; non-specic Ab on surface; low or high pH	110	Dammer *et al.*, 1996
Streptavidin/ biotin	Biotin covalently bound to nanotube tips; streptavidin linked to surface by biotin groups	Free biotin in medium; unmodified nanotube tips	200	Wong *et al.*, 1999
Streptavidin or avidin/biotin	Biotin covalently attached *via* linkers to glass micro-beads and surfaces; avidin was further adsorbed to both, such that free biotin groups were still available for infrequent bond formation	Linkers terminated in chemical groups inactive in attaching biotin; free biotin	5 – 170, depending on loading rate	Merkel *et al.*, 1999
Avidin/biotin	Biotin covalently attached *via* PEG spacer, avidin adsorbed to the mica	Free biotin	56	Kamruzzaha n *et al.*, 2006
Avidin/biotin	Avidin adsorbed on mica, biotin attachedto an AFM tip *via* PEG linker	Avidin injection into solution	80	Kienberger *et al.*, 2006
Avidin/biotin	Avidin on tip *via* glutaraldehide biotin on glass plate		236	Piramowicz *et al.*, 2006

1.2.7 Determination of molecule dimensions

AFM has also been used for three-dimensional imaging of single proteins under their physiological conditions. Precise measurements of molecular dimensions of the proteins are still very challenging due to their weak attachment to mica (or glass), inherent elasticity of the biological materials and tip convolution effects. Molecular volumes of proteins have been determined by AFM and correlated with molecular weight (Equations 1.2 and 1.3). These provide a method of distinguishing between single and multimeric proteins, which may also correlate with their molecular weights. The assumption is that proteins have a spherical shape, although measurements of diameters at the half maximal height prevent overestimation due to the geometry of the tip (Schneider, 1998).

$$V_m = \left(\frac{\pi h}{6}\right)\left(3r^2 + h^2\right) \qquad \text{(Equation 1.2)}$$

h = the particle height and r = the radius at half-height of the protein.

$$V_c = \left(\frac{M_0}{N_0}\right)\left(V_1 + dV_2\right) \qquad \text{(Equation 1.3)}$$

M_0 = molecular mass of protein, N_0 = Avogadro's number (6.022×10^{23} mol^{-1}), V_1 = the partial specific volume of the protein (0.747 cm^3 g^{-1}), V_2 = the partial specific volume of water (1 cm^3 g^{-1}) and d = the extent of protein hydration (assumed to be 0.4 mol H_2O / mol per protein).

1.3 Aims of this thesis

The motor activity of EcoR124I and its ability to self-assemble provide potential uses of the enzyme to act as a nanoactuator within a biosensor for toxicity, since subunit disassembly has been observed in the presence of hydrophobic compounds.

The main aim of the project was to investigate the forces necessary to hold MTase and HsdR subunits together as a holoenzyme. Dynamic force spectroscopy (DFS) was used to obtain kinetic information on this novel system.

The assembly of proteins on the functionalised mica surfaces was also investigated using AFM imaging (in air and in liquid); molecular volume measurements of deposited proteins were also obtained and analysed.

AFM force curves on biological systems have not previously been extensively performed at Portsmouth and as a consequence it was important to look at the well known model system of avidin-biotin to improve local capability in this area. A clearer insight into the model system was required to enable comparison with a novel GST-HsdR(PrrI)-MTase system.

Chapter 2

Material and Methods

2.1 Bacterial strains

Strain	Genotype	Origin
E. coli JM109(DE3)	*endA*1, *recA*1, *gyr*A96, *thi*-1, *hsdR*17(r_K-, m_K+), *relA*1, *supE*44, Δ(*lac-proAB*), [F', *traD*36, *proAB*, *lac*I^qZΔM15], λ(DE3)	(Yanish-Perron *et al.*, 1985)
BL21(DE3)	F^-, *omp*T, *hsd*S_B(r_B-, m_B-), *dcm*, *gal*, λ(DE3)	(Studier and Moffatt, 1986) (Weiner *et al.*, 1994)

2.2 Plasmids

pGEX-2T	Amp^r, GST-tag, thrombin cleavage site	(Smith and Johnson, 1988)
pGEX(PrrI)	Recombinant plasmid carrying a hybrid *hsdR* gene produced from fusion of the *hsdR* gene of EcoPrrI (first 200 amino acids) and the *hsdR* gene of EcoR124I (amino acids 201 to gene end) inserted into the vector pGEX2T	(Firman, K., personal communication)
pJS4M	Derivative of pUC119 and pET3a over-producing M EcoR124I MTase from T7 promoter	(Patel *et al.*, 1992)

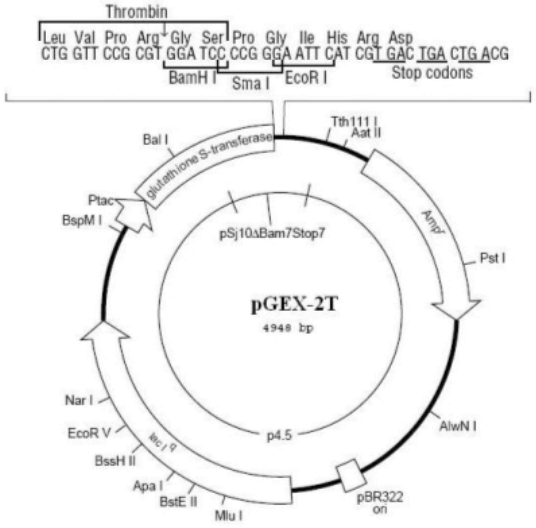

Figure 2.1. Plasmid map of pGEX-2T. Adapted from http://www.pasteur.ac.ir/ researchDepartment/GeneBank/Plasmid.htm. The GST Gene Fusion System, *i.e.*, pGEX-2T, is a versatile system for the expression, purification, and detection of fusion proteins produced in *E. coli*. Expression in *E. coli* yields fusion proteins with the GST moiety at the amino terminus and the protein of interest at the carboxyl terminus.

2.3 Proteins

Protein	**Activity**	**Reference**
M.EcoR124I (MTase)	DNA Methyltransferase composed of HsdM and HsdS subunits in a stoichiometry of M_2S	(Patel *et al.*, 1992)
HsdR(R124)	Restriction subunit	(Zinkevich *et al.*, 1997)
GST-HsdR (PrrI) and HsdR(PrrI)	A hybrid (restriction subunit) protein as detailed above.	(Dutta. C, Weiserova. M, Lisle. W, Firman K, unpublished observation)

2.4 Oligonucleotides

30 mer oligonucleotides were used as an oligoduplex for gel retardation assays. The sequence was: EMSA Fluor-30 bp Fluoro-$^{5'}$ CCG TGC AGA ATT CGA GGT CGA CGG ATC CGG $^{3'}$. The recognition site for EcoR124I is highlighted in red.

2.5 Primers used for PCR

Lambda 2097-(2397sR)-3097 For	$^{5'}$GGC CGC TGC TGG GAT ACT GGC GGG ATT GA$^{3'}$
Lambda 2097-(2397sR)-3097 Rev	$^{5'}$GCG CGC GCC GGA AAA AAG ACC CGA CGA TA $^{3'}$
Biotin-lambda-EcoR124I-5′	biotin CAA CCG AAG AAT GCG ACA CTG AC
Biotin-lambda-EcoR124I-3′	CCC AGC GTT AAC GGT GAT GGT GT
R124 substrate 250 bp central F	$^{5'}$AGC AGA TTT ATA ACC GCT TCA CAC T $^{3'}$
R124 substrate 250 bp central R	$^{5'}$ CTG CCA GCG GGA AAT ACT GAT$^{3'}$

The first two pairs of primers were used to produce 1 kB DNA fragments with the recognition site for EcoR124 placed at 1/3 of the DNA length (Lambda 2097-(2397sR)-3097 For, Rev) and in the centre (Biotin-lambda-EcoR124I). Shorter fragments (250 bp), with the target site placed in the centre, were produced using R124 substrate (250 bp central F and R).

2.6 Culture media

2.6.1 Lennox broth agar

Bactotryptone (10 g), bactoyeast extract (5 g), bactoagar (15 g) and sodium chloride (5 g) were dissolved in water (AnalaR), the pH adjusted to 7.2 (NaOH, 1 M), the solution made up to 1 L and autoclaved immediately.

2.6.2 Lennox broth (LB) media

Bactotryptone (10 g), bactoyeast extract (5 g) and sodium chloride (5 g) were dissolved in water (AnalaR), the pH adjusted to 7.2 (NaOH, 1 M), the solution made up to 1 L and autoclaved immediately.

2.6.3 2× TY buffer

Bactotryptone (16 g), bactoyeast extract (10 g) and sodium chloride (5 g) were dissolved in water (AnalaR), the pH adjusted to 7.2 (NaOH, 1 M), the solution made up to 1 L and autoclaved immediately.

2.7 Standard solutions

2.7.1 Ampicillin stock

Ampicillin (sodium salt) was dissolved in water (AnalaR) to a concentration of 100 mg mL^{-1}, filtered through a 0.2 μm filter and stored at 4 ºC for no more than 1 month.

2.7.2 AMP-pnp stock

Adenosine 5′-(β,γ-imido) triphosphate tetralithium salt hydrate (53 mg), was dissolved in water (AnalaR, 0.8 L) and adjusted to pH 7.0 (NaOH, 0.1 M). The volume was made up to 1 mL with water (AnalaR) to provide a final concentration of 100 mM. The solution was aliquoted into 100 μL volumes and stored at -70 °C.

2.7.3 ATP stock (100 mM)

Adenosine 5′-triphosphate (disodium salt; 60 mg) was dissolved in water (AnalaR; 0.8 mL) and adjusted to pH 7.0 (NaOH, 0.1 M). The volume was made up to 1 mL with

water (AnalaR) to provide a final concentration of 100 mM. The solution was aliquoted into 100 µL volumes and stored at -70 °C.

2.7.4 ATP-γ-S stock (100 mM)

Adenosine 5′-[γ-thio] triphosphate tetralithium salt (54.7 mg), was dissolved in water (AnalaR; 0.8 mL) and adjusted to pH 7.0 (NaOH; 0.1 M). The volume was made up to 1 mL with water (AnalaR) to provide a final concentration of 100 mM. The solution was aliquoted into 100 µL volumes and stored at -70 °C.

2.7.5 Deposition buffer

HEPES buffer (100 mM, pH 7.4; 200 µL) and $MgCl_2$ (100 mM; 50 µL) were diluted in water (AnalaR; 750 µL) to the final concentration of 20 mM HEPES and 5 mM $MgCl_2$. The solution was filtered sterilised through a 0.2 µm filter into 1 mL aliquots.

2.7.6 EDTA (500 mM)

EDTA, dipotassium salt dehydrate (186.12 g) was dissolved in water (AnalaR) and adjusted to pH 8 (NaOH; 1 M). The volume was made up to 1 L using water (AnalaR) and autoclaved.

2.7.7 Isopropylthiogalactoside (IPTG) stock (1 mM)

IPTG (2.38 g) was dissolved in water (AnalaR; 10 mL) and filtered through a 0.2 µm filter. This stock solution was always made immediately before it was required.

2.7.8 10× PBS

NaCl (80 g), KCl (2 g), Na_2HPO_4 (11.5 g) and KH_2PO_4 (2 g) were dissolved in water (AnalaR; 1 L) and autoclaved.

2.7.9 Sodium hydroxide (10 M)

Sodium hydroxide (NaOH; 40 g; Sigma-Aldrich) was dissolved in water (AnalaR; 80 mL). The volume was made up to 100 mL with water (AnalaR).

2.7.10 TAE buffer (50×)

Tris base (242 g), glacial acetic acid (57.1 mL) and EDTA (18.6 g) was made up to 1 L with water (AnalaR). The solution was then filtered sterilised through a 0.2 µm filter and stored at room temperature until required.

2.7.11 Tris.HCl (1 M)

Tris (hydroxymethyl)aminomethanne.HCl (Tris.HCl; 60.57 g; Sigma-Aldrich) was dissolved in water (AnalaR; 480 mL) and adjusted to the required pH with concentrated hydrochloric acid. The volume was made up to 500 mL with water (AnalaR) and autoclaved.

2.7.12 Dilution buffer for proteins

NaCl (5 M; 0.6 mL), Tris.HCl (1 M; pH 8; 0.1 mL), EDTA (0.5 M; 20 µL) and glycerol (5 mL) were mixed together, made up to 10 mL using water (AnalaR) and filtered sterilised (0.2 µm). The final concentration of the solution was NaCl (300 mM), Tris.HCl pH 8 (10 mM), EDTA (1 mM), glycerol (50 %).

2.7.13 Disruption buffer (10×)

Disruption buffer was made from Tris.HCl buffer (0.5 M; pH 6.8; 1.2 mL), glycerol (1 mL), SDS (10 %; 2 mL), bromophenol blue (0.1 %; 0.5 mL) and water (4.8 mL) to the final volume of 9.5 mL. 2-Mercaptoethanol (50 µL) was mixed with the aliquots of stock solution (450 µL) before use. For non-denaturing gels, addition of SDS and 2-mercaptoethanol was omitted in preparation of disruption buffer.

2.8 Microbial techniques

2.8.1 Preparation of competent cells

JM109(DE3) or BL21(DE3) cells were grown overnight in L-Broth media, supplemented with ampicillin (100 µg mL^{-1}). The overnight culture (1 mL) was added to LB medium (100 ml; 250 mL flask), shaken at 37°C until an OD_{600} of 0.5 was reached. Cells were cooled on ice, collected by centrifugation and resuspended in TFB1 buffer (RbCl, 100 mM; RbCl, $MnCl_2$, 50 mM; potassium acetate, 30 mM; $CaCl_2$, 10 mM; pH 5.8), kept on ice for a further 90 min. After collection by centrifugation, cells were resuspended in TFB2 buffer (MOPS, 10 mM; RbCl, 10 mM; $CaCl_2$, 75 mM; glycerol, 15 %; pH 6.8)**.** The competent cells were stored at -70 °C after being frozen in liquid nitrogen.

2.8.2 Transformation of competent cells

An aliquot (200 µL) of competent cells (stored as above), but thawed slowly on ice, was added to 1 µL of the required plasmid DNA in a sterile Eppendorf tube and the mixture was left on ice for 20 min. A 90 s heat shock at 42 °C was applied to the cells followed by incubation with LB-broth (90 min at 37 °C). An aliquot (100 µL) of transformed

cells was spread on an LB agar plate containing ampicillin (100 µg mL^{-1}) and incubated over night at 37 °C.

2.9 Protein techniques

2.9.1 SDS PAGE gel preparation and electrophoresis

SDS-PAGE protein gels were made with stacking and resolving gel. The resolving gel was composed of Tris.HCl (375 mM; pH 8.0), acrylamide solution (10 %) and SDS (0.1 %). The stacking gel was composed of Tris.HCl (125 mM; pH 6.8), acrylamide solution (6 %) and SDS (0.1 %). The addition of APS (10 %) and TEMED (8 µL) started the reaction of polymerisation. Samples were diluted in disruption buffer (Section 2.7.13) and boiled for 2 min before loading (Laemmli, 1970). Electrophoresis was carried out at 120 V after loading of the samples onto the gel, until the bromophenol blue dye front had reached the bottom of the gel. The gel was then submerged in a stain solution (Section 2.8.3) containing Coomassue brilliant blue dye for 1 h before being washed and submerged in destain solution. Gels were visualised by transillumination.

2.9.2 Stock SDS running buffer (10×)

Glycine (144 g), Tris base (30 g) and SDS (10 g) were dissolved in distilled water and adjusted to pH 8.3 using concentrated HCl. The volume was made up to 1 L with distilled water. Running buffer for non-denaturated PAGE was made up in the same manner, with the exclusion of SDS.

2.9.3 Staining solution for PAGE gels

Coomassie brilliant blue (2.5 g) was dissolved in methanol (400 mL) and glacial acetic acid (70 mL). The volume was then adjusted to 1 L with distilled water.

2.9.4 Destain solution for PAGE gels

Destain solution was prepared by mixing methanol (400 mL) and acetic acid 70 mL with distilled water (530 mL).

2.9.5 5× SDS loading buffer

SDS loading buffer was prepared by mixing 1M Tris.HCl (0.5 mL; pH 6.8), SDS (20 %; 0.8 mL), glycerol (1.6 mL), bromophenol blue (1 %; 0.2 mL), β- mercaptoethanol (0.4 mL) with distilled water (4.5 mL).

2.9.6 Protein markers

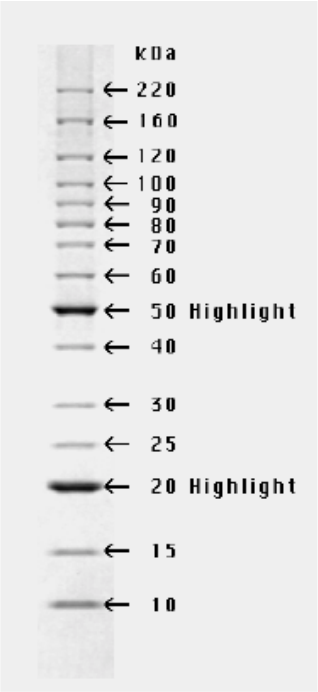

Figure 2.2. Invitrogen Bench Mark ™ Protein Ladder.

2.9.7 Protein production test

The ability of the cells to overproduce HsdR and MTase was determined after successful transformation. L-broth (3 mL) plus ampicillin was inoculated with a colony of the required recombinant. This was grown overnight at 37 ºC with shaking. The overnight cultures were sub-cultured by the addition of culture (200 µL) into aliquots (10 mL) of fresh medium plus antibiotics in universal bottles (30 mL). The cells were grown for 2 – 3 h at 37 ºC with shaking. If required, they were induced with IPTG (1 mM) to promote over-expression of HsdR. Induced and non-induced cells were then incubated at 24 ^{o}C for 2 h, after which they were centrifuged to obtain a pellet and re-suspended in 5× SDS loading buffer (50 µL) (Section 2.9.5). The samples were heated to 100 ^{o}C for 5 min, using a heat-block, to denature the proteins and then loaded onto an SDS gel (10 %) alongside a marker (benchmark protein ladder – Invitrogen). The gel was run at 40 mA (constant) until the dye reached the bottom of the gel. The gel was stained by immersion in Coomassie brilliant blue (Section 2.9.3) at 65 ^{o}C for 30 min and destained using destain solution (Section 2.9.4) at room temperature on a rocker.

2.9.8 Protein production (large scale)

Overnight cultures of *E. coli* containing the appropriate recombinant plasmid (2× YT medium, ampicillin, grown from a freshly transformed single colony) were transferred into fresh 2× YT medium (1 L) supplemented with ampicillin (100 µg mL^{-1}) and incubated at 37 °C for 4 h (Optical density 0.6 – 1 at λ = 600 nm). Cultures were induced with IPTG (1 M) and grown overnight at 24 °C. The cells were harvested by centrifugation and stored as a cell paste at -20 °C.

2.9.9 Purification of HsdR(PrrI)

HsdR(PrrI) was overproduced in *E. coli* BL21(DE3) from plasmid pGEX-2T HsdR(PrrI). Singles colonies of the pGEX-2T HsdR(PrrI) clone transformed into the bacterial strain were used to inoculate LB media (10 mL) containing ampicillin (150 mg mL^{-1}) grown overnight at 37 °C. The cultures were then used to inoculate 2× YT Broth (500 mL) and grown at 37 °C until mid-log. The addition of IPTG (1 mM) was used to induce protein production and cultures were grown overnight at 24 °C with shaking at 200 rpm. The cells were harvested by centrifugation at 3000 g for 30 min at 4 °C. The pellet of cells was re-suspended in sonication buffer (50 mL) (1× PBS; DTT (1 mM); PMSF (0.1 mM); benzamidine (1 mM) and 1 non-EDTA protease tablet) and sonicated for a total time of 10 min at a 40 % amplitude in bursts of 3 s with a recovery time of 9 s off. The sonicate was centrifuged at 3,500 g for 30 min (to remove any remaining cell debris), followed by centrifugation at 200,000 g for 2 h. The supernatant was directly loaded on to a pre-equilibrated GSTrap™ glutathione column (GE Healthcare, Amersham, UK). The sample was exchanged into Buffer A (10 mM Tris.HCl; pH 8.0; NaCl (0.2 M); EDTA (1 mM); DTT (1 mM) on column. After washing, the elution buffer (Tris.HCl (10 mM; pH 8.0), NaCl (0.2 M), EDTA (1 mM), DTT (1 mM) and glutathione (10 mM)) was used to remove the proteins from the column. Fractions containing pure GST-HsdR(PrrI) were pooled, made to 50% glycerol and stored at -20 ºC to prevent degradation.

A column trace of purified GST-HsdR(PrrI) (Figure 2.3) showed the locations at which the eluent absorbed UV light and defined peaks at fractions 28, 29, 30 were analysed on SDS PAGE gel (Figure 2.4a). The concentration of protein was obtained by the

Nanodrop ND-1000 (Lab-Tech International, Ringer, East Sussex, UK) method by measuring the absorbance at 280 nm.

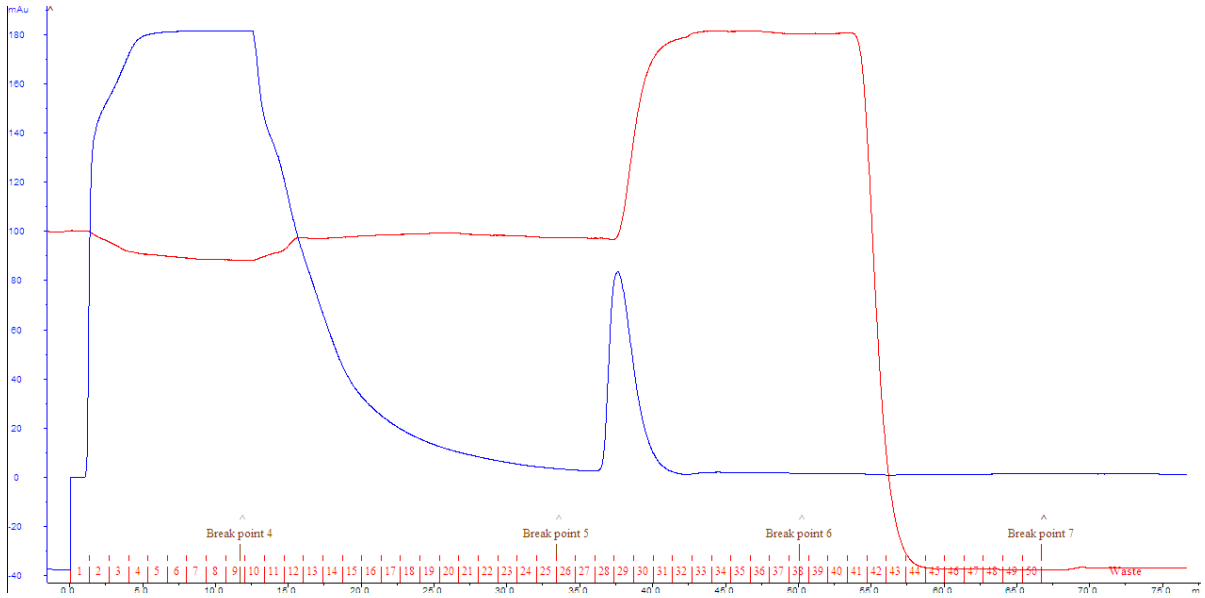

Figure 2.3. Column profile for GST-HsdR (PrrI) from an ÄKTA prime FPLC system. Column trace produced from affinity GSTrap FF column using AKTA-Prime, 4 ml fractions were collected at a flow rate of 5 ml min^{-1}. The blue line represents the UV absorbance of the eluent at the injected fractions, whilst the red line represents the NaCl concentration.

2.9.10 On column cleavage

GST-HsdR(PrrI) was cleaved from the GST by addition of cleavage buffer (5 mL: Tris.HCl (50 mM; pH 8.0), NaCl (50 mM), EDTA (1 mM) and thrombin (3 U ml^{-1}), incubated overnight at 24 °C; fractions were collected and analysed by gel electrophoresis. GST (26 kDa) obtained after cleavage from the column is shown in Figure 3.4b.

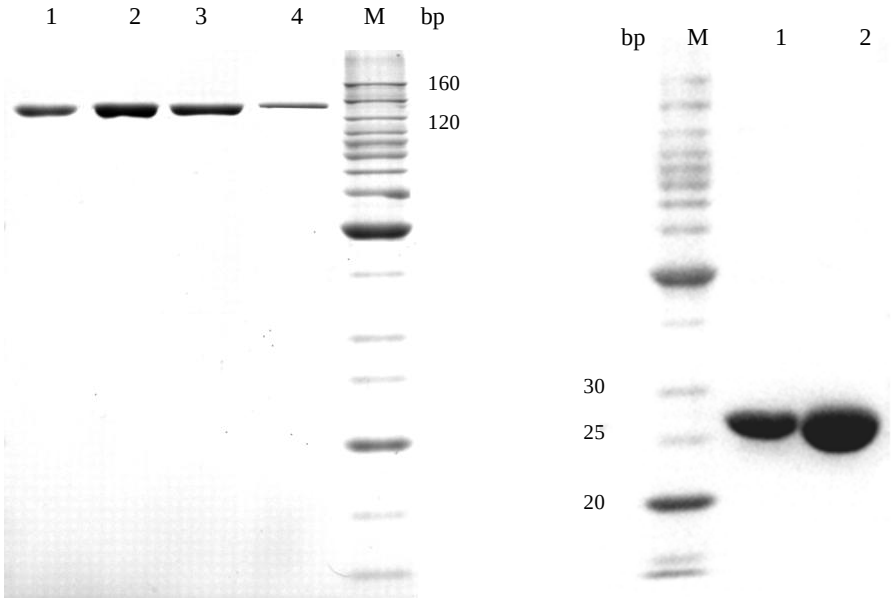

(a) (b)

Figure 2.4 SDS-PAGE of purified GST-HsdR (PrrI) (a) and (b) GST obtained from the cleavage on the column (Section 2.8.8): (a) Fractions of purified GST-HsdR (PrrI) were run on an SDS-PAGE gel and stained with coomassie blue stain (lines 1-4), M: Invitrogen Bench Mark^{TM} Protein ladder; (b) GST sample obtained from the cleavage on the column (lines 1,2), M: Invitrogen Bench Mark^{TM} Protein ladder.

2.9.11 Determination of protein concentration

Samples indicating the presence of proteins were chosen based on the UV wavelength scan using the Nanodrop ND-1000 and the absorbance determined at a wavelength of 280 nm. The amino acid sequence of the proteins as deposited in the Rebase online database was used and the molecular weight was determined (Prot-Param) as was the molar extinction co-efficient (E_M). The E_M was calculated by the number of Y, W and C residues in the protein, multiplied by their individual E_M. Protein concentration in mg mL^{-1} was determined using these data and the sample volume.

2.9.12 Purification of MTase

MTase from the EcoR124I system was overproduced in JM109(DE3) from the plasmid pJS4M (Patel *et al.,* 1992) following 16 h growth. Cells were then harvested by centrifugation at 3,500 g for 30 min. The cell pellet was re-suspended in sonication

buffer (Tris.HCl (50 mM; pH 8.0), glucose (20 %), DTT (3 mM), EDTA (5 mM), PMSF (0.1 mM) and benzamidine (1mM)), and sonicated for a total time of 10 min at a 40 % amplitude in bursts of 9 s with a recovery time of 9 s off. The sonicate was centrifuged at 3,500 g for 30 min followed by centrifugation at 200,000 g for 2 h. The supernatant produced was then made to NaCl (500 mM) and protamine sulphate (10 mg mL^{-1}), gently mixed for 30 min at 4 ºC and the DNA pelleted by centrifugation at 27,000 g for 30 min. The supernatant was subjected to a 70% ammonium sulphate fractionation followed by centrifugation at 12,000g for 30 mins. The MTase was purified by a chromatography method (Taylor *et al.*, 1992). The pellets were re-suspended in buffer A (Tris.HCl (50 mM; pH 8.0), NaCl (50 mM) and EDTA (1 mM)) and desalted using a pre-equilibrated HiTrap™ desalting columns (GE Healthcare) (10 mL total column volume). The desalted fractions were then directly loaded on to a pre-equilibrated HiTrap™ DEAE columns (GE Healthcare) (10 mL total column volume) and eluted over a 100 mL gradient of NaCl (50 mM to 500 mM) using Buffer B (Tris.HCl (50 mM; pH 8.0), NaCl (1 M) and EDTA (1 mM)). Fractions containing MTase were pooled and desalted into Buffer C (Tris.HCl (50 mM; pH 8.0), NaCl (100 mM) and EDTA (1 mM)) as previously described. The desalted fractions were pooled and loaded onto a pre-equilibrated HiTrap™ heparin column (GE Healthcare) and protein eluted using a 100 mL gradient of 100 mM to 1 M NaCl using buffer B. The column profile obtained from the last step of purification has been shown in (Figure 2.5). Fractions containing pure MTase were pooled, as shown in Figure 2.6. The concentration of protein was obtained by the Nano drop method by measuring absorbance at 280 nm, made to 50% glycerol and stored at -20 ºC until required.

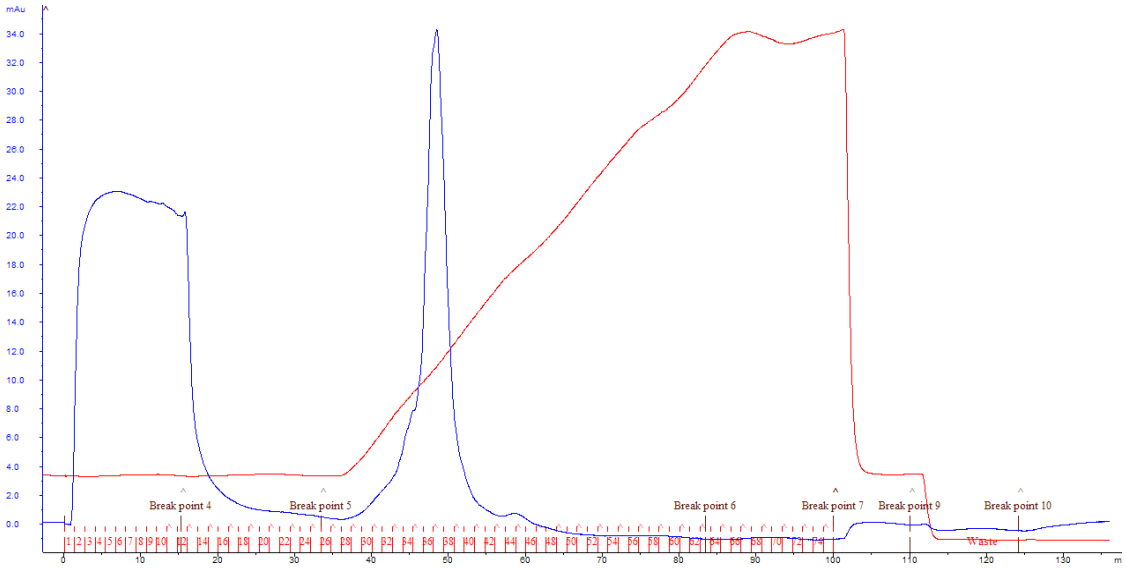

Figure 2.5. Heparin chromatography elution profile of MTase. Proteins were eluted using a 100 mL gradient of NaCl (100 mM to 1 M) (sharp, blue peak). The blue line represents the UV absorbance of the eluent at the injected fractions; red line represents the NaCl concentration.

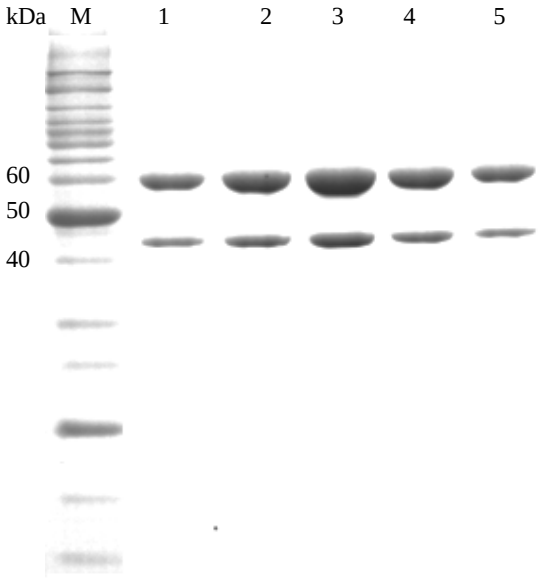

Figure 2.6. SDS-PAGE of purified MTase. Fractions of purified MTase: Lines 1-5 represent an example of purified MTase, two bands, characteristic for HsdS (46 kDa) and HsdM (58 kDa) subunits have been observed, marker (M) - Invitrogen Bench Mark^{TM} Protein ladder.

The MTase, GST-HsdR(PrrI), HsdR(PrrI) and HsdR(R124I) proteins (Figure 2.7) were used in AFM studies (Figure 2.7).

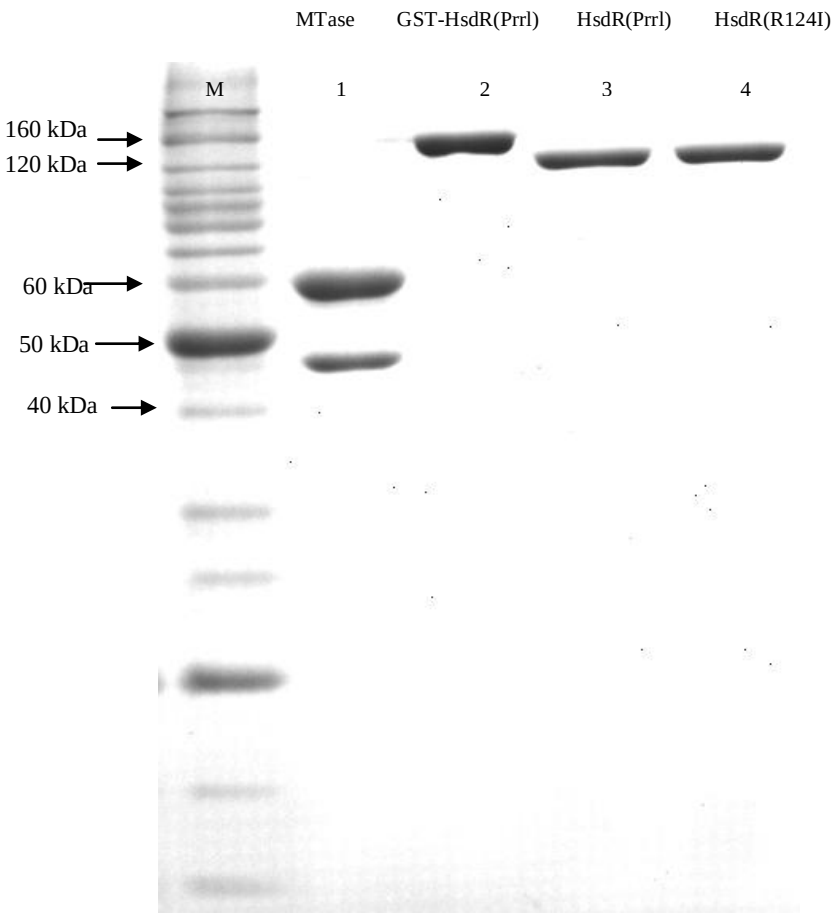

Figure 2.7. SDS-PAGE gel of purified MTase and HsdR subunits. Marker (M) - Invitrogen Bench Mark™ Protein ladder, line 1 represent MTase, line 2: GST-HsdR(PrrI), line 3: HsdR(PrrI) (after cleavage from GST), line 4: HsdR(R124I). The GST-HsdR(PrrI) (146 kDa) was found to be the biggest from all HsdR subunits as expected due to the presence of GST (26 kDa). Cleavage of GST resulting the same size (120 kDa) of HsdR(PrrI) and HsdR(R124I).

2.9.13 Electrophoretic Mobility Shift Assay

The enzyme activity in DNA-protein interaction *in vitro* was investigated using the EMSA method. DNA-protein complexes migrate more slowly than free fluor-labelled DNA (Garner and Revzin, 1981; Fried and Crothers, 1981). MTase and HsdR proteins

were diluted in dilution buffer (Section 2.7.12). The complex was formed following a10 min incubation at room temperature before the addition of a fluor-labelled oligoduplex; this was allowed to bind to the DNA for 10 min. The samples were loaded onto a 6 % Native Gel (40 % Acrylamide / Bisacrylamide (AA / BAA) (19:1), (1.5 mL), 50× TAE (0.2 mL), DTT (1 M; 30 µL), APS (10 %; 10 µL), dH_20 (8.27 mL) pre-run for 1 h (100 V; 4 ºC). The EMSA was run at 100 V / 4 ºC until the marker had migrated 2/3 of the gel. DNA-protein complexes were imaged using Fujifilm FLA-5000 phosporimager (laser at λ473 nm at 550 V and a green filter λ575 nm). The picture was analysed in Image Gauge V 4.0 on an Apple Macintosh.

Electrophoretic Mobility Shift Assay confirmed the formation of both R_1- and R_2-complexes, MTase and unbound 30bp florescein-labelled DNA (with EcoR124I central binding site) (Figure 2.8).

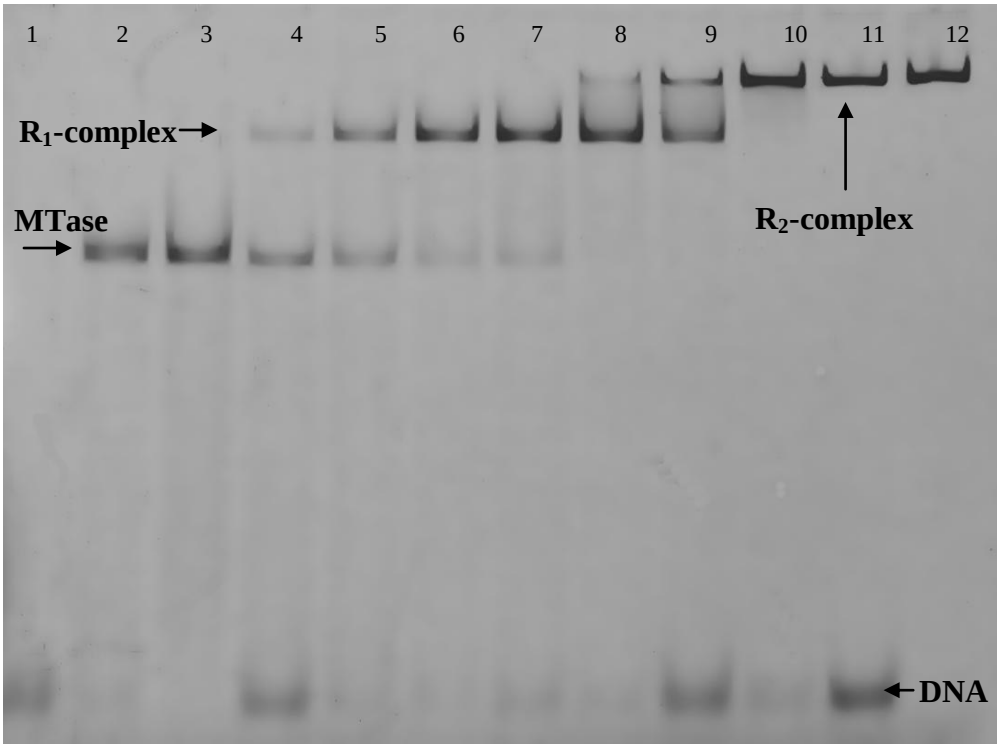

Figure 2.8. Electrophoretic Mobility Shift Assay for EcoR124I(PrrI). MTase (100 nM) was titrated with increasing amounts of HsdR(PrrI) (20 nM – 700 nM) to produce first R_1-complex and then R_2-complex (from left to right). Complexes were incubated with fluorescein-labelled 30 bp oligoduplex. Samples were run on a 6 % native polyacrylamide gel at 100 V at 4 °C. The location of free DNA, MTase; R_1- and R_2-complex is shown with arrows. The DNA-MTase complex was observed until the molar ratio of MTase:HsdR(PrrI) reached 1:1 (Line 7). The R_1-complex appeared (Line 4) at the ratio of 1MTAse (100 nM): 0.2 HsdR(PrrI) (20 nM). The full shift to R_2-complex was observed for ratios higher than 1 MTase: 3 HsdR(PrrI).

Line	Sample
1	100 nM DNA
2	100 nM DNA, 100 nM MTase
3	100 nM DNA, 200 nM MTase
4	100 nM DNA, 100nM MTase, 20 nM hsdR
5	100 nM DNA, 100nM MTase, 60 nM hsdR
6	100 nM DNA, 100nM MTase, 80 nM hsdR
7	100 nM DNA, 100nM MTase, 100 nM hsdR
8	100 nM DNA, 100nM MTase, 150 nM hsdR
9	100 nM DNA, 100nM MTase, 200 nM hsdR
10	100 nM DNA, 100nM MTase, 300 nM hsdR
11	100 nM DNA, 100nM MTase, 500 nM hsdR
12	100 nM DNA, 100nM MTase, 700 nM hsdR

2.10 DNA techniques

2.10.1 Preparation of agarose gels

50× TAE buffer (2 mL) was diluted with water (AnalaR; 100 mL) and added to agarose (1 g). The agarose percentage used was dependent on the size range of DNA/RNA fragments to be resolved (Maniatis *et al*., 1982). The mixture was boiled in a microwave and cooled in a water bath (65 °C); ethidium bromide solution was added to a final concentration of 0.5 μg mL^{-1}. Gels were then poured into plates with the combs inserted and allowed to set at room temperature, after which the combs were removed. A 1× TAE containing ethidium bromide solution (0.5 μg mL^{-1}) was then poured into the gel tank, so as to cover the gel and the wells. DNA fragments were separated based on size and then visualised using a transilluminator (G: BOX Syngene) and depending upon the size of the DNA fragment, the sizes were estimated by comparison with the DNA ladder.

2.10.2 Electrophoresis

Gels were run horizontally at 40 V for 15 min and then increased to 100 V until full separation occurred, using the marker to compare DNA fragment size. The gels were visualised *via* UV transillumination (Alpha Invotec Corp), which was able to detect the fluorescence of the ethidium bromide that had intercalated with the DNA.

2.10.3 DNA ladders

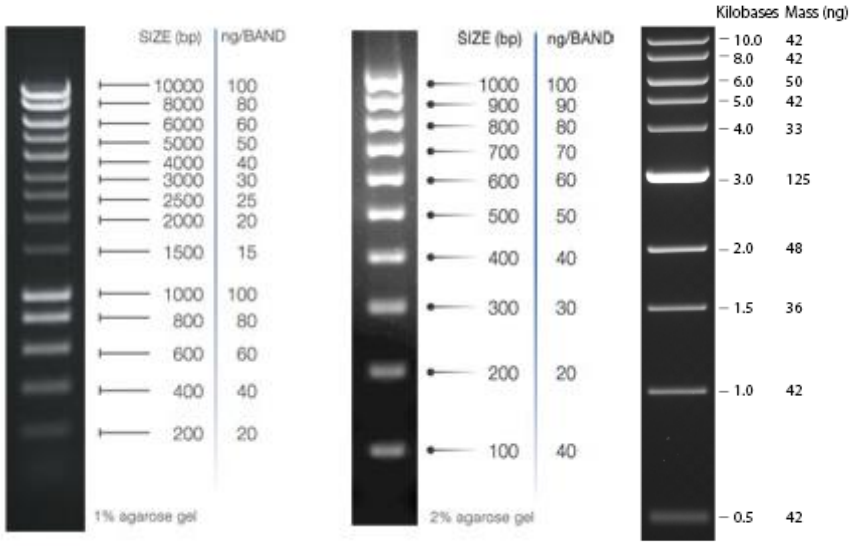

(a) (b) (c)

Figure 2.9. (a) Bioline hyperladder I; (b) hyperladder IV DNA ladder; and (c) 1k ladder NEB.

2.10.4 DNA sample preparation

Samples (total volume 10 µL) were prepared in water with the addition of DNA loading buffer (60% v/v glycerol; 100 mM EDTA; pH 8; 1% w/v bromophenol blue and 1% xylene cyanol) and a total of ~5 ng DNA loaded per lane of gel.

2.10.5 Miniprep plasmid isolation

From the incubated plates containing freshly transformed bacteria, a colony was picked from the plate using a sterile inoculating loop and placed into L-broth (3 mL) with antibiotic (ampicillin, 150 mg mL^{-1}; 3 µL) and grown at 37 ºC overnight with vigorous shaking. An aliquot (1.5 mL) was taken, pelleted and re-suspended in lysis buffer (glucose (50 mM), Tris-HCl (25 mM; pH 8), EDTA (10 mM) and lysozyme (4 mg mL^{-1}; 200 µL)) and incubated at room temperature for 5 min. To the sample mixture of NaOH/SDS (NaOH (0.2 M); SDS (1 %)) was added (400 µL) after which the sample was stored on ice for 5 min. Ammonium acetate (7.5 M; 300 µL) was added to neutralise the alkali and incubated on ice for 10 min to allow high molecular weight RNA, protein and chromosomal DNA to precipitate. Samples were incubated for 10 min on ice then centrifuged (10,000 rpm for 5 min) to remove cell debris. The supernatant was retained and transferred into a new tube. Isopropanol (0.6 volumes; 500 µL) was added and the sample was incubated at room temperature for 10 min. After further centrifugation (15,000 rpm for 10 min), the supernatant was removed by aspiration. The plasmid DNA was washed with ethanol (70 %; 1 mL) and spun for 4 min. The supernatant was again removed by aspiration and the tubes dried by inversion at room temperature for 15 min. DNA pellets were dissolved in TE (100 µL), containing 1:100 stock RNase A (20 mg mL^{-1}) and incubated on ice for 15 min. Aliquots (10 µL: sample (8 µL) and 5× DNA loading dye (2 µL)) were run on a 0.8 % agarose gel alongside a size marker (Figure 2.10).

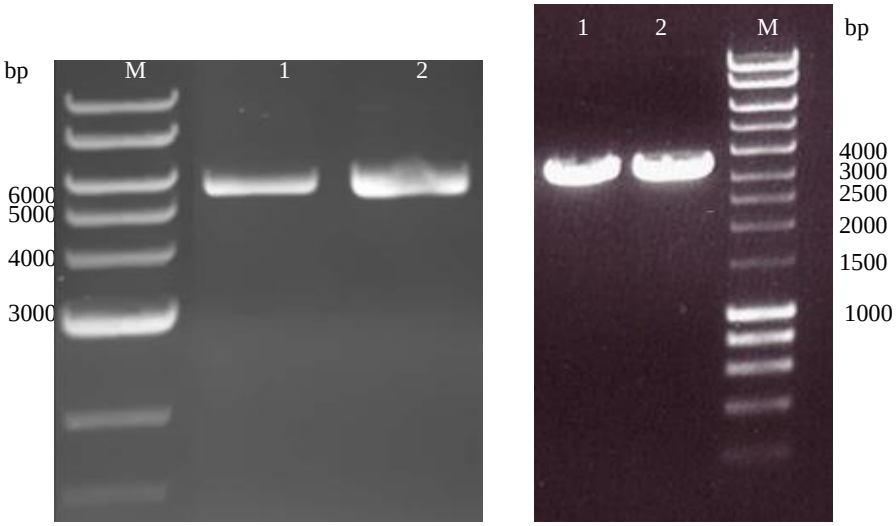

Figure 2.10. Miniprep plasmid isolation. 0.8% Agarose gels loaded with samples (10 µL: 5× loading dye (2 µL) and miniprep sample (8 µL)) obtained from the miniprep procedure: (a) lines 1,2 represent BL21(DE3) transformed with pGEX-2T taken from miniprep, M (1 kB ladder – NEB); (b) lines 1,2: samples of JM109(DE3) + pJS4M from miniprep M (Hyperladder I-Bioline).

2.10.6 Miniscale preparation of plasmid DNA using Quiagen miniprep kit

Mini scale plasmid preparation was carried out using *E. coli* JM109 (DE3) with the Qiaprep spin miniprep kit detailed in the Quiagen manual.

2.10.7 PCR of lambda DNA

All PCR reactions were carried out using a Stratogene Robocycler in thin walled, dome capped PCR tubes in 50 µL volumes. Accuzyme mix (25 µL), the template (25 ng μL^{-1}) and forward and reverse primers (10 µM; 2 µL) were added to the PCR tube. The DNA was amplified by initial melting step at 94 ºC for 5 min and a final extension step of 68 ºC for 5 min, 40 steps of thermal cycling of melting (94 ºC for 1 min), annealing (60 ºC for 30 s) and 68 ºC for 1min (elongation).

For imaging of EcoR124I-DNA complexes and for length measurements, DNA (1 kB) fragments with a single recognition site for EcoR124I at 300 bp and in the centre were produced by PCR (Figure 2.11a); a smaller DNA fragment (250 bp) was also produced by PCR with the same recognition site at the centre (Figure 2.11b).

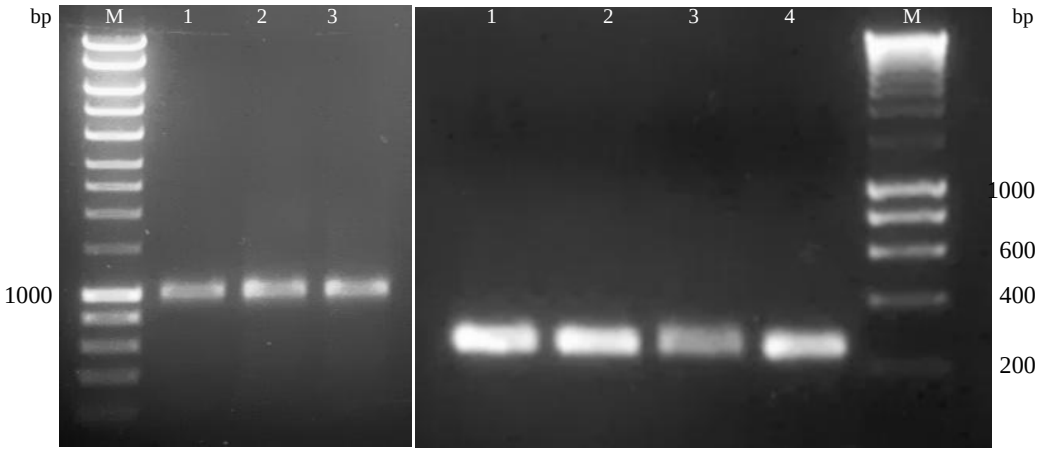

(a) (b)

Figure 2.11. PCR products on an agarose gel: (a) 1 % agarose gel of 1000 bp products; M (marker) Hyperladder I (Bioline), lines 1-3 represent aliquots (5 µL) of the 50 µL PCR reaction; (b) 2 % agarose gel represent 250 bp PCR products; M Hyperladder I (Bioline), lines 1-4 show 5 µL aliquots.

2.10.8 Phenol chloroform extraction of DNA

An equal volume of buffer-saturated phenol:chloroform (1:1) was added to the DNA solution and thoroughly mixed (vortexed; 10 s) and then spun (microcentrifuge; 3 min). The organic and aqueous layers were separated by centrifugation (13,000 rpm; 10 min) and the supernatant carefully removed. These steps were repeated until an interface was not longer visible. An equal volume of chloroform was added to the aqueous layer, spun for 3 min and the aqueous layer was transferred to a new tube.

2.10.9 Ethanol precipitation

The DNA sample was adjusted to high salt by addition of 1/10 volume sodium acetate, to the final concentration of 0.3M and 2.5 volumes of cold ethanol (100 %) added. Samples were incubated at -20 ºC overnight and the precipitated DNA was collected by centrifugation (13,000 rpm in a microcentrifuge; 10 min). The supernatant was decanted, ethanol (70 %; 1 mL) was added and the pellet collected by centrifugation. The supernatant was carefully decanted, the pellet was air dried and re-suspended in filter sterile water. DNA was quantified by Nanodrop and stored at -20 ºC.

2.11 Atomic force microscopy experiments

AFM studies were carried out using a MultiMode/NanoScope IV Scanning Probe Microscope (Digital Instruments, Santa Barbara, CA, USA) using the J-scanner (max. xy = 200 µm). AFM imaging was performed in air (T = 22 °C; RH = 21 %) and in liquid (PBS buffer, pH 7.4 and ultrapure water H_2O; T = 22 °C) in TappingMode® using silicon/silicon nitride cantilevers with integrated tips (air: t = 1.7 – 2.3 µm, l = 130 ± 5 µm, w = 35 ± 5 µm, ν_0 = 115 – 190 kHz , k = 2.5 – 10 N m^{-1}, R ~ 10 nm; RMS amplitude = 0.8 V; Model: NSG01, NT-MDT, Russia; liquid: t = 0.55 – 0.66 µm, l = 120 – 125 µm, w = 20 – 25 µm, ν_0 = 56 – 75 kHz, k = 0.32 N m^{-1}, R = 2 – 3 nm; Model: SNL-10; Digital Instruments, Veeco Metrology Group, Santa Barbara, CA, USA).

Images were obtained at a scan rate of 1 – 2 Hz and the set-point adjusted to minimise tip-sample interactions. Images, recorded in topography mode with pixel size of 512 × 512, were subsequently processed using NanoScope software (V 6.11r1, Digital Instruments, Santa Barbara, CA, USA).

The Millipore Simplicity purification system (18.2 MΩ cm at 25 °C; ultrapure water) was used to obtain the water for all experiments. All buffers were filtered through a 0.2 µm pore size filter (Ministart-plus, Sartorius Stedim, Biotech, Germany) prior to use.

2.11.1 Imaging in air

2.11.1.1 Mica pre-treatment with PLL

Freshly cleaved muscovite mica (Agar Scientific, Stansted, Essex, UK), mounted on a nickel disc (dia. 1 cm^2), was placed on the AFM scanner using with double-sided adhesive tape. Images of mica (5 and 10 µm) were obtained as a control prior to protein immobilisation. Poly-L-lysine (PLL) (6 µL, 0.01 %, MW 70 000 – 150 000 g mol^{-1}; Sigma-Alrich, Poole, UK), used for protein immobilisation, was placed directly on the freshly cleaved mica and incubated for 2 min; this surface was then washed with pure water (2 mL) and dried with in a stream of N_2.

2.11.1.2 Visualisation of DNA on mica in the presence of different cations

DNA stock was diluted to the final concentration of 10 nM with HEPES buffer (20 mM; pH 7.4 containing $MgCl_2$ (5 mM), $CaCl_2$ (10 mM) or $NiCl_2$ (1 mM)). Mica was freshly cleaved and an aliquot of the sample (5 µL) was deposited on the surface and incubated at room temperature for 2 min; this was then washed with water (1 mL) and gently dried with a stream of N_2.

2.11.1.3 Imaging of MTase and HsdR

MTase or HsdR stocks were diluted to a final concentration of 10 nM with HEPES buffer (20 mM; pH 7.4) containing $MgCl_2$ (5 mM). An aliquot of the sample (5 µL) was

deposited on the PLL pre-treated mica surface (Section 2.10.1.1) and incubated at room temperature for 2 min, washed with water (1 mL) and gently dried in a stream of N_2.

2.11.1.4 Immobilisation of MTase-DNA

DNA (250 bp or 1 kB; 5 nM) was incubated with MTase (10 nM) in HEPES buffer (20 mM; pH 7.4) containing $NiCl_2$ (10 mM), $CaCl_2$ (10 mM) or $MgCl_2$ (5 mM) at room temperature for 5 min. The mixture (5 µL) was deposited on the mica surface, followed by 2 min incubation, rinsing with pure water and dried with N_2.

2.11.1.5 Imaging R_1-complex on mica

The R_1-complex was obtained by incubation of the MTase (10 µL) and HsdR subunits (10 µL) in an equal molar ratio (100 nM) in AFM buffer (NaCl (300 nM), Tris-HCl (pH 8)) at room temperature for 5 min. The stable complex was diluted 10× in HEPES buffer (20 mM; pH 7.4) containing $MgCl_2$ (5 mM) and an aliquot of the sample (5 µL) placed on the PLL pre-treated mica (Section 2.10.1.1) for a 2 min incubation; the surface was then rinsed with pure water and dried with N_2.

2.11.1.6 Imaging of the DNA-R_1-complex

The R_1-complex was obtained by incubation of the MTase (10 µL) and HsdR (10 µL) subunits in an equal molar ratio (100 nM) in AFM buffer (NaCl (300 nM), Tris-HCl (pH 8)) at room temperature for 5 min. The stable complex was diluted 10× in HEPES buffer (20 mM; pH 7.4) containing $MgCl_2$ (5 mM) or $CaCl_2$ mixed with DNA (1 kB or 250 bp; 5 nM) at a molar ratio of 2:1 followed by a 5 min incubation at 37 °C. An aliquot of the sample (5 µL) placed on the PLL pre-treated mica (Section 2.10.1.1) for a 2 min incubation; the surface was then rinsed with pure water and dried with N_2.

2.11.1.7 Visualisation of R_2-complex

MTase and HsdR were diluted to 100 nM in AFM buffer. The R_2-complex was produced by incubation of MTase (10 nM) and HsdR(R124I) (50 nM) in HEPES buffer (20 mM); pH 7.4) containing $MgCl_2$ (5 mM) for 5 min at room temperature, followed by 5 min at 37 °C with the DNA (1 kB and 250 bp DNA; 5 nM). An aliquot of the DNA-protein mixture (5 µL) was placed on the PLL pre-treated mica (Section 2.10.1.1) for 2 min incubation; the surface was then rinsed with pure water and dried with N_2.

2.11.1.8 Visualisation of EcoR124I in the presence of ATP-γ-S and AMP-pnp cofactors

The R_1-complex (10 nM) was incubated with DNA (1 kB; 5 nM), as described in (Section 2.10.1.6). ATP-γ-S or AMP-pnp was added the reaction mixture (to a final concentration of 2 mM) and incubated for 30 s at room temperature. The mixture (5 µL) was deposited on PLL pre-treated mica (2 min incubation), rinsed with pure water (1 mL), quickly dried in a stream of N_2 and directly imaged.

2.11.1.9 Images of translocating EcoR124I

The R_1-complex was incubated with DNA (Section 2.10.1.6) followed by the addition of ATP to the final concentration of 0.5 mM; an aliquot (10 µL) was immediate deposited on PLL pre-treated mica, where the mixture was incubated for 15 s, rinsed with pure water (1 mL) and dried in a stream of N_2.

2.11.1.10 Images of increasing concentration of MTase

MTase (1 nM – 300 nM; 5 µL) in PBS buffer (pH 7.4) was placed onto PLL pre-treated mica (Section 2.10.1.1) and incubated for 2 min. The surface was then washed with

water (2 mL) and dried in a stream of N_2. The integrity of the MTase layer without aggregation (made using 200 nM) for imaging in liquid was confirmed.

2.11.1.11 Imaging of avidin

Avidin stock was diluted to a final concentration of 750 nM in PBS (pH 7.4; NaCl (15 mM); NaH_2PO_4 (5 mM)). An aliquot (5 µL) was placed on PLL pre-treated mica (Section 2.10.1.1) and incubated for 5 min, rinsed with water (2 mL) and dried in a stream of N_2.

2.11.2 Imaging in liquid

2.11.2.1 Visualisation of DNA on mica in the presence of (Mg^{2+} and Ni^{2+}) (in aqueous)

PLL (10 µL) was deposited on the mica surface followed by a 2 min incubation at room temperature, rinsed with pure water (2 mL) and dried in a stream of N_2. The DNA (1 kB; 10 µL), diluted to a final concentration of 10 nM with HEPES buffer (20 mM; pH 7.4) containing $NiCl_2$ (10 mM), was deposited on the mica. After an incubation time of 2 min, the sample was rinsed with water (1 mL) and dried in a stream of N_2. In a parallel experiment, $MgCl_2$ (10 mM) replaced $NiCl_2$ (10 mM).

2.11.2.2 Monolayer of MTase and HsdR in PBS buffer

MTase (200 nM) or GST-HsdR(PrrI) (200 nM) in PBS buffer (pH 7.4; 10 µL) was placed onto PLL pre-treated mica (Section 2.10.1.1) and incubated for 5 min. The surface was then washed with PBS (1 mL) and water (1mL) and directly imaged.

2.11.2.3 Monolayer of GST

GST, diluted to a final concentration of 0.8 µM in PBS buffer, pH 7.4, was deposited on PLL pre-treated mica (Section 2.10.1.1) and after a 5 min incubation, rinsed with PBS buffer (pH 7.4; 1 mL) and water (1 mL) and directly imaged.

2.11.2.4 Monolayer of avidin preparation

Avidin (0.75 µM) in PBS (NaCl (150 mM); NaH_2PO_4 (5 mM)); pH adjusted to 7.4 using NaOH) was diluted with 9 volumes of water and an aliquot (10 µL) placed on mica. After 15 min, the substrate was rinsed with PBS (1 mL) and imaged in PBS.

2.11.2.5 Imaging of the avidin monolayer using MAC Mode

Topography images of dense avidin monolayers (1.5 µM) on mica in PBS buffer (pH 7.4) after 15 min of incubation were obtained using a MacMode dynamic force microscope (5500 AFM; Agilent, Chandler AZ, USA). Magnetized cantilevers were driven by a solenoid with amplitude oscillation of 8 kHz and scanning was performed at 1 Hz.

2.11.3 Contour length measurements of DNA molecules

Lengths of DNA molecules were calculated using Image J (V 1.38; National Institute of Mental Health, Bethesda, Maryland, USA). The spatial scale was defined by entering the image width in pixels. The segmented line tool was used to outline the DNA contour and the pixel distance converted to a length in nanometres (Figure 2.12).

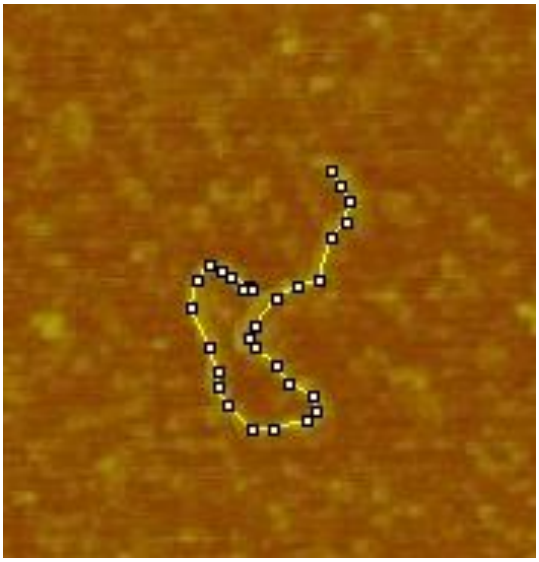

Figure 2.12. An illustration of selection of a DNA contour for DNA length measurements.

2.11.4 Force spectroscopy studies

Force *versus* distance curves were acquired in PBS buffer pH 7.4, using Si_3N_4 cantilevers with integrated tips integrated tips (t = 0.59 – 0.61 µm, l = 315 – 325 µm, w = 18 – 26 µm, ν_0 = 4 – 10 kHz, k_{nom} = 0.01 N m^{-1}, R = 20 – 60 nm; Model: MLCT-AUNM, Veeco Instruments, Dordan, France). The position of the laser was not altered during any of the adhesion experiments. Force *vs.* distance curves were obtained at a scan rate of 1.03 Hz (for avidin-biotin and antibodies measurements) and a sensor response (V nm^{-1}), obtained from the withdraw curve, was measured to convert the deflection scale (y-axis) from V to nm. The ramp size was set to 400 nm and a relative trigger of 10 nm was used. Arrays of 10 × 10 force measurements were obtained for multiple force curve acquisition, although single force curves were also obtained were necessary using single ramp mode.

2.11.4.1 Spring constant determination

It is necessary to determine the spring constant (*k*) of each AFM cantilever used in force-distance experiments since nominal values provided by manufacturers often vary by a factor of two or more.

A number of equations have been used in the literature to determine *k*, however the "gold standard" is yet to be found. The applicability of these depends on the cantilever shape (beam-shaped or V-shaped) and the limitations of each method have been reviewed (Clifford and Seah, 2005). The thickness *(t)* of the cantilever usually differs from wafer to wafer. Cleveland's dynamic deflection method (Cleveland *et al.*, 1993) was considered to be inappropriate as there was a high chance of breaking the cantilever on completion of the force measurements when attempting to attach a microsphere end-mass (the position of applied mass is also critical). The use of the reference cantilever method (Eve *et al.*, 2002; Clifford & Seah, 2005; Jing *et al.*, 2007) has been found to be highly dependent on the position of measured tip in touching the end of the reference cantilever, thus giving inconsistent results (Lamprou *et al.*, 2010). The use of the Sader method is reserved for beam-shaped cantilevers (Sader *et al.*, 1999), however the simplicity of the parallel beam approximation for V-shaped tips was considered. A few of the more suitable techniques are compared below.

The dimensional-model approach for a V-shaped cantilever uses Equation 2.1; the factor 2 is replaced by 4 for beam shaped cantilevers (Butt *et al*., 1993).

$$k = \frac{Ewt^3}{2l^3} \qquad (2.1)$$

where l = length of cantilever from base to the tip apex, w = cantilever width (measured perpendicular to L; Figure 2.13), t = cantilever thickness, E = Young's Modulus of Si_3N_4 (185 GPa (Hazel and Tsukruk, 1999)).

Equations 2.2 – 2.4 have also been reported (Albrecht *et al*., 1990, Sader and White, 1993; Sader, 1995):

$$k = \frac{Ewt^3}{2l^3}\left(1 + \frac{b^2}{4l^2}\right)^{-2} \tag{2.2}$$

$$k = \frac{Ewt^3}{2l^3}\left(1 + \frac{4w^3}{b^3}\right)^{-1} \tag{2.3}$$

$$k = \frac{Ewt^3}{2l^3}\cos\theta\left(1 + \frac{4w^3}{b^3}(3\cos\theta - 2)\right)^{-1} \tag{2.4}$$

where b = width at the base of the cantilever, θ = half angle between the two legs, w = width of the leg parallel to the front edge, l = the length measured straight out to the apex (Figure 2.13).

Sader (1995) investigated the use of the formulas presented in Equations 2.1 – 2.4 and found the percentage errors of each to be 16 %, 25 %, 13 % and 2 %, respectively.

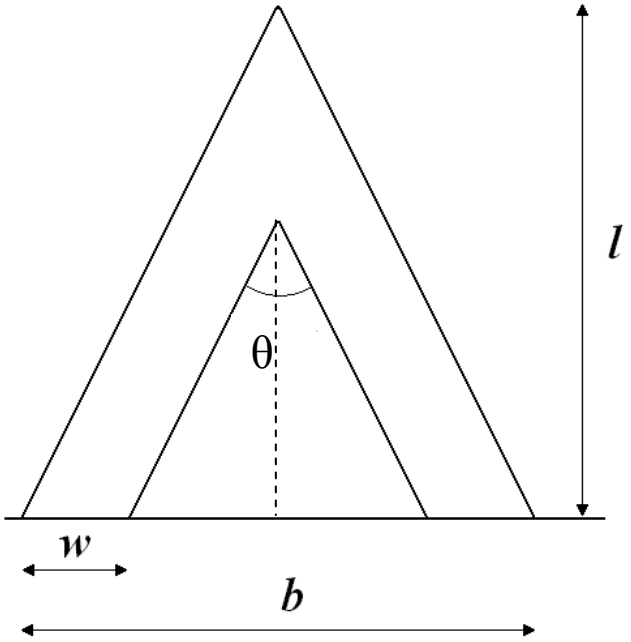

Figure 2.13. Length *l*, width *w*, tip base width *b* and angle θ parameters used to determine *k* using dimensional methods for V-shaped cantilevers.

Using the geometric method, an error in *k* can result from the difficulties in measuring *t* (even with SEM), giving rise to an error of *ca.* 3 % (Kim *et al*., 2010). Errors in *E*, and hence *k*, may also arise from the non-stoichiometry of Si_3N_4 and the use of thin gold-coating layers. Hazel and Tsukruk (1999) included the bi-component nature of V-shaped cantilevers and determined the effective *E* value of 185 GPa.

To alleviate the need of *t* measurements, Equation 2.5 (Clifford and Seah, 2005) included resonant frequency and density of Si_3N_4, although the latter parameter also contains the uncertainty (which is also a cube term), due to the variations in stoichiometry of Si_3N_4 in the fabrication process:

$$k = (512)^{0.5}\pi^3 M_e^{1.5} w \frac{(L_V\sqrt{\rho})^3}{\sqrt{E}} \quad (2.5)$$

where, ρ = density of Si_3N_4 (3000 kg m^{-3} (Hazel and Tsukruk, 1999)) and M_e = normalised effective mass (0.163), $(512)^{0.5}\pi^3 M_e^{1.5} = 46.17$ (Clifford and Seah, 2005).

The thermal noise method is the most desired method for soft cantilevers and has the advantage in not requiring cantilever dimensions (Hutter and Bechhoefer, 1993). The uncertainly of this method has been assessed to be 15 – 20 % (Clifford and Seah, 2005), 10 – 20 % (Gibson *et al*., 1996) and 5-25 % (Kim *et al*., 2010). Equation 2.6 is shown in its simplest form, although for practical reasons, higher modes of oscillation are often used (Kim *et al*., 2010).

$$k = \frac{k_B T}{\langle z_c^2 \rangle} \tag{2.6}$$

where k_BT = Boltzmann constant (1.38×10^{-23} J K^{-1}); T = temperature and $\langle z_c^2 \rangle$ is the mean square cantilever displacement.

In a typical experiment, a power spectral density analysis of the cantilever oscillation is measured and the area integrated under the oscillation curve. Implementation of this method was not available during this project. Towards the very end of the project, however, a CellHesion 200 AFM (JPK Instruments, Berlin, Germany) did become available for a short period, although the experimental part of work the thesis was complete. The *k* values could not been compared due to some tips that were used in experiments had become destroyed.

Table 2.1 shows the values of measured parameters, necessary to determine *k* with dimensional methods and Table 2.2 details the values of *k* obtained using Equations 2.1 – 2.5.

Table 2.1. Physical properties of tips used to determine k. The range values given by manufacturer (l = 315 – 325 μm, w = 18 – 26 μm, t = 0.59 – 0.61 μm, ν_0 = 4 – 10 kHz.

Tip	l / μm	w / μm	t / μm	b / μm	2θ / °	ν / kHz
T1	314.7	20.4	0.62	220.5	37.0	9.01
T2	319.1	22.3	0.61	220.2	37.5	8.95
T3	318.5	20.4	0.63	223.3	37.0	8.76
T4	316.5	21.1	0.60	222.1	36.5	9.08
T5	319.1	22.3	0.60	220.2	37.5	8.58
T6	320.4	21.7	0.59	220.5	36.0	8.42
T7	314.7	22.3	0.60	220.8	37.0	9.15
T8	322.3	21.7	0.62	220.8	37.0	8.79

The *l, w, b* measurements were obtained using a Zeiss Axiovert 200M inverted microscope; *t* values were obtained using a low vacuum scanning electron microscope (uncoated specimens).

Table 2.2. Values of *k* determined using different equations within the dimensional method; k_{nom} = 0.01 N m^{-1}.

Tip[a]	*k* / N m^{-1}				
	Equation 2.1	Equation 2.2	Equation 2.3	Equation 2.4	Equation 2.5
T1	0.014	0.011	0.014	0.014	0.007
T2	0.014	0.012	0.014	0.014	0.008
T3	0.014	0.011	0.014	0.014	0.009
T4	0.013	0.011	0.013	0.013	0.008
T5	0.014	0.011	0.014	0.013	0.009
T6	0.013	0.011	0.012	0.012	0.009
T7	0.014	0.010	0.014	0.014	0.008
T8	0.014	0.011	0.014	0.014	0.009

The *k* values obtained with the dimensional method were close to the nominal value stated by the manufacturer (0.01 N m^{-1}). Only values obtained with Equation 2.5, where *t* was replaced with ρ, were smaller, which is with agreement with elsewhere (Lamprou *et al.*, 2010). Equations 2.1, 2.3 and 2.4 gave the same value, where the latter two required additional measurement (*b* and/or θ) and therefore, the simplest Equation (2.1) was used to calculate *k*.

2.11.4.2 Tip cleaning

Prior to force distance measurements silicon nitride cantilevers were washed by immersion with chloroform (3 x10 min) and dried gently with stream of nitrogen, two methods of cleaning were used:

(1) Pirahna solution (3:1 concentrated sulphuric acid, 33 % (v/v): 30 % aqueous hydrogen peroxide): Samples were immersed for 30 min, rinsed with deionised water (force distance measurements of avidin-biotin-glutaraldehyde method).The gold layer was found to detach from the cantilever using Pirahna solution and so method 2 was used for rest of the experiments.

(2) UVO cleaner®-ozone cleaning device, model 42 (Jelight Company Inc, Irvine, CA, USA) was used to remove any contaminants and generate a more polar surface (increases presences of surface OH groups) by treating for 30 min.

Prior to imaging, cantilevers were washed by immersion in chloroform (Fisher Scientific) (3 × 10 min) and dried gently with in a stream of N_2. After protein imaging, cantilevers were cleaned by 4 immersion steps: SDS (20%; 10 min), pure water (3 × 10 min), ethanol (3 × 10 min) and ultra pure water (3 × 10 min) and dried with N_2.

2.11.4.3 Tip and sample functionalisation for avidin-biotin measurements (glutaraldehyde method)

Silicon nitride cantilevers were modified according to the method described by Luckham and Smith (1998). Before use, APTES (Sigma-Aldrich) was freshly distilled under vacuum. A desiccator (5 L) was flooded with Ar to remove air and moisture. APTES (30 µL) and triethylamine (10 µL) (Sigma-Aldrich) were placed into two trays in the desiccators along with the AFM cantilevers positioned close-by on a clean, inert surface. After 120 min of incubation, the trays with APTES and triethylamine were removed and the desiccator was flooded with Ar for 5 min and the cantilevers left inside for 2 days. Cantilevers were immersed in glutaraldehyde (2.5 %; Sigma-Aldrich) for 20

min, rinsed with water and finally incubated with avidin from egg white (1 µM; Fisher Scientific, Loughborough, UK) in PBS buffer (PO_4^{3-} (20 mM), NaCl (150 mM); pH = 7.2) at 22 °C for a 10 min incubation. Functionalised cantilevers were stored at 4ºC (up to 2 days). The sample surface was coated with biotin (Fisher Scientific UK), diluted in PBS (0.4 µM) in a similar way as described for the cantilevers, however amino-functionalisation with APTES was replaced with PLL treatment of mica (Section 2.10.1.1).

AFM force measurements were recorded between avidin immobilised on AFM cantilevers and biotin on mica using a retract velocity of 1 µm s^{-1}

2.11.4.4 F-d measurements of avidin-biotin (NHS-PEG_{12}-biotin)

Aminofunctionalisation (ethanolamine hydrochloride method)

The silicon nitride cantilevers were cleaned in the ozone cleaner for 30 min, immersed in chloroform and dried with a gentle stream of N_2. Cantilevers were modified with amino groups using ethanolamine hydrochloride (3.3 g; Sigma-Aldrich) dissolved in DMSO (6 mL; Fisher Scientific) by heating to 70 °C. Once all material had dissolved, molecular sieves (*ca.* 10% v/v; 4 Å) were added. The solution was cooled to room temperature and dissolved air was removed by degassing in a desiccator under vacuum for 30 min. The cantilevers were placed in the ethanolamine hydrochloride/DMSO solution on top of the glass plate. Overnight incubation was followed by washing with DMSO (3 ×) and ethanol (3 ×), and dried in a stream of N_2.

PEGylation

Biotin-PEG-NHS (1 mg) was dissolved in chloroform (1 mL). Triethylamine (30 µL) was added to the mixture to start coupling reaction and the ethanolamine-coated cantilevers were immediately immersed in the mixture and left for 2 h. After incubation, the cantilevers were washed with chloroform (3 × 10 min immersion) and used for force-distance measurements.

2.11.4.5 Tip functionalisation for HsdR-MTase measurements

The amino-functionalisation of AFM cantilevers was obtained using the ethanolamine hydrochloride method (Section 2.10.4.4).

PEGylation using MAL-PEG$_{12}$-NHS

Amino functionalised AFM cantilevers were coupled to a PEG spacer (MEL-dPEG$_{12}$-NHS ester; n = 12; 53.3 Å; QuantaBiodesign; Powell, OH, USA) *via* the NHS ester group. PEG (1 mg) was dissolved in chloroform (1 mL) and triethylamine (30 µL) was added. The cantilevers were covered with an inverted beaker to prevent chloroform evaporation and incubated in the PEG solution at room temperature for 2 h; they were then washed in chloroform (3 × 10 min immersion) and dried in a stream of N_2.

Coupling with GST-HsdR(PrrI)

The maleimide (MEL) group at the other end of the linker reacted with thiol group in cysteine of glutathione. PEGylated cantilevers were immersed for 1 h in glutathione (10 mM) dissolved in PBS buffer (pH 7.4) and after the required time, cantilevers were washed in PBS buffer and immersed in HsdR (1 µM) solution in PBS buffer and

incubated for 30 min at room temperature. Freshly prepared tips were used for force-distance experiments; remaining tips were stored in PBS buffer at 4 °C.

2.11.4.6 Modification of AFM tips with antibodies

Silicon nitride AFM cantilevers were derivatised with primary amines (ethanolamine hydrochloride method, Section 2.10.4.1). The PEG linker (NHS-PEG_{12}-MAL), previously used in GST-HsdR(PrrI)-MTase measurements, was attached to the AFM cantilevers (Section 2.10.4.5). The sulfhydryl groups, necessary for attachment to the maleimide ended tips, could then be added to the antibodies using Traut's reagent, which is able to react with primary amines available on the side chain of antibody lysine residues.

Modification of antibodies with sulfhydryl groups

Antibodies (anti-GST, polyclonal; Abcam) were diluted in coupling buffer: PBS-EDTA (50 mM Phosphate, 0.15 M NaCl, 10 mM EDTA, pH 8) and Traut's Reagent (20 μL) was added to the solution. The mixture was then incubation for 45 min at room temperature. MicroSpin G-25 columns were used to purify the modified antibody from excess Traut's Reagent. Collected fractions containing antibodies were identified by Nanodrop.

Attachment of modified antibodies onto AFM tips

The PEGylated cantilevers were incubated with the antibody solution (0.1 mg mL^{-1}) for 4 h at room temperature. Modified tips were washed with coupling buffer and PBS and immediately used or stored at 4 °C (2 days max).

Force-distance measurements were recorded between antibodies attached to AFM cantilevers and a layer of GST/GST-HsdR on mica at a retract rate of 1.2 μm s^{-1}.

2.11.4.7 Control experiments (F-d experiments)

For each investigation, a control experiment was performed using with the same cantilevers used in the functionalised systems to ensure that the interactions observed between pairs of molecules were specific. The binding sites of proteins attached on the mica surface of avidin (NHS-PEG_{12}-biotin method) and GST-HsdR(PrrI) (MTase-HsdR studies) were blocked through the injection of free biotin (0.2 mg mL^{-1}) and HsdR, respectively. This was followed by incubation in PBS buffer (pH 7.4) for 10 min at room temperature and subsequently, AFM F-d measurements were obtained.

Control experiments of antibodies-GST and antibodies-GST-HsdR studies were carried out by using F-d measurements between antibody-functionalised cantilevers and mica pre-treated with PLL.

Chapter 3

Optimising the conditions for AFM imaging of DNA

3.1 Introduction

Biological materials require suitably prepared surfaces for AFM studies. In the literature, a number of methods for adaptation of conditions to suit different surfaces have been described, such as glass, gold, highly oriented pyrolytic graphite (HOPG) and mica, of which the latter is usually most suited for DNA imaging (Hansma and Laney, 1996) using the AFM.

3.1.1 Muscovite mica surface

Atomically flat muscovite mica is composed of negatively charged layers, each consisting of two tetrahedral SiO_4 layers crosslinked by aluminium ions surrounded by hydroxyl groups (Figure 3.1) (Nishimura *et al.*, 1995). These layers are connected to a positively charged interlayer of potassium cations *via* weak electrostatic bonds. The cleavage of mica, using adhesive tape, disrupts the structure of the basal layer of oxygen atoms with exposition of the K^+ ions (Muller *et al.*, 1997), which, in air, are completely neutralised by the negatively charged aluminosilicate lattice. In water, at neutral pH, the K^+ ions can easily dissociate from the surface resulting in negatively charged mica (Pashley, 1981; Claesson *et al.*, 1986).

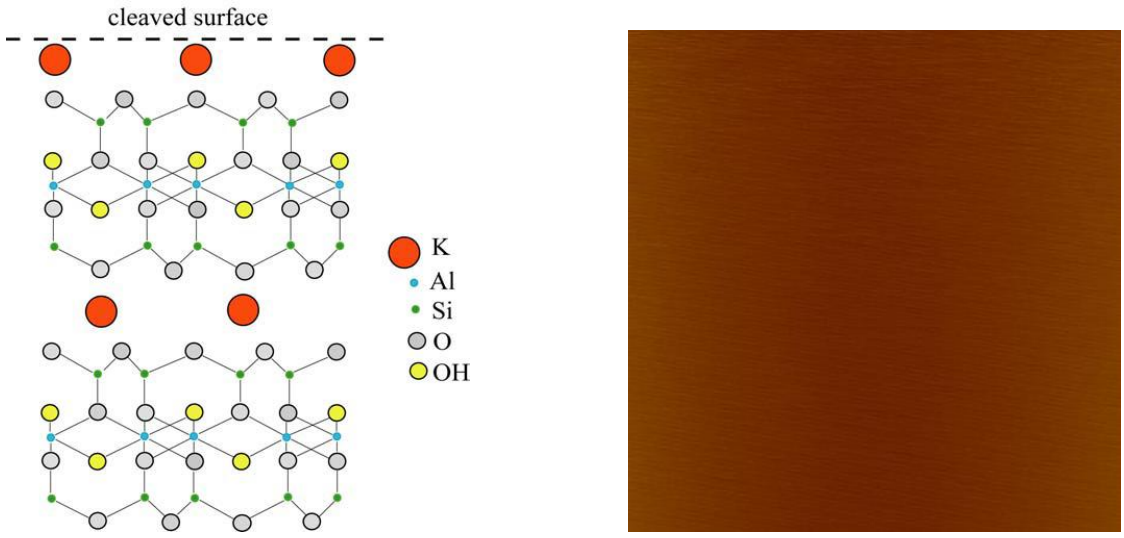

(a) (b)

Figure 3.1. (a) Layered structure of mica surface (vertical slice); adapted from www.ism.cnr.it/english/linee/MD.P06.006.php; (b) AFM image in air (tapping mode) of a flat mica surface (R_a = 0.022 nm; size 10 µm × 10 µm; z-scale 3 nm).

3.1.2 Methods of DNA immobilisation on mica

Successful, reproducible and high-resolution imaging of DNA and proteins, or studies of DNA-protein and protein-protein interactions on surfaces using the AFM require stable immobilisation of biomolecules. Very strong attachment of DNA to mica, however, may destroy some of the physiological activity of the DNA and change the conformation. If DNA binding is too weak, there is a risk that biomolecules could be swept away by the AFM tip.

One of the standard methods for DNA immobilisation is based on using divalent cations to act as an electrostatic bridge between hydroxyl groups on the mica surface and the negative phosphate groups of the DNA backbone (cations in the buffer shield electrostatic charges and thus lower the repulsion between DNA and mica). The first

AFM images of DNA molecules in air were implemented on mica treated with Mg^{2+} ions (Bustamante *et al.*, 1992; Vesenka *et al.*, 1992). Later studies showed that other cations (Ca^{2+}, Ni^{2+}, Co^{2+}, La^{3+} and Zr^{4+}) could be also used for DNA imaging (Bustamante *et al.*, 1992, Thundat *et al.*,1992; Benzilla *et al.*, 1995). The adhesion of DNA molecules was also observed when Mg^{2+} was present in the buffer and, therefore, mica pre-treatment with cations was not necessary (Hansma *et al.*, 1993a; Bezanilla *et al.*, 1995; Bustamante and Rivetti, 1996; Bustamante *et al.*, 1997). This approach has been successfully applied in the study of DNA-protein complexes and has become the most widely used due to the simplicity of sample preparation (Erie *et al.*, 1994; Guthold *et al.*, 1994; Zlatanova *et al.*, 1994; Bustamante and Rivetti, 1996; Bustamante *et al.*, 1997; Rippe *et al.*, 1997; Wyman *et al.*, 1997; Dame *et al.*, 2003; Modesti *et al.*, 2007; van der Linden *et al.*, 2009).

The strength of the adsorption of DNA molecules has been optimised by varying the concentration and type of cations (Guthold *et al.*, 1994; Thomson *et al.*, 1996; Hansma *et al.*, 1996; Pastre *et al.*, 2003; 2006). However, the cation used was found to influence the secondary and topological structures of DNA on mica and the cations were able to bind either phosphate groups or base sites of DNA. For example, Mg^{2+} was able to bind to the phosphate groups of DNA only, whereas, binding to the phosphate groups and to bases of DNA has been observed in the presence of divalent metal ions such as Ni^{2+}, Ca^{2+}, Cd^{2+}, Zn^{2+} and Co^{2+} in one report, although is unlikely (Hackl *et al.*, 2005). The size of the ionic radii of the transition metal cation present in the buffer seems to be also related to the binding ability. Divalent cations with small radii (0.69 Å (Ni^{2+}) – 0.74 Å (Zn^{2+})) were able to fit into cavities above the recessed hydroxyl groups in the mica

lattice and neutralise the negative charge of the mica (Gaines, 1957; Pashley *et al.*, 1985). The Mg^{2+} ion with an ionic radius of 0.65 Å, similar to Ni^{2+} (0.69 Å), was small enough to enter the mica cavities, whereas Ca^{2+} (ionic radius 0.99 Å) was too large (Nishimura *et al.*, 1995). However, DNA immobilisation by Mg^{2+} and Ca^{2+} was found to be too weak to obtain reproducible images in liquid, whereas Ni^{2+} provided reproducible visualisation of DNA molecules without observed movement (Benzilla *et al.*, 1994). A schematic diagram showing immobilisation of DNA on mica with divalent metal ions is shown in Figure 3.2.

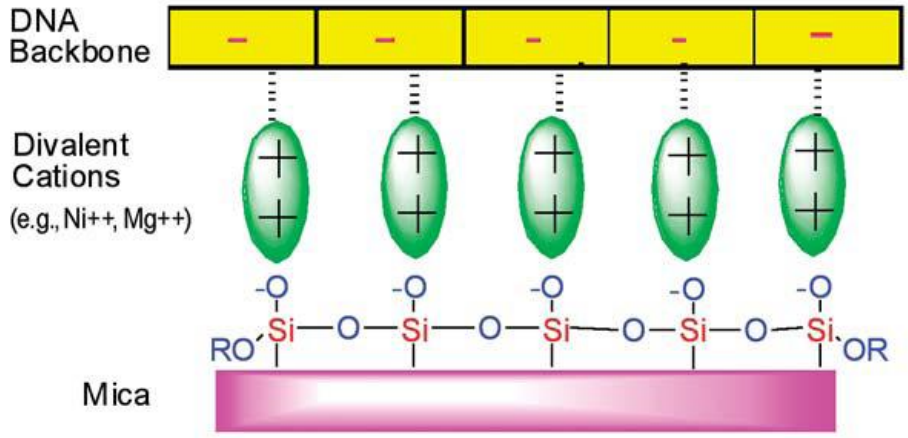

Figure 3.2. DNA immobilisation on mica with divalent metal ions. Adapted from (Johnson, 2008).

Another common approach in DNA deposition is chemical functionalisation of mica with APTES, which exposes positively charged amino groups allowing binding to negatively charged DNA molecules (Lyubchenko, 2001). Mica functionalisation with aminopropyl (AP) has also been used for DNA imaging in air and liquids (Lindsay *et al.*, 1992; Lyubchenko *et al.*, 1993a; Lyubchenko *et al.*, 1993b). Surface functionalisation with 1-(3-aminopropyl)silatrane (APS) has become an alternative method to the use of AP-mica (Shlyakhtenko *et al.*, 2000; Tiner *et al.*, 2001; Shlyakhtenko *et al.*, 2003; Lyubchenko *et al.*, 2009). Mica pre-treatment with PLL, a

positively charged cationic polymer, is also commonly used for the attraction of negatively charged DNA to the surface and successful visualisation of DNA-proteins complexes (Berge *et al.*, 2000, van Noort *et al.*, 2004).

3.1.3 AFM imaging in liquid

An AFM operating in liquid has the great advantage of being able to follow dynamic and structural changes of single molecules and study the interactions between macromolecules in physiological buffer in real time. Imaging in liquid allows for better control of forces applied to the sample, since capillary forces between the tip and the surface when operating in an air environment, due to adsorbed water layers, are eliminated (Drake *et al.*, 1989). Deformation of soft biological samples can be reduced by removal of the undesirable and often destructive forces and the artefacts related to washing and drying of the samples are eliminated (Schulz *et al.*, 1998).

The literature reports that the addition of Ni^{2+} ions to the buffer provides stable imaging of DNA in liquid (Bezanilla *et al.*, 1994) and it has been postulated that mica treatment with $NiCl_2$ provides this increased stability without changes to the DNA conformation (Vesenka *et al.*, 1992; Hansma *et al.*, 1995). Co^{2+} and Zn^{2+} ions have also been found to bind DNA with enough strength to allow stable imaging in water, or in buffer solution (Bezanilla *et al.*, 1994; Thomson *et al.*, 1996).

3.1.4 Tip convolution

Imaging artefacts can arise when the scanning tip has a radius comparable to, or larger than the lateral size of the imaged object. As the tip scans over the sample, the sides of the tip make contact before the apex leading to image broadening; this is also known as tip convolution. Imaged features appear wider, whereas the holes present on the surface appear smaller (narrower and often less deep) (Figure 3.3).

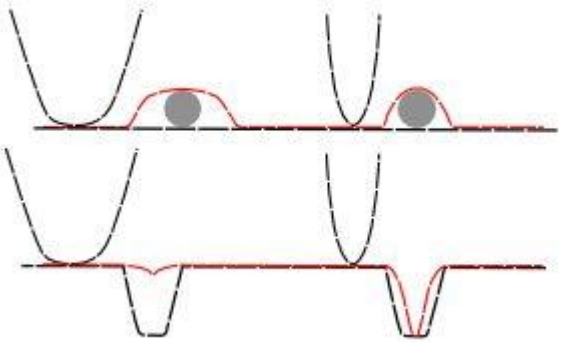

Figure 3.3. Artefacts resulting from tip-sample convolution (Eaton and West, 2010).

3.1.5 Aims

The aim of the work described in this chapter was to optimise the conditions necessary for AFM imaging of DNA so that DNA-EcoR124I complexes could be imaged under ideal conditions for the rest of the project. Whilst much of this work is not novel, a systematic approach to imaging was considered to be critically important both to gain experience of handling the large motor proteins as single molecules, but also to improve the local knowledge base of the AFM work using biomolecules. Imaging in air and water and in the presence of divalent cations (Mg^{2+}, Ca^{2+} and Ni^{2+}) in the deposition buffer (Chapter 2) was explored and the use of PLL pre-treated mica was investigated.

DNA fragments of 250 and 1000 bp, obtained from lambda DNA by PCR amplification, were used for imaging.

3.2 Results and discussion

3.2.1 AFM imaging of DNA in the presence of divalent cations

3.2.1.1 Effect of magnesium ions

DNA (1 kB) visualisation in the presence of Mg^{2+} in deposition buffer was first investigated. The Mg^{2+} present in the deposition buffer was necessary for DNA adsorption to the mica through salt bridge formation (Shao *et al.*, 1995). Deposition buffer contained *N*-(2-hydroxyethyl)piperazine-*N*'-2-ethanesulfonic acid (HEPES) instead of Tris, based on previous experiments showing that more DNA binds to untreated mica in HEPES than in Tris buffer (Bezanilla *et al.*, 1994). The pH of HEPES buffer is also more stable over time. HEPES-Mg^{2+} buffer stabilises the binding of DNA to mica which improves the spreading of DNA and provides good DNA coverage (Hansma *et al.*, 1993).

DNA strands and few connected molecules were observed (Figure 3.4). The transition between DNA desorption and adsorption is dependent on the concentration of Mg^{2+}. A lower DNA binding and a gradual release of molecules resulting in a low surface density was observed when [$MgCl_2$] < 5 mM (Pastre *et al.*, 2009). An optimal $MgCl_2$ concentration of 5 mM for DNA immobilisation was chosen for the further investigation of the DNA complex with proteins.

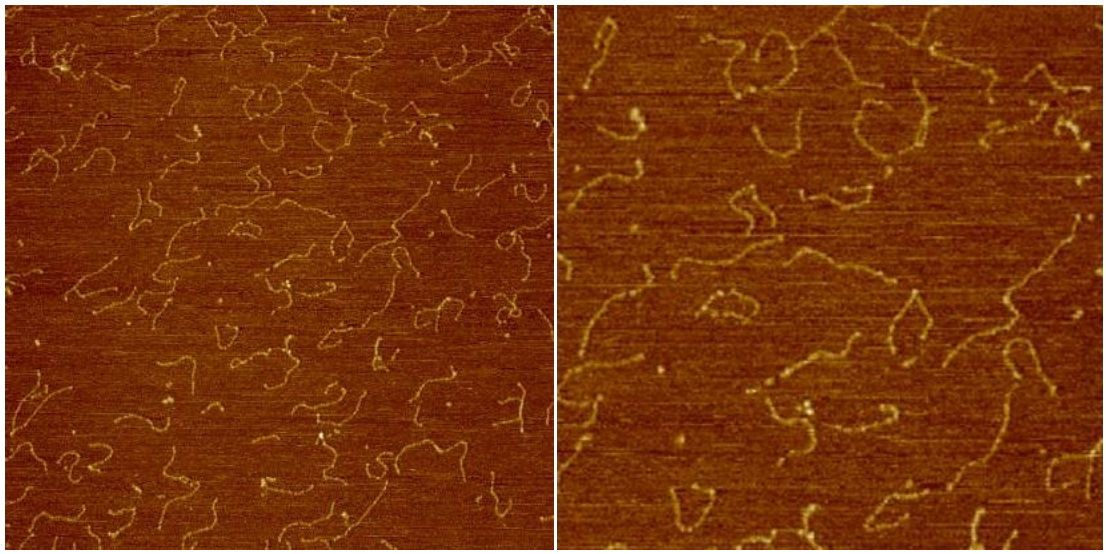

(a) (b)

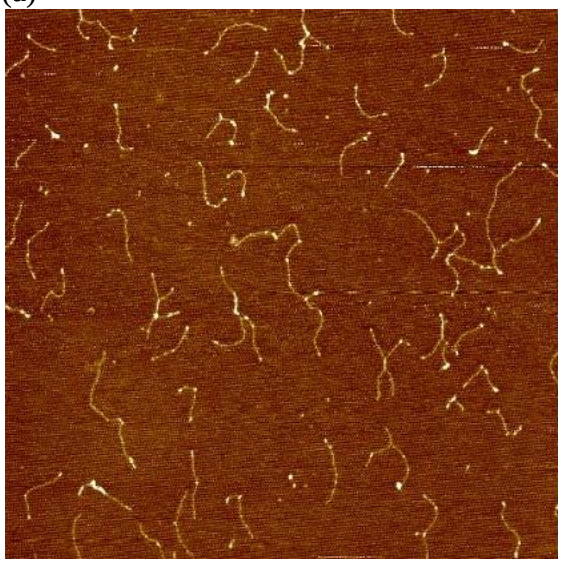

(c)

Figure 3.4. Typical AFM images of DNA (10 nM; 1 kB) in deposition buffer (HEPES (20 mM); pH 7.4) containing $MgCl_2$ (5 mM). Sizes of images (a,c) 2.5 µm × 2.5 µm; z-scale (a) 3 nm, (c) 1.5 nm; image (b) 1.3 µm × 1.3 µm; z-scale 3 nm; imaged in air under ambient conditions.

The salt concentration in the buffer is also an important factor concerning the geometry of DNA in solution and on the surface (Tessmer *et al.*, 2005). AFM images of DNA-protein complexes were shown to have a better quality if proteins that require a high salt concentration, for the binding reaction, were diluted before the deposition step to minimise the salt crystals formation during the drying step (Bustamante and Rivetti,

1996). However, DNA binding to the mica surface can be affected by the surface potential, which becomes more negative at low Na^+ concentrations (Pashley, 1981).

DNA molecules that were rod-shaped had a tendency to form connections, this in some cases could be problematic for obtaining DNA length measurements. The majority of experiments were performed using DNA with a length of 1 kB, although, in the next series of experiments, shorter DNA strands (250 bp) were also investigated (Figure 3.5).

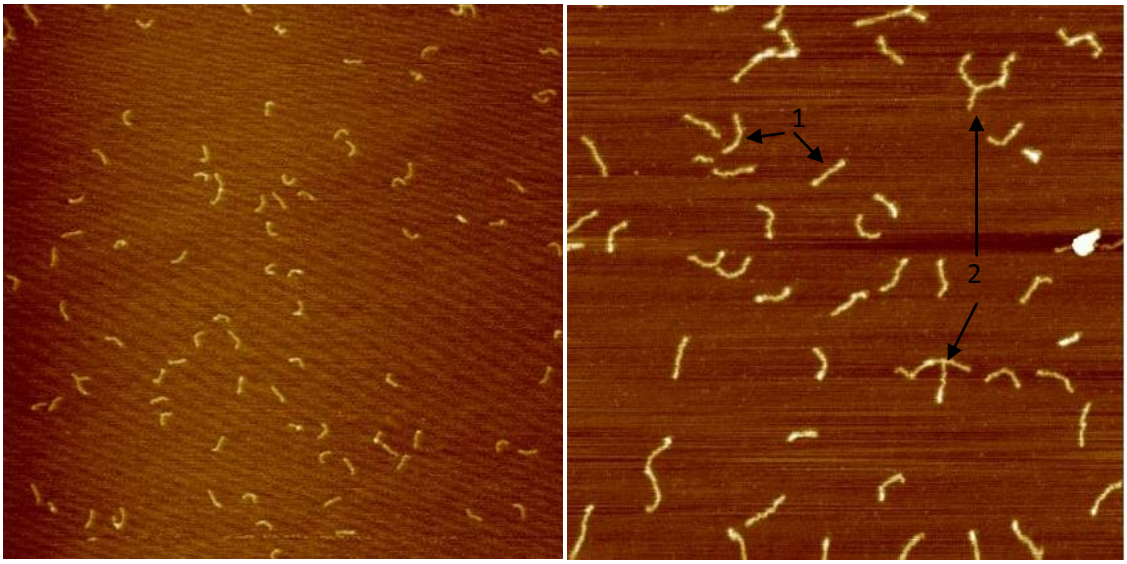

(a) (b)

Figure 3.5. Typical AFM images of DNA (250 bp) (10 nM) deposited on mica; size (a) 2.5 µm × 2.5 µm; z-scale 2 nm; (b) 1 µm × 1 µm; z-scale 3 nm; imaged in air under ambient conditions.

The shortened DNA (10 nM; 250 bp) showed the presence of straight strands (arrows numbered as 1); although, multimolecular connections could be observed (arrows numbered as 2) (Figure 3.5b). At higher DNA concentrations (*ca.* 50 nM), string-like networks of agglomerated DNA were seen (Figure 3.6a). Here, adsorbed DNA

molecules may have acted as a nucleation sites for further DNA adsorption. Dilution of this network, however, did not lead to the observation of clearly defined individual molecules (Figure 3.6b).

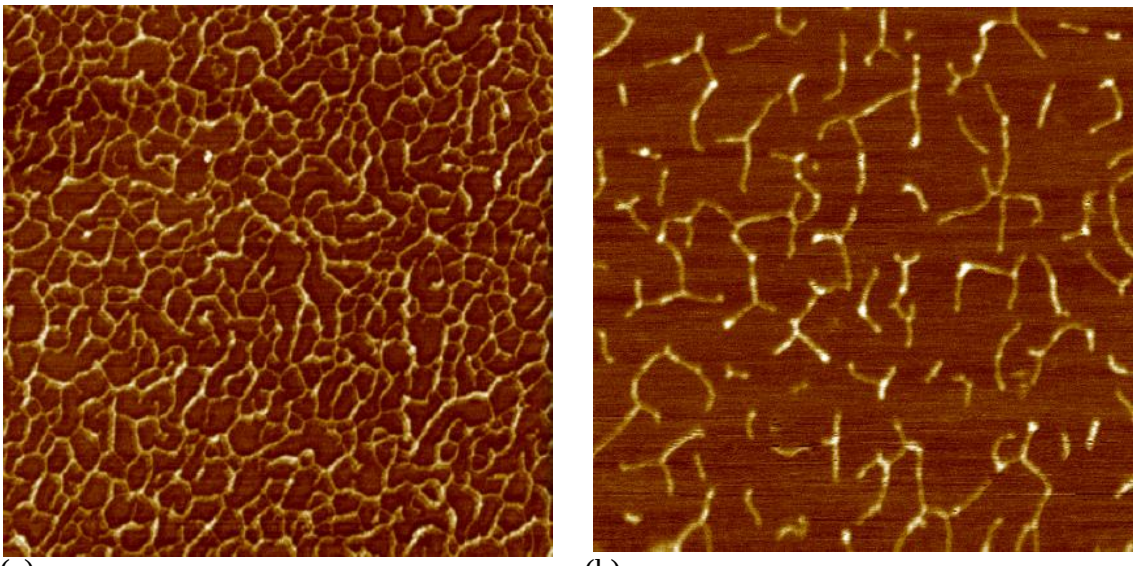

(a) (b)

Figure 3.6. Typical AFM images of DNA (250 bp) multimolecular networks observed at high DNA concentration (50 nM). Size (a) 1.7 µm × 2.5 µm; z-scale 3 nm; (b) 1 µm × 1 µm; z-scale 2 nm.

DNA strands able to contact or overlap each other, resulting in multimolecular network formation, were also observed on SAMs of 11-mercaptoundecanoic acid (MUDA) on gold (Song *et al.*, 2005). Two factors have been used to explain the formation of the DNA networks: Mg^{2+} acting as a glue between the DNA strands on the surface forming networks (a bridge between DNA phosphate groups and MUDA carboxylate groups) and a high concentration of NaCl in the solution, where DNA molecules are close to being neutralised by electrostatic repulsion of the negatively charged phosphate backbone (Shlyakhtenko *et al.*, 2003).

3.2.1.2 Mica pre-treatment with PLL

The effect of PLL on DNA imaging was also investigated, previous AFM studies of DNA-enzyme complexes have shown a strong attraction to the mica in the presence of PLL (Berge *et al.*, 2000; van Noort *et al.*, 2004). A weak DNA condensation in the presence of PLL has also previously been observed with AFM (Hansma *et al.*, 1998). Mann *et al.* (2008) postulated that DNA condensation depends on the length of PLL and DNA concentration. Condensation is monomolecular at low DNA concentrations and multimolecular (multiple molecules clustered) at higher DNA concentration.

A typical procedure used here involved spotting PLL (0.01 %) onto a freshly cleaved mica surface, allowing a 2 min incubation, followed by rinsing with pure water and drying in a stream of N_2. Mica prepared following this method resulted in featureless images of low surface roughness (R_a = 0.077 nm; xy scale = 10 µm × 10 µm; Figure 3.7).

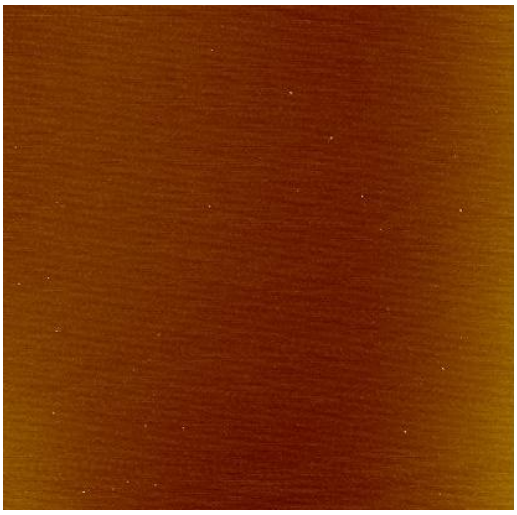

Figure 3.7. A featureless AFM image of PLL pre-treated mica (R_a = 0.077 nm); size 10 µm × 10 µm; z-scale 3 nm.

The PLL treatment did not increase the surface roughness of mica. This observation was in agreement with Bussiak *et al.* (2003).

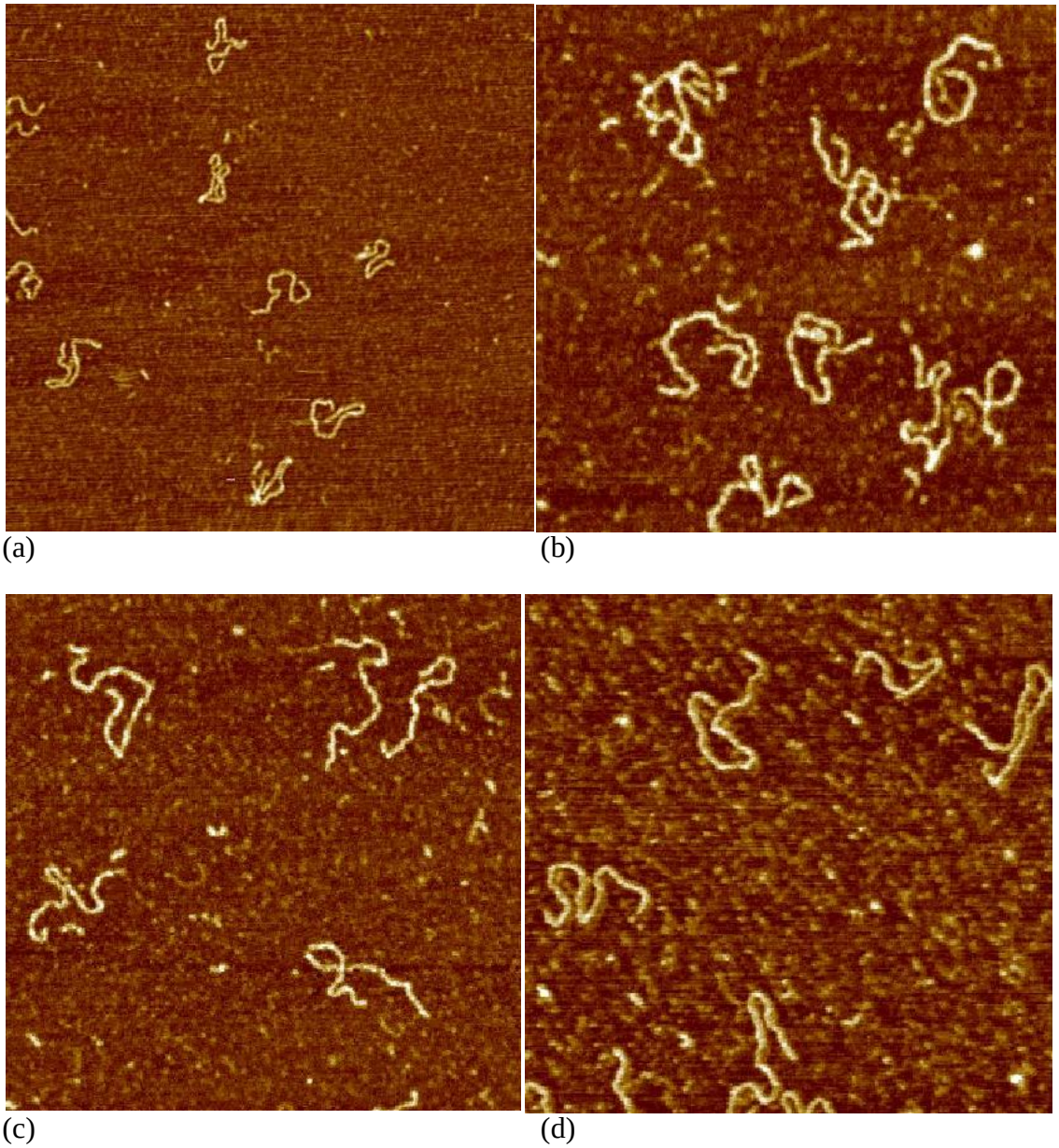

Figure 3.8. Typical AFM images of DNA (1 kB) on PLL pre-treated mica; size (a) 1.3 µm × 1.3 µm; z-scale 1.5 nm; (b) 612 nm × 612 nm; z-scale 1.5 nm; (c) 602 nm × 602 nm; z-scale 1.5 nm; (d) 660 nm × 660 nm; z-scale 1.5 nm.

DNA deposited on PLL pre-treated mica (Sections 2.10.1.1 and 2.10.1.2) resulted in coiled molecules with a contour length that was difficult to measure (Figure 3.8).

Accurate length measurements were necessary for further analysis of the translocation process and formation of loops.

3.2.1.3 Effect of calcium ions

The next studies investigated the use of Ca^{2+} for DNA imaging (Section 2.10.1.2). The images showed that Ca^{2+} allowed greater binding of DNA (more DNA molecules were enumerated at the same cation concentration compared to Mg^{2+}), although a partial salt layer was present in most images (Figure 3.9). However, in Figure 3.9 (c), instabilities of the tip-sample interactions were observed, which were caused by attractive/repulsive regions between the tip and the sample surface.

3.2.1.4 Effect of nickel ions

The strong adsorption of Ni^{2+} ions during pre-treatment neutralises the mica surface, with the K^+ ions being exchanged for Ni^{2+} ions (Ni^{2+} are not replaced by monovalent cations) (Koppelman and Dillard, 1977). The high ionic strength is necessary to lower the entropic repulsion between DNA and mica, which overcomes the electrostatic attraction (at low ionic strength), even if the mica is partially neutralised (Pastre *et al.*, 2007).

DNA (1 kB) in HEPES buffer (20 mM; pH 7.4) containing $NiCl_2$ (1 mM) was deposited on mica, incubated for 2 min, rinsed with pure water (1 mL) and dried with N_2 and imaged in air (Figure 3.10). More DNA strands were visible suggesting greater binding. The visible globular features surrounding the DNA molecules may indicate contamination or impurities; their size and shape were similar to proteins and may therefore provide difficulties when identifying protein-DNA complexes (Chapter 4).

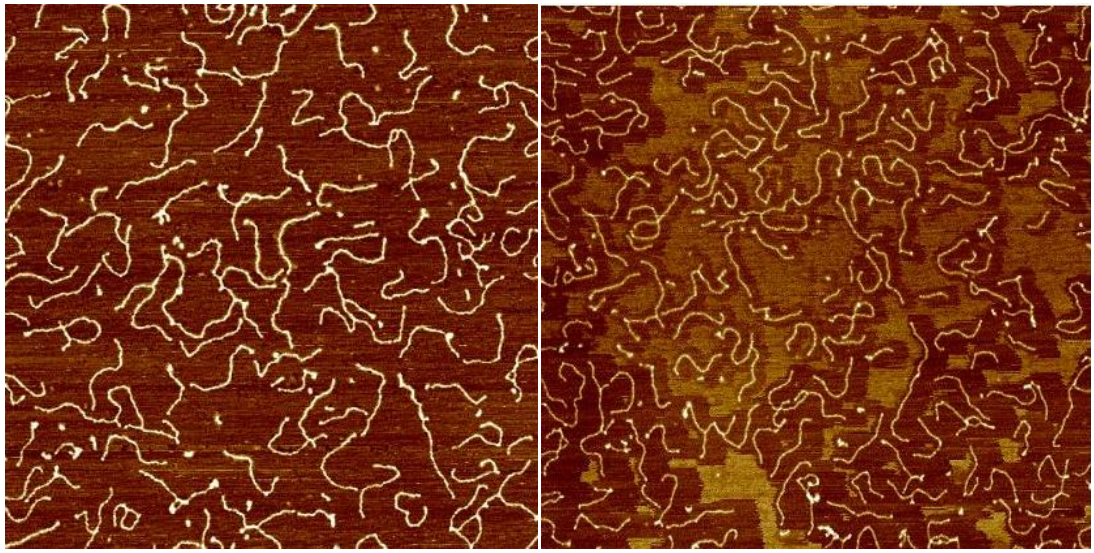

(a) (b)

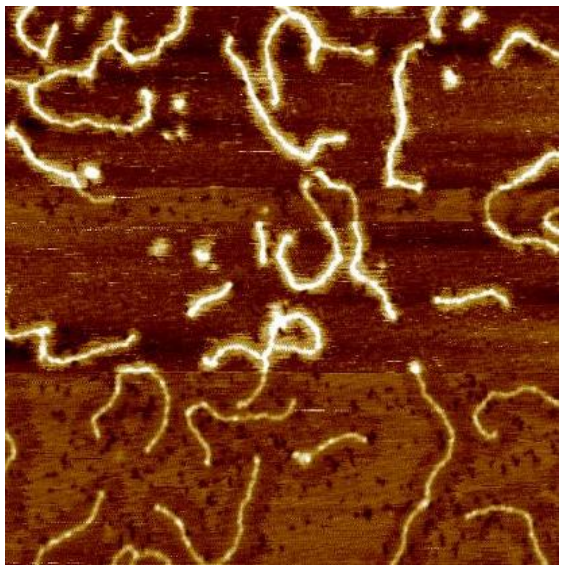

(c)

Figure 3.9. Typical AFM images of DNA (1 kB) in the presence of HEPES buffer (20 mM; pH 7.4) containing $CaCl_2$ (10 mM) after deposition on mica, incubation for 2 min, rinsing with pure water and gently drying in a stream of N_2; size (a) 2 μm × 2 μm; z-scale 1.5 nm; (b) 2.5 μm × 2.5 μm; z-scale 1.5 nm; (c) 1 μm × 1 μm; z-scale 1.5 nm. Dark regions show holes in salt layer present on the mica surface.

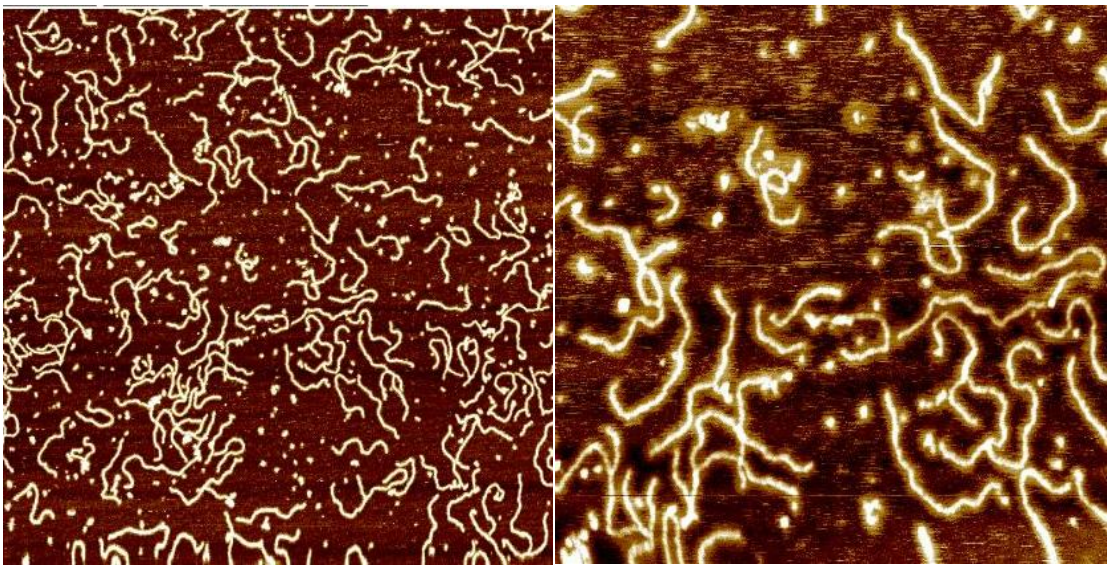

(a) (b)

Figure 3.10. Typical AFM images of DNA (1 kB) on mica in the presence of Ni^{2+} (in air); size (a) 2.5 µm × 2.5 µm; z-scale 1.5 nm; (b) 1µm × 1 µm; z-scale 1.5 nm.

3.2.2 The influence of cations used for immobilisation on DNA length measurements

The next step of this work was to determine the contour length of DNA (Section 2.10.3), in the presence of different divalent ions in deposition buffer, supplemented with an investigation of the influence of PLL on mica pre-treatment.

The DNA length, based on the assumption that DNA is in B form with an inter-base distance of 0.34 nm (Watson *et al.*, 1988), should be 340 nm for 1 kB DNA fragments and 85 nm for short (250 bp) DNA fragments. Extended DNA molecules are desired for accurate measurements of DNA length and for further localisation of site-specific binding of proteins to DNA molecules. DNA images obtained from previously described cations (Mg^{2+}, Ca^{2+}, Ni^{2+}) present in the deposition buffer were analysed to determine the contour length of the visualised molecules (Figure 3.11).

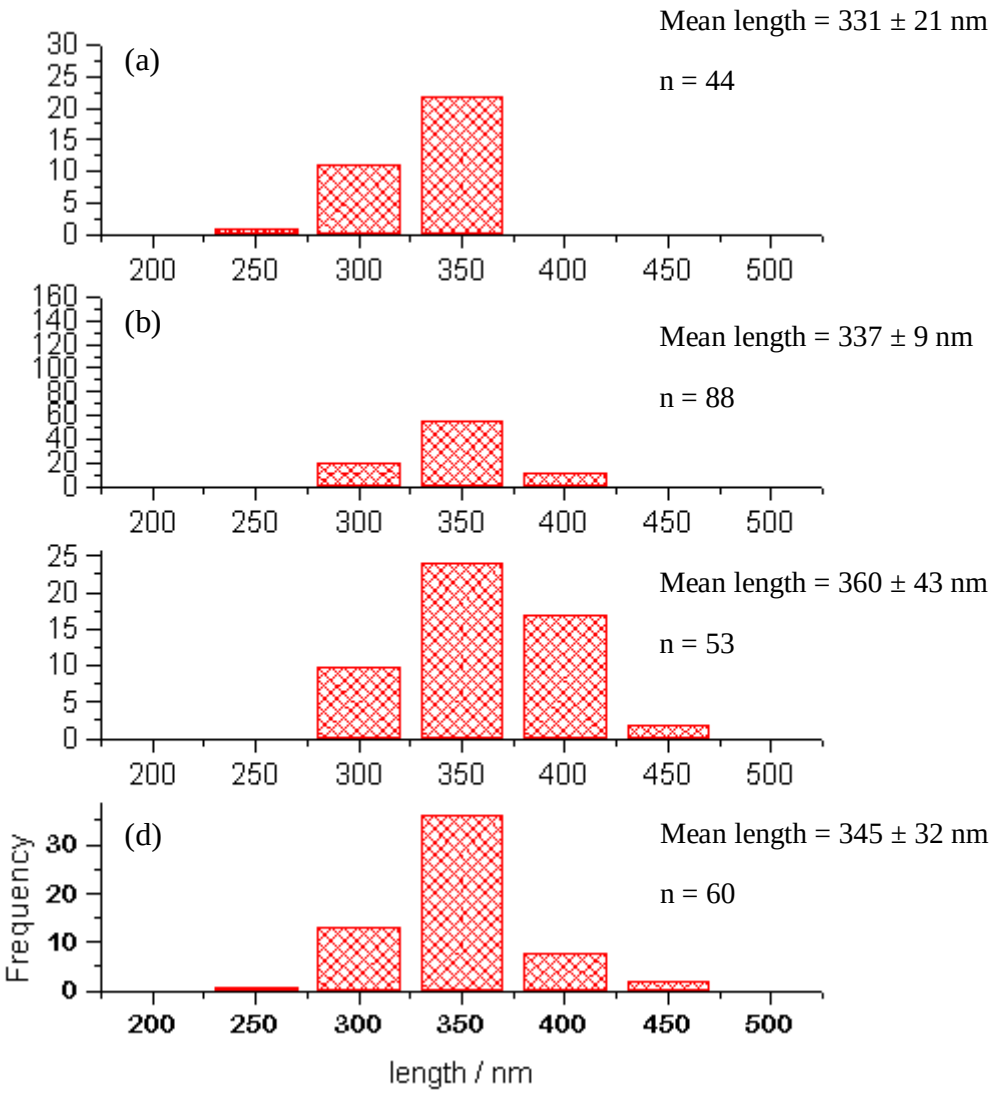

Figure 3.11. Distribution of contour lengths of DNA (1 kB) obtained by varying the cation type present in the deposition buffer; (a) Mg^{2+} ions; (b) Ca^{2+} ions; (c) Ni^{2+} ions and (d) Mg^{2+} ions and PLL treated mica.

The length distribution obtained for different cations should be in an agreement to the theoretical value of 340 nm (0.34 nm × 1000 bp). The largest spread in contour length values was observed after Ni^{2+} and Mg^{2+} (after mica pre-treatment with PLL) was used, however the mean value of 345 ± 32 nm obtained for DNA length measurements in the

presence of Mg^{2+} in the presence of PLL was the closest to the theoretical value, however, higher values may represent possible distortion of the helix. The length distribution measured for shorter DNA (250 bp) deposited on mica pre-treated with PLL and Mg^{2+} in the solution showed a mean length of 84 ± 4 nm, close to the theoretical value (85 nm) (Figure 3.12). Contour lengths of shorter DNA fragments were easier to measure than longer fragments due to the absence of coiling and therefore reducing errors in their measurement. In addition, short DNA fragments ≤ 400 bp have been reported to not condense due to the small attractive interactions per base pairs (Widom and Baldwin, 1980). DNA condensation occurs when *ca.* 70 – 90 % of its charge is neutralised by multivalent cations (Blumfield, 1997).

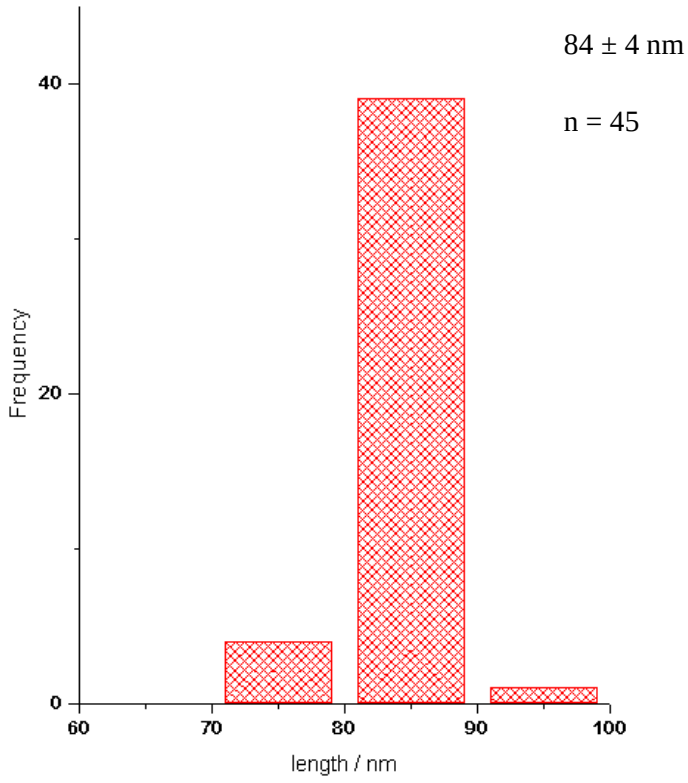

Figure 3.12. Distribution of contour lengths of DNA (250 bp) deposited on mica surface pre-treated with PLL.

3.2.3 Height and width measurements of DNA molecules imaged with AFM

The theoretical diameter of a DNA molecule, deduced from the Watson-Crick model, is 2 nm (Watson and Crick, 1953). The height of DNA molecules adsorbed on mica, as measured by tapping mode AFM, however, is always less than the theoretical value, *e.g.*, 0.5 nm (Liu *et al.*, 2005), 0.7 nm (Moreno-Herrero *et al.*, 2003) and 0.8 nm (Yunchang *et al.*, 2004). Under ambient conditions, DNA molecules are embedded in a salt layer, used for binding molecules to the mica surface, which distorts measured DNA height. In water, DNA molecules become fully hydrated (the salt layer is not present) and an increase in height has been reported, although, the theoretical height of 2 nm is not obtained (Lyubchenko *et al.*, 1992; Kasas, *et al.*, 1997; Moreno-Herrero *et al.*, 2003). Dehydration of the sample, mechanical deformation of the molecule induced by the AFM tip, the attractive capillary forces mediated by the thin water layer on the sample surface, attractive interactions with the mica surface and humidity, all play a role in the reduction of DNA height measurements.

In air, the presence of salt, mainly NaCl and $MgCl_2$, in the buffers during DNA preparation, can be used to account for the appearance of holes or other defects not present on a fresh mica surface. Moreno-Herrero *et al.* (2003) suggested that the salt layers are almost always present on mica when DNA is prepared from a buffer solution. After drying of a prepared sample, DNA molecules become trapped in this salt layer. Sometimes this layer is not complete and exposes the underlying mica.

Another possible source of height reduction is due to the induced strain owing to the compression of the DNA molecule by the electrostatic interaction of the molecule with the mica surface. In aqueous solutions, electrostatic forces are very high and keep molecules away one from each other; this electrostatic interaction binds the molecules to the substrate (DNA is a highly charged polymer). A model of height reduction of measured DNA molecules has been proposed for air and liquid by Moreno-Herrero *et al.* (2003) (Figure 3.13).

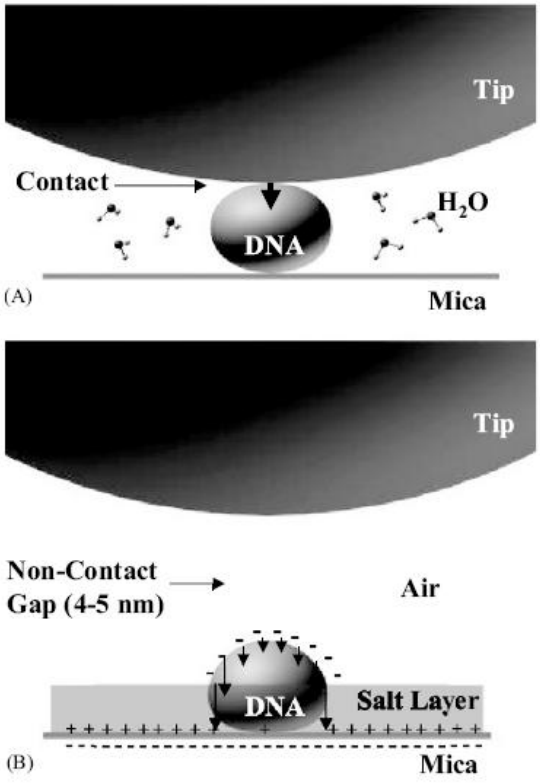

Figure 3.13. DNA height reduction in measurements obtained in liquid (a) and in air (b); adapted from Moreno- Herrero *et al.* (2003).

DNA imaged in aqueous solution, where no salt layer is present (Figure 3.13a), exhibits a height less than the theoretical value due to compression of the molecule by the tip. The height reduction measured in air (Figure 3.13b) may be due to the electrostatic

interaction between the biomolecule and the mica surface and also the presence of the salt layer, hydrated layer or capillary layer.

The height measurement has been obtained for the DNA molecules deposited on the mica surface in the presence Mg^{2+}, Ca^{2+} and Ni^{2+} imaged in air. The holes indicating voids in the salt layer, created during drying of the surface, were observed. Part of the molecule, trapped in the layer of salt, was observed to be faint on the lighter background; whereas, brighter parts of the DNA molecules and darker mica were attributed to the salt layer being removed from mica, (Figure 3.14).

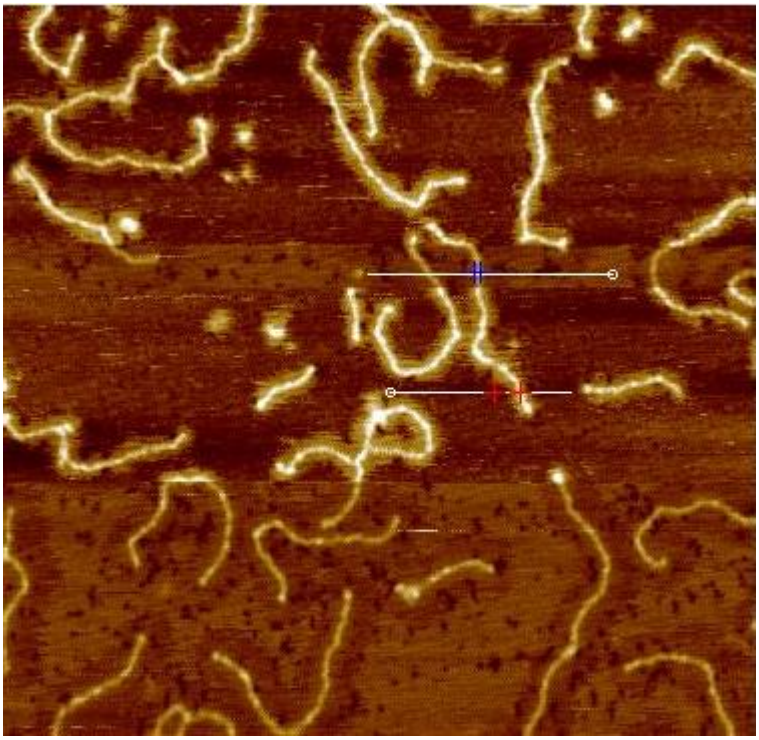

Figure 3.14. Typical AFM image (in air) of DNA (1 kB) adsorbed on the mica surface in the presence of $CaCl_2$. Line-profiles denote positions where heights and widths were measured. DNA is partially covered by the salt layer remaining on the surface after deposition; size: 1 µm × 1 µm; z-scale 2 nm.

For DNA deposited in the presence of Ca^{2+} ions, heights and widths of DNA molecules in the absence of salt layers were found to be 0.81 nm and 8.0 – 10.0 nm, respectively

(Figure 3.15a,b). In the presence of the salt layer, the height and width were 0.43 nm and 8.0 nm, respectively (Figure 3.15c,d).

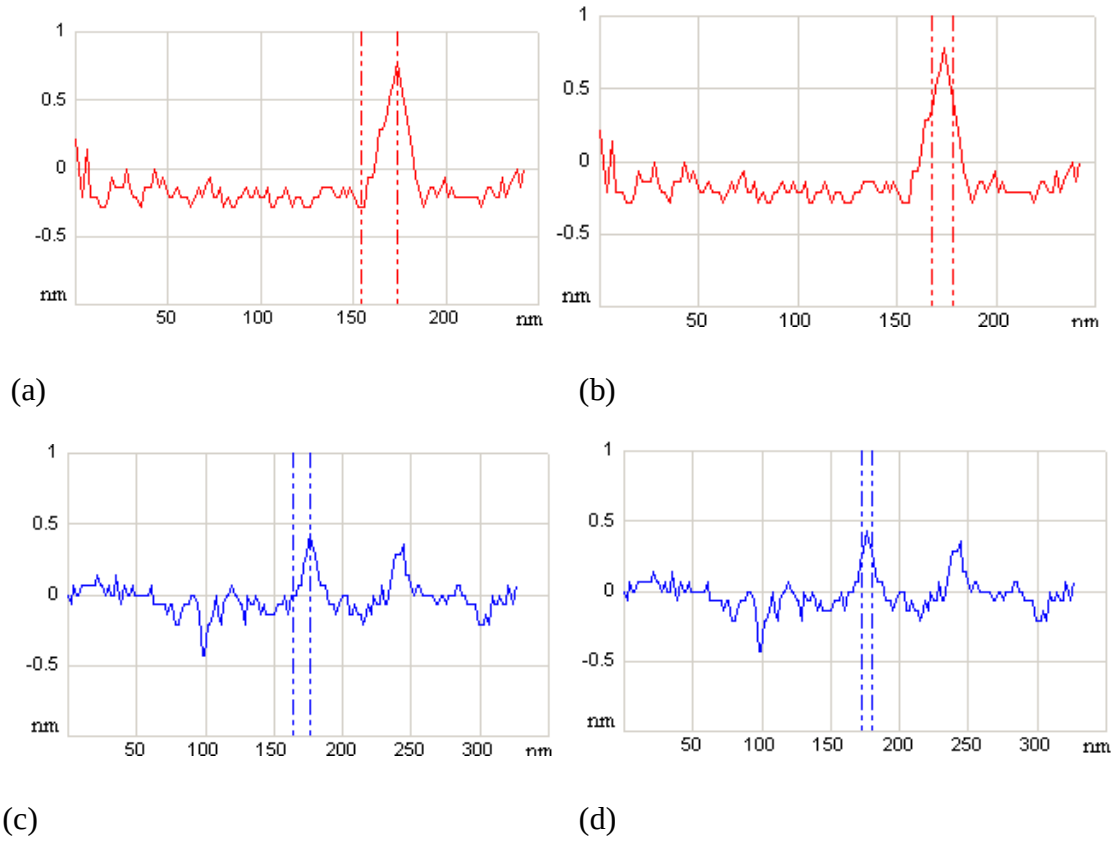

Figure 3.15. Line-profiles showing heights (left hand side) and widths (at half height; right hand side) of DNA molecules in the absence (a,b) and presence (c,d) of a salt layer.

According to the tip dilation phenomena (broadening of the lateral dimensions of the surface topography, where the vertical resolution of AFM is not affected by the finite size of the probe), the higher molecules look wider. This was confirmed by the current measurements, where smaller DNA heights in the presence of salt appeared thinner (3.15a,c). The height of the basal salt layer was found to be 0.35 nm (Figure 3.16).

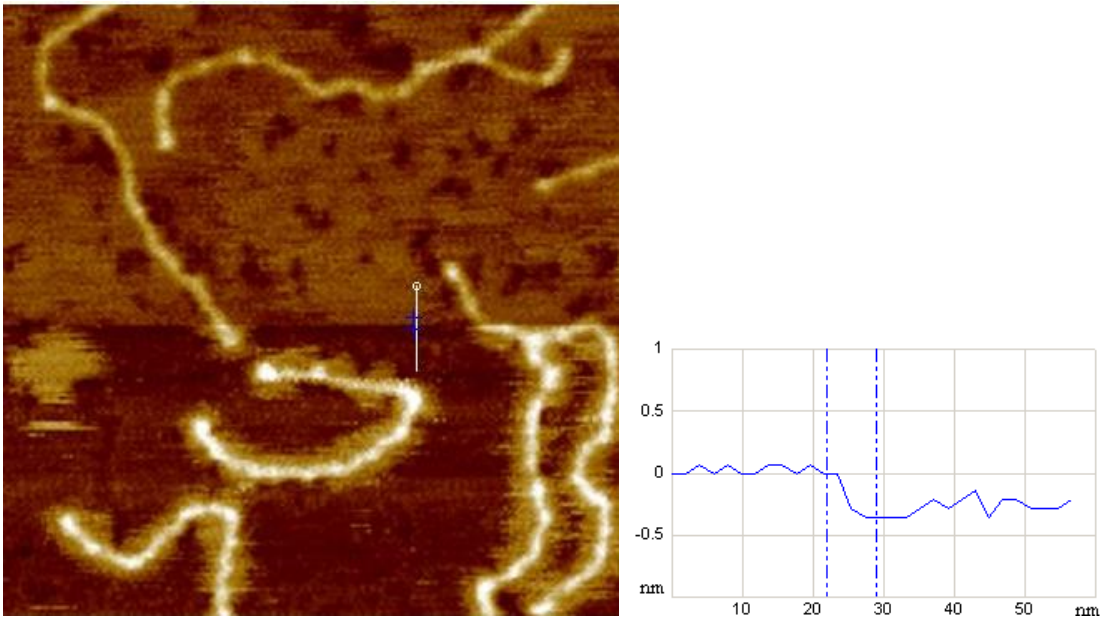

Figure 3.16. AFM image and line-profile showing thickness of salt layer (0.35 nm); size: 387 nm × 387 nm.

The height of DNA observed in the salt layer was about half of the value of molecules free from salt (0.43 and 0.81 nm, respectively), which corresponds to the value of the measured basal salt layer (0.35 nm). A similar trend was observed by Moreno-Herrero *et al.* (2003), where heights of DNA molecules embedded in the salt layer were found to be lower (0.70 ± 0.20 nm) than those obtained in the absence of the salt layer (1.50 ± 0.20 nm); however, the latter value was higher than corresponding values found in the present work.

The occurrence of broadening caused by the tip radius (Bustamante *et al.*, 1992) is the reason why widths of DNA appear to be larger (11 – 14 nm) than the theoretical values (Allen *et al.*, 1992; Vesenka *et al.*, 1994; Ramirez-Aguilar and Rowlen, 1998).

The nominal value of the tip radius (10 nm) used for DNA imaging (NSG01; NT-MDT, Russia) was used to calculate the width using the model described by Engel, *et al.* (1997). The DNA was assumed to have a cylindrical shape, which links the apparent and the real widths of a spherical sample, the width at half-maximum could be calculated (Equation 3.1).

$$S = 2\sqrt{RD + \frac{D^2}{4}} \approx 2\sqrt{RD} \qquad \text{(Equation 3.1)}$$

where S is the width measured at half-height, R is the tip radius (10 nm), D is the true width of the molecule (2 nm). The approximation is valid when $R \geq D$, which is usually the case. The theoretical value of the width measured at half-height was found to be 8.9 nm, which is in close agreement with the experimentally measured width.

An increase of height of the DNA, in the absence of salt layer, was observed for all cations. The measured heights of DNA molecules (embedded in the salt layer) in the presence of Mg^{2+}, Ni^{2+} and Ca^{2+} were found to be 0.50 ± 0.06 nm, 0.57 ± 0.12 nm and 0.43 ± 0.05 nm, respectively; whereas, measurements of DNA taken in regions of the sample where the salt layer had been removed were almost double: 0.90 ± 0.05 nm, 1.03 ± 0.14 nm and 0.81 ± 0.21 nm, respectively. The height measurements of DNA in the presence of different cations, in the absence and presence of the salt layer, are shown in Figure 3.17.

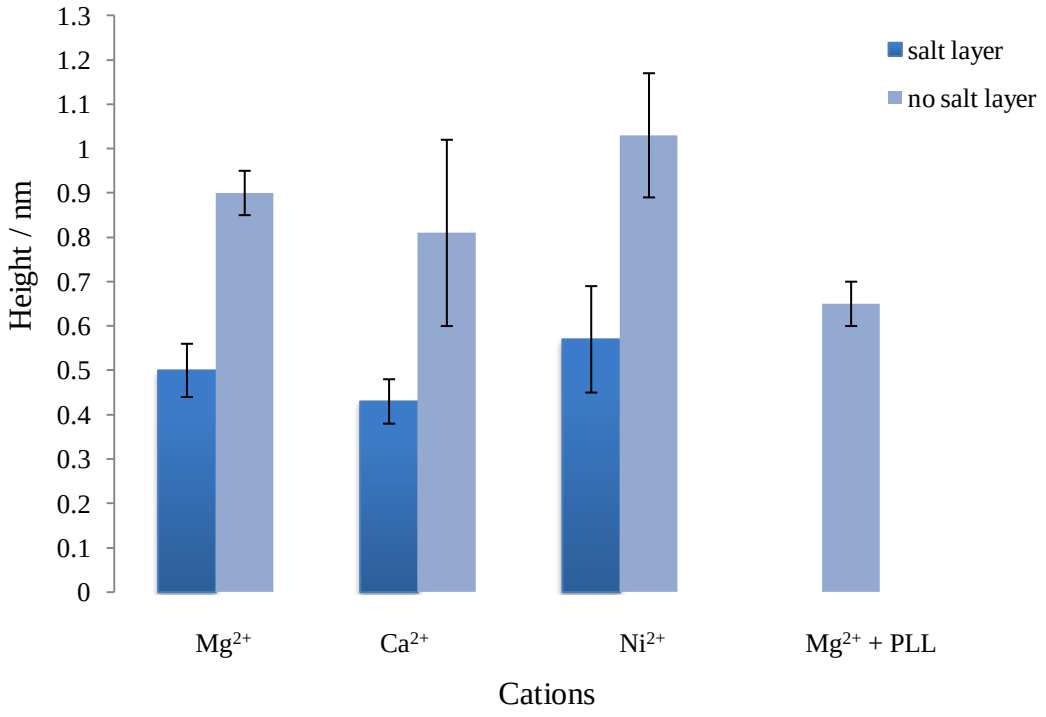

Figure 3.17. Height measurements of DNA molecules after deposition from HEPES buffer containing different cations in the presence (dark bars) and absence (light bars) of salt layers; n = 25 (Mg^{2+}), n = 50 (Ca^{2+}), n = 25 (Ni^{2+}), n = 25 (Mg^{2+} + PLL). Error bars show SD.

The heights of DNA molecules were dependent on the presence of a salt layer, but less dependent on the type of cation. The lowest height (0.43 ± 0.05 nm) was recorded for DNA in the presence of a salt layer from a deposition buffer containing Ca^{2+} ions.

The holes, indicating voids in the salt layer, were not observed after mica pre-treatment with PLL and the measured height of DNA molecules in the presence of Mg^{2+} was found to be 0.65 ± 0.05 nm. This value is greater than the heights of DNA embedded in salt layers obtained with Mg^{2+}, Ca^{2+} and Ni^{2+}, but lower than DNA heights deposited in the absence of the salt layers from these cations. The influence of the salt layer, the greatest source of error, could be eliminated by pre-treating the mica with PLL.

Similar comparisons were made between measured widths of DNA molecules in the absence and presence of salt layers from deposition buffers containing Mg^{2+}, Ca^{2+} and Ni^{2+} ions (Figure 3.18).

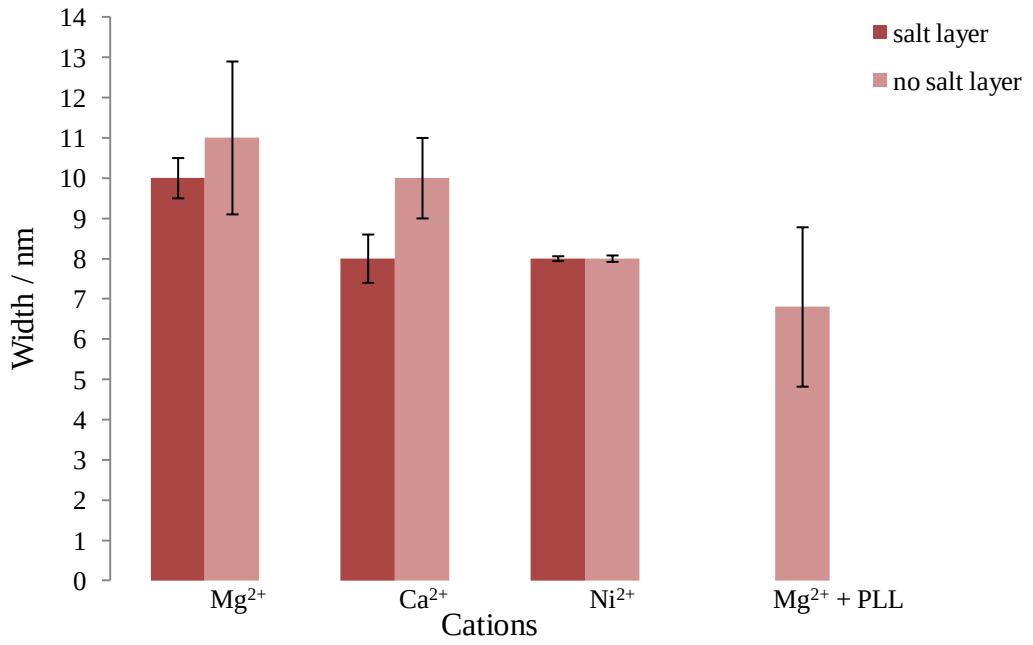

Figure 3.18. Width measurements of DNA molecules after deposition from HEPES buffer containing different cations in the presence (dark bars) and absence (light bars) of salt layers; n = 25 (Mg^{2+}), n = 50 (Ca^{2+}), n =25 (Ni^{2+}), n = 25 (Mg^{2+} + PLL). Error bars show SD.

Width measurements of molecules embedded in the salt layer showed little variation with the type of cation used in the deposition buffer. In the presence of the salt layer, measured widths were generally smaller (Mg^{2+} = 10.0 ± 1.0 nm; Ca^{2+} = 8.0 ± 1.0 nm, Ni^{2+} = 8.0 ± 0 nm) than those not associated with a salt layer (11.0 ± 2.0 nm; 10.0 ± 1.0 nm and 8.0 ± 0 nm, respectively).

3.2.4 DNA imaging in aqueous environments

Initially, DNA was imaged in a liquid environment in the presence of Ni^{2+} ions, although it was unknown as to whether these species may affect DNA-EcoR124I activity and/or interactions (Chapter 4). Mg^{2+} ions are known to provide only weak binding between DNA and mica and so are not generally suited for AFM imaging in liquid.

Both Ni^{2+} and Mg^{2+} ions were investigated. Tapping mode AFM images were acquired in pure water, using the same tip and procedure, for both cation treatments (Figure 3.19); DNA height and width measurements were also obtained.

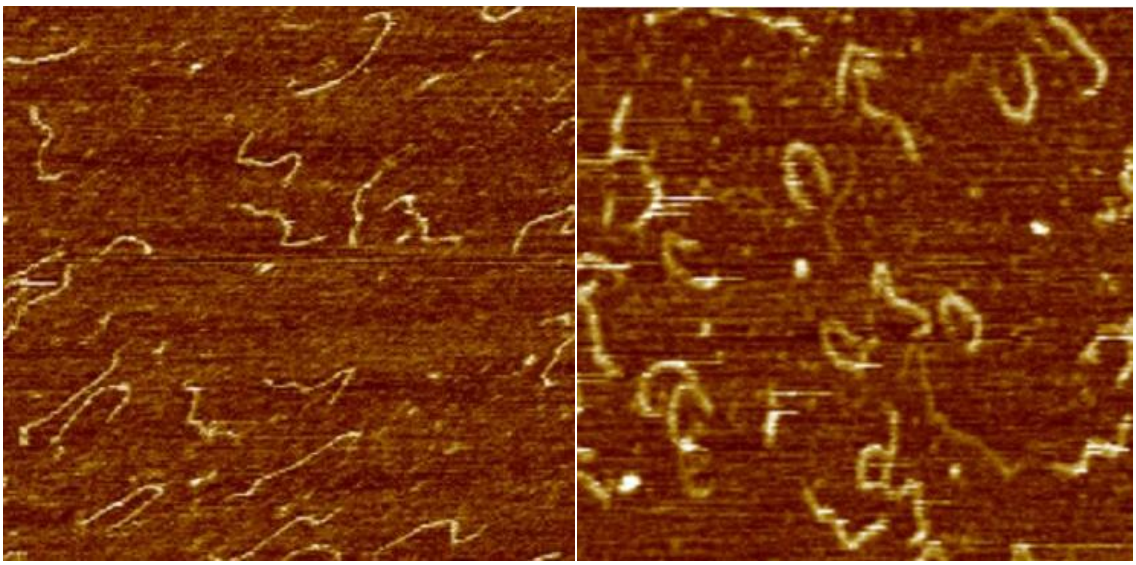

(a) (b)

Figure 3.19. Typical AFM images of DNA (1 kB) obtained in pure water on PLL pre-treated mica from a HEPES (20 mM; pH 7.4) deposition buffer containing (a) $NiCl_2$ (10 mM) and (b) $MgCl_2$ (10 mM); sizes (a) 492 nm × 492 nm; z-scale 2 nm; (b) 533 nm × 533 nm; z-scale 3 nm.

Images in water could be obtained when the mica surface was pre-treated with PLL, as observed by Bussiek *et al.* (2003). A 2 min incubation on mica allowed visualisation of DNA structure in aqueous solution for both Ni^{2+} and Mg^{2+} cations. In a control experiment, where mica was not pre-treated with PLL but in the presence of Mg^{2+}, DNA strands were not observed. DNA height and width measurements (NanoScope software) obtained when Ni^{2+} was present in the deposition buffer were found to be 0.72 ± 0.10 nm and 5.0 ± 1.0 nm, respectively. Even without direct measurement, a visible difference in DNA width could be observed when compared to strands deposited from an Mg^{2+}-containing buffer. DNA molecules imaged on the Ni^{2+}-treated surface appeared thinner and more stretched. These observations were confirmed using height measurements where the width measured using Mg^{2+} was 9.0 ± 1.0 nm; the height of the DNA also increased to 0.85 ± 0.07 nm, larger than that measured using Ni^{2+} ions (0.72 ± 0.10 nm; n = 30 molecules for each cation).

The height of DNA molecules measured in the presence of Mg^{2+} in water (0.85 ± 0.07 nm) was larger than that observed in air (0.65 ± 0.05 nm). In the presence of Ni^{2+} ions, the height in water (0.72 ± 0.1 nm) was less than that in air (1.03 ± 0.14 nm) (after the salt layer was removed) and larger than values obtained for molecules trapped in the salt layer (0.57 ± 0.12 nm). The comparison in the former case, however, could not be made due to the fact that in air the widths and heights of measured DNA molecules were obtained without PLL pre-treatment of mica.

Imaging in water, with Mg^{2+} ions, did not improve the width measurements (9.0 ± 1.0 nm and 7.0 ± 2.0 nm in water and air, respectively), therefore the visualisation of DNA-

protein complexes was performed an air, as it is a simpler and more reproducible method.

3.3 Conclusions

A range of experiments based on DNA immobilisation on mica in the presence of different cations was obtained to optimise imaging of DNA, necessary for the study of subsequent protein (EcoR124I)-DNA interactions. PLL deposited on the mica prior to DNA immobilisation provided a uniform layer; the height and width measurements were obtained without the uncertainty produced by the partially present salt layer. The contour length of measured DNA strands in the presence of PLL on mica compatible with the theoretical value. Mg^{2+}, necessary to determine the optimal conditions for the enzyme activity and absolutely required for restriction by EcoR124I in the native environment, seemed to be the most suitable cation for DNA-protein studies. Imaging in liquid, in the presence of Mg^{2+}, did not improve the accuracy of width measurements, necessary for further molecular volume calculation, therefore DNA-proteins visualisation (Chapter 4) was performed in air, an easier and more reproducible method.

Chapter 4

AFM imaging of the EcoR124I-DNA complex

4.1 Introduction

4.1.1 Imaging of DNA-protein complexes

AFM has been widely used for visualisation of DNA-protein complexes (Lyubchenko *et al.*, 1995; Berge *et al.*, 2000; van Noort *et al.*, 2004; Bennink *et al.*, 2003). These have included Type I R-M enzymes, mostly EcoKI (Ellis *et al.*, 1999; Berge *et al.*, 2000; Neaves *et al.*, 2009) and EcoR124I (van Noort *et al.*, 2004). Whilst the distinction between proteins and DNA is obviously straightforward, observing differences between subunit composition of fully functional complexes with DNA is very difficult and requires many observations and detailed image analysis. The previous chapter described the background observations necessary to this work, including optimising visualisation of DNA and the effect of different cations.

The visualisation of DNA interacting with proteins may be inhibited when molecules are fixed to the mica surface without the ability for movement. Loose-binding to the surface is necessary as parts of the DNA must be free to move around and interact with proteins, although other parts of the molecule must be tethered to the supporting surface to prevent movement by the AFM tip. This will enable AFM imaging of complexes at a resolution sufficient to follow dynamic interactions (Bennink *et al.*, 2003). When Mg^{2+} is present in the deposition buffer, these ions partly exchange K^{+} at the mica surface

(Hansma and Lanley, 1996). Additionally, Mg^{2+} is extremely important in maintaining enzyme activity (Aggrawal, 1995), binding to the DNA molecules (Thielking *et al.*, 1992) and is essential for DNA translocation and cleavage activity.

4.1.2 Molecular volume

The orientation of proteins on a surface and the electrostatic interactions between macromolecules and the tip can affect AFM height measurements of proteins (Muller and Engel, 1997). Viani *et al.* (1999) showed a linear dependence between protein volume, determined by AFM, and molecular mass. Volume measurements have become a reliable method to obtain the stoichiometries of protein-protein assemblies (Schneider *et al.*, 1998) and for the determination of protein-protein association constants (Ratcliff *et al.*, 2001).

The molecular volume of the proteins based on molecular weight of the molecules (V_c) have been determined using Equation 4.1 (Edstrom *et al.*, 1990) and predicted from the particle dimensions derived from AFM images (V_m) (Equation 4.2) (Schneider *et al.*, 1998)

$$V_c = \left(\frac{M_0}{N_0}\right)(V_1 + dV_2) \qquad \text{(Equation 4.1)}$$

where M_0 = the molecular mass of protein, N_0 = Avogadro's number (6.022×10^{23} mol^{-1}), V_1 = the partial specific volume of the protein (0.747 cm^3 g^{-1}), V_2 = the partial

specific volume of water (1 cm^3 g^{-1}) and *d* = the extent of protein hydration (assumed to be 0.4 mol H_2O / mol per protein, and

$$V_m = \left(\frac{\pi h}{6}\right)(3r^2 + h^2) \qquad \text{(Equation 4.2)}$$

where *h* = the particle height and *r* = the radius at half height of the protein, with the assumption that the protein is spherical.

4.1.3 Adenosine 5'-O-(3-thio)triphosphate

Adenosine 5'-O-(3-thio)triphosphate (ATP-γ-S; Figure 4.1b) is a close, non-hydrolysable analogue of ATP (Figure 4.1a), where one of the γ-phosphate oxygen atoms is replaced by a sulphur atom. ATP-γ-S functions as an inhibitor of ATP-dependent processes and is hydrolysed at a dramatically slower rate than ATP.

Adenosine 5'-(β,γ-imido) triphosphate (AMP-pnp; Figure 4.1c) is one of the competitive inhibitors in most of the ATP-dependent systems and binds in the same manner to ATP, although it cannot be hydrolysed. The N atom placed between the β- and γ-phosphate groups, as a replacement of the oxygen, prevents the transfer of the γ-phosphate to the substrate peptide during hydrolysis.

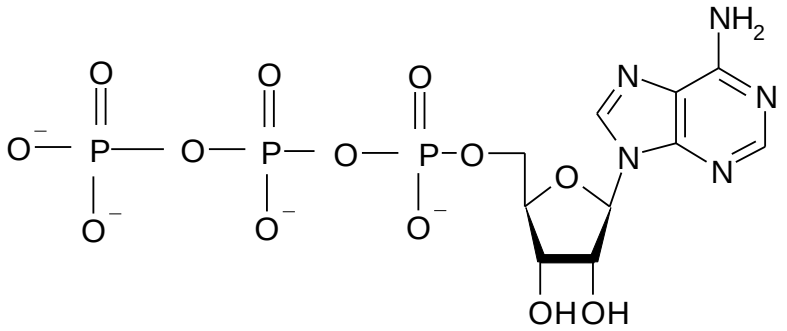

(a)

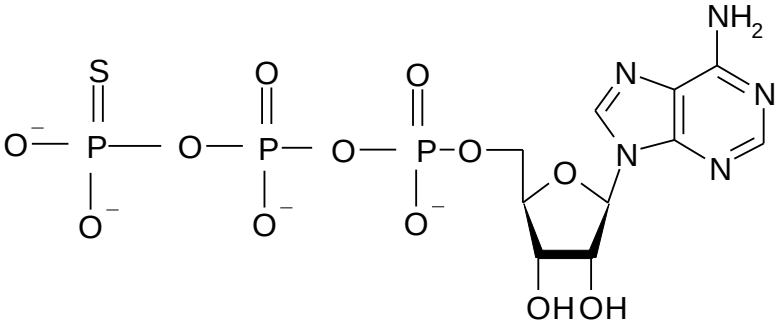

(b)

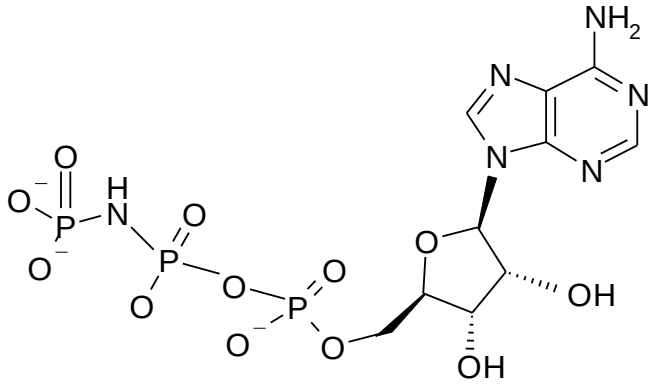

(c)

Figure 4.1. Chemical structures of (a) adenosine 5′-triphosphate (ATP), (b) adenosine 5'-O-(3-thio)triphosphate (ATP-γ-S) and (c) adenosine 5'-(β,γ-imido)triphosphate (AMP-pnp).

4.1.4 Aims

Visualisation of MTase and HsdR subunits directly deposited on mica was investigated to provide stable attachment of proteins necessary for further force spectroscopy studies to measure protein-protein interactions (Chapter 6). The assembly of the EcoR124I holoenzyme, bound to DNA on mica, was performed, where the specific binding of the enzyme to DNA was identified by length measurements of DNA fragments (DNA was designed to have a recognition sequence for EcoR124I in the middle or at 1/3 of the length of the DNA strands). The influence of Mg^{2+}, Ca^{2+} and Ni^{2+} cations, which affect immobilisation (Chapter 3), on molecular motor assembly was studied. Molecular volume measurements from the sizes of imaged molecules were obtained for subunits and complexes directly deposited on mica and bound to DNA to confirm subunit assembly or detect eventual dimerisation. The translocation activity of the enzyme was confirmed in the presence of ATP. The influence of ATP analogues on the holoenzyme assembly and stability, was also investigated.

4.2 Results and discussion

4.2.1 MTase and MTase-DNA complexes on mica

Initial experiments to determine the dimension of the proteins of the EcoR124I R-M enzyme involved visualisation of MTase on mica and specifically bound to DNA.

4.2.1.1 AFM imaging

The first step in the study of assembly of the holoenzyme was to visualise MTase (the core of the EcoR124I enzyme; M_2S_1) directly deposited on the mica surface (in the presence of Mg^{2+}, Ca^{2+} and Ni^{2+} ions in the deposition buffer) and compare the height and width parameters with MTase bound to DNA (1 kB). In addition, it was important to demonstrate specific DNA binding by confirming that the recognition binding site for MTase was at the centre or at 1/3 of the length of the DNA.

The MTase was incubated with the DNA in the ratio 2:1. Only 2 complexes (from 7 images) were observed for MTase bound to DNA in the presence of Ni^{2+} ions, of which only one was specifically bound; the remainder of the DNA molecules did not have proteins attached (data not shown). The lack of DNA-MTase complexes was assumed to be due to very tight binding of the DNA to the mica in the presence of Ni^{2+} ions or an influence of Ni^{2+} itself on MTase binding to DNA. The efficient interaction between DNA and MTase was therefore considered to be compromised and Ni^{2+} was disqualified from further investigations.

The ability of Ca^{2+} to promote DNA binding without catalysis has been widely used to mimic Mg^{2+} in equilibrium binding and structural studies to give an inactive enzyme-Ca^{2+}-DNA complex (Vipond and Halford, 1995; Newman *et al.*, 1998; Galburt and Stoddard, 2002; Yang *et al.*, 2006;). DNA-MTase complexes were prepared using $CaCl_2$ (10 mM) in place of $NiCl_2$ in the deposition buffer. However, very few DNA-

MTase complexes were observed (Figure 4.2). It is known that enzymes acting with nucleic acids sometimes show a lack of activity with Ca^{2+} ions.

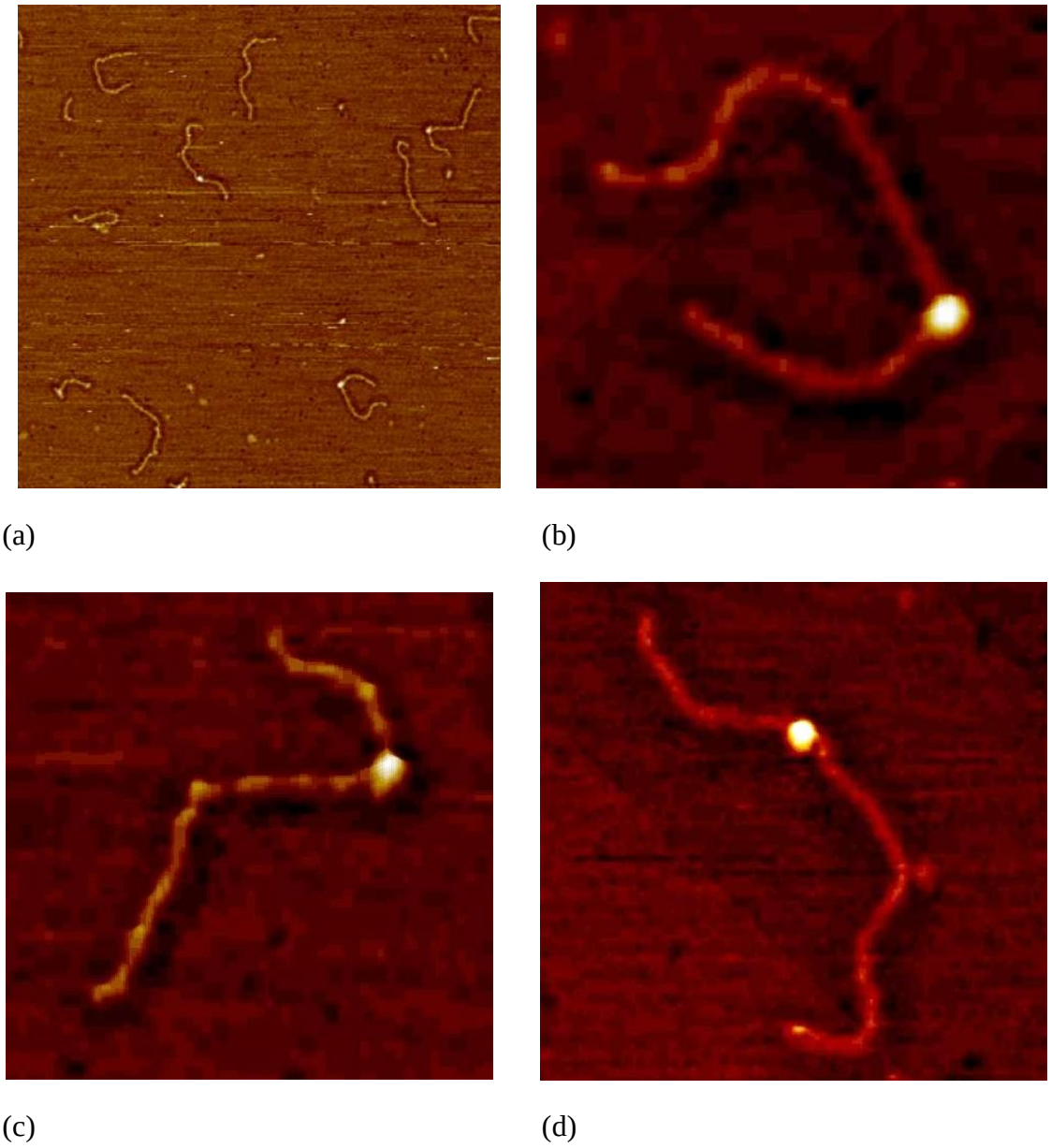

Figure 4.2. Typical AFM images (in air) of MTase specifically bound to DNA (1 kB, recognition site at 1/3 along length) on mica. Sample deposited from HEPES buffer (20 mM; pH 7.4) containing $CaCl_2$ (10 mM); (a) MTase bound to DNA where only few complexes could be observed; MTase bound to binding site (1/3 of DNA length); sizes (a) 1.6 × 1.6 µm; z-scale 2 nm; (b-d) magnifications of (a).

MTase was next visualised on untreated mica (adsorption) and PLL pre-treated mica. However, in the absence of PLL, not many MTase proteins could be observed in repeated experiments. With PLL, isolated MTase molecules were uniformly deposited over the mica surface (Figure 4.3).

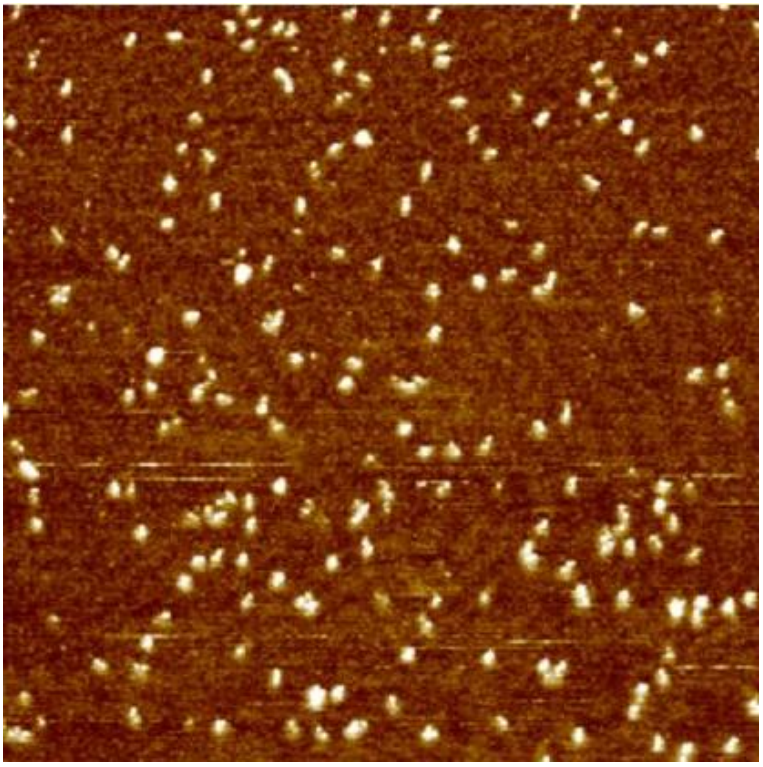

Figure 4.3. A typical AFM image of MTase (diluted to 10 nM) on PLL pre-treated mica deposited from HEPES buffer (20 mM; pH 7.4) containing $MgCl_2$ (5 mM); size 1.4 µm × 1.4 µm; z-scale 2 nm.

4.2.1.2 Dimensions of surface-bound MTase and MTase-DNA complexes

The heights and widths of MTase proteins and MTase-DNA complexes were next determined using the NanoScope software (Chapter 2). A line-profile across 3 MTase molecules shows the homogeneity of their measured heights (1.36 nm) and widths (21 nm) (Figure 4.4).

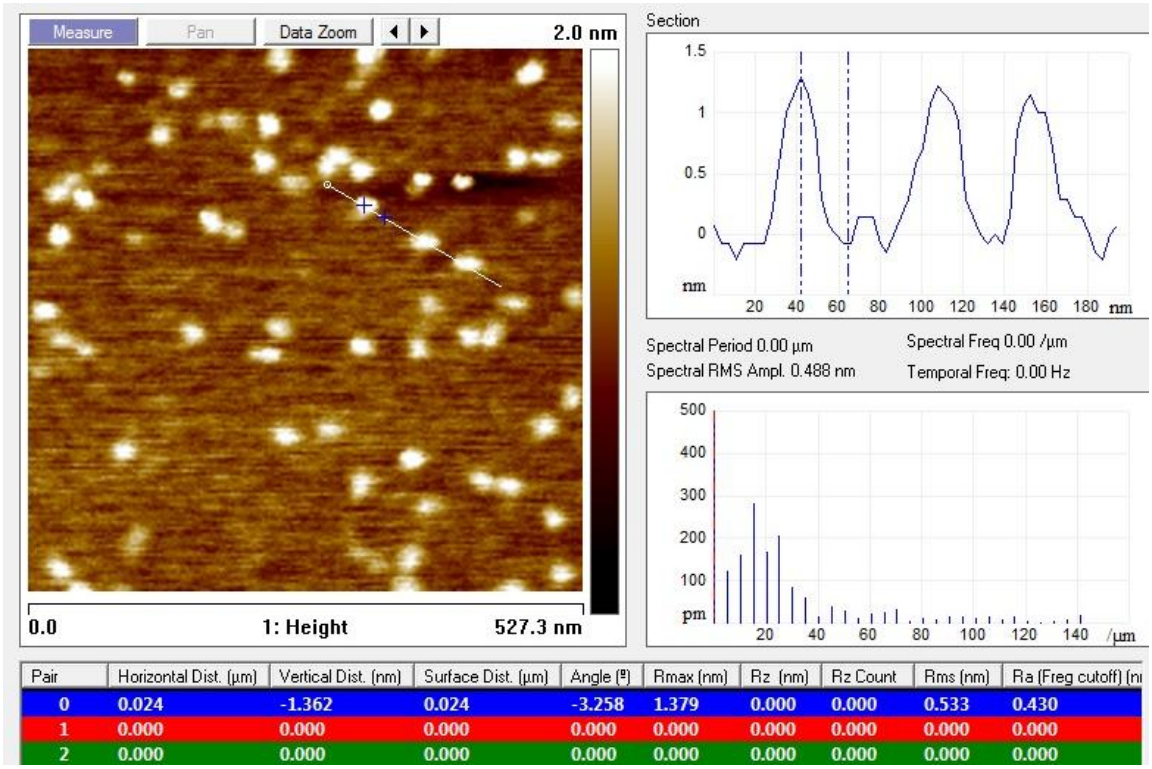

Pair	Horizontal Dist. (µm)	Vertical Dist. (nm)	Surface Dist. (µm)	Angle (º)	Rmax (nm)	Rz (nm)	Rz Count	Rms (nm)	Ra (Freq cutoff) (n
0	0.024	-1.362	0.024	-3.258	1.379	0.000	0.000	0.533	0.430
1	0.000	0.000	0.000	0.000	0.000	0.000	0.000	0.000	0.000
2	0.000	0.000	0.000	0.000	0.000	0.000	0.000	0.000	0.000

Figure 4.4. A typical line-profile across 3 MTase molecules showing similar heights and widths.

Height and width measurements of single molecules were obtained from horizontal and vertical sections through their centres. The tip-convolution effect was minimised by taking width measurements at half-height. The mean heights of MTase proteins bound to DNA were larger (1.60 ± 0.08 nm) than those directly deposited on mica (1.35 ± 0.07 nm; n = 30, obtained from 3 images (Figure 4.5). The conformation of proteins directly deposited on mica was more disorganised than MTase specifically bound to DNA and therefore an increase of height for MTase-DNA complexes would not necessarily be equal to a simple sum of their respective heights. A change in quaternary structure of MTase has been observed on binding to DNA, as evidenced by a reduction in size of the enzyme from 180 to 112 Å (Taylor *et al.*, 1994). The hinge bending domains in the HsdS subunit (which acts as a pivot for HsdM subunits) bound to the DNA was

proposed to determine the rotation of HsdM subunits towards the DNA. The average widths measured for both cases were comparable (21.0 ± 0.3 nm and 20.0 ± 0.5 nm for isolated and complexed proteins, respectively; Figure 4.5).

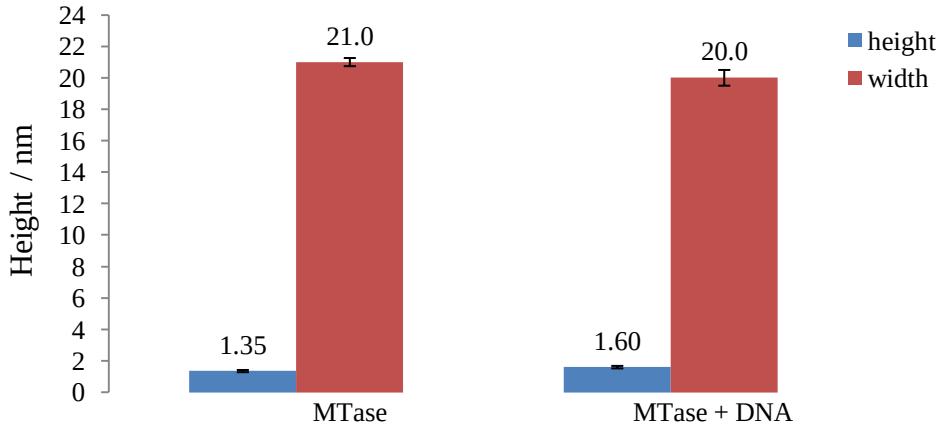

Figure 4.5. Mean height (blue columns) and width (red columns) of MTase proteins from isolated molecules (10 nM) and MTase-DNA complexes deposited on PLL pre-treated mica (n = 30).

The specificity of bound molecules was confirmed by measuring the distance from the bound proteins to the end of the DNA (ImageJ software) (Figure 4.6). The MTase recognition site was in the middle of the molecule for the 1 kB (Figure 4.6 a) and 250 bp DNA (Figure 4.6 b) and also at 1/3 along the length for a different 1 kB strand(Figure 4.6c). MTase may find the specific sites on DNA by two mechanisms (Berg *et al.*, 1981): diffusion from the buffer or non-specific binding at first and then moving along the DNA molecule until the specific binding sites is found (Dowd and Lloyd, 1990). A typical AFM image of MTase specifically bound to a central recognition site on DNA is shown in Figure 4.7.

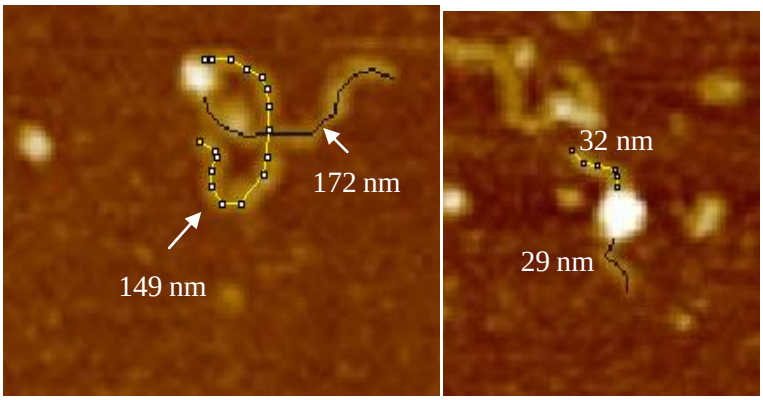

(a) (b)

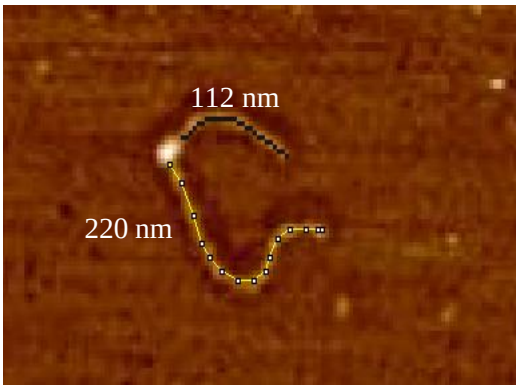

(c)

Figure 4.6 Length measurements of the arms of DNA determined with bound MTase. DNA with the recognition binding site in the middle: (a) 1kB; (b) 250 bp; and (c) DNA with the target site in 1/3 of the DNA length.

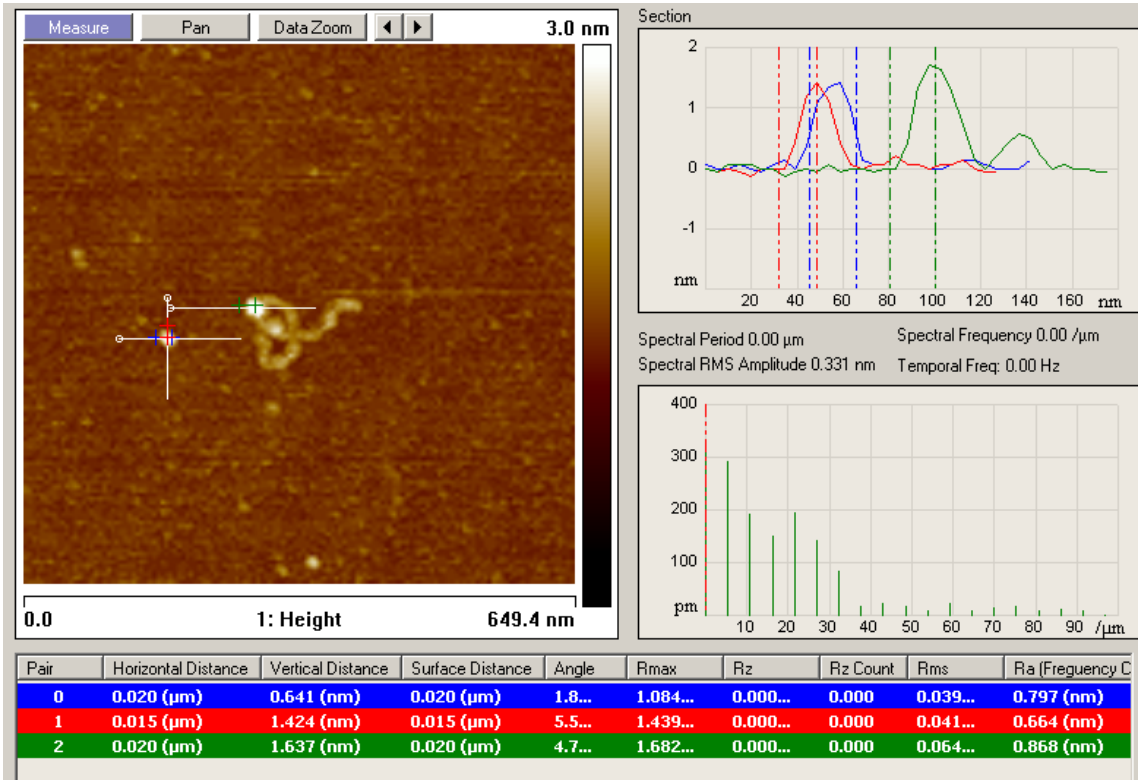

Figure 4.7. A typical AFM image of a specifically-bound MTase-DNA complex (height 1.64 nm) deposited on mica pre-treated with PLL in the presence of Mg^{2+} in HEPES deposition buffer; an unbound MTase (height 1.42 nm) is also seen; size 649 nm × 649 nm; z-scale 3 nm.

4.2.1.3 Molecular volume calculations of MTase and MTase-DNA complexes

To determine oligomeric states of proteins in large DNA-protein assemblies, volume analysis of proteins in the AFM images was required. Using Equation 4.2, the molecular volumes (V_m) of isolated MTase molecules and MTase specifically bound to DNA were calculated to be 235 ± 10 nm^3 and 253 ± 20 nm^3, respectively.

$$V_m = \left(\frac{3.14 \times 1.35}{6}\right)(3 \times 10.5^{\,2} + 1.35^2) = 235\ \text{nm}^3 \qquad \text{(Equation 4.3)}$$

The volume obtained from the molecular weight of the protein (V_c; Equation 4.1) was calculated to be 308 nm^3 (Equation 4.4).

$$V_c = \left(\frac{162000}{6.022 \times 10^{23}}\right)(0.747 + 0.4 \times 1) = 3.08 \times 10^{-19} \qquad \text{(Equation 4.4)}$$

$$V_c = 308 \text{ nm}^3$$

That V_m was less than V_c may be related to a number of factors: the conformation change of MTase specifically bound to DNA compared to being randomly deposited on mica; a flattening process of molecules interacting with mica resulting in reduced heights; and/or dehydration during sample drying. The latter explanation is likely to be the most important factor. For example, if the hydration value was halved, V_c becomes 254 nm^3. The homogeneity of the height, width and molecular volume data suggest that the imaged proteins were indeed MTase molecules.

4.2.2 AFM imaging of HsdR (motor) subunits

The HsdR subunit, responsible for the motor activity of the enzyme and necessary in the assembly of the R_1-complex and the holoenzyme (R_2-complex), was visualised in a similar manner to MTase using AFM. The HsdR(R124I), the hybrid subunit HsdR(PrrI) and a version of HsdR fused with GST (GST-HsdR(PrrI)) were used in these investigations.

HsdR molecules, diluted in deposition buffer (as for the MTase) to a concentration of 10 nM were adsorbed on PLL pre-treated mica and imaged using the AFM (Figure 4.8).

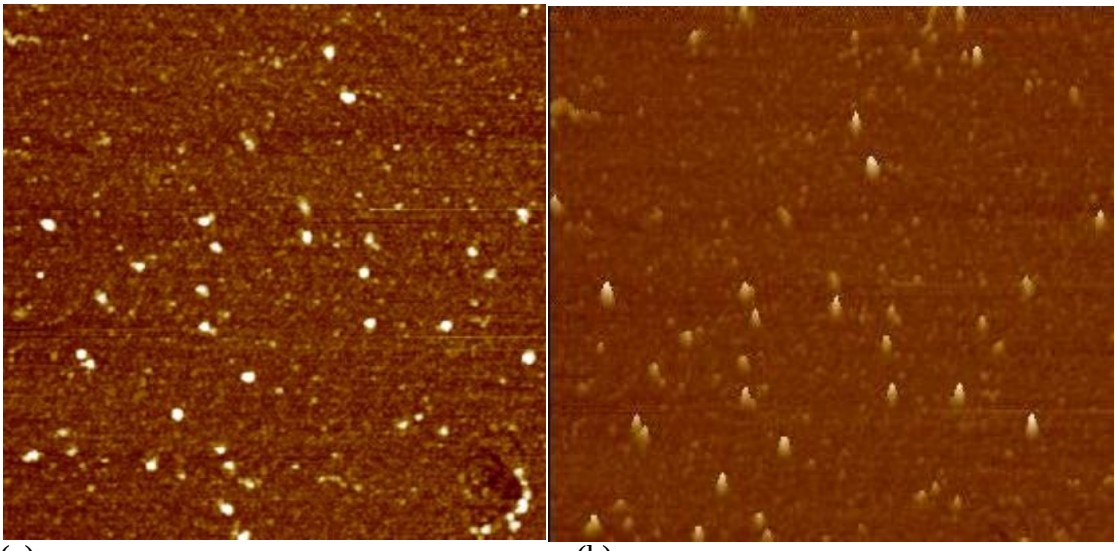

(a) (b)

Figure 4.8. Typical AFM images (in air) of purified HsdR(PrrI) (10 nM) subunits deposited from HEPES buffer (20 mM; pH 7.4) containing $MgCl_2$ (5 mM) on PLL pre-treated mica; size 977 nm × 977 nm; z-scale 2 nm; (a) 2D image; (b) pseudo-3D image (same area).

Single particles were observed for samples containing HsdR(R124I), HsdR(PrrI) and GST-HsdR(PrrI) and their dimensions are summarised in Table 4.1. V_m was calculated from height and width data

Table 4.1. Dimensions of HsdR(R124I), HsdR(PrrI) and GST-HsdR(PrrI) from AFM measurements (images not shown). Means and standard deviations are shown; n = number of molecules measured.

	Height / nm	Width / nm	V_m / nm^3	n
HsdR(R124I)	1.50 ± 0.05	19.0 ± 0. 3	215 ± 19	25
HsdR(PrrI)	1.50 ± 0.10	18.5 ± 1.1	208 ± 27	25
GST-HsdR(PrrI)	1.55 ± 0.05	20.0 ± 0.5	243 ± 21	53

GST-HsdR(PrrI) had the largest dimensions in keeping with the additional 26 kDa protein GST at the N-terminus. V_c was calculated to be 227 nm^3 for HsdR (R124I) and HsdR(PrrI) or 276 nm^3 for GST-HsdR(PrrI). The smaller values of V_m from AFM measurements could be due to flattening of the protein on the surface and protein dehydration during the drying process.

4.2.3 AFM imaging of assembled EcoR124I R_1-complex

Typical AFM images of R_1-DNA (250 bp and 1 kB) complexes (Section 2.11.1.6) are shown in Figure 4.9.

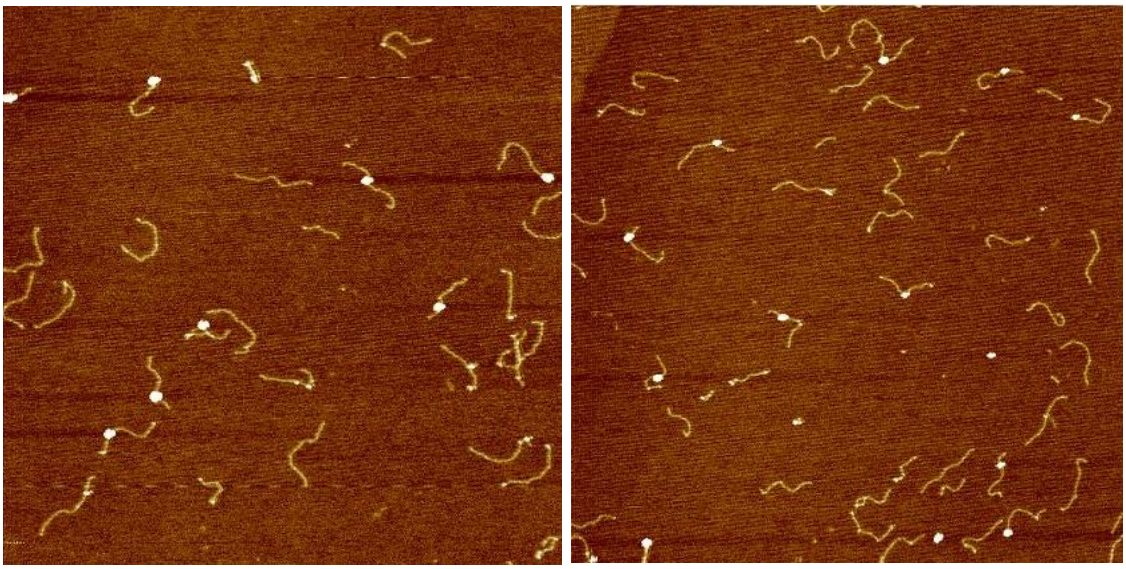

(a) (b)

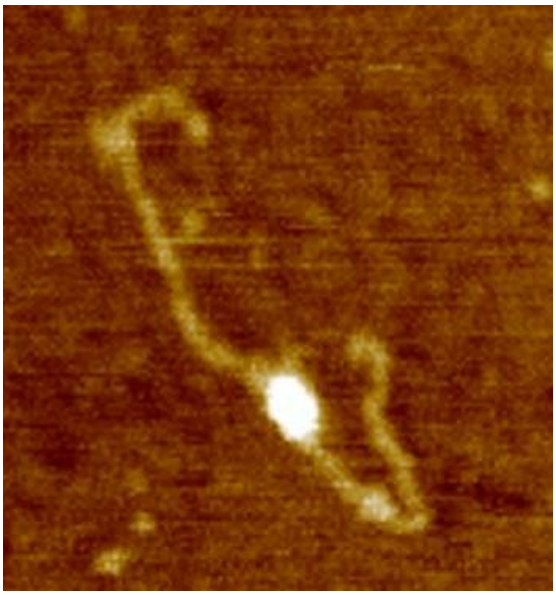

(c)

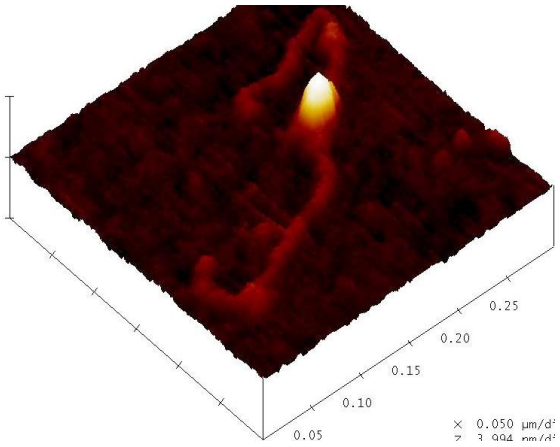

(d)

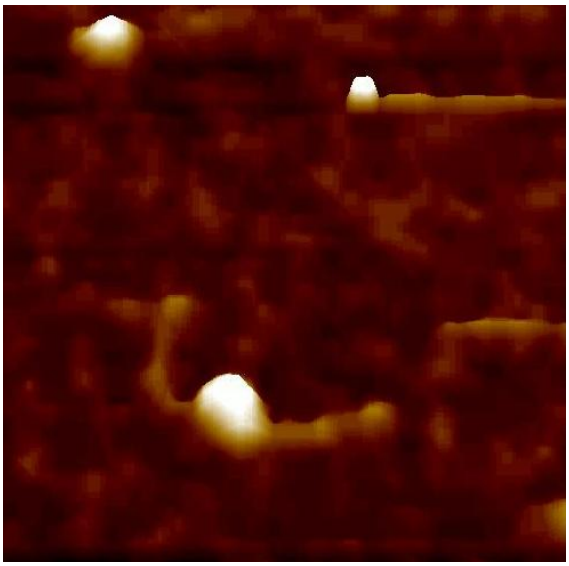

(e)

Figure 4.9. (a,b) AFM images of R_1-complexes specifically bound to DNA (1 kB; recognition site 1/3 of the length of the strand);image sizes (a) 2.3 µm × 2.3 µm; z-scale 2 nm; (b) 2.9 µm × 2.9 µm, z-scale 2 nm; (c) the magnification of an R_1-complex bound to DNA (1 kB) with the recognition binding site at the centre of the DNA; pseudo-3D view (d); size 394 nm × 394 nm; z-scale 3 nm; (e) R_1-complex bound at the centre of DNA (250 bp); size 150 nm × 150 nm; z-scale 2 nm.

Complexes showed only one protein to be attached to the DNA strand (at the concentrations used), indicative of specific binding (Figure 4.9). Isolated protein molecules, however, were observed close to neighbouring DNA strands or at the end of DNA strands, which may indicate that complexes were swept during the drying step or

scanning with the AFM tip (Figures 4.9a,b). The presence of R_1-DNA complexes specifically bound to DNA was established to be *ca.* 20 % (the remainder being DNA with no proteins attached).

Height and width measurements were determined for complexes randomly bound to the mica surface and compared with the same parameters obtained for R_1-complexes bound to DNA (Figure 4.10).

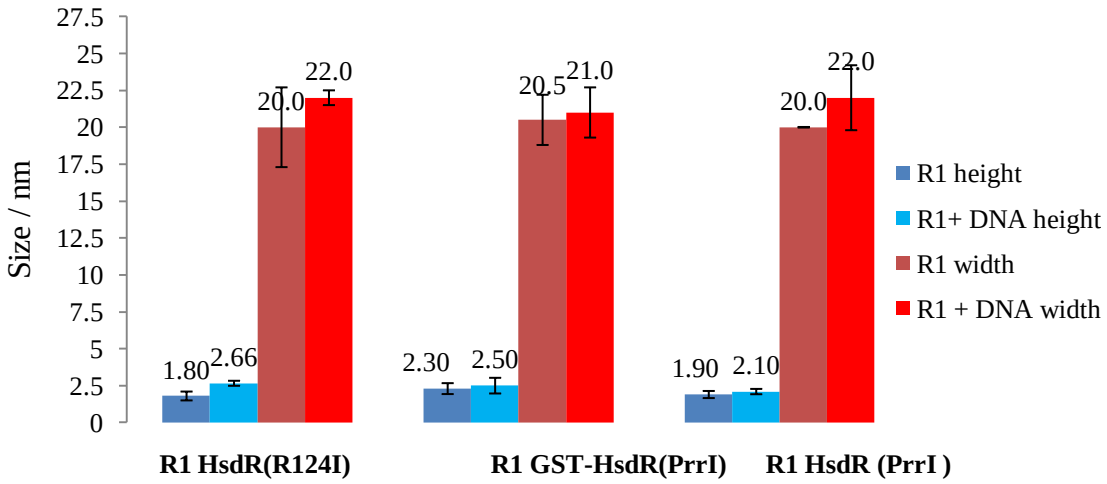

Figure 4.10. Height and width measurements of unbound R_1-complexes (dark blue and maroon) and R_1-complexes specifically bound to DNA (light blue and red) deposited on PLL pre-treated mica. HsdR(R124I), GST-HsdR(PrrI) and HsdR(PrrI) were used to assemble different R_1-complexes. Error bars represent standard deviation.

Independent of the HsdR type, mean height and width parameters increased when R_1-complexes were specifically bound to DNA, although error bars were found to overlap. The change in height observed when the R_1-complex involving HsdR(R124I) became specifically bound to DNA (1.80 ± 0.30 nm and 2.66 ± 0.17 nm, respectively). The width also changed when the complex bound to DNA (20.0 ± 2.7 nm and 22.0 ± 0.5 nm, respectively). The R_1-complex involving GST-HsdR(PrrI)

showed the increase in mean height on binding with DNA (2.30 ± 0.37 nm to 2.50 ± 0.53 nm, respectively); the width values also altered (20.5 ± 1.7 nm and 21 ± 1.7 nm). When HsdR(PrrI) was used, a slight change in mean height and width values of the R_1-complex (1.90 ± 0.24 nm to 2.10 ± 0.18 nm and 20.0 ± 0.1 nm to 22.0 ± 2.2 nm, respectively) were observed.

It was postulated that R_1-complexes may have become dissociated into constituent MTase and HsdR subunits prior to specific binding to DNA. This was because the proteins on the DNA chains sometimes appeared to have different sizes or intensities (Figure 4.11). For example, in Figure 4.11a, molecules 1 – 4 seem to be of similar size, and larger than molecules 5 and 6. This was supported by V_m calculations, 1 – 4 being R_1-complex (458 ± 44 nm^3) and 5 and 6 (237 ± 8 nm^3) being MTase proteins. V_c for the R_1-complex was 534 nm^3. In Figure 4.11b, molecule 1 appears to be smaller than molecule 2, again, confirmed by V_m calculations (261 and 538 nm^3, respectively), 1 and 2 to be MTase and the R_1-complex, respectively.

4.2.4 AFM imaging of R_2-complex bound to DNA

The R_2-complex (Section 2.10.1.7) is not as stable as the R_1-complex, since the HsdR subunit can easily dissociate; this probability increases during the washing step. The two DNA-protein complexes shown in Figure 4.12 are assumed to be R_2-complexes specifically bound to DNA. The V_m of these complexes, numbered 1 and 2, were 463 and 692 nm^3, respectively, corresponding to the R_1- and R_2-complexes (V_c 534 and 762 nm^3 when HsdR(R124I) was used).

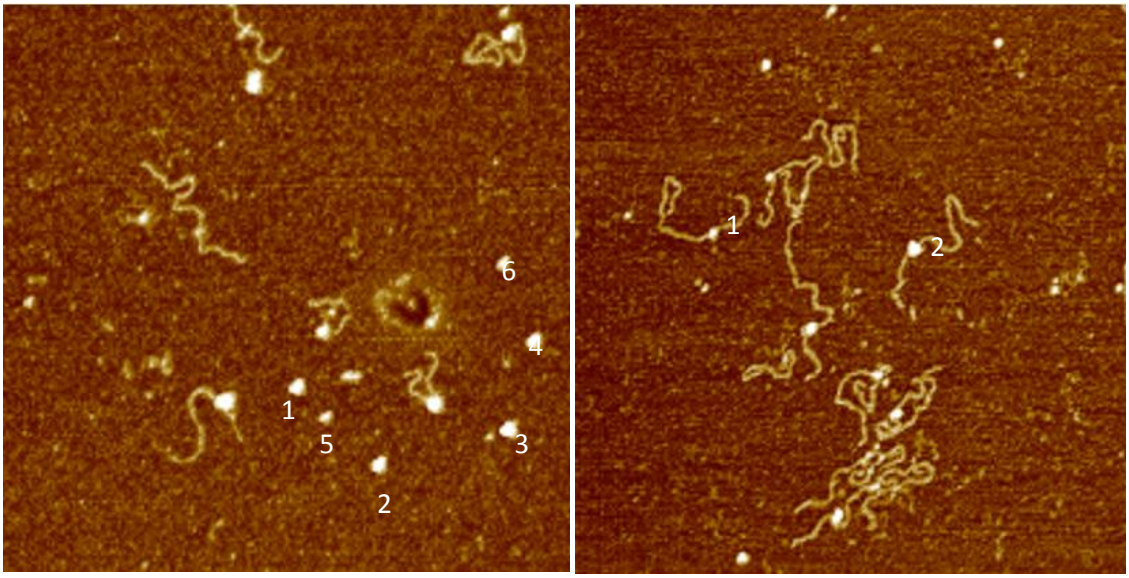

(a) (b)

Figure 4.11. AFM images of R_1-complexes (using the HsdR(R124I) submit) on DNA (1 kB; recognition site at 1/3 of length) showing difference in sizes of bound complexes; sizes (a) 972 nm × 972 nm; z-scale 2.5 nm; (b) 1 µm × 1 µm; z-scale 2.5 nm.

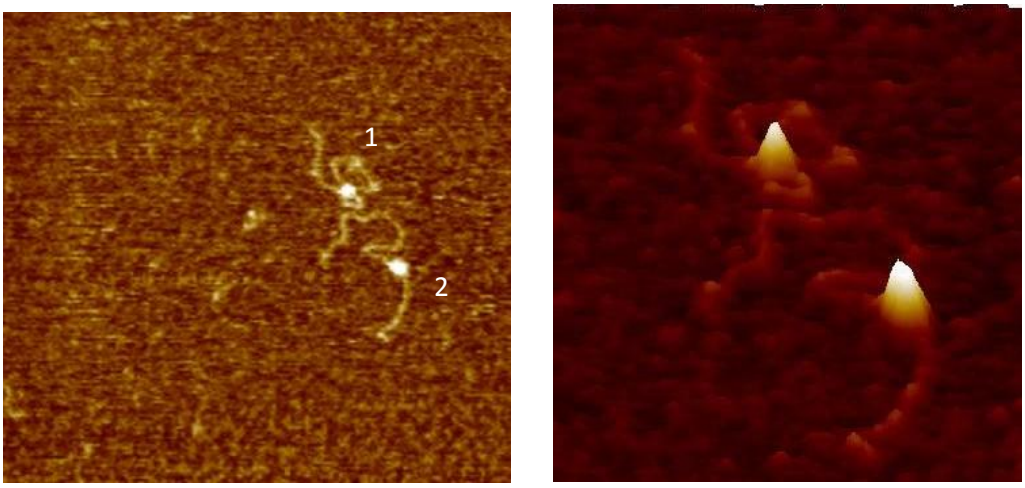

(a) (b)

Figure 4.12. AFM images of the "R_2-complex" deposited on PLL pre-treated mica from HEPES buffer (20 mM; pH 7.4) containing $MgCl_2$ (5 mM) deposited on PLL pre-treated mica; size 690 nm × 690 nm; z-scale 3.2 nm; (a) 2D image; (b) pseudo-3D image (same area).

Based on V_m measurements, R_2-complexes were rarely observed, in agreement with an (EMSA) experiment where the EcoR124I complex (diluted to 10 nM) could only be

observed as 10 % of the total complexes observed (Janscak *et al.*, 1998). An explanation for the rarely detected R_2-complex may be that the concentration used for visualisation of single molecules was much lower than the dissociation constant of the R_2-complex (2.4×10^{-7} M) and, therefore, dissociation may be occurring. Another example is shown in Figure 4.13, where R_1-complexes (smaller proteins) can be seen at the top-right of the image and a larger R_2-complex in the lower-left quadrant.

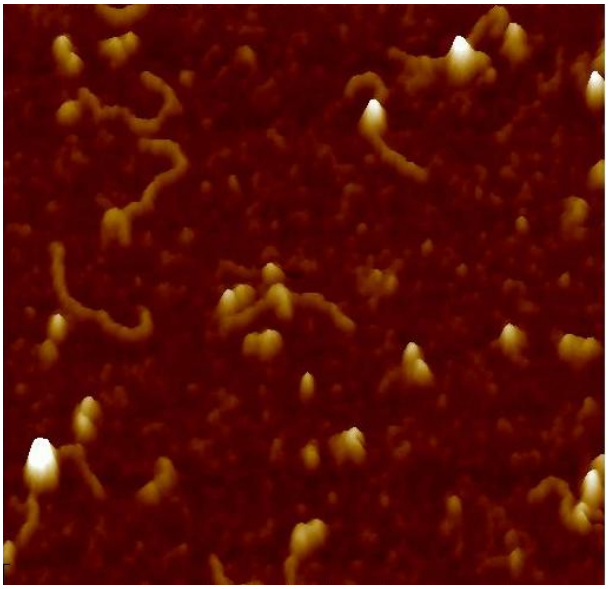

Figure 4.13. An AFM (pseudo-3D) image of "R_2-complexes" specifically bound to the recognition site on DNA (250 bp); size 350 nm × 350 nm; z-scale 3 nm.

4.2.5 Effect of ATP-γ-S and AMP-pnp cofactors on the assembly of EcoR124I

The next investigations were aimed at imaging the R_1-complex with DNA after addition of ATP-γ-S, used to trap initial translocation complexes (van Noort *et al.*, 2004). In parallel experiments, AMP-pnp was used in place of ATP-γ-S. V_m calculations were carried out before and after the addition of these cofactors.

The R_1-complex was incubated with DNA (1 kB), as described in Section 4.2.3. ATP-γ-S (or AMP-pnp) was added the reaction mixture (to a final concentration of 2 mM) and incubated for 30 s at 22 °C). The mixture was deposited on PLL pre-treated mica, rinsed with pure water (1 mL), quickly dried in a stream of N_2 and directly imaged. R_1-complexes bound to DNA in the presence of ATP-γ-S are shown in Figure 4.14.

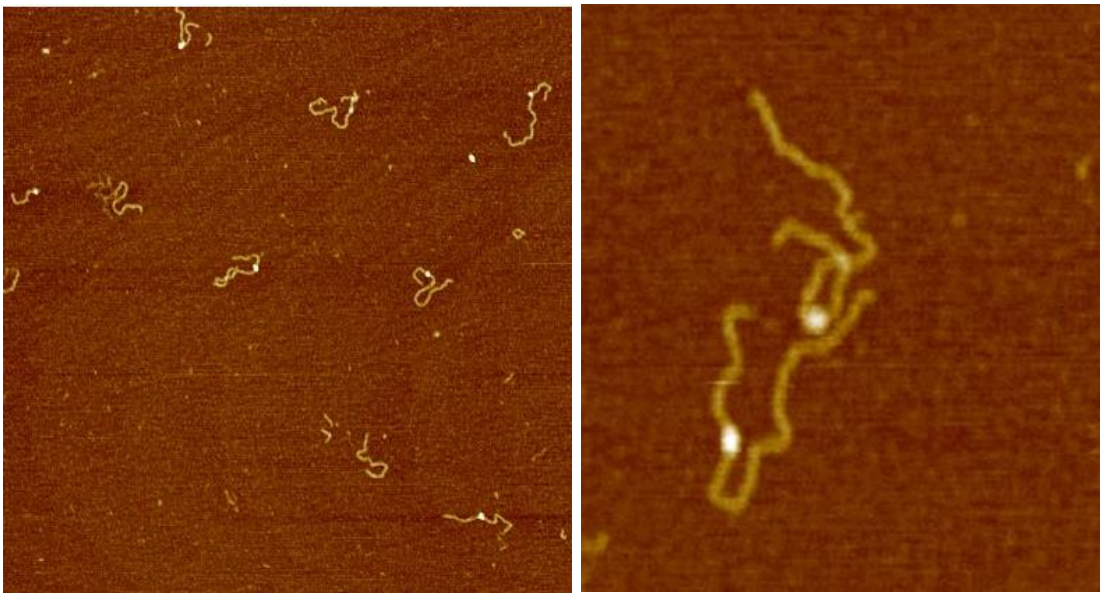

(a) (b)

Figure 4.14. AFM images of the R_1-complex (HsdR(R124I) used) specifically bound to DNA (1 kB; recognition site 1/3 along its length) in the presence of ATP-γ-S (2 mM) on PLL pre-treated mica; size (a) 1.7 µm × 1.7 µm; z-scale 2 nm; (b) 489 nm × 489 nm; z-scale 4.6 nm.

In AFM studies of EcoR124I in the presence of ATP-γ-S, van Noort *et al.* (2004) observed, for the R_1-complex, a small bulge that was sensitive to single-stranded DNA nucleases, indicative of non-duplex DNA (Figure 4.15a). This was the result of DNA melting when the enzyme switched from recognition to translocation mode, causing an

associated shortening of the DNA contour length of 8 nm. A shortening of the DNA length by 11 nm was also noted for the R_2-complex.

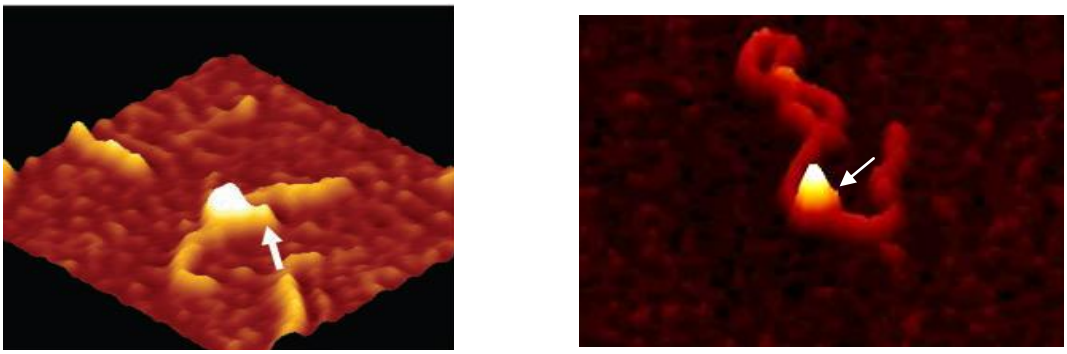

(a) (b)

Figure 4.15. AFM images of initial complex formation of the R_1-complex with DNA in the presence of ATP-γ-S, showing (a) small bulge from van Noort *et al.* (2004), size 125 nm × 270 nm, z-scale 3 nm; and (b) bulge was also observed in present work, size 270 nm × 270 nm, z-scale 3 nm.

The current studies confirmed the appearance of the bulge after the addition of ATP-γ-S (Figure 4.15 b), however the shortening of the DNA length was not investigated.

Expanding loops during imaging of EcoR124I complex bound to DNA in the presence of ATPγS were not observed, which confirms that translocation takes places only in the presence of ATP. Neaves *et al.* (2009) studied the influence of ATP-γ-S on EcoKI and showed dimerisation and the existence of expanding loops of the DNA bound to the complex, indicating the translocation process. The dimerisation and expanding loops in the presence of ATP-γ-S have never been observed for EcoR124I.

4.2.6 Molecular volume measurements of R_1-complexes before and after addition of ATP-γ-S and AMP-pnp

Values of V_m were calculated for the R_1-DNA complexes, where HsdR(R124I), GST-HsdR(PrrI) and HsdR(PrrI) were used in the assembly of the R_1-complexes before the addition of ATP-γ-S and AMP-pnp cofactors (Figure 4.16).

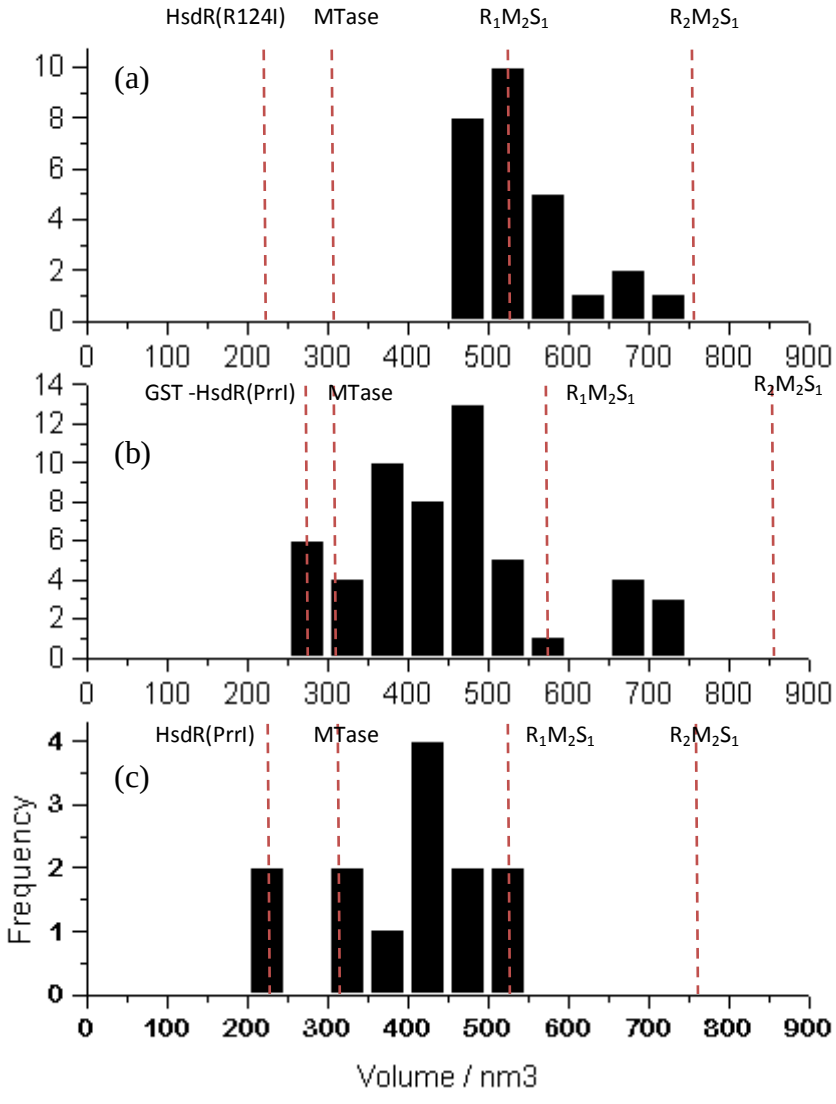

Figure 4.16. Distribution of V_m of R_1-complexes specifically bound to DNA without cofactors. R_1-complexes were constructed from (a) HsdR(R124I), (b) GST-HsdR(PrrI) and (c) HsdR(PrrI). The dotted lines show V_c for various subunits and complexes.

The V_m values calculated for MTase-HsdR(R124I) complexes (R_1-complexes) with DNA (250 bp) indicated homogeneity (Figure 4.16a) and were consistent with V_c (534 nm^3) for the R_1-complex. A few unstable R_2-complexes were also seen. For the R_1- and R_2-complexes (constructed from GST-HsdR(PrrI)) with DNA, V_c values were calculated to be 585 and 861 nm^3, respectively. A wider distribution in V_m was observed (Figure 4.16b), suggesting the presence of R_1-complexes and MTase bound to DNA. For HsdR(PrrI) involved in the R_1-complex, not many complexes were seen, perhaps reflecting weaker binding of the hybrid subunit to MTase.

The next series of V_m calculations from were obtained from MTase-HsdR(R124I) (R_1-complexes) specifically bound to DNA before (Figure 4.17a) and after the addition of ATP-γ-S (Figure 4.17b) and AMP-pnp (Figure 4.17c).

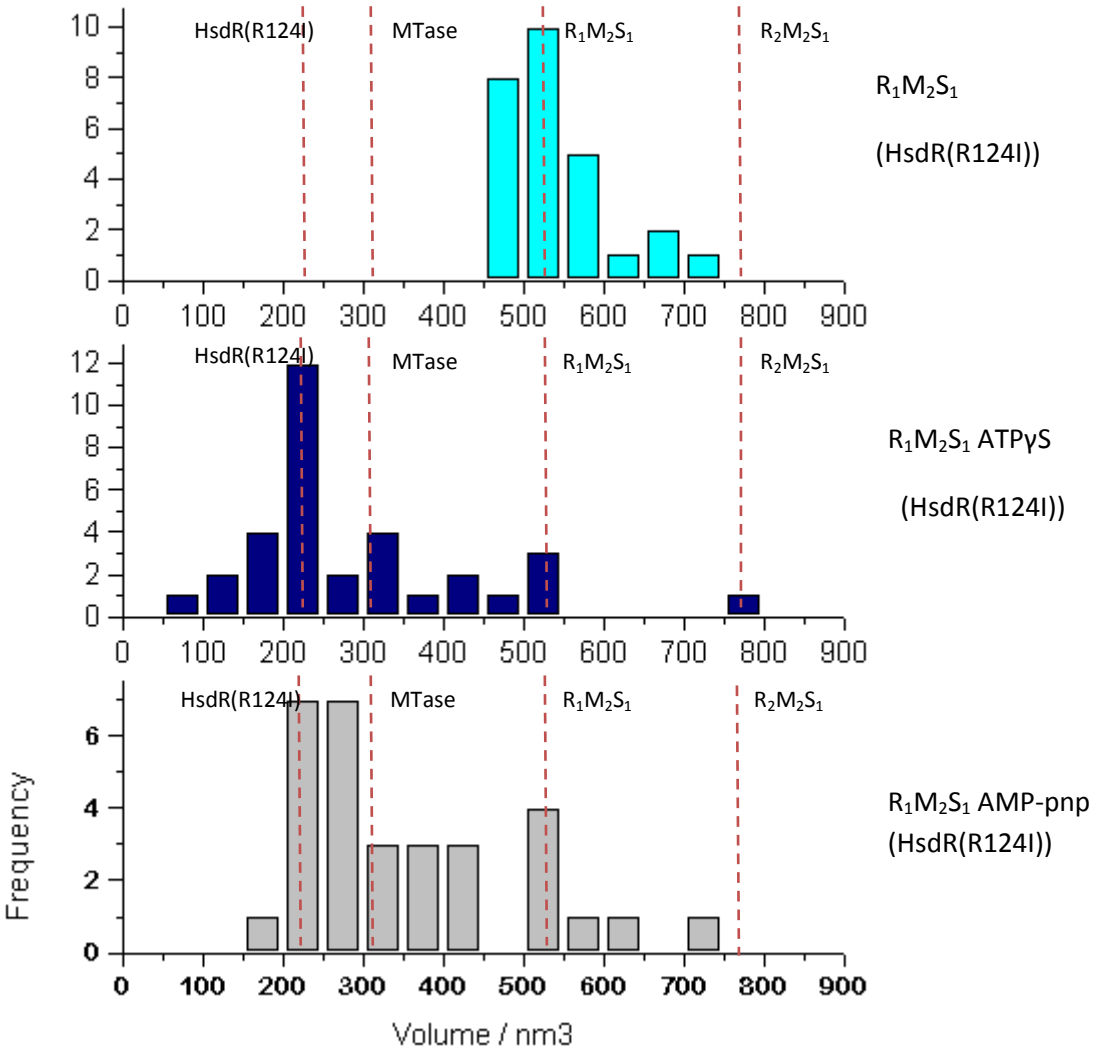

Figure 4.17. Distribution of V_m of MTase-HsdR(R124I) (R_1-complexes) before (a) and after the addition of cofactors ATP-γ-S (b) and AMP-pnp (c).

In the presence of ATP-γ-S and AMP-pnp, a smaller number of DNA-R_1-complexes (based on V_m) were observed (Figures 4.17b and c, respectively). The addition of ATP-γ-S is suggested to freeze an initiation complex, which is unable to translocate, resulting in instability and dissociation of HsdR subunit, therefore MTase bound to the DNA

were the dominant species. The AMP-pnp also reduced the number of R_1- and R_2-complexes, however more R_1-complexes were observed compared to the use of ATP-γ-S, suggesting a decrease in dissociation of the HsdR subunit. This may involve the lack of hydrolysis in the presence of AMP-pnp.

The variation of V_m was obtained for GST-HsdR(PrrI)-MTase (R_1-complexes) before (Figure 4.18a) and after the addition of ATP-γ-S (Figure 4.18b) and AMP-pnp (Figure 4.18c).

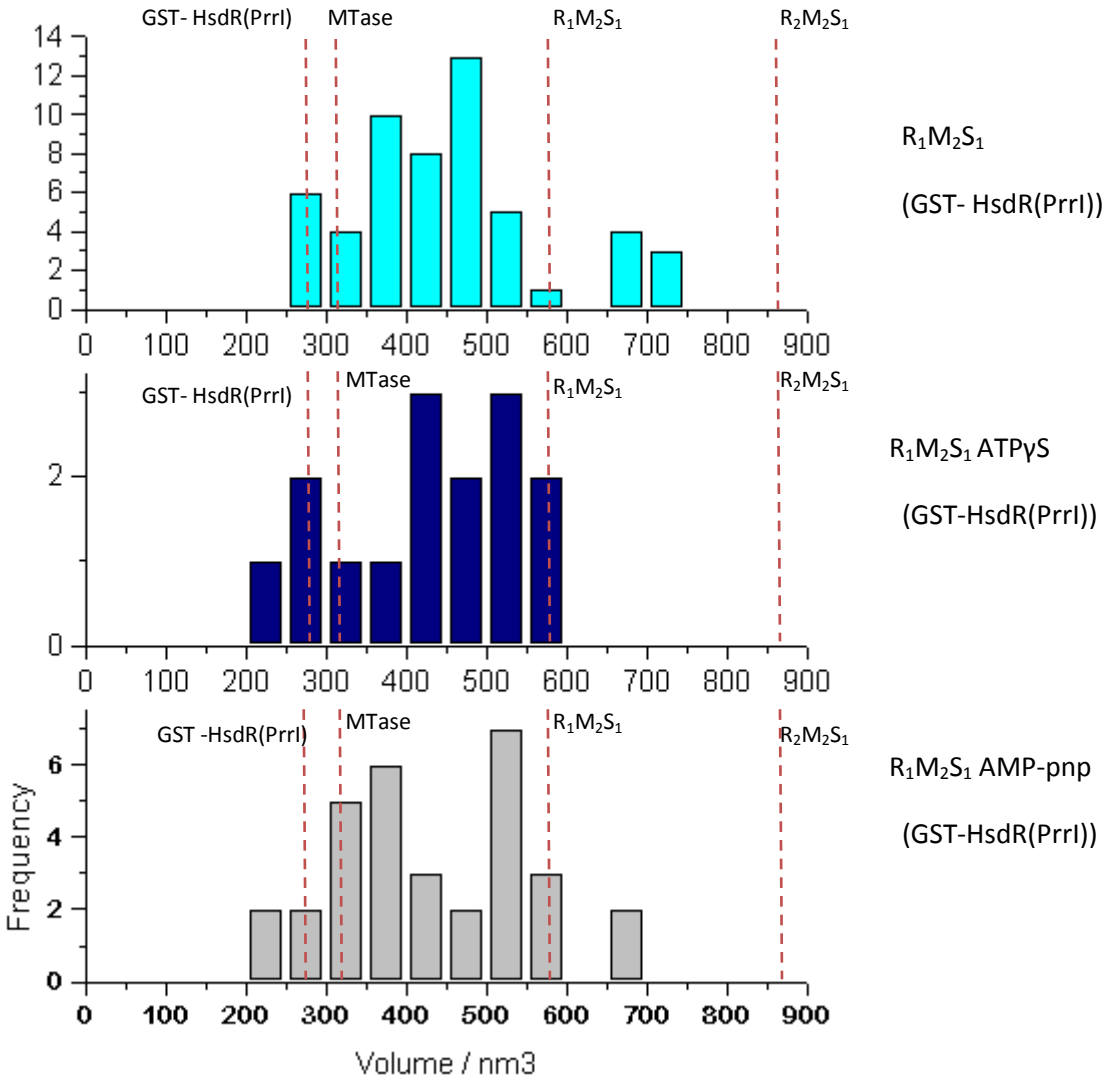

Figure 4.18. Distribution of V_m of GST-HsdR(PrrI)-MTase fused with GST R_1-complexes before (a) and after the addition of cofactors ATP-γ-S (b) and AMP-pnp (c).

V_m values obtained from R_1-DNA complexes, comprised of GST-HsdR(PrrI), were larger than with HsdR(R124I) as expected from their differences in V_c. Fewer complexes, however, were observed.

Very few R_1-complexes comprised of HsdR(PrrI) fusion were observed. V_m calculations showed the presence of mostly MTase bound to DNA after the addition of cofactors which may indicate stronger dissociation of HsdR subunit (Figure 4.19).

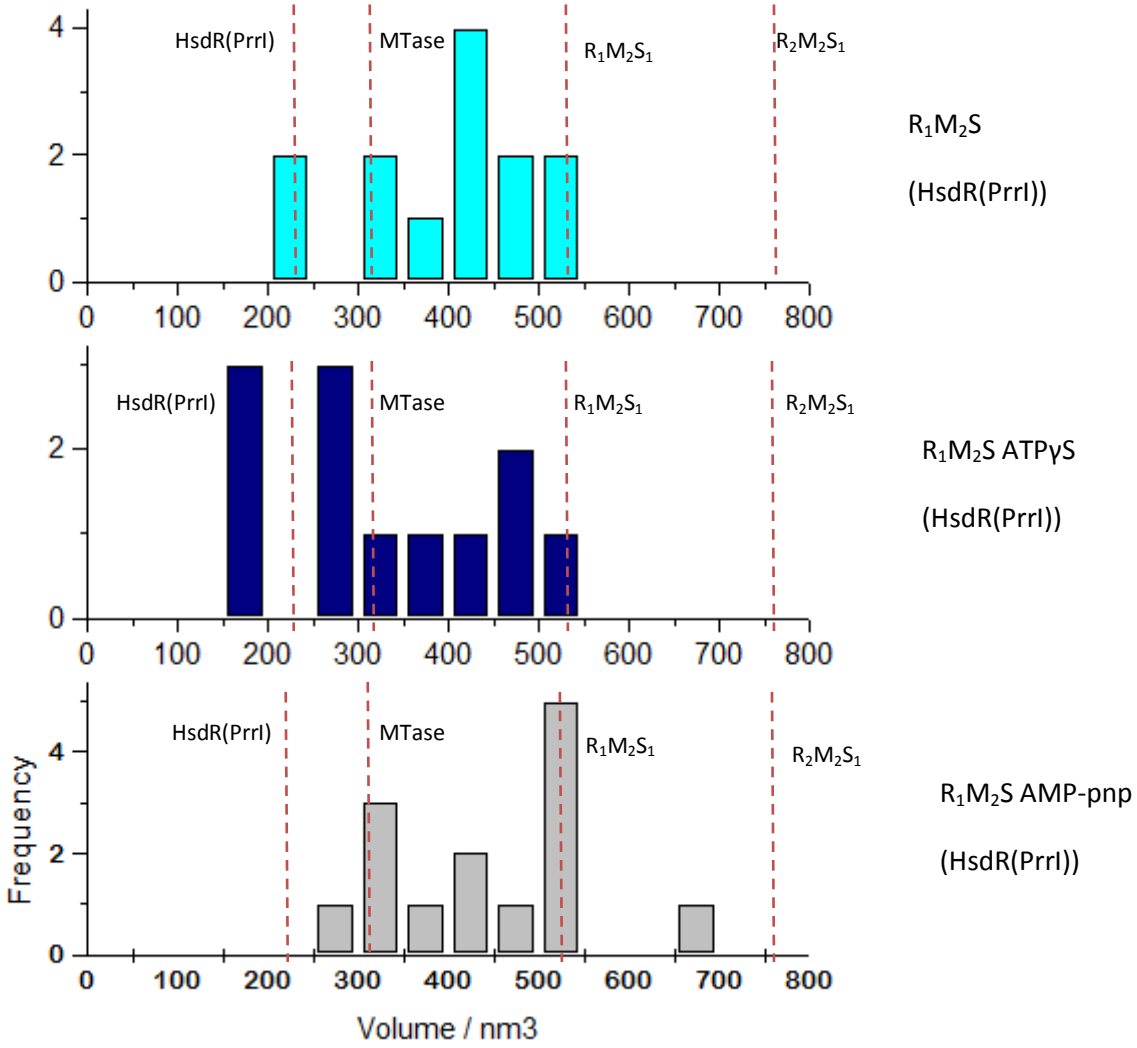

Figure 4.19. Distribution of V_m of MTase-HsdR(PrrI) (R_1-complexes) before (a) and after the addition of cofactors ATP-γ-S (b) and AMP-pnp (c).

Based on V_m measurements, R_1-complexes were present before and after addition of cofactors, however the number analysed was small. Seidel *et al.* (2005) indicated differences in EcoR124I dissociation in the presence of ATP. They proposed that the addition of ATP involved changes in the complex conformation prior to translocation

and that the stability of the subunits could be altered. The non-hydrolysable analogues may also affect the enzyme stability. It was previously reported that the GST tag may increase the stability of the target protein, that may confirm the present observation that more R_1-complexes were observed for the HsdR(PrrI) subunit fused with GST than without fusion.

4.2.7 Visualisation of DNA translocation with EcoR124I in the presence of ATP

DNA translocation by the EcoR124I restriction enzyme is preceded by the recognition of 'foreign' DNA that requires an ATP-dependent switch from methylase to motor (R_1) or endonuclease (R_2) activity. The structural changes of DNA appear as a result of initiation of translocation (van Noort *et al.*, 2004).

An investigation of the translocation at the single molecular level in the presence of ATP, the cofactor required for this process (hydrolysed by HsdR subunit), was therefore carried out.

AFM studies with EcoKI (another Type I R-M enzyme) suggested a model of rapid dimerisation of the enzyme (Figure 4.20), as the result of a conformational changes induced by specific binding to DNA containing two recognition sites for EcoKI prior to translocation in the absence of ATP (Berge *et al.*, 2000).

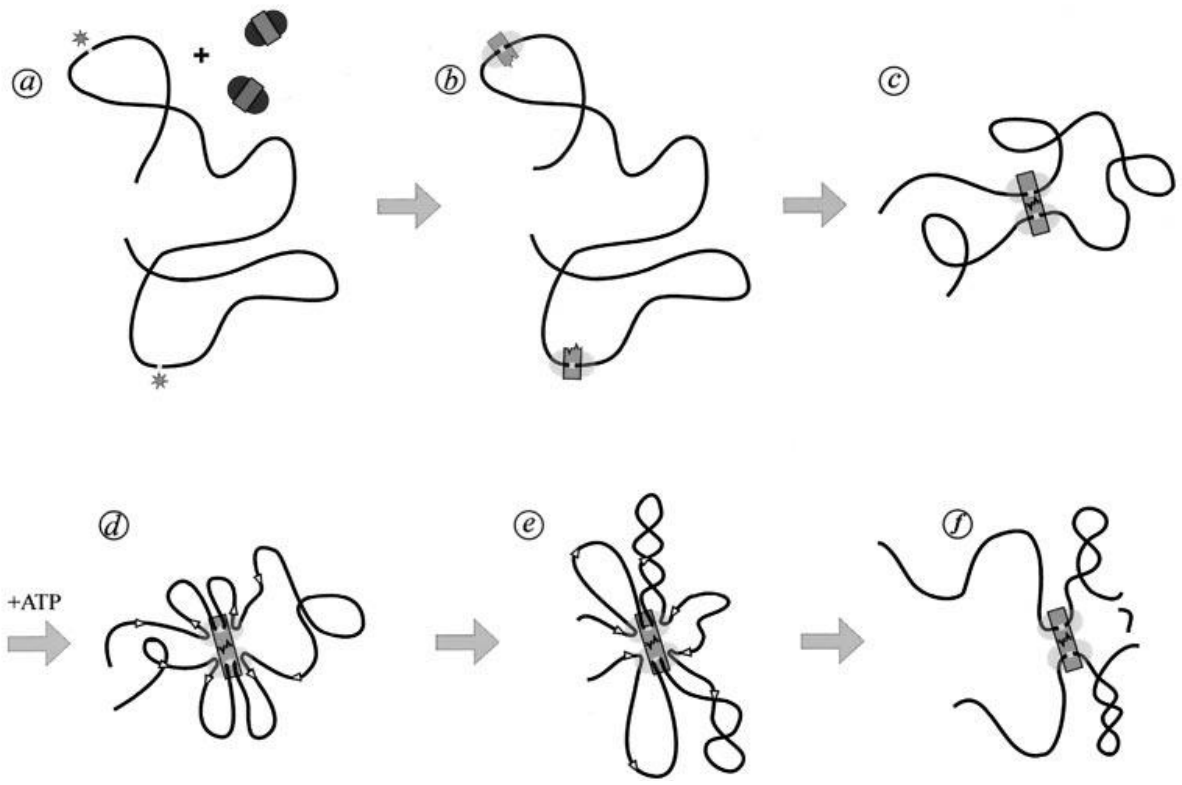

Figure 4.20. Model of *Eco*KI dimerisation on plasmid DNA containing two recognition sites for the enzyme (Berge *et al.*, 2000).

Neaves *et al.* (2009) confirmed the previous observation of EcoKI dimerisation in the presence of two recognition sites before the translocation process. The extended investigations showed that dimerisation of EcoKI did not occur before binding to DNA and takes place on specific sites before looping. The significant looping of DNA molecules containing a single EcoKI target site was observed, indicating the appearance of looping between a specific binding site and a non-specific region of the DNA. A comparison of the Berge model (Berge *et al.*, 2000) and the new model, based on the existing data with additional information, is shown in Figure 4.21.

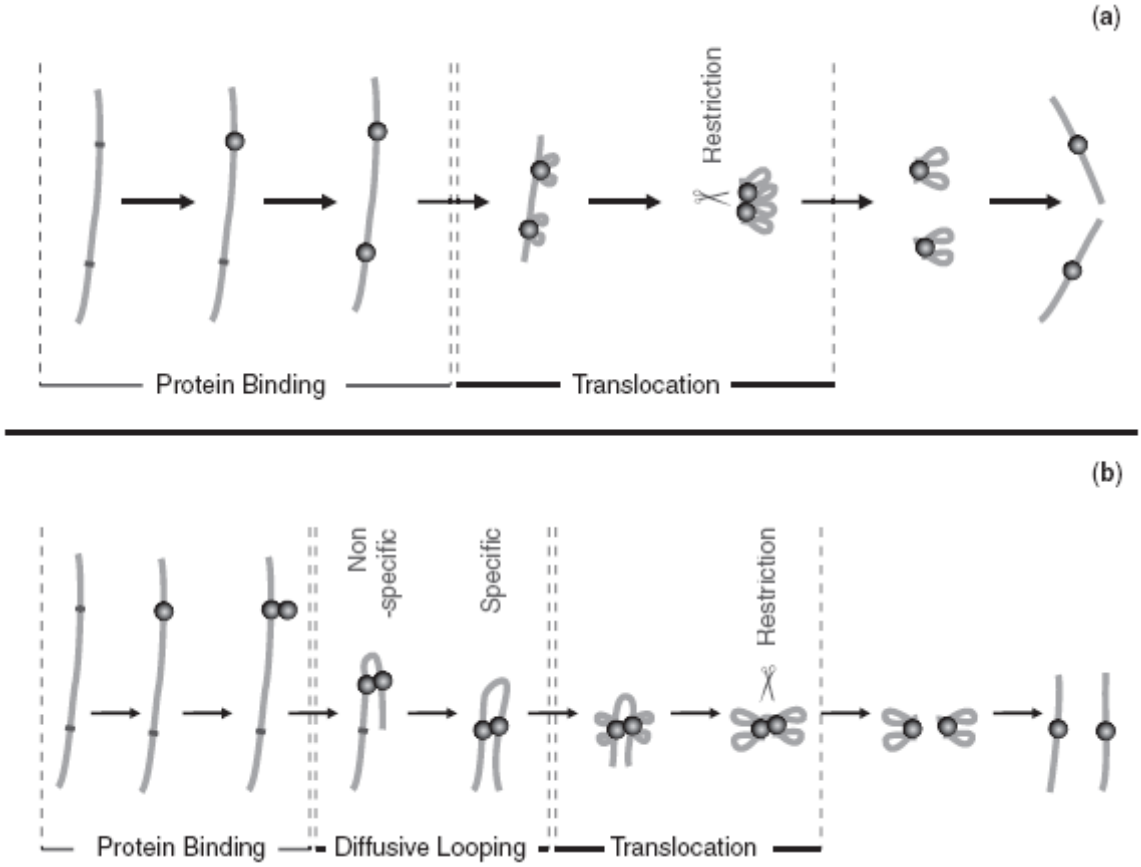

Figure 4.21. Comparison of models proposing binding, translocation and restriction of EcoKI to linearised DNA. (a) Model previously proposed by Berge *et al.* (2000), where EcoKI monomers individually bind to each site and translocation occurs independently from both sites, translocation stops when monomers meet, restriction occurs. In a new model supplemented by Neaves *et al.* (2009) (b) the dimerisation occurs at the same binding site. Here, a monomer of EcoKI binds to one site and then a second monomer binds to the same site. Diffusive loops are formed by dimerised complexes with non-specific regions of DNA until it is stabilised by contact with the second target site for EcoKI. Translocation proceeded from both sides of both monomers. Fully contracted diffusive loops between monomers halt the translocation process resulting in restriction.

AFM studies of translocation of EcoR124I, by van Noort *et al.* (2004), did not show dimerisation preceding this process, although translocation could be observed for both R_1-complexes (one loop) (Figure 4.22a) and R_2-complexes, where two expanding loops were imaged (Figure 4.22b). The translocation process possible for both R_1- and R_2-complexes was also confirmed in single molecule studies using a magnetic tweezer

setup; the dimerisation of the EcoR124I was also not observed (Seidel *et al.*, 2005). This latter process is assumed to be important for EcoKI, but not for EcoR124I.

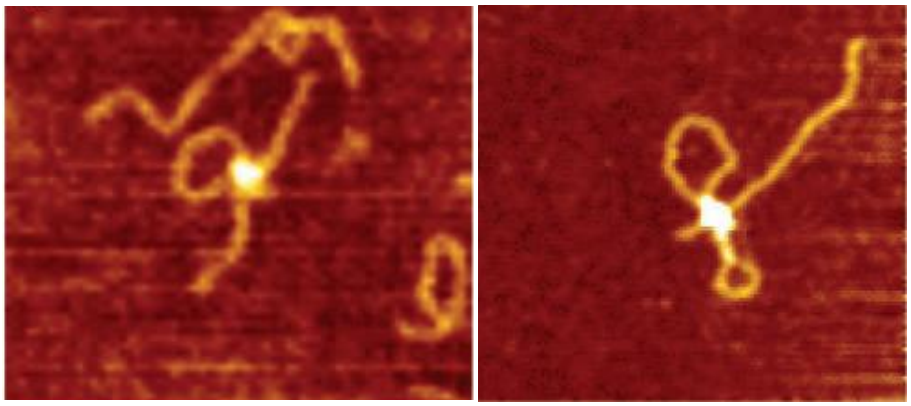

(a) (b)

Figure 4.22. AFM images of the translocation process observed for (a) an R_1-complex, where only one loop was observed and (b) an R_2-complex, where two loops were present (van Noort *et al.*, 2004); size 250 nm × 250 nm; z-scale 3 nm.

The visualisation of the translocation process for EcoR124I provided additional conformation that a fully functional enzyme, even when the interactions with the surfaces were involved.

Deposition of the translocating complex on the mica (Section 2.10.1.9) stopped the reaction and provided a snapshot of the process. A few complexes having a single loop were imaged, suggesting the translocation process was proceeded by an R_1-complex (Figure 4.23). This was supported by V_m measurements.

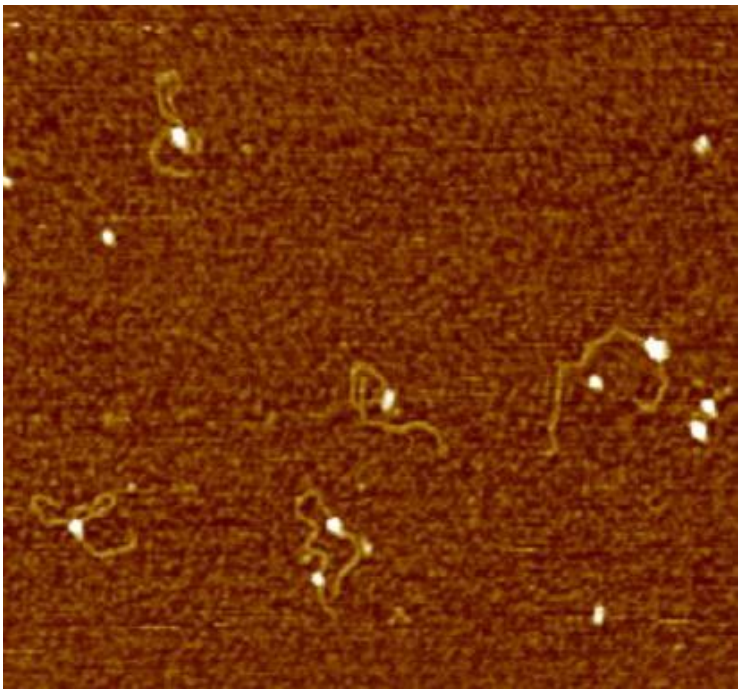

(a)

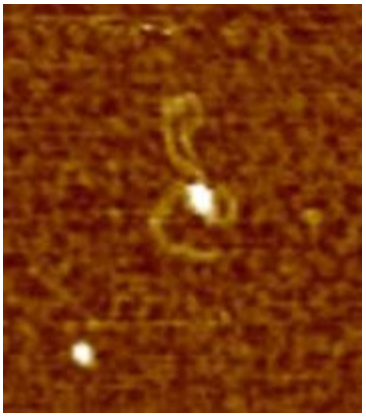

(b)

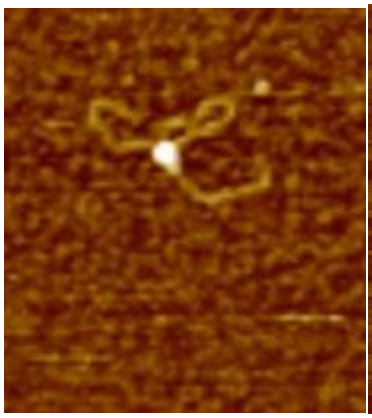

(c)

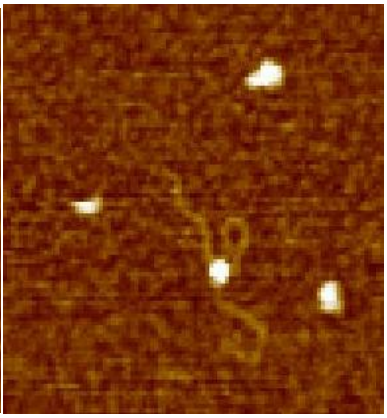

(d)

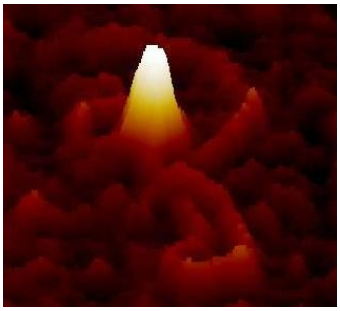

(b')

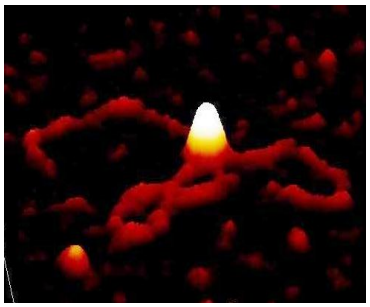

(c')

(d')

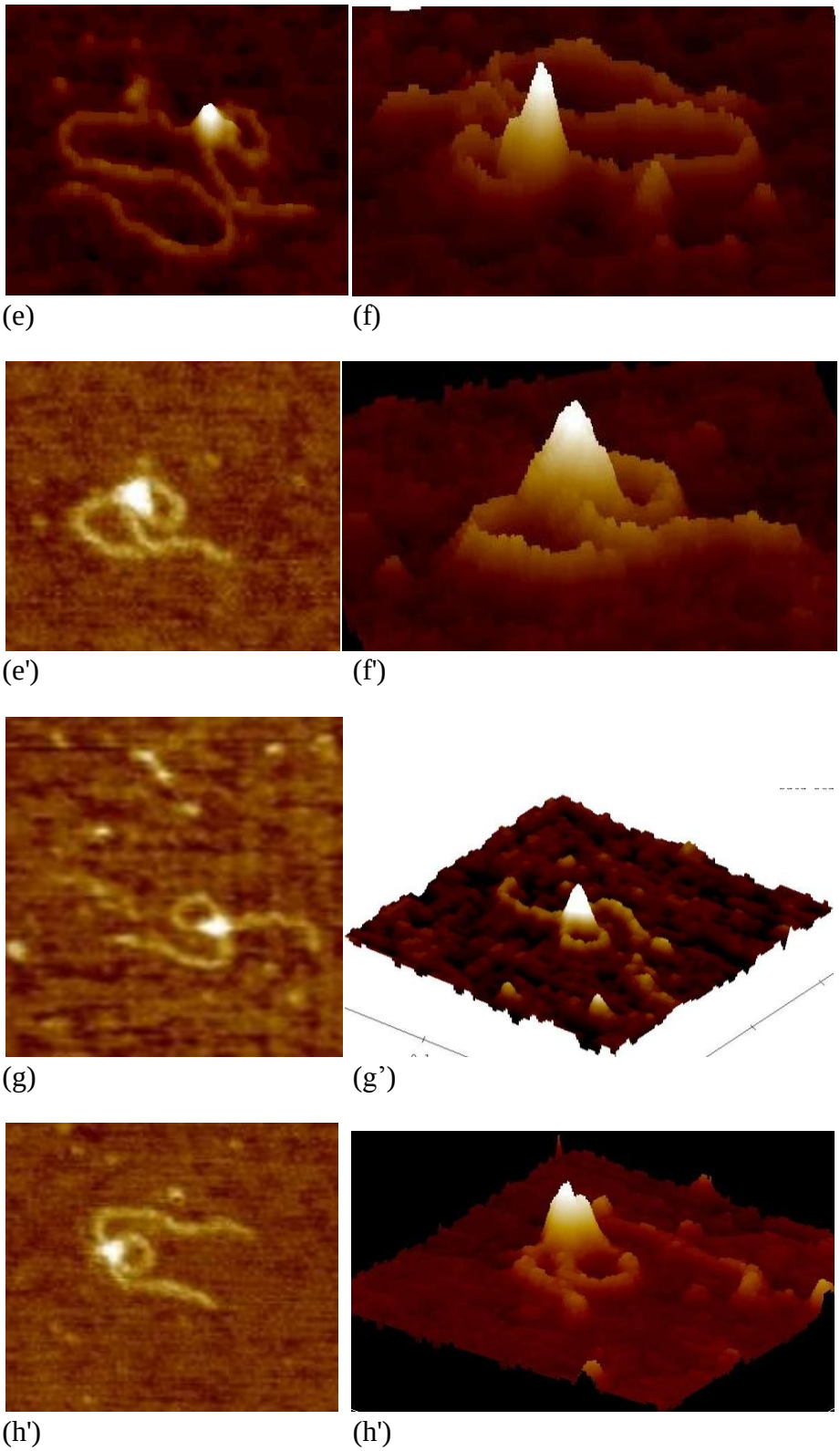

Figure 4.23. AFM images showing EcoR124I motor activity, resulting in translocation with looping of DNA (1 kB) in the presence of ATP (0.5 mM) after incubation (30 s) on PLL pre-treated mica: (a) Size 957 nm × 957 nm, z-scale 3 nm; (b-d), and pseudo-3D versions (b'-d'), showing magnifications of observed DNA supercoiling; (e-h) showing further DNA-R_1-complexes with expanding loops.

The presence of expanding loops, characteristic of translocation, was only observed in the presence of ATP. The dimensions and V_m values of proteins associated with DNA were analysed, together with the size of observed loop and length of the DNA arms. An example of height measurements of EcoR124I, suggesting translocating DNA, is showed in Figure 4.24.

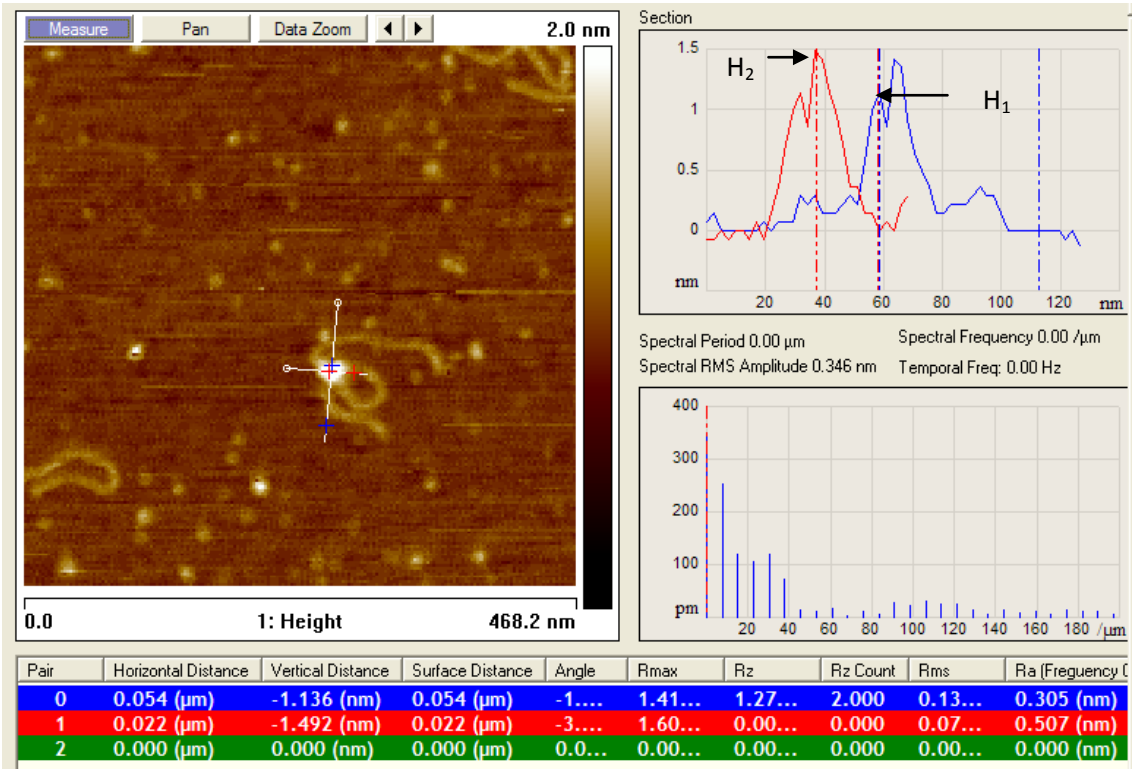

Pair	Horizontal Distance	Vertical Distance	Surface Distance	Angle	Rmax	Rz	Rz Count	Rms	Ra (Freguency
0	0.054 (µm)	-1.136 (nm)	0.054 (µm)	-1....	1.41...	1.27...	2.000	0.13...	0.305 (nm)
1	0.022 (µm)	-1.492 (nm)	0.022 (µm)	-3....	1.60...	0.00...	0.000	0.07...	0.507 (nm)
2	0.000 (µm)	0.000 (nm)	0.000 (µm)	0.0...	0.00...	0.00...	0.000	0.00...	0.000 (nm)

Figure 4.24. A typical AFM image with line-profiles showing heights of an R_1-DNA complex and the presence of a DNA loop following the addition of ATP.

The height measurements of the complex in Figure 4.24 show the presence of two peaks representing different heights: H_1 at *ca.* 1.2 nm, of similar height for MTase, and H_2, being 1.5 nm and characteristic of the HsdR subunit. The presence of two peaks, not seen for all measured complexes, may be due to MTase and HsdR having become dissociated during the translocation with ATP. However, this suggestion needs further investigation.

Ten DNA-R_1-complexes were analysed. For these complexes, the combined DNA length of the loop (87 ± 20 nm, corresponding to *ca.* 256 bp) and arms (112 ± 19 nm and 96 ± 17 nm) were found to be less (295 ± 33 nm) than the complete length of DNA used in the translocation experiment (340 nm), the difference being due to DNA remaining "buried" by the enzyme.

The translocation rate of the single motor subunit of an R_1-complex measured with magnetic tweezers was found to be 550 ± 30 bp s^{-1} (Seider *et al.*, 2004), in agreement with previously reported values for a high rate (400 ± 32 bp s^{-1}) from bulk measurements (Firman and Szczelkun, 2000). Present studies showed the average size of the loop to be 256 bp after 30 s incubation on the mica surface. The significant decrease in translocation rate from AFM measurements may indicate an influence of additional interactions between DNA and the enzyme with the surface, which were absent in the bulk media. For example, mica may "freeze" the complex.

4.3 Conclusions

Stable and reproducible imaging of MTase and HsdR subunit molecules were obtained on mica pre-treated with PLL. Imaged DNA-protein complexes confirmed the presence of only one enzyme molecule specifically bound to DNA.

A decrease in the number of DNA-protein complexes was observed in the presence of Ni^{2+} and Ca^{2+}. This may be attributed to stronger DNA binding to mica caused by Ni^{2+} or that the Ni^{2+} may affect the stability of the proteins and their binding to DNA. For

Ca^{2+}, the decrease in the number of DNA-protein complexes may be due to the known decrease in activity for some enzymes acting nucleic acids with these ions.

The V_m of the measured subunits or complexes, were smaller than theoretical values V_c, and were thought to be due to flattening as a result of dehydration of the molecules during the sample preparation drying step. The most DNA-R_1 complexes were observed when the HsdR(R124I) was used in the assembly of the R_1-complex, which would be expected as this is the native subunit for the MTase. A predicted increase in the measured volume was detected for GST-HsdR(PrrI), which corresponds to the presence of the GST fusion protein. In contrast, only a small number of complexes were observed for HsdR(PrrI) involved in the assembly of the R_1-complex, supporting unpublished evidence that complexes incorporating this hybrid subunit are less stable than those with the wild-type subunit.

The addition of ATP-γ-S in all cases showed a decrease in the number of imaged complexes, suggesting induced dissociation of HsdR from the complex. Calculated V_m indicated the presence of MTase bound to DNA in the majority of the complexes observed. More DNA-R_1-complexes (assumed from V_m measurements) were seen in the presence of AMP-pnp, which may indicate a slower process of dissociation with this ATP analogue. Addition of ATP confirmed the ability of the enzyme for translocation, but at no point was dimerisation, as seen for EcoKI, observed for EcoR124I.

Chapter 5

Force-distance measurements of a model system: biotin-avidin

5.1 Introduction

Recently developed single molecule manipulation techniques, including atomic force microscopy (Binnig *et al.*, 1986), optical tweezers (Ashkin *et al.*, 1990), magnetic tweezers (Smith *et al.*, 1992), glass microneedles (Kashino *et al.*, 1988) and the biomembrane force probe (BFP) (Evans *et al.*, 1995), have become indispensable tools for the structural and functional investigation of single biomolecules (Table 5.1).

The use of single molecule tools allows forces involved in intra- and intermolecular interactions to be directly quantified (Clausen-Schaumann *et al.*, 2000). These methods have been applied to study intermolecular forces of nucleic acids, receptor-ligand, proteins (*e.g.*, molecular motors) and proteins unfolding. The whole range from entropic forces at several femtoNewtons (Smith *et al.*, 1992) to the rupture of covalent bonds at a few nano Newtons (Grandbois *et al.*, 1999) can be investigated (Figure 5.1).

Table 5.1. Comparison of (the most commonly used) single-molecule force spectroscopy methods (Clausen-Schaumann *et al.*, 2000; Neuman and Nagy, 2008; Michaelis *et al.*, 2009).

Method	AFM	Optical tweezers	Magnetic tweezers
Force range / pN	10 – 100 000	0.1 – 150	0.001 – 100
Resolution / nm	< 0.1	0.1 – 2	2 – 10
Dynamic range / ms	≥ 0.1	≥ 0.1	≥ 10
Probe size / μm	100 – 250	0.25 – 5	0.5 – 5
Limitations	Large high-stiffness probe; large minimal force; nonspecific	Photodamage; sample heating; nonspecific	No manipulation (Force hysteresis)
Typical applications	DNA, RNA, proteins, receptor-ligand pairs	DNA, actin, molecular motors, proteins	Mechanical properties of DNA, RNA, DNA translocases, helicases, nucleosome remodelling complexes

For studies with nucleic acids, the force range of interest lies in the range 0.1 – 100 pN (Oberhauser and Carrion-Vazquez, 2008). The unbinding force of complementary DNA strands has been found to be *ca.* 70 pN (Lee *et al.*, 1994; Strunz *et al.*, 1999); whereas, sequence-specific base-pair forces (9 pN for AT and 20 pN for GC) were determined by unzipping the synthetic sequences of DNA (Rief *et al.*, 1999a). Leger *et al.* (1999), using a glass microneedle, investigated the coupling of stretching and twisting DNA molecules up to forces of 150 pN.

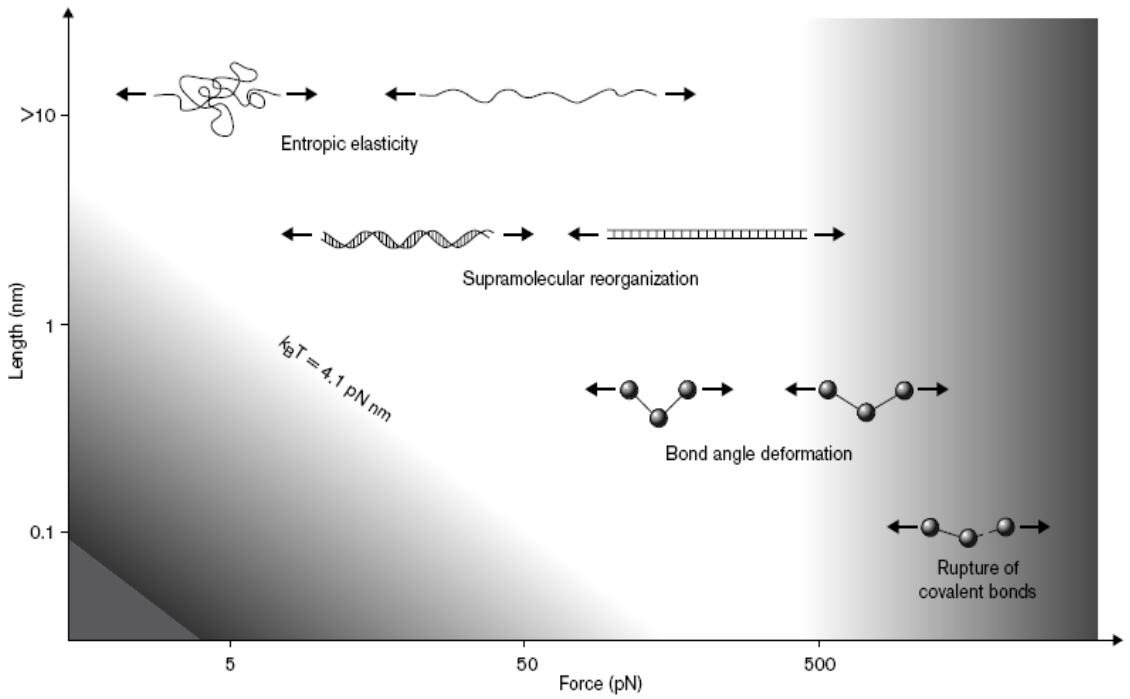

Figure 5.1. Typical forces and length (logarithmic) scales in single molecule force spectroscopy. The experimental accessibility of mechanical information is limited to the light areas of the plot. The shaded area in the lower left corner indicates the region of limited thermal stability of molecular structures (length multiplied by force = thermal energy, k_BT = 4.1 pN nm at room temperature). The upper limit to the accessible experimental force range is determined by the rupture of covalent bonds at several nN. Adpted from Clausen-Schaumann *et al.* (2000).

The activity of proteins and their complexes, through conformational changes, often involve the conversion of stored or supplied chemical energy into mechanical work (Oberhauser and Carrion-Vazquez 2008). Optical tweezers allow the detection of forces and distances (0.1 nm) in the range reported for molecular motors and is probably the most widely used tool for studying their mechanics. This technique has been used to investigate the process known as "working stroke" for actomyosin complex, producing force and movement attributed to conformational changes. The movement of actomyosin was found to be 5.5 nm (Veigel *et al.*, 1998). The stalling forces of a kinesin motor (5 – 7 pN) were reported with a displacement step of 8 nm (Svoboda and Block, 1994; Kojima *et al.*, 1997), whereas, forces in range of 21 – 27 pN, required to

stall the RNA polymerase motor were obtained by Wang *et al.* (1998). One of the best studied motor systems is the portal packing motor from bacteriophage (Smith *et al.*, 2001). The motor is able to pack DNA against external forces as high as 65 pN; during this packaging process an internal pressure of *ca.* 50 atm was developed.

Seidel *et al.* (2004), using a magnetic tweezer setup, described the translocation and processivity of EcoR124I in the presence of ATP. Independent work of two motor subunits has been shown with the re-setting process being due to dissociation of the R_1-complex, which also showed lower processivity of translocation. The translocation rate of *ca.* 500 bp s^{-1} for both motors was reported.

AFM has been used to investigate the mechanical properties (stretching) of titin and the large sarcomeric protein of striated muscle (Rief *et al.*, 1997). The forces required to unfold individual domains ranged from 150 – 300 pN and were dependent on the pulling speed whereas, forces required to mechanically unfold spectrin (cytoskeletal protein) repeats were found to be 25 – 35 pN (Rief *et al.*, 1999b).

5.1.1 Measurement of biotin-avidin interactions

The avidin-biotin complex has been widely studied using AFM spectroscopy due to the high affinity and specificity of the system. Literature values of rupture forces between avidin and biotin, however, have varied widely from 56 to 410 pN (Table 1.5). The measurement of such forces are affected by immobilisation methods, state and orientation of the complex, buffer, pH, temperature used (Moy *et al.*, 1994b). Merkel *et al.* (1999) demonstrated that the loading rate (R_f; rate of force alteration with time)

applied to the avidin-biotin varied over six orders of magnitude, corresponding with the variation of force values. Dissociation of the ligand-receptor bond is a non-equilibrium dynamic process; therefore R_f has to be considered. The most probable rupture force (f^*) is a function of R_f (Evans and Ritche, 1997), however many reports have not presented enough information about the applied force and therefore interpretation and comparison of the measured forces is not often possible. It is therefore unclear as to which values of rupture force are correct.

Many publications present an ideal situation of a single interaction between avidin-biotin. The tetrameric structure of avidin allows the interactions and binding of more than one biotin (up to four), increasing the probability of observing multiple events before a final separation (Guo *et al.*, 2008). Figure 5.2 shows the interaction between a single avidin molecule attached to the apex of an AFM tip with one (a) and two (b) biotin molecules.

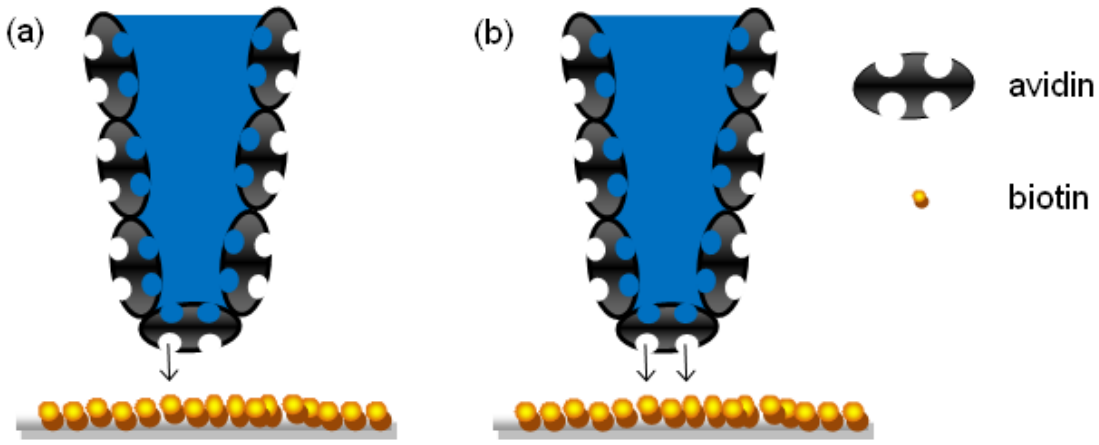

Figure 5.2. A model showing the ideal interaction between avidin and biotin with the possibility of single (a) and double (b) interactions. The arrows shows an interaction between single avidin molecule having two available binding sites able to interact with one or two biotin molecules.

The immobilisation method is another important factor that can affect adhesion measurements. Proteins can attach more weakly at some locations on the surface than others and molecules may adsorb in such a way that they "lay" on the surface to form multilayers. When avidin is attached to the surface, the existence of avidin mutlilayers can be verified by AFM imaging. When a small part of the surface is scratched with the tip, the height measurement across the hole can be compared to the expected size of the protein.

Various shapes of single force curves will result from differing numbers of biotin-avidin unbinding events. In the case where one peak is observed, care must be taken to distinguish between whether the adhesion is due to a "hard interaction" or a single (or concurrent) biological interaction. The former is characterised by a "sharp" adhesion peak, with a linear region immediately before the maximum adhesion point (Figure 5.3a) (Lee *et al.*, 2007). Hard interactions should normally be ignored in AFM force spectroscopy of interacting biological functionalities, although they are often included erroneously. The specific interaction has a curved region before the maximum adhesion event (Figure 5.3b).

The hard interaction is due to a non-specific interaction between a non-functionalised region of the Si_3N_4 tip and the underlying substrate, which may or may not be biotinylated (Figure 5.4).

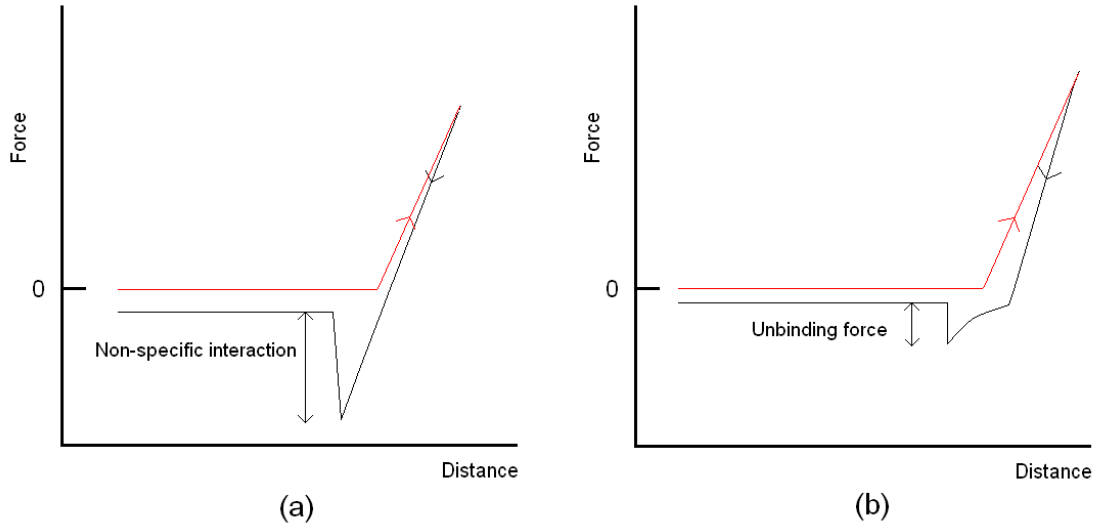

Figure 5.3. Schematic diagrams showing typical AFM force-distance curves arising from (a) non-specific ("hard") and (b) specific (unbinding) interactions between functionalised surfaces. Red curve = approach curve; black curve = retract curve.

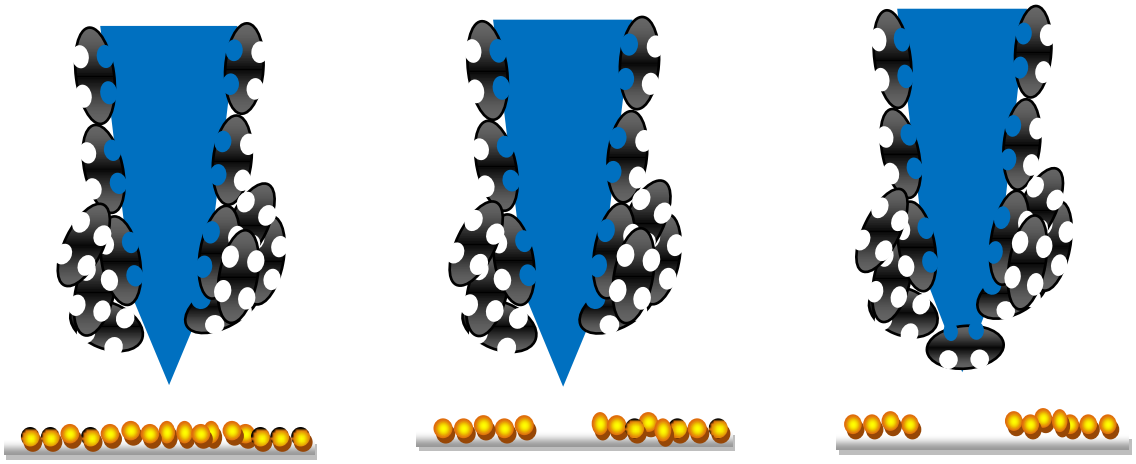

Figure 5.4. Models showing origin of non-specific ("hard") interactions. The most likely reason for "hard" contact is that part of contact region either the AFM tip, or the surface or both is not functionalised with proteins. Black shapes represent avidin; yellow spheres represent biotin (as in Figure 5.1).

The unbinding forces of avidin-biotin complexes are proportional to the change in enthalpy of the complex formation, although they are independent of changes in the free energy. The unbinding process is adiabatic with entropic changes occurring after unbinding. The enthalpy change (ΔH) for the avidin-biotin complex is reported to be -21.5 kcal mol^{-1} (Moy *et al.*, 1994), (9.00×10^4 J mol^{-1}; corresponding to an energy of 1.46×10^{-19} J (Equation 5.1)

$$E = \frac{\Delta H}{N_A} \qquad \text{(Equation 5.1)}$$

where N_A = Avogadro Constant (6.02×10^{23} mol^{-1}).

Moore and Kuhl (2006) reported the biotin-avidin bond energy to be 35 k_BT, which corresponds to 1.44×10^{-19} J (Boltzmann Constant, $k_B = 1.38 \times 10^{-23}$ J K^{-1}; T = 298 K), which is in agreement with the value obtained from Equation 5.1.

Interpretation of multiple-event AFM force-distance curves in the literature is generally restricted to the last adhesion peak (F_{final}). The remainder of this section focuses on other peaks in the multiple-event retract curve to see whether any useful information may be obtained.

The complexity in the multiple-event force-distance curves arises from the many possible unbinding interactions that are possible in the "real" system, some of which are shown in Figure 5.5. It is possible that a multilayer of avidin and/or biotin may play a

significant role in the observed interactions, leading to binding away from the apex of the AFM tip. The random orientation of avidin molecules on the tip will also contribute to this problem.

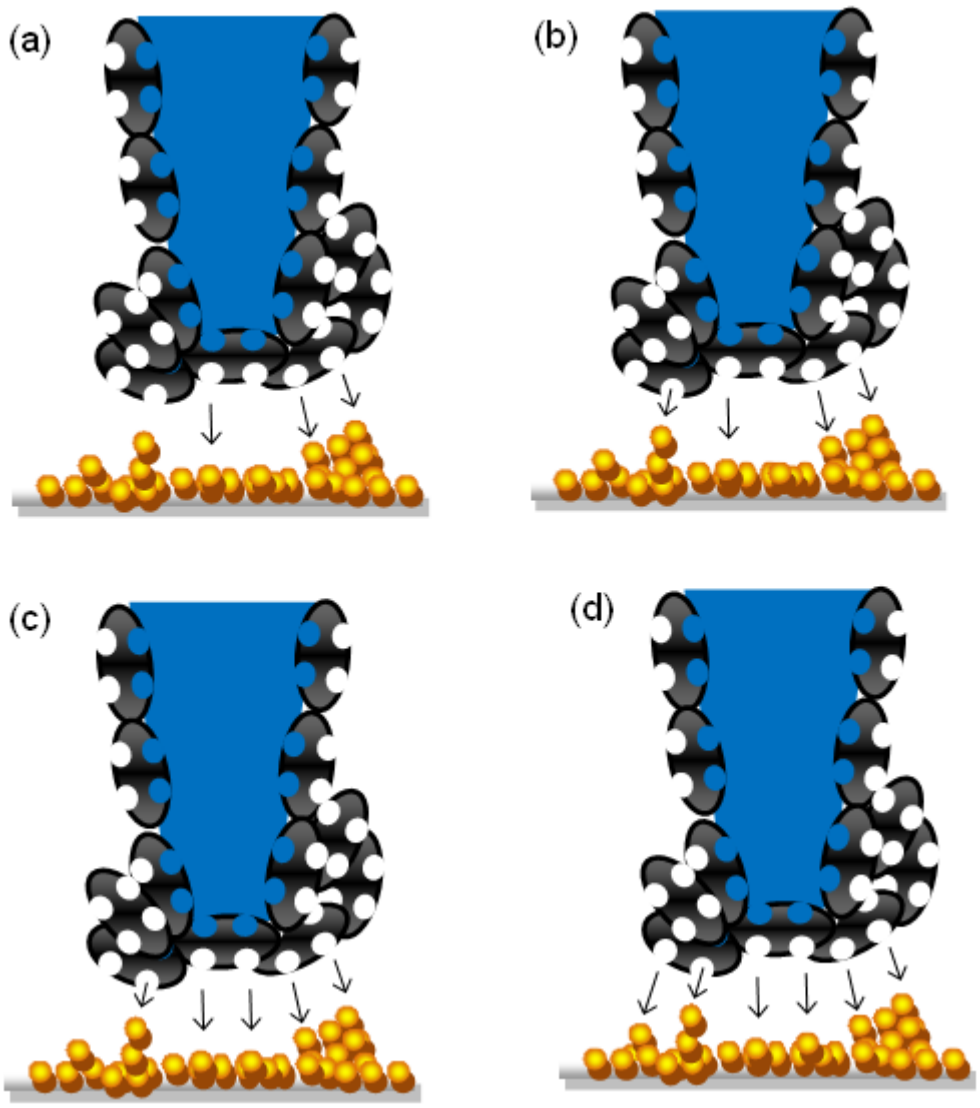

Figure 5.5. Possible scenarios of avidin-biotin binding leading to multi-event AFM force-distance curves; three (a), four (b), five (c) or six (d) interactions are indicated. Black shapes represent avidin; yellow spheres represent biotin (as in Figure 5.2).

Biotin-streptavidin interactions have also been determined using AFM. Streptavidin is a homologue of avidin, where the structural and binding properties are similar to that of avidin (Green, 1975). The avidin-biotin interaction is stronger than that of streptavidin-

biotin due to the presence of three additional hydrogen bonds and hydrophobic interactions in avidin (Weber *et al.*, 1989; Livnah *et al.*, 1993b). Typical literature values for the biotin-streptavidin interaction include: 126 ± 2.3 and 207 ± 5.8 pN (R_f = 189 and 2300 pN s^{-1}, respectively; Yuan *et al.*, 2000) and 257 ± 25 pN (Moy *et al.*, 1994). Further literature for biotin-avidin and biotin-streptavidin are shown in Table 1.5.

5.1.2 Covalent attachment of biotin and avidin to surfaces

The binding of molecules of interest to an AFM tip should be much stronger than the intermolecular forces to be measured to avoid problems of "stripping" of the molecules from the tip. Improved immobilisation to the AFM tip can be achieved by the use of strong, covalent bonds (1 – 2 nN), which are at least ten times stronger than the expected forces (Grandbois *et al.*, 1999).

5.1.2.1 Glutaraldehyde

Glutaraldehyde is an effective protein crosslinking reagent, although the reaction mechanism of glutaraldehyde with protein amino groups is not clearly understood. Glutaraldehyde can react with several functional groups of proteins, such as amine, thiol, phenol, and imidazole, because the most reactive amino acid side-chains are nucleophiles. Aso and Aito (1962) found that spontaneous polymerisation of glutaraldehyde, occurred in aqueous solutions and at room temperature. Kawahara *et al.* (1992) also reported that most of the studies neglected possible solvent effects on the glutaraldehyde structure, which was found to react with water in various ways. Water is

the solvent in which commercial glutaraldehyde is supplied and in which the crosslinking reaction with proteins is carried out. The high reactivity of glutaraldehyde toward proteins at around neutral pH is based on the presence of reactive residues in proteins and molecular forms of glutaraldehyde (reduced and cyclised products) in aqueous solution, leading to many possible reaction mechanisms. However, Jansen *et al.* (1971) showed that the optimum pH for the glutaraldehyde-protein reaction varied from protein to protein. Broun (1969) reported that low concentrations of glutaraldehyde were not able to form sufficient crosslinks to effect precipitation of the protein.

5.1.2.2 PEG linker used in force distance studies of biotin-avidin interactions

A flexible poly(ethylene glycol) (PEG) linker, widely used in force distance measurements, enables strong and site directed attachment of proteins to an AFM tip (Metzger *et al.*, 1999; Jeppesen *et al.*, 2001; Kamruzzahan *et al.*, 2006; Ebner *et al.*, 2007b). Tethering of the bio-ligand to the AFM tip, *via* a PEG linker, allows for rapid and free reorientation of the immobilised species when the AFM tip is at or near the sample surface (Hinterdorfer *et al.*, 1996). PEG is a hydrophilic molecule and attachment to proteins and other biomolecules increases their solubility and decreases aggregation. Non-toxicity and non-immunogenenicity of PEG allows for good attachment to surfaces and conjugated to molecules without interfering with cellular functions or target immunogenenicity.

The bending of the cantilever before the unbinding event is known to reflect the nonlinear elasticity of PEG and allows for easy discrimination of specific unbinding

events, which are preceded by nonlinear PEG stretching, from nonspecific tip adhesion, which would lack this nonlinear delay (Kienberger *et al.*, 2000).

It was reported that PEGylated biotin (especially long spacers) has a lower affinity for avidin than biotin (Kaiser *et al.*, 1997). This has been attributed to steric hindrance, where the long PEG chain can block the binding sites of avidin preventing close approach of biotin; however, the strong (*ca.* 10^8 M^{-1}) affinity is sufficient for PEG to function as an effective linker (Ke *et al.*, 2007).

Theoretically, the binding of a tethered biotin to the avidin attached to a mica surface is expected to be dependent on the binding energy E_0 of the biotin-avidin bond and the length and molecular structure (which determines the flexibility) of the tether. For the avidin-biotin pair, E_0 is very large (35 k_BT, where k_B is the Boltzmann constant and T is absolute temperature), so that binding can be expected to occur once the biotin is within a few Angströms of the avidin (Florin *et al.*, 1994; Leckband *et al.*, 1994). Compared to the polymer tether (941.1 g mol^{-1}) used in this work, biotin is a small molecule (244.3 g mol^{-1}) and therefore the intrinsic translational and rotational mobility is much higher than the PEG linker. The binding mechanism of the avidin-biotin system, as a consequence of above factors, is expected to be controlled mainly by the dynamics of the polymer tether, *i.e.*, by the energetics associated with extended polymer configurations. The binding efficiency, however, is not a direct function of the tether length, but related to different chain conformations in the PEG spacers. The average distance between the grafting sites (distance between neighbouring chains attached at the surface, d) and the radius of gyration (Flory radius, R_F) are important factors in two

possible, stable conformations (extended or coiled) of PEG chains. R_F is used to describe the dimensions of the polymer and is calculated as the root mean square distance of points along the length to the centre of gravity of the chain.

For coiled conformations, each chain occupies roughly half a sphere with the radius comparable to R_F for the polymer dissolved in a good solvent (Equation 5.3)

$$R_F = an^{3/5} \qquad \text{(Equation 5.3)}$$

where a is the size of the monomer and n is the number of monomer units.

The distance d is a function of concentration; when $d > R_F$, the chains develop as random coils (Figure 5.6a), whereas for $d < R_F$ the chains adopt a fully extended state (Figure 5.6b) (Gennes, 1980). At a low grafting concentration, the hydrophilic PEG chains are in a random-coil conformation, while an extended conformation is formed at a high grafting concentration, due to lateral repulsion (Alexander, 1977).

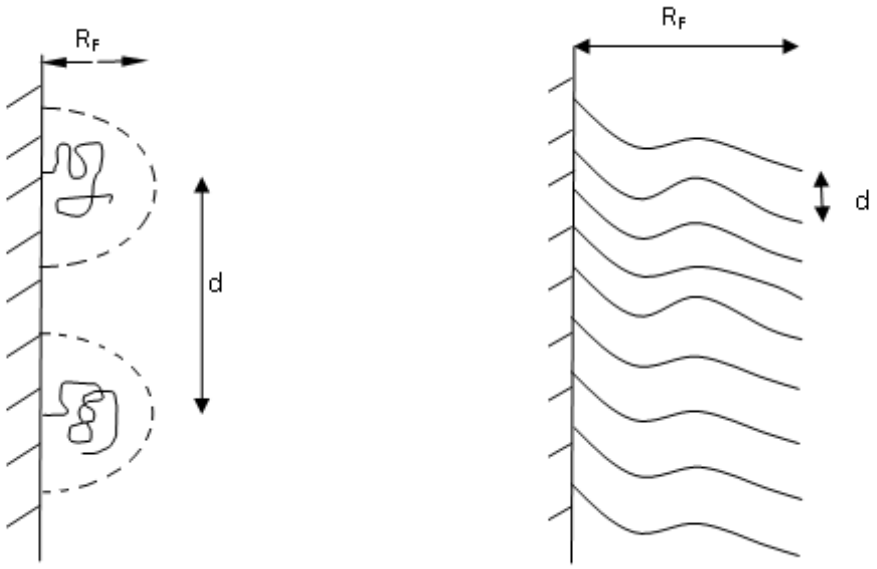

(a) (b)

Figure 5.6 Schematic diagram showing two PEG conformations: (a) random coil ($d > R_F$) and (b) fully extended ($d < R_F$) (Gennes, 1980).

5.1.3 Aims

The aim of this chapter was to measure biotin-avidin interactions as a model system for comparisons with the novel HsdR(PrrI)-MTase system investigated in Chapter 6. As a consequence, experience of the capability of the AFM for direct measurement of inter-molecular force measurement was gained. Although biotin-avidin interactions have been studied using AFM, a wide range of forces have been reported in the literature due to a number of factors discussed in the previous sections. A clearer insight into the biotin-avidin system was therefore required, not least if other protein-protein interactions are to be examined with confidence.

The first studies used avidin attached to an amino-functionalised Si_3N_4 AFM tip using glutaraldehyde (Figure 5.7) and a biotinylated mica surface. The amino groups were applied to the Si_3N_4 tip using APTES, the avidin molecules were attached to the AFM tip using glutaraldehyde as a crosslinker. Mica surface pre-treated with PLL, was coated with biotin (glutaraldehyde was used to fix the molecules). Visualisation of biotin on mica was not possible due to the small size of the molecules. Different scenarios of biotin deposition were also considered (Figure 5.5).

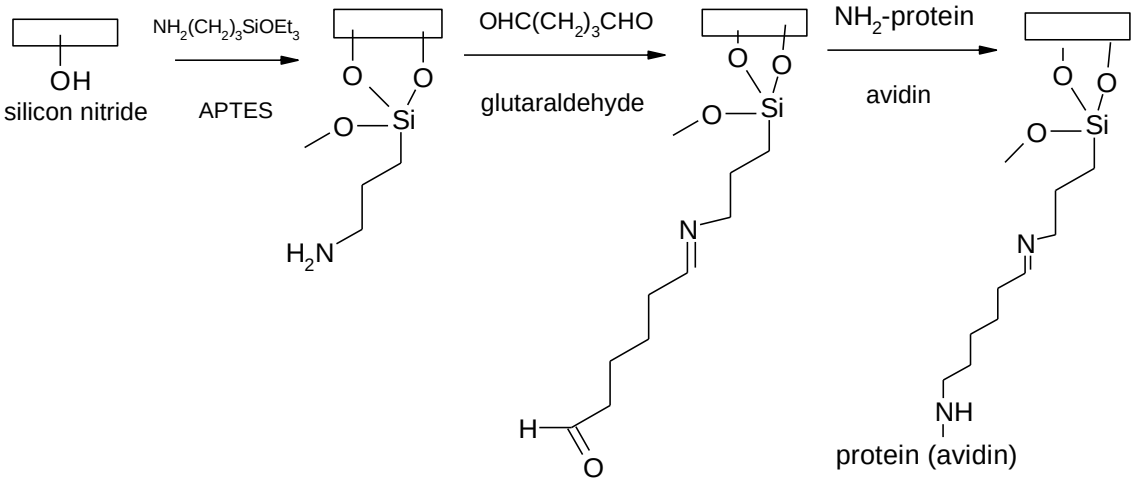

Figure 5.7. Idealised structures for the derivatisation of a Si_3N_4 tip.

In the second part of this work, biotin was covalently linked to an amino-functionalised Si_3N_4 AFM tip by means of a hetero-bifunctional PEG linker (biotin-dPEG$_{12}$-NHS) (Quanta Biodesign; Powell, OH, USA; Hinterdorfer *et al.*, 1996). The surface amino groups reacted with the *N*-hydroxysuccinimide (NHS) ester group of the hetero-bifunctional PEG linker resulting in amide bond formation (Figure 5.8). By

functionalising the tip at sufficiently low concentration, the ability to carry out single-molecule experiments was anticipated. The positively charged avidin layer was immobilised on the mica surface by simple adsorption.

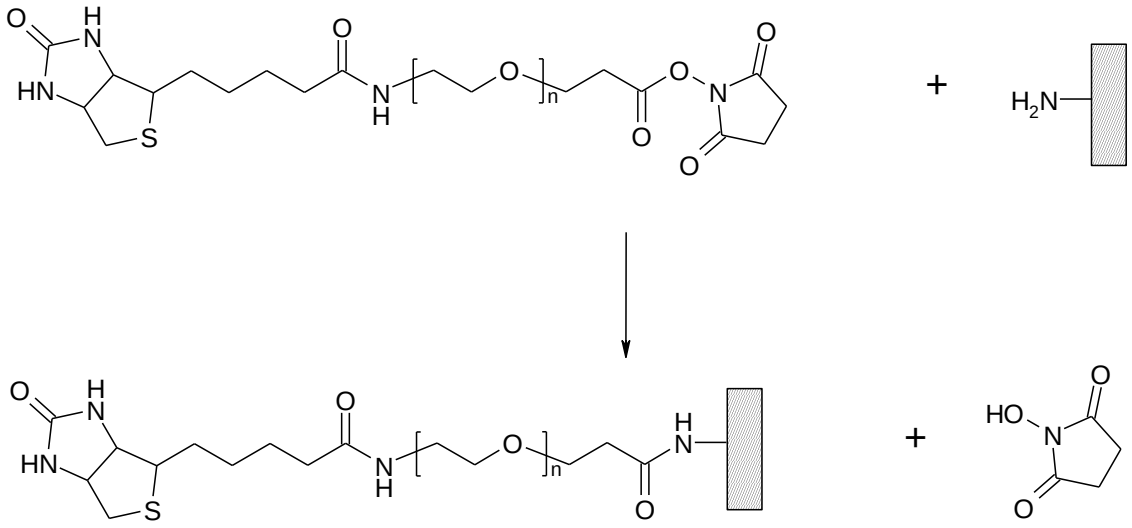

Figure 5.8. Coupling of a biotinylated PEG linker (biotin-dPEG$_{12}$-NHS; n = 12; Quanta Biodesign) to an amino-terminated Si_3N_4 AFM tip. The *N*-hydroxysuccinimide (NHS) ester group at one end of the PEG linker reacts specifically and efficiently with an NH_2 group on the Si_3N_4 to form a stable amide bond; biotin on the other end of the tether is available for force distance measurements.

5.2 Results and discussion

5.2.1 Force-distance measurements of the avidin-biotin complex using glutaraldehyde attachment

Typical examples of force-distance (retract) curves (analysed using the PUNIAS software (V 1.1 e 1.1, France)) showing multiple events for the interaction between avidin linked to a Si_3N_4 AFM tip and biotin attached to mica (Section 2.10.3.3) are shown in Figure 5.9.

The most important factor in force curves interpretation, where there are multiple events, is to distinguish between real events and eliminate the baseline noise. The last event in some cases was difficult to distinguish from the background noise and so magnifications of these regions were made also using the PUNIAS software. The horizontal regions of the retraction curves in b′ and c′ may have been produced by peeling of the PEG linkers, since there is no change in force with distance and the area under the curve represents energy (work done) associated with the process.

The control experiments were carried out between an uncoated Si_3N_4 tip (functionalised with avidin) and the mica surface after each step of functionalisation. Adhesion peaks were not observed for the uncoated Si_3N_4 tip with mica (Figure 5.10a). A distinct adhesion peak was detected between Si_3N_4 (modified with avidin) and the mica pre-treated with PLL (Figure 5.10b) and a similar shaped peak was observed for the interaction between Si_3N_4 and a biotin layer on PLL pre-treated mica (Figure 5.10c).

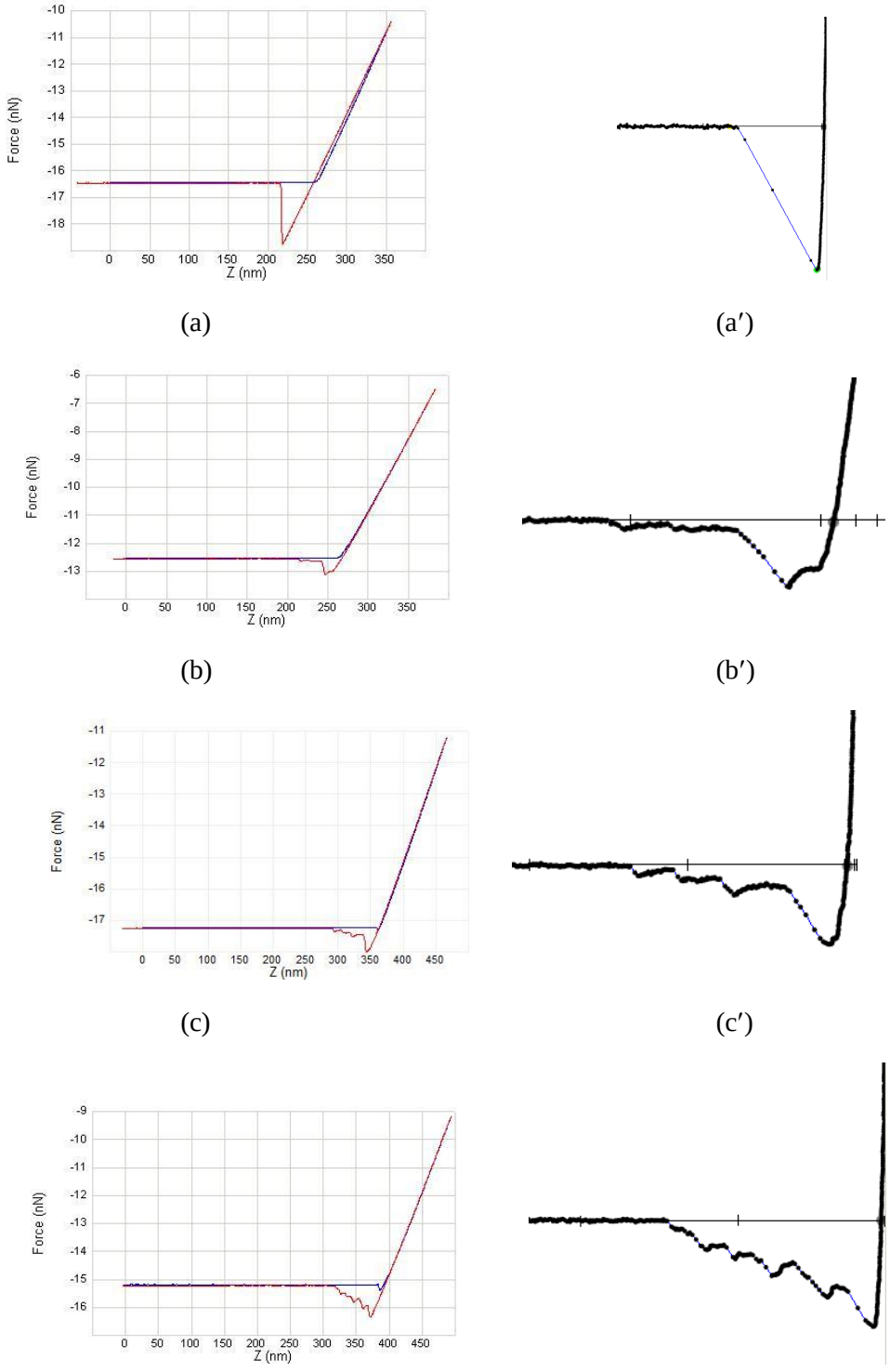

Figure 5.9. Typical force-distance curves obtained from the separation of an avidin coated tip with a biotinylated mica surface (approach curves (blue); retract curves (red)). Various interactions are possible: (a) the hard interaction between the tip and a mica surface (control); (b) hard interaction followed by a single (or multiple, but concurrent) biotin-avidin interaction(s); (c),(d) multiple biotin-avidin interactions (sequential and possibly also concurrent); (a′)-(d′) show magnified force-curves from the PUNIAS software with the baseline set to zero force.

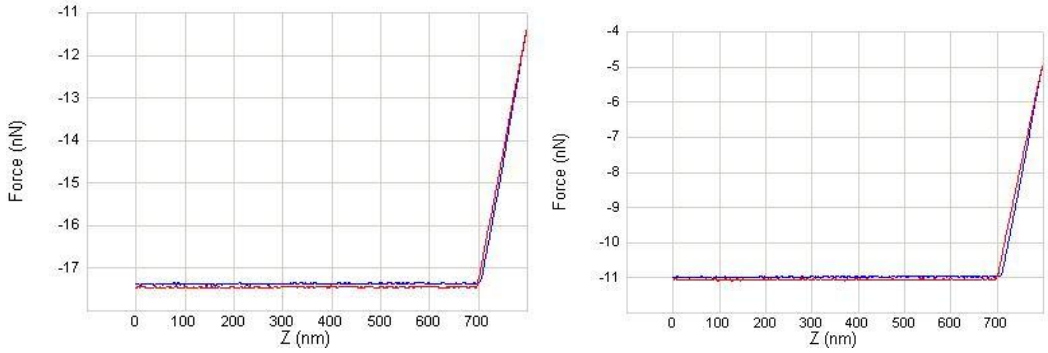

(a)

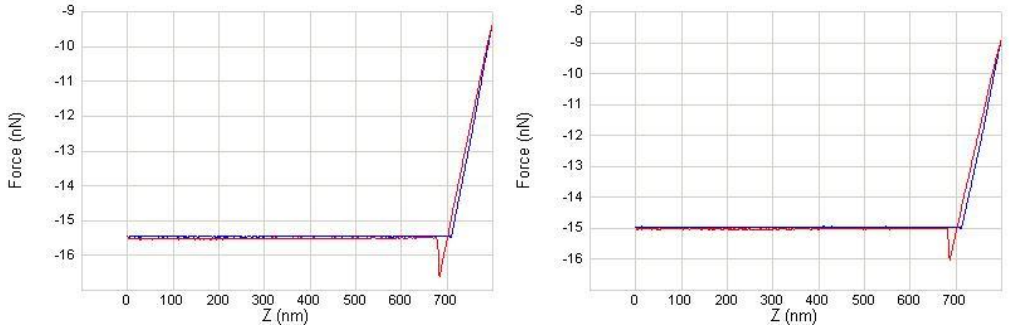

(b)

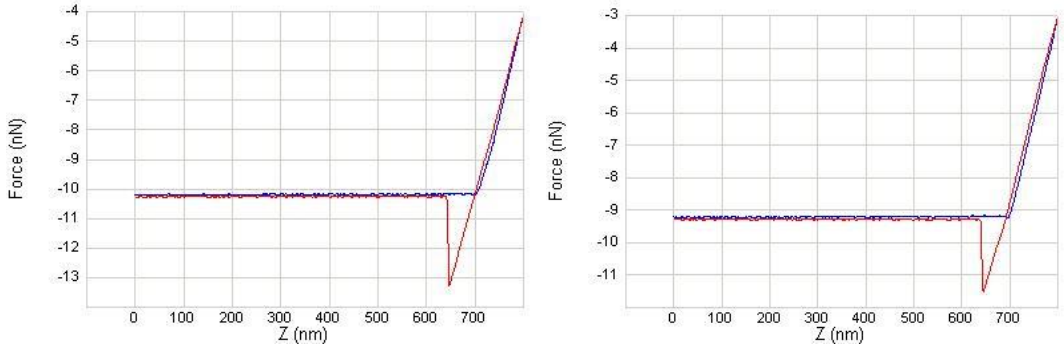

(c)

Figure 5.10 Typical force-distance curves obtained between Si_3N_4 and (a) and mica surface, (b) an mica treated with PLL and glutaraldehyde and (c) mica covered with PLL, glutaraldehyde and biotin (1 µg ml^{-1}).

The last adhesion event in a multiple peak force-distance curve is generally considered to be due to the rupture of a single bond (Figure 5.11) (Janshoff *et al.*, 2000). F_{final} is commonly defined as the "rupture force" (symbolised as f^* (Yuan *et al.*, 2000); F_i (Lo *et al.*, 2001; Piramowicz *et al.*, 2006); and F_u (Moy *et al.*, 1994)).

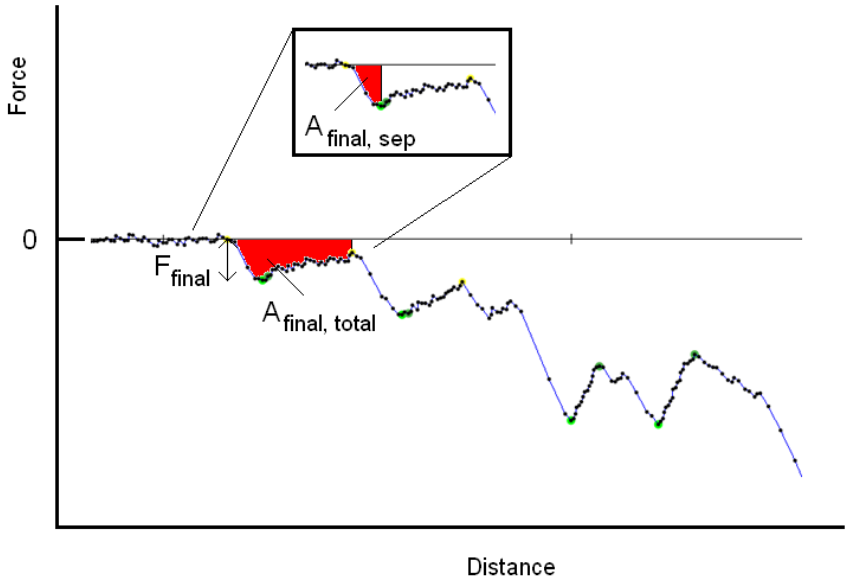

Figure 5.11. Force (F_{final}) and work ($A_{final,total}$ and $A_{final,sep}$) parameters for the last adhesion peak obtained from a typical force-distance curve.

Sixty multiple force-distance curves were analysed using PUNIAS software, where F_{final} was measured to be 56 ± 13 pN for the first distribution and second, third and fourth maxima at 98 ± 15, 161 ± 3 and 225 ± 9 pN, respectively (Figure 5.12). The values and periodicity match those reported by Florin *et al.* (1994).

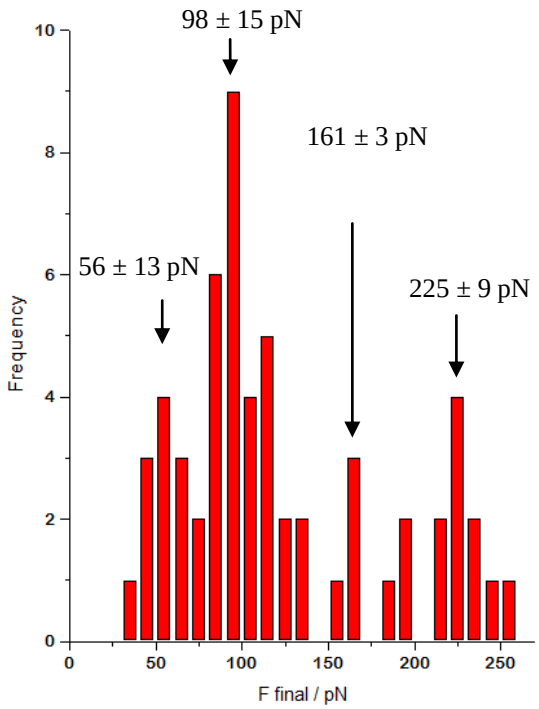

Figure 5.12. Distribution of F_{final} values obtained from biotin-avidin interactions (the biotin molecules were attached to the mica surface pre-treated with PLL and glutaraldehyde; AFM tip was functionalised with avidin after treatment with APTES where the amine functionalised tip was activated with glutaraldehyde; n = 60). F_{final} = 56 ± 13 pN and second, third and fourth force maxima at 98 ± 15, 161 ± 3 and 225 ± 9 pN (bin size 10).

The first force maxima also corresponded with a rupture force of 56 pN, at a loading rate of 10.4 nN s^{-1}, reported for the biotin-avidin system in which biotin was attached to an AFM tip using a PEG linker and avidin was adsorbed on mica (Kamruzzahan *et al.*, 2006). This is likely to be due to the rupture of a single biotin-avidin interaction.

The second and third force maxima at 98 ± 15 and 161 ± 3 pN seem to correspond with the 96 and 150 pN values also reported by Kamruzzahan *et al.* (2006), attributed to the simultaneous unbinding of two or three biotin residues, respectively. In the former case, it is unknown as to whether the rupture corresponds to two interactions on the same avidin molecule or concurrent from two molecules. The frequencies of the second maxima were *ca.* twice as large as those observed for the other maxima. This might be expected since simultaneous breakage of two biotin-avidin bonds from the same avidin molecule should be less probable than breakage of single bonds. The two other binding sites on avidin will be non-accessible to biotin as they are on the other side of the molecule, buried amongst the immobilisation matrix.

Literature values of 160 ± 20 pN have been reported by Moy *et al.* (1994) and Wong *et al.* (1999), although in the latter case, this peak was attributed to the breakage of a single bond, with two concurrent ruptures at 320 pN. In view of the results reported here and other literature values, these are likely to be due to the rupture of higher numbers of molecules. A higher force of 510 pN (loading rate 3.9 nN s^{-1}) was also reported by Piramowicz *et al.* (2006).

The area under the force-distance curve is a measure of the work done (energy) in separating the tip from the surface. In the case of the biotin-avidin system, $A_{final,sep}$ and $A_{final,total}$ refer to the work done associated with the final rupture event (Figure 5.11), the former being the area after F_{final} and $A_{final,total}$ the area under the whole final peak. The $A_{final,sep}$ and $A_{final,total}$ were obtained from 60 force-distance curves using the PUNIAS software.

$A_{final,total}$ and $A_{final,sep}$ give the total and separation energies (Figure 5.13), which were calculated to be 649 ± 311 pN nm ($6.49 \times 10^{-19} \pm 3.11 \times 10^{-19}$ J) and 262 ± 226 pN nm ($2.62 \times 10^{-19} \pm 2.26 \times 10^{-19}$ J), respectively (Figure 5.13). The $A_{final,sep}$ value compared with the energy measured with Equation 5.1 (1.46×10^{-19} J) corresponds to the rupture of 1.8 (*ca.* 2) avidin-biotin bonds, consistent with the second force maxima (98 ± 15 pN) also suggesting the rupture of 2 bonds. This may be due to a single avidin molecule with 2 available binding sites or 2 avidin molecules each using a single binding site, as detailed above. The large errors associated with these measurements are probably due to various degrees of peeling, previously described, and hence the area data must be interpreted with caution.

A typical force-distance curve obtained from an avidin-coated AFM tip and a biotinylated surface is shown in Figure 5.14. The retraction curve shows six events, in addition to the first hard interaction peak. This feature is almost always the largest adhesion value, although not all force curves show the hard interaction. The force of the first peak is termed F_0. As the AFM tip is pulled away from the surface, biotin-avidin bonds starts to break simultaneously or sequentially. The total area under the complete force-distance curve (A_0) represents the work done by the tip during retraction to break the bonds between all interacting molecules including the hard interaction. The total unfolding length (l), measured over the complete width of the force curve (distance between F_0 and F_{final}) and complete rupture of all the interactions, was also noted (Figure 5.14).

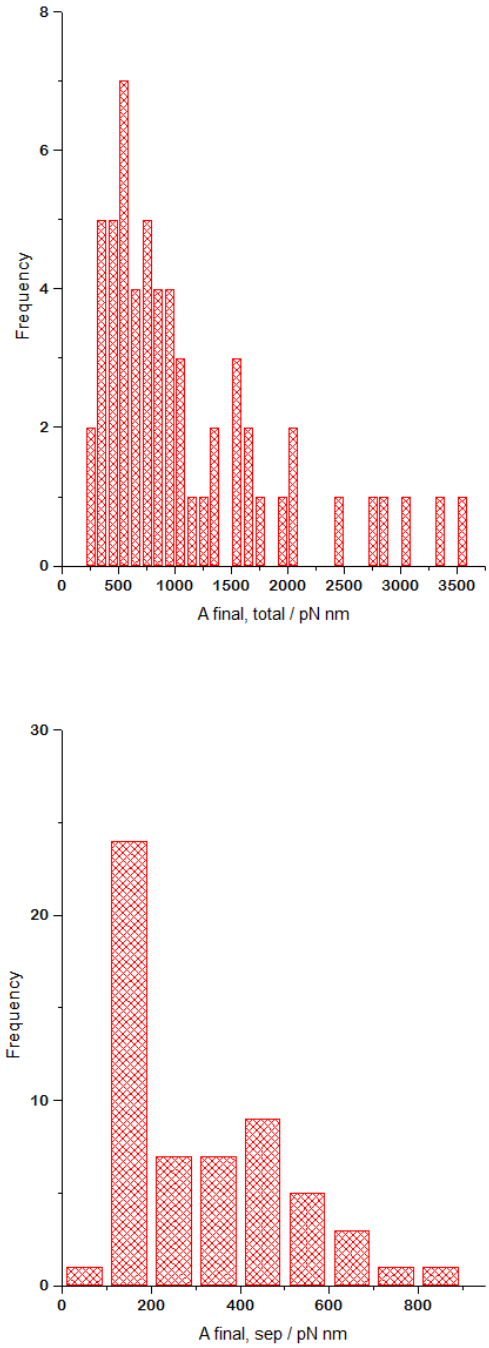

Figure 5.13. Histograms of $A_{final,total}$ (top) and $A_{final,sep}$ (bottom) calculated from the last adhesion peak in multiple-peak force-curves between an avidin tip and a biotinylated surface (n = 60 force-distance curves). Mean $A_{final,total}$ and $A_{final,sep}$ = 649 ± 311 and 262 ± 226 pN nm, respectively.

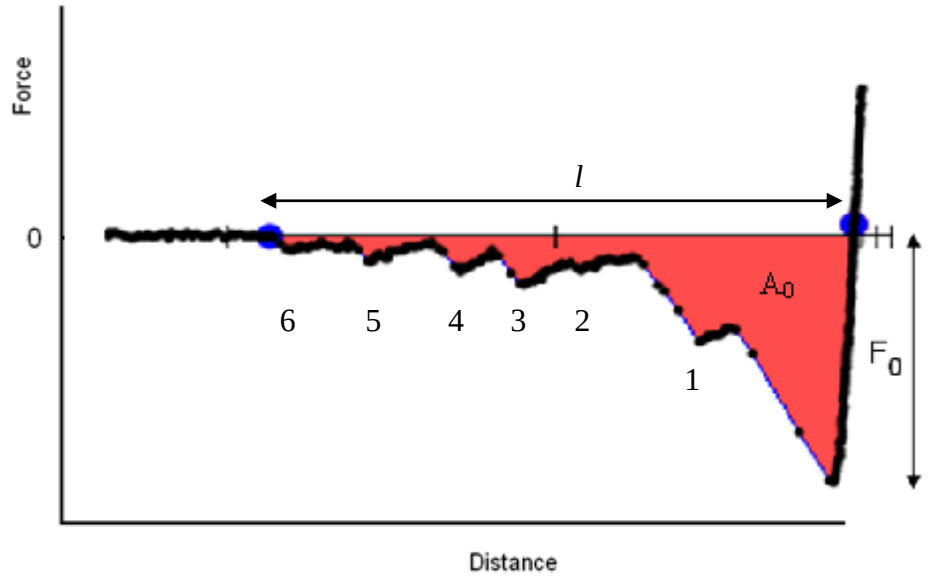

Figure 5.14. A typical AFM force-distance biotin-avidin retract curve obtained using the PUNIAS software. At least six separation events (numbered), excluding the first hard interaction, are present. The horizontal regions found in peaks 2 and 6 are probably attributed to tip sliding, where no change in force was observed. F_0 = maximum force; A_0 = work done by AFM tip to rupture bonds between all interacting molecules, including the hard interaction, l = unfolding length.

The mean F_0, A_0 and l values obtained from 60 force-distance curves were 592 ± 136 pN, 13.1 ± 5.0 nN nm and 47 ± 16 nm respectively (Figure 5.15). It is difficult to comment on the magnitude of these data since the interactions are convoluted with that from the hard interactions. The process was repeated, although if a hard interaction was observed in the force-distance curve, F_0 (now termed F_1) was chosen as the second peak and the area under the first peak omitted from the A_0 calculation (now termed A_1) (Figure 5.16).

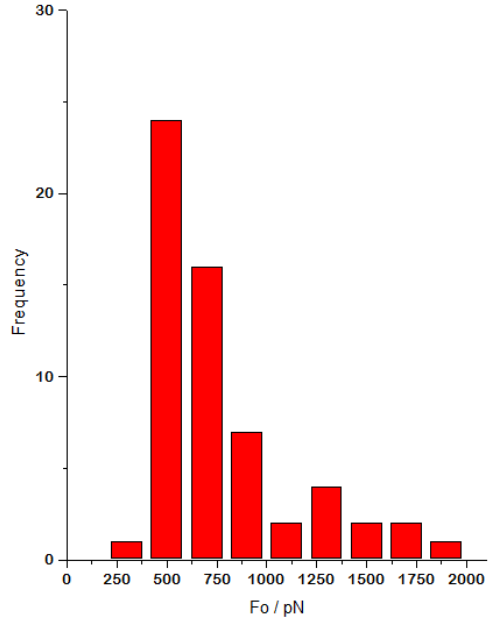

(a)

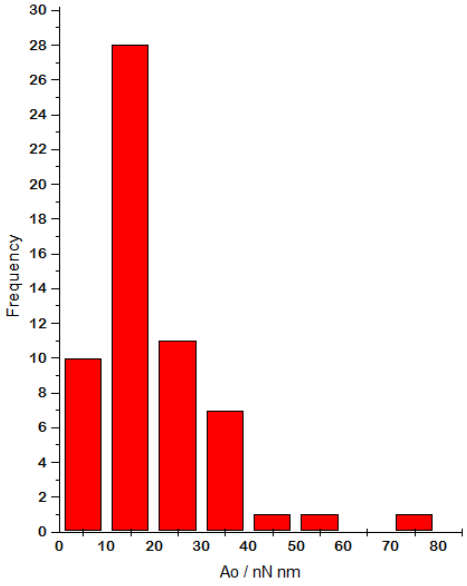

(b)

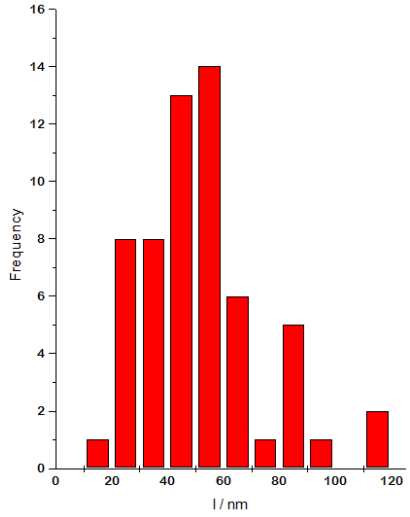

(c)

Figure 5.15. Histograms of (a) maximum rupture force (F_0) corresponding to the first adhesion peak of the biotin-avidin complex; (b) total area (A_0); (c) unbinding length (l) (n = 60 force-distance curves). Mean F_0 = 592 ± 136 pN; mean A_0 = 13.1 ± 5.0 nN nm; mean l = 47 ± 16 nm.

The next step was to exclude first hard interaction peak in the area and force measurements.

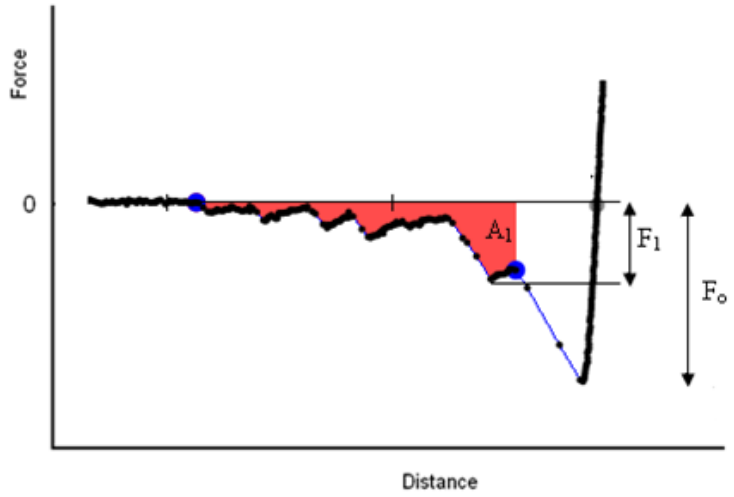

Figure 5.16. A typical avidin-biotin AFM force-distance curve showing F_1, and A_1. The blue circles show the range for calculation of A_1.

Mean values of F_1, A_1 and number of events (excluding the hard event) were calculated to be 360 ± 200 pN, 8.3 ± 4.2 nN nm and 3, respectively (Figure 5.17). Assuming the force of a single avidin-biotin interaction to be 56 pN (Kamruzzahan *et al.*, 2006), as was indeed observed (56 ± 13 pN), the number of avidin-biotin bonds corresponding to a force of 360 ± 200 pN (F_1) was 6.4 ± 3.6. This might correspond to 3 avidin molecules, each with 2 binding sites, although the error is quite large due to peeling interactions. Since the work done in breaking a single avidin-biotin bond is 35 k_BT (1.44 × 10^{-19} J; Moore *et al.*, 2006), the number of bonds ruptured for 8.29 ± 4.19 nN nm (82.9 × 10^{-10} ± 41.9 × 10^{-10} J) would be 58 ± 29.

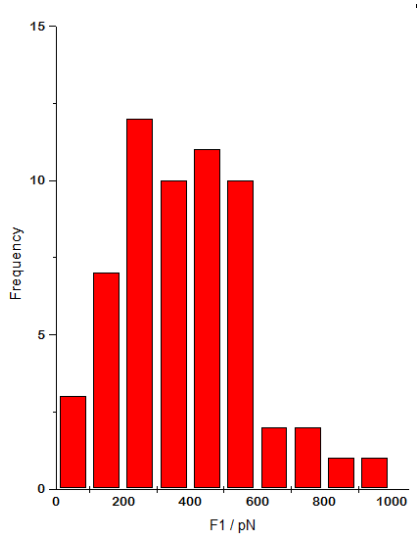

(a)

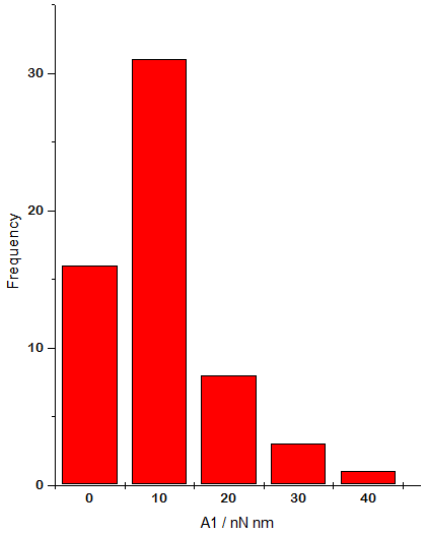

(b)

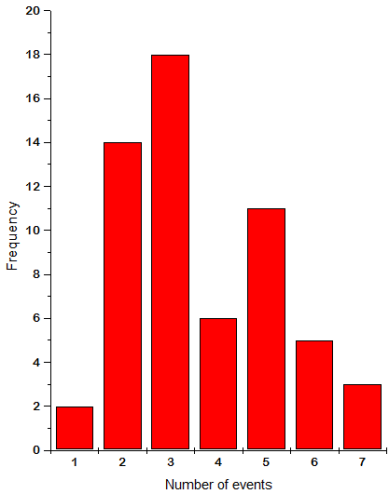

(c)

Figure 5.17. Histograms of (a) maximum rupture force (F_1) corresponding to the first adhesion peak of the biotin-avidin complex, (b) total area (A_1), and (c) number of adhesion events (excluding hard interaction) (n = 60 force-distance curves). Mean F_1 = 360 ± 200 pN; mean A_1 = 8.3 ± 4.2 nN nm; mean number of events = 3.

The theoretical number of bonds that are possible may be estimated from the tip radius and the dimensions of an avidin molecule. The height (diameter) of an avidin molecule has been reported to be 4.5 nm (Helm *et al.*, 1991), corresponding to an area of 63.6 nm^2 ($A = \pi r^2$). The contact surface area of the tip can be assumed to be a hemisphere ($A = 2\pi r^2$). The nominal tip radius for the probe used (MLCT-AUNM, Veeco) is 20 nm (max. 60 nm), corresponding to an area of 2513 nm^2 (max. 22 619 nm^2). Therefore the number of avidin molecules covering this area could be *ca.* 40 (max. 356). The number of avidin molecules is likely to be lower than this, since the contact area is less than the area defined by the radius of the tip.

Due to the presence of multiple events with the glutaraldehyde as a crosslinking reagent, it was necessary to improve the detection of single interactions. Therefore, a more sensitive approach using a PEG linker was next investigated.

5.2.2 Force-distance studies of biotin-avidin using a PEG linker

5.2.2.1 Probe microscopy imaging of the avidin layer

A simple, rapid and reproducible method was found for the irreversible immobilisation of avidin to the negatively charged muscovite mica surface in PBS buffer. The positively charged avidin tetramers were strongly bound to freshly cleaved ultra-flat mica, due to its high isoelectric point (pI = 10), as previously found with the protein lysozyme (pI = 11) (Raab *et al.*, 1999).

Initially the monolayer of avidin on mica for force-distance measurements was imaged using Tapping Mode® imaging in air. A monolayer of avidin was obtained by increasing the concentration of protein until a reasonable coverage without the presence of many aggregates was obtained with an avidin concentration of 0.05 mg mL^{-1} (0.75 µM) (Figure 5.18), which is within agreement with the literature (Ebner *et al.*, 2007b).

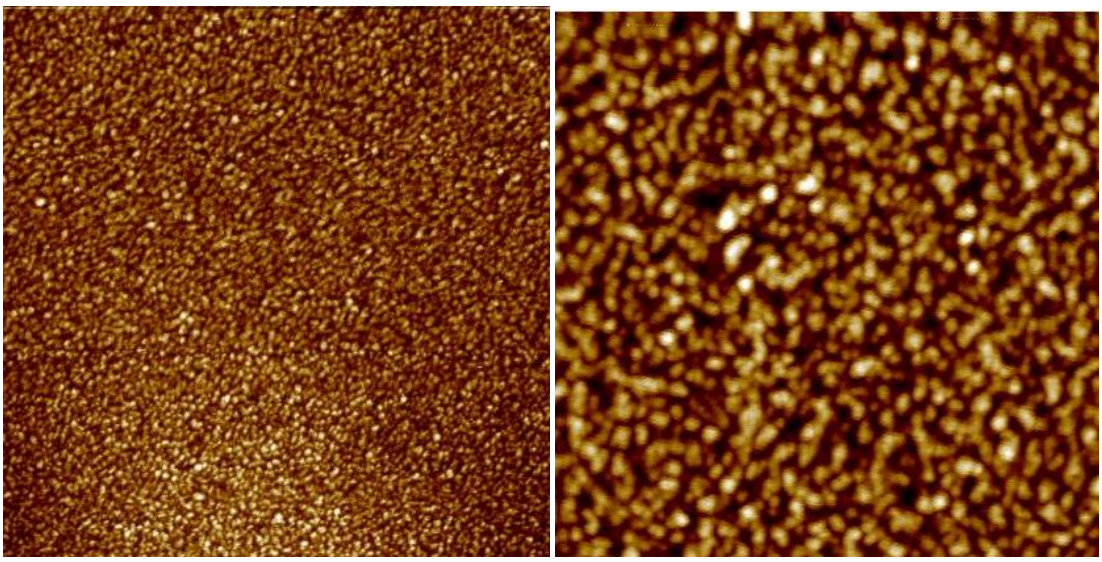

(a) (b)

Figures 5.18. Typical AFM images an avidin monolayer obtained in air (Tapping Mode®): prepared using 0.75 µM avidin (a) size 1.6 µm × 1.6 µm, z-scale 4 nm; (b) magnification of image a, size 500 nm × 500 nm, z-scale 4 nm. A few aggregates of avidin visible.

The height of the avidin molecules was found to be much smaller (1.5 – 2 nm) than predicted from the dimensions of avidin (*ca.* 4 nm), possibly due to dehydration of the molecules and subsequent flattening. In some cases, "halos" around avidin molecules were observed (Figure 5.19a), which may correspond to dehydration or tip instability. Obtaining images of avidin molecules in air was fairly difficult as artefacts were commonly observed (Figure 5.19b).

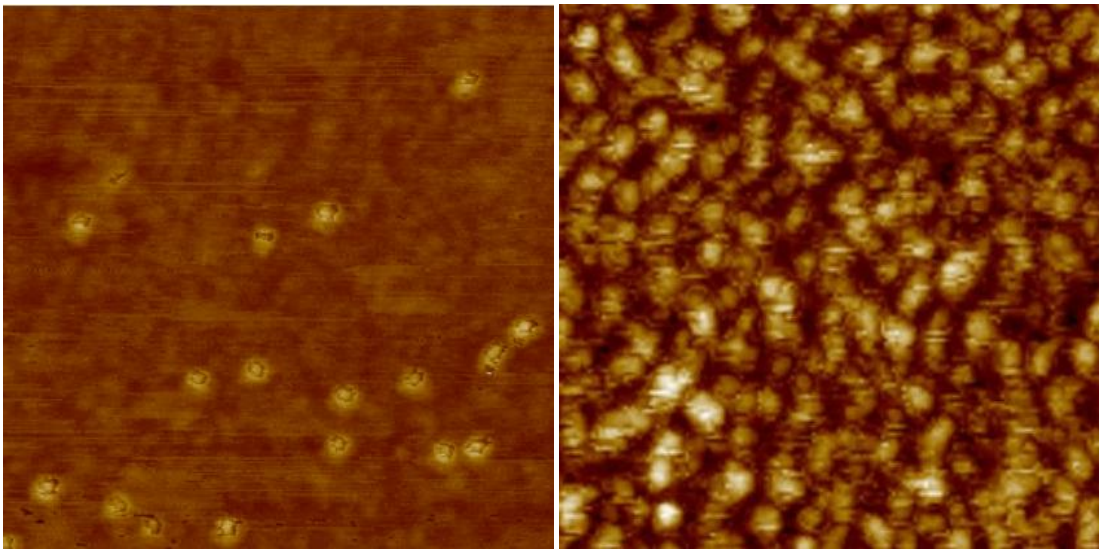

(a) (b)

Figures 5.19. AFM images of avidin molecules attached to mica obtained in air (Tapping Mode®) (a): size 295 nm × 295 nm, z-scale 4 nm; (b) size 295 nm × 295 nm, z-scale 4 nm.

5.2.2.2 Avidin layer visualisation using MAC mode

All force spectroscopy experiments were carried out in PBS buffer; therefore the visualisation of the monolayer, in a liquid environment, was essential to prove the stability of the coverage of the mica with avidin molecules.

To investigate the stability of the avidin monolayer on mica in liquid, imaging was carried out using AFM (Magnetic AC ("MAC") mode) (Agilent 5500 AFM, Wokingham, Berkshire) allowing direct studies of avidin-biotin interactions. This mode oscillates the cantilever magnetically to provide tapping imaging of delicate biological samples. A typical MAC mode AFM image of an avidin monolayer (prepared using 0.1 mg mL^{-1} in PBS buffer at pH 7.4) is shown in Figure 5.20. After producing a 500

nm × 500 nm hole in the layer a height of 3 – 4 nm was recorded, which is in agreement to the literature value (Pugliese *et al.*, 1993). This confirms dehydration effects play role during the AFM imaging in air as described previously.

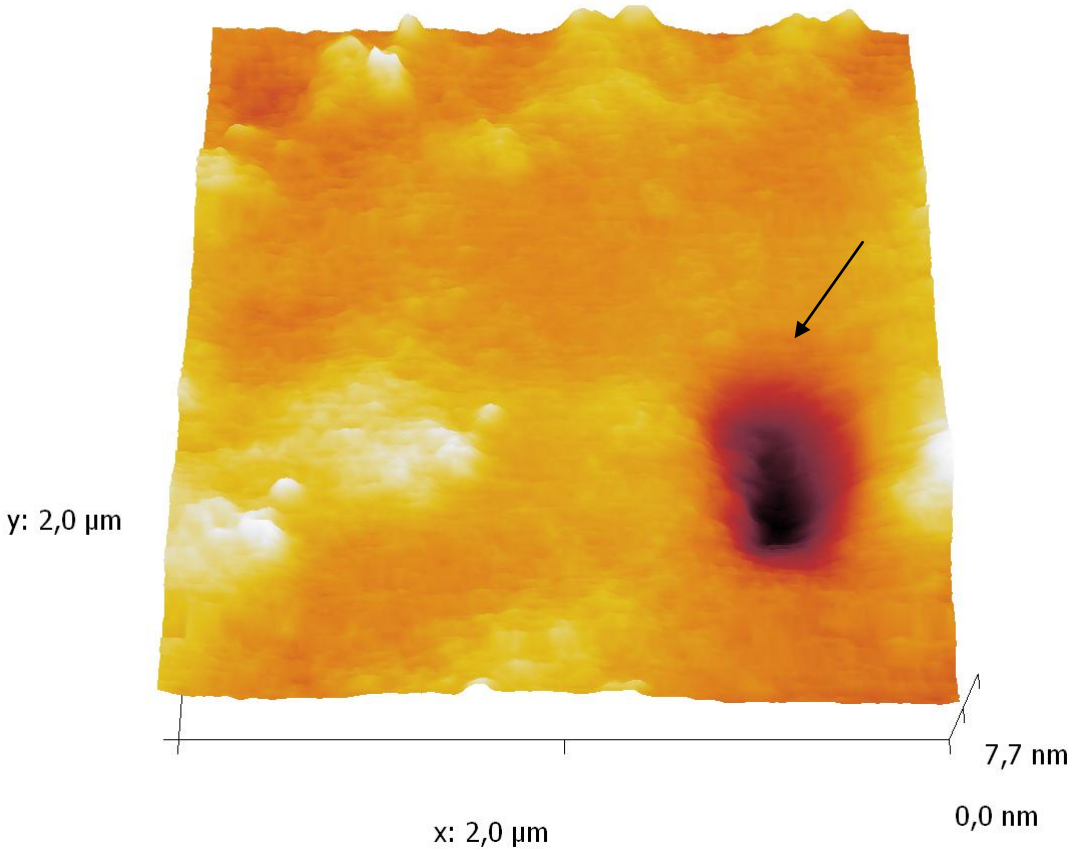

Figure 5.20. AFM MAC mode topography image of a dense avidin monolayer on mica (0.1 mg mL^{-1} in PBS buffer (pH 7.4) after 15 min of incubation. The height of the avidin monolayer was observed to be 3-4 nm after scanning in contact mode at several nN force; a "hole" (presented with arrow) of 500 nm in xy, and about 4 nm in z-direction was generated by removing the avidin layer to expose bare mica.

5.2.2.3 Length measurements of the PEG linker

Knowledge of the PEG spacer length is important in AFM force spectroscopy since tip-mica distance is the sum of the extended total spacer length and the height of the protein

(Riener *et al.*, 2003). The length of fully extended PEG tether (*L*) can be measured using Equation 5.3 (Jeppesen *et al.*, 2001)

$$L = a\,n \qquad \text{(Equation 5.3)}$$

where *n* is the number of ethylene glycol monomer units (*n* = 12, in this case) and *a* is the length of each monomer (0.35 nm) (Jeppesen *et al.*, 2001).

Therefore, in this case, L = 4.2 nm (0.35 nm × 12). The length of the spacer has been reported by the manufacturer (Quanta Biodesign) to be 4.76 nm, a value obtained using ChemDraw (CambridgeSoft, measured from the first atom in the PEG chain to the last atom). The sum of the spacer length (4.2 nm) and the height of avidin (dimensions: 56 Å × 50 Å × 40 Å) (Pugliese *et al.*, 1993) give the total expected distance of *ca.* 10 nm.

The purity of the commercially available PEG tethers range from 80 – 98 % (mixtures of different oligomer sizes in broadly or narrowly defined molecular weight) and therefore the length of the spacer should agree with the theoretical length.

An example of a force-distance plot shown in Figure 5.21. The specific rupture distance (*x*) is 10 nm, which is in agreement with the length of the spacer (*L* = 4.2 nm) plus the height of avidin molecule (*ca.* 4.5 nm). Theoretically, a shorter distance maybe achieved if the PEG linker is immobilised to the AFM tip further away from the apex. Alternatively, a distance grater then 10 nm maybe observed if a higher molecular weight PEG impurity is being stretched (Riener *et al.*, 2003).

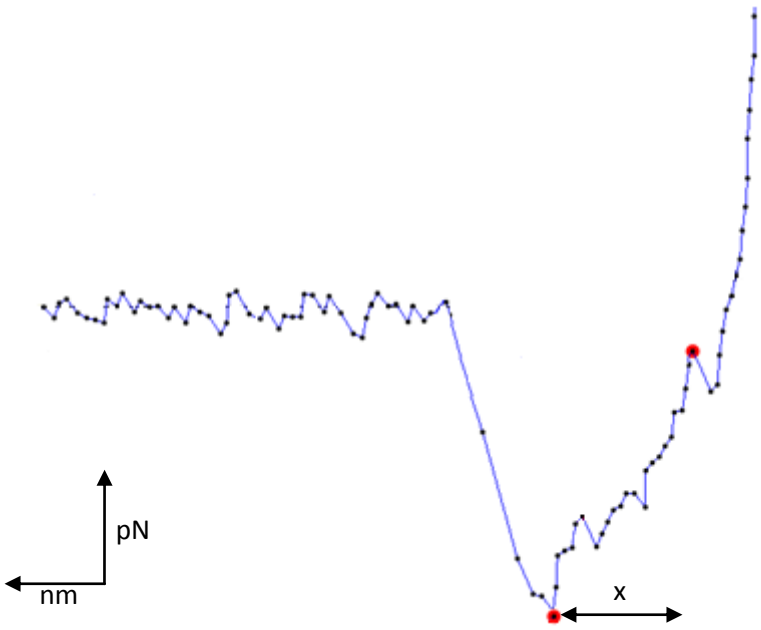

Figure 5.21. Typical AFM force-distance (retract) curve between biotinylated tip (with biotin-dPEG$_{12}$-NHS) and avidin on mica; *x* (*ca.* 10 nm) marks the specific rupture distance between point of maximum adhesion and point of zero force.

5.2.2.4 Types of interactions between biotin attached to the AFM tip via PEG linker and avidin on mica surface

Data interpretation and the distinction between specific unbinding events and non-specific interactions is time consuming and requires the analysis of thousands of force-distance curves. A low concentration of PEGylated biotin at the end of an AFM tip provide a good opportunity to study single molecule interactions between biotin and the avidin layer on mica (Figure 5.22a-c). However, the large area of the tip, free from biotin gives the possibility for a nonspecific interaction between the tip and the mica surface. Three possibilities of binding in the force-distance experiments using PEG as a tether are shown in Figure 5.22. These are (i) specific unbinding events (preceded by the nonlinear stretching of PEG) between biotin on the tip and the avidin on mica (Figure

5.22a-d); (ii) nonspecific (direct tip-substrate adhesion) binding, between the bare part of the tip and the mica surface functionalised with a monolayer of avidin (Figure 5.22e-f), where the force curve exhibited the same gradient before and after the point of zero force (*Fz*; Figure 5.22f); and (iii) a combination of both interactions, where a hard interaction and the specific unbinding event (Figure 5.22g,h).

5.2.2.5 Rupture force measurements of avidin-biotin interactions in the presence of PEG linker

Having established a stable avidin monolayer on mica, subsequent studies were focused on measuring specific unbinding forces to a freely orientated PEGylated biotin on an AFM tip. Force-distance measurements (10 × 10 array, n = 10) using two PEGylated biotin tips and two avidin-mica surfaces in PBS buffer, showed 132 specific unbinding events (binding probability of 13.2 %). Histograms of force values were plotted and fitted to Gaussian curves (Origin 4.10, Northampton, MA, US). Three force distributions were found (Figure 5.23a,b) with peaks at *ca.* 47, 93 and *ca.* 142 pN. 77 % of all analysed unbinding events for avidin-biotin (101, from 132 curves) correspond to a rupture force (F) of 47 ± 9.5 pN; 14 % of measurements showed unbinding events at 93 ± 7 pN and a third maximum (7.5 %) represented forces of 143 ± 4 pN. The 47 ± 9.5 pN maximum is in close agreement with the published values (43, 52, 58 pN), where a PEG linker was used as a tether (Riener *et al.*, 2003; Ebner *et al.*, 2007; Kamruzzahan *et al.*, 2006), respectively. The remaining 868 force curves showed hard interactions with just a few (3 max) exhibiting multiple interactions.

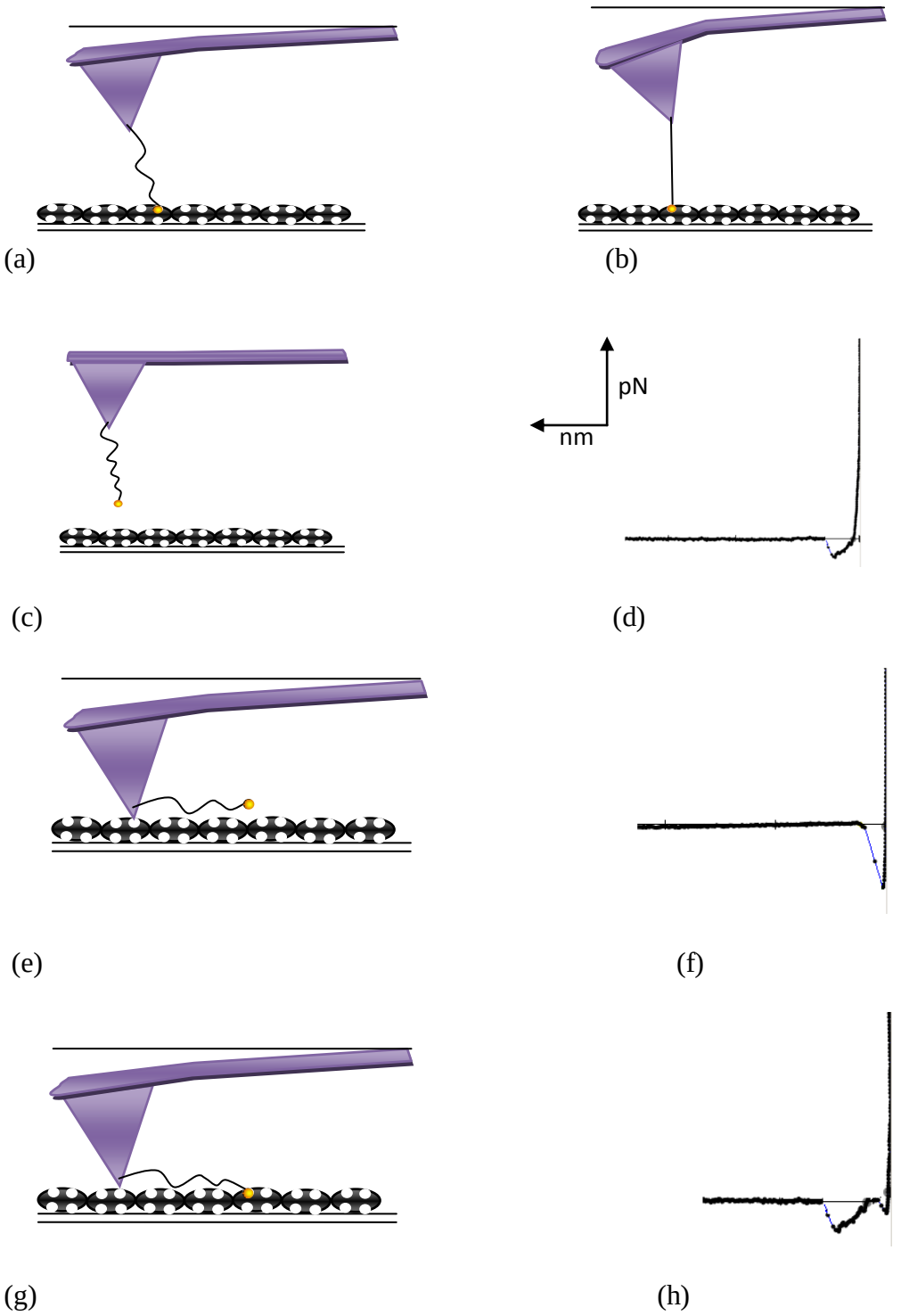

Figure 5.22. Schematic of possible types of interactions between biotin and avidin in the presence of a PEG linker and corresponding example AFM force-distance retraction curves. Specific binding between biotin and avidin molecules (a-c) and an example of retraction curve (d), where a change in gradient before and after *Fz* is observed. Direct, nonspecific adhesion between the tip and the surface (e) and corresponding typical retraction curve (f) showing no change in gradient before and after *Fz*. Simultaneous binding between the tip, biotin and avidin on the surface (g), showing a hard interaction (silicon nitride-avidin) followed by stretching of the PEG tether in the specific unbinding event (h).

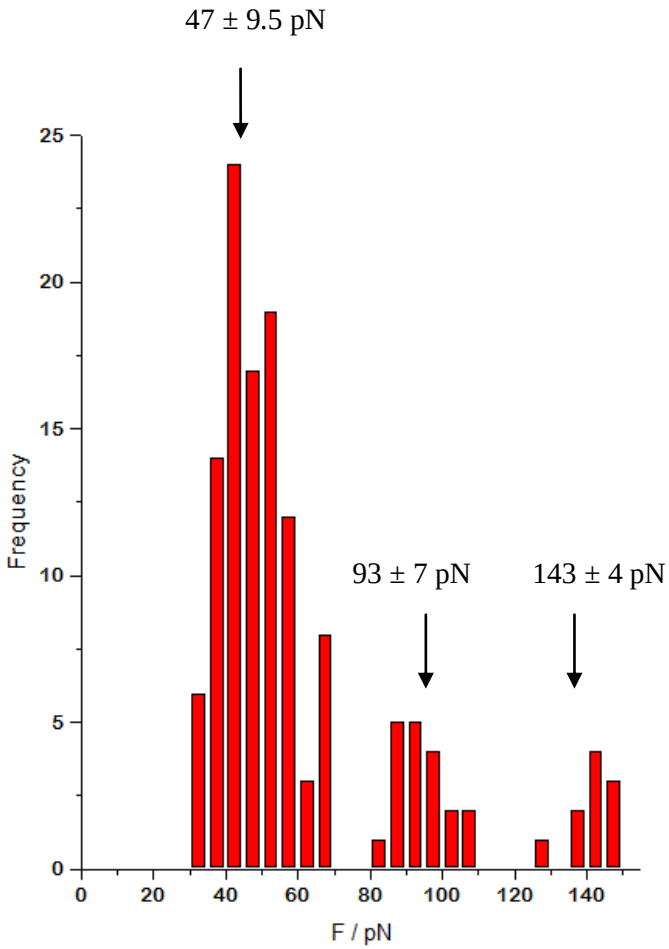

Figure 5.23. AFM force-distance measurements between a PEGylated biotin tip and avidin on mica in PBS (pH 7.4); (a) force histogram showing three force rupture maxima. The distribution at 47 ± 9.5 pN (77%), 93 ± 7 pN (14%) and 143 ± 4 pN (7.5%). (bin size 5) are shown.

Kamruzzahan *et al.* (2006) obtained the same force distribution profile to that observed in this present work, but with three peaks at 58, 96 and 150 pN. The detected three force maxima show an interesting periodicity: the second maximum (93 pN) shows the force exactly twice that of the first (47 pN) and the third maximum (143 pN) is three times bigger than the first maximum. Since the 47 pN value obtained seems to be a typical unbinding force of a single biotin-avidin interaction, the peak maxima at 93 and 143 pN probably reflect the simultaneous breakage of two and three bonds respectively, between biotin on the tip and avidin molecules immobilised on the mica surface. The

two or three biotin residues may have been located on two or three different tether molecules causing such simultaneous unbinding events with twice or thrice the unbinding force of one avidin-biotin bond, however higher forces (> 160 pN) indicating four interacting molecules were not observed.

These force maxima are also in close agreement with F_{final} values (56 ± 13, 98 ± 15 and 161 ± 3 pN) reported using the glutaraldehyde method (Section 5.2.1), although the peak at 225 ± 9 pN was not observed, probably due to their being less interacting molecules with the PEG linker. The ability to routinely observe lower forces (47 pN) using the PEG spacer may be due to a more freely oriented biotin molecule. With the glutaraldehyde method the force peak maximum at 98 ± 15 pN, corresponding to two biotin-avidin interactions, was predominated over the single interaction (by a factor of 2).

Control experiments to prove specificity

Specificity of unbinding events recorded between avidin and biotin was investigated by a blocking experiment where free biotin (0.2 mg mL^{-1}) was injected into the PBS buffer. Identical force distance measurements to that carried out previously, using the PEGylated biotin-avidin system, were repeated using the PBS buffer containing free biotin, following a 10 min incubation period (Figure 5.24 shows a typical force curve). For 95.5% of all the force curves analysed, no binding events were observed confirming blocking of the avidin binding sites with free biotins.

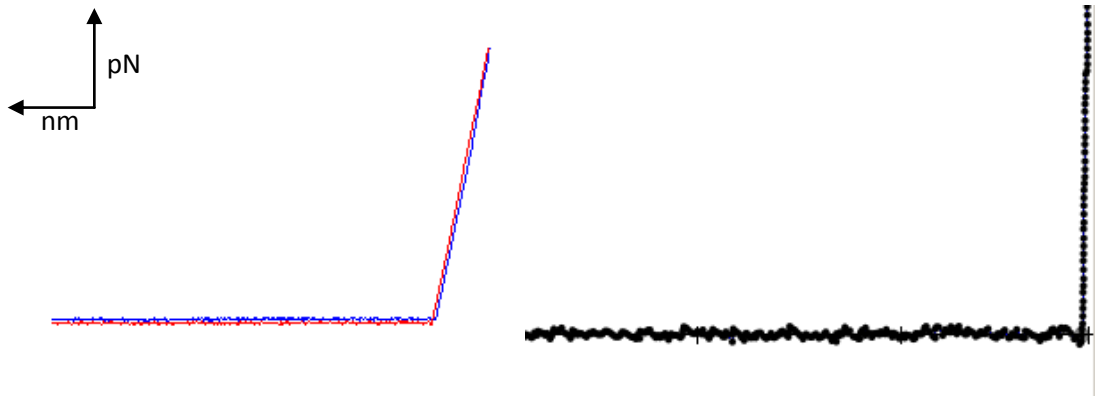

(a) (b)

Figure 5.24. AFM force curves obtained from the interactions between PEGylated biotin tip and avidin on mica in PBS buffer (pH 7.2) containing free biotin (0.2 mg mL^{-1}): (a) Blue = approach curve, red = retract curve and (b) magnification of retract curve (PUNIAS software).

5.3 Conclusions

Biotin-avidin interactions have been measured between avidin attached to the AFM tip and biotin to the mica surface (using glutaraldehyde crosslinking for attachment) and a biotinylated tip (with a PEG linker) and avidin attached to mica. In the former case, many multiple adhesion events (max seven) were observed in the majority of force curves; the last adhesion event (F_{final}) showed four possible values of 56 ± 13, 98 ± 15, 161 ± 3 and 225 ± 9 pN, the first corresponding to a single biotin-avidin bond. The other three force maxima are quantised multiples of the single interactions, showing the rupture of 2, 3 and 4 bonds.

When a PEG linker was used, single biotin-avidin interactions (47 ± 9.5 pN) were also measured, as was a periodicity between force maxima showing two other peaks at 93 ± 7 and 143 ± 4 pN, corresponding to the rupture of two and three avidin-biotin bonds.

Using the PEG and glutaraldehyde methods allowed the acquisition of similar force values corresponding to a single bond rupture, however in the former attachment single interactions were mostly detected (~ 70% of analysed force-distance curves), whereas for the latter method obtained forces represented mostly two interactions. The use of the PEG linker allowed more sensitive measurements to be made using smaller numbers of interactions. This detailed study of the well-known biotin-avidin model system will allow meaningful interpretation of AFM force curves from the novel HsdR-MTase system investigated in the next chapter.

The data obtained in the first part of the chapter reflects the learning process in force spectroscopy studies. The difficulties in the interpretation of the force distance curves representing multiple interactions and the lack of a blocking experiment, are the reasons the data needs to be treated with caution. The single force values obtained were similar to those reported by Kamruzzahan *et al.* (2006), however forces are dependent on the loading rate, and also the average rupture force at any particular velocity is not sufficient for the determination of the strength of the molecular bond.

Chapter 6

Force spectroscopy studies with EcoR124I

6.1 Introduction

In this chapter, an *in vitro* assembled version of EcoR124I incorporating the GST-HsdR(PrrI) subunit and the wild-type-MTase was studied for the first time using AFM force spectroscopy. The investigations built upon the biotin-avidin 'model' experiments of the previous chapter, where PEGylated biotin was covalently linked to an AFM tip and separated from an avidin layer on mica. The use of the PEG linker was to improve the chances of observing single-molecule interactions. Dynamic force spectroscopy (DFS) was used to obtain kinetic information on this novel system.

6.1.1 Dynamic force spectroscopy

DFS has been found to be a powerful tool for the characterisation of the dynamic properties of biomolecular complexes and provides new insights into the energy landscape of binding interactions. By the exposition of the single bond to an external force, the lifetime of the bond shortens and barriers present in the energy landscape become lower (Bell, 1978). The breakage of the bond can be detected by measuring the rupture force during retraction of the AFM tip. This method provides useful information about kinetic parameters: dissociation rate of the bond k_{diss}, position of energy barrier x_{diss} and lifetime of the bond $\tau(0)$.

The natural lifetime of the bond can be reduced by the application of force accelerating rupture of the bond between a pair of molecules. The rupture of the bond is a result of the lowering of the energy barrier due to the applied force, where the increase in dissociation rate of the bond and concomitant decrease in association rate can be observed.

The lifetime of the bonds formed between pairs of interacting molecules is characteristic of particular molecules and spontaneous dissociation occurs when the intermolecular potential of the dissociation landscape exceeds the energy acquired through Brownian excitation (Evans, 1999). The external force produced by the AFM tip reduces the natural lifetime of the bond (Evans, 2001). The dissociation and association rates under the applied external force $k_{diss}(f)$ and $k_{ass}(f)$ can be described by Equation 6.1a and b.

$$k_{diss}\,(f) = k_{diss}(0)\exp\left\lfloor\frac{f\,x_{diss}}{k_BT}\right\rfloor \qquad \text{(Equation 6.1a)}$$

$$k_{ass}\,(f) = k_{ass}(0)\exp\left\lfloor-\frac{f\,x_{diss}}{k_BT}\right\rfloor \qquad \text{(Equation 6.1b)}$$

where $k_{diss}(0)$ and $k_{ass}(0)$ are natural dissociation and association rates, respectively, f is the applied force, x_{diss} is the distance of the energy barrier to rupture, k_BT is thermal energy (4.1 pN nm).

The dissociation rate of the bond is characteristic for any particular pair of molecules and varies between 10^{-6} and 10^{1} s^{-1} (Schwesinger *et al.*, 2000; Merkel, 2001, Zhang *et al.*, 2002). $\tau(0)$, in the absence of an external force, for ligand-receptor complexes this value varies between 10^{-4} s and a few min and can be measured using Equation 6.2.

$$\tau(0) = \frac{1}{k_{diss}(0)} \quad \text{(Equation 6.2)}$$

Unbinding forces between a pair of molecules, measured at constant pulling velocity, represent only a single point in a continuous spectrum of bond strength (Evans and Ritchie, 1997). Bell's model has been extended: f is assumed to vary linearly with time (t) (Equation 6.3a),

$$f = R_f . t \quad \text{(Equation 6.3a)}$$

where R_f is the rate of force alteration with t, termed the loading rate (Equation 6.3b).

$$R_f = \frac{dF}{dt} \quad \text{(Equation 6.3b)}$$

The equation of the probability density $N(t)$ of a molecular complex dissociating under the force f at time t shows that rupture forces are dependent on R_f at which the load (force) is applied to the bond (Equation 6.4).

$$\frac{dN(t)}{dt} = -k_{diss}(R_f t)N(t) \quad \text{(Equation 6.4)}$$

R_f can be determined as the product between the effective spring constant k_s (stiffness) of the system (the elasticity of both cantilever k_c and bound molecules k_b) (Yuan *et al.*, 2000) and the velocity υ in which the force is applied (in practice, the retraction speed of the AFM tip) (Equation 6.5).

$$R_f = k_s \upsilon \qquad \text{(Equation 6.5)}$$

The measured forces necessary to rupture the bond existing between molecules in the complex increase over time during pulling experiment with increasing value of R_f (Hinterdorfer and Dufrene, 2006). R_f can be varied by changing υ and/or by using a number of different cantilevers (k_c) (Yuan *et al.*, 2000). k_s may be measured using Equation 6.6

$$\frac{1}{k_s} = \frac{1}{k_c} + \frac{1}{k_b} \qquad \text{(Equation 6.6)}$$

and from the slope of an AFM force-distance (retract) curve (Figure 6.1).

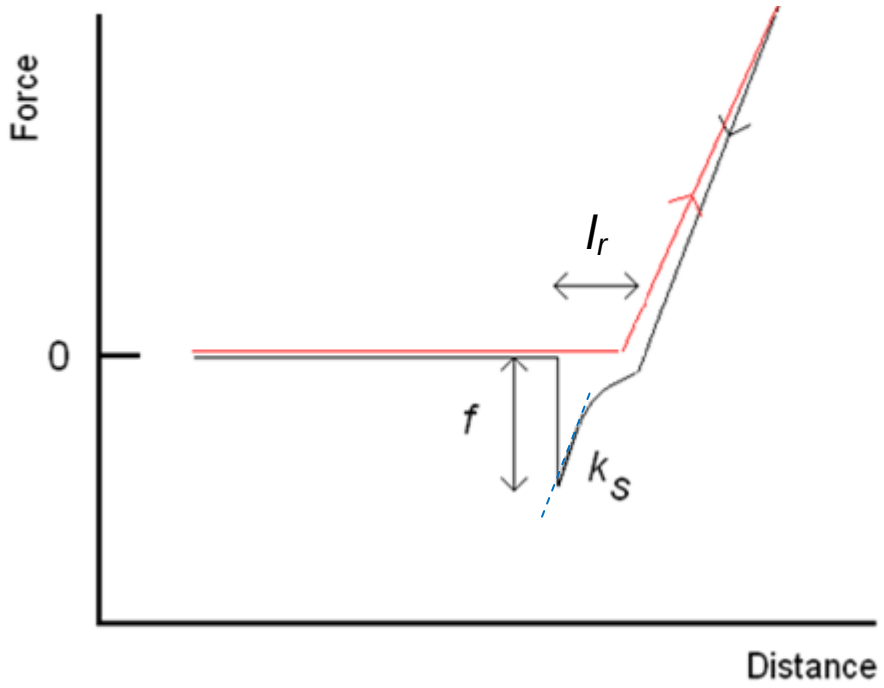

Figure 6.1. Determination of k_s from an AFM force-distance curve; l_r = rupture length; retract curve (black), approach curve (red).

The retraction velocity in AFM is usually in the range of 10 – 10 000 nm s^{-1}, although, in practice, the upper and lower limits are *ca.* 5,000 nm s^{-1} and 100 nm s^{-1} due to hydrodynamic effects and duration / signal-to-noise problems, respectively (Lee and Marchant, 2003).

The most probable binding force required to rupture a molecular complex bond (f^*; mean force) is related to R_f as shown in Equation 6.7. A plot of f^* *vs.* ln(R_f) (Equation 6.8) enables x_{diss} and $k_{diss}(0)$ to be calculated from the gradient and intercept, respectively (Equations 6.9 – 6.12) (Evans and Ritchie, 1997). R_f must be obtained over several orders of magnitude.

$$f^* = \frac{k_B T}{\Delta x} \ln\left(\frac{R_f}{k_{diss}(0)\frac{k_B T}{\Delta x}}\right) \quad \text{(Equation 6.7)}$$

$$f^* = \frac{k_B T}{x_{diss}} \ln\left(\frac{x_{diss}}{k_{diss}(0).k_B T}\right) + \frac{k_B T}{x_{diss}} \ln R_f \quad \text{(Equation 6.8)}$$

$$a = \frac{k_B T}{x_{diss}} \ln\left(\frac{x_{diss}}{k_{diss}(0).k_B T}\right) \quad \text{(Equation 6.9)}$$

$$b = \frac{k_B T}{x_{diss}} \quad \text{(Equation 6.10)}$$

$$k_{diss}(0) = \frac{1}{b} e^{-\frac{a}{b}} \quad \text{(Equation 6.11)}$$

$$x_{diss} = \frac{k_B T}{b} \quad \text{(Equation 6.12)}$$

The idealised situation is where the complex consists of only two (bound and unbound) states, separated by one transition state and only single energy barrier at a given position along a specific reaction path has been considered. The activation energy for the dissociation held by the molecular complex is the difference in energy between the

bound state (low energy) and the transition state (*i.e.*, maximum of the energy barrier) to which the system must be raised before dissociation can occur (Lee *et al.*, 2007).

In the absence of an applied force, the bound state (shown as 'A' in Figure 6.2a) with the minimum energy aspires to the unbinding state ('B', Figure 6.2a) at higher energy; the energy barrier, including a transition state, needs to be overcome. An applied force lowers the energy barrier (blue line) by $Fx_{diss,}$ tilting the energy landscape and lowering the energy barrier relative to k_BT (thermal energy) at the transition state (x_{diss}; distance between bound state and location of maximum barrier) and the thermal force scale k_BT / x_{diss} emerges to become tilted by a mechanical potential. x_{ass} represents the distance between the maximum energy barrier and the unbound state.

According to the theoretical predictions (Evans and Ritchie, 1997), f rises linearly with the R_f on a half-logarithmic scale, which is characteristic for a single-energy barrier in the thermally activated regime (Merkel *et al.*, 1999) (Figure 6.2b).

Most biomolecular interactions consist of large numbers of small interactions, involving two or even more energy barriers. DFS of avidin-biotin and streptavidin-biotin complexes have shown multiple energy barriers in the dissociation pathway, revealed by distinct linear regions in the f^* *vs.* R_f plots (Merkel *et al.*, 1999).

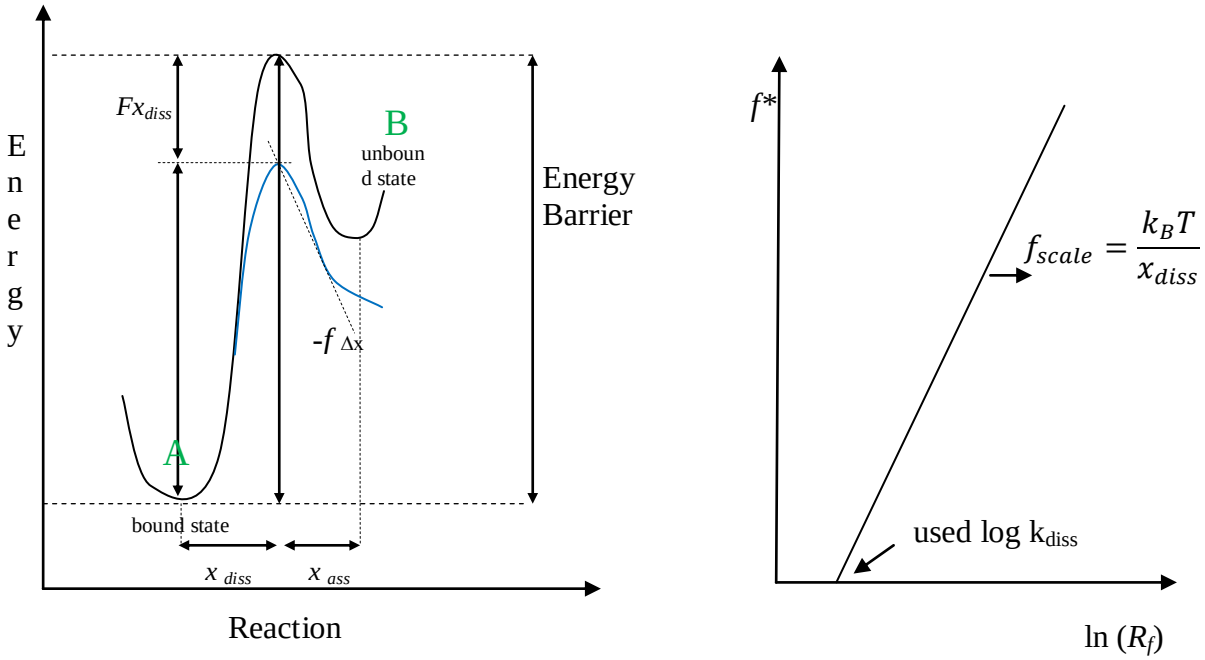

Figure 6.2. (a) Schematic diagram of the energy landscape showing the dissociation of the bond in the absence and presence of an external, applied force (black and blue lines, respectively); (b) DFS spectrum showing f^* *vs.* ln(R_f) is a straight line, indicative of the single energy barrier with one transition state seen in (a). Adapted from Evans, 1999.

Figure 6.3a shows the energy landscape of a system with two energy barriers with different heights. In a situation where no force is applied, the second barrier is higher than the first one. Tilting of the energy landscape through the application of an external force causes the first, smaller barrier to exceed the second barrier (Evans, 1998). Two linear regions in the DFS spectrum are characteristic of a system having two energy barriers shown (Figure 6.3b). The energy landscape of the thermally driven dissociation can be described using the dissociation rate $k_{diss.}$

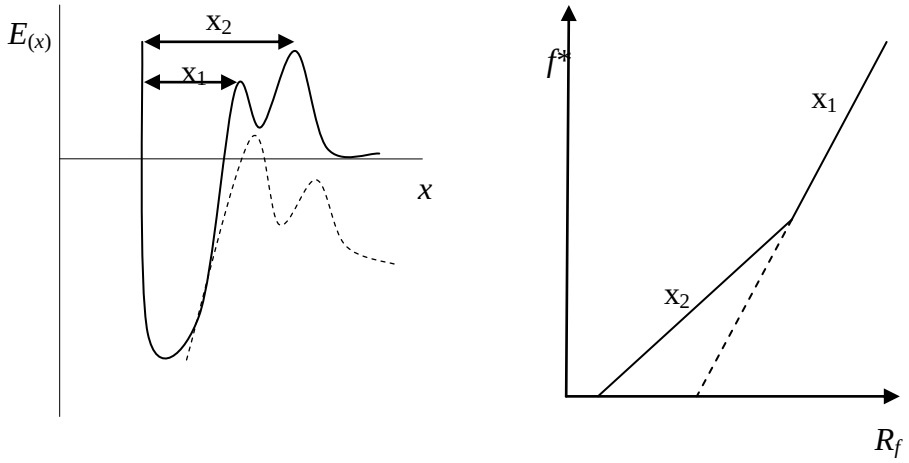

(a) (b)

Figure 6.3. (a) Energy landscape with two energy barriers. In the absence of an applied force, the second energy barrier is higher than the first peak. As the energy landscape becomes tilted under an applied force, the relative heights of the barriers change until eventually the first energy barrier becomes more prominent; (b) f^* *vs.* $\ln(R_f)$ (DFS spectrum) for a cascade of two sharp energy barriers. Adapted from Evans, 1999.

Kinetic parameters ($k_{diss}(0)$ and x_{diss}) have been obtained for streptavidin-biotin (Yuan *et al.*, 2000), leukocyte function-associated antigen-1 and intercellular adhesion molecule-1 (Zhang *et al.*, 2002), ryanodine receptor 1 (RYR1)-anti-RYR1 (Kada *et al.*, 2001) and selectins and glycoproteins (Fritz, 1998; Evans *et al.*, 2001).

6.1.2 AFM force resolution

The lower limit (noise) of soft cantilevers used in this work (k_{nom} = 10 pN nm^{-1}; MLCT-AUNM, Veeco, Santa Barbara, CA, USA) was assessed to be around 10 pN (Jung *et al.*, 2007). Thermal vibration of AFM cantilevers limits the force resolution in AFM. For typical soft cantilevers (k_{nom} = 10 to 100 pN nm^{-1}), the thermal vibration amplitudes of the free cantilevers at room temperature (25 °C) varies from 0.2 to 0.64 nm, respectively, corresponding to force fluctuations between 6 pN and 20 pN, which set up the lower limit (noise) of force resolution.

6.1.3 Structure of antibodies

Some aspects of this chapter will involve attaching antibodies to an AFM tip and measuring specific antibody-antigen interactions.

The immunoglobulins, also known as antibodies, are proteins produced by the immune system (lymphocytes B) as a response to the presence of harmful substances, called antigens. In the moment of recognition of the antigen by the antibody, high specific bonding occurs, strong enough to inactivate or neutralise the antigen. The specificity of the antibody can be defined as the functional ability to discriminate between the target antigen and other chemically similar structures. IgG antibodies are large molecules (150 kDa) resulting from a tetramer structure (Figure 6.4), consisting of four peptide chains: two identical heavy chains (linked to each other and to a light chain, each by disulfide bonds) and two identical light chains, all together forming a flexible Y-shaped structure. The ends of the two identical halves each contain an identical antigen binding site (Fab), whereas the fragment involved in the process necessary to destroy the antigen is called Fc, which consists of two equals segments of the H chains. Heavy and light chains contain variable (V) and constant (C) regions. The former region contains antigen-binding sites and recognises a particular antigen and is responsible for the specificity of antigen binding. The different classes of antibody (IgM, IgG, IgE, IgA, IgD) contain different variable regions (V) in the heavy chains. The constant region (C) is responsible for the structure of the antibody molecule and its recognition by other components of immune system. In all types of IgG, the conservative regions of the L chains (C_L) contain the same sequence of amino acids and likewise the same region in

the heavy chains (C_H) are identical and can be divided into three segments (C_H1, C_H2, C_H3) (Freifelder, 1987).

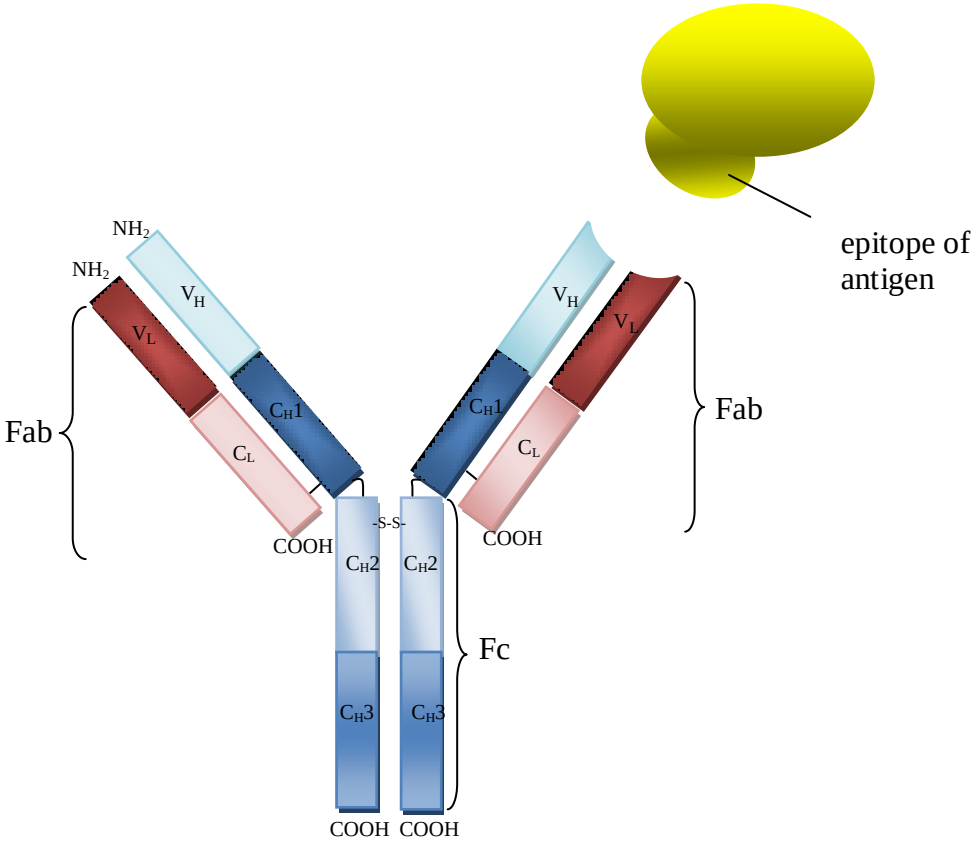

Figure 6.4. Schematic structure of an antibody molecule. The blue blocks represent heavy chains with the presence of particular regions; V_H is the variable and three conservative (C_H1, C_H2, C_H3) regions. The red and pink blocks represent variable (V_L) and conservative (C_L) regions in the light chains, respectively. The IgG molecule binds two antigens, one at each of the two binding sites in a V region (Fab). Conservative regions (C_H2 and C_H3) of heavy chains represent the Fc fragment.

6.1.4 Aims

For the first time, DFS studies of the GST-HsdR(PrrI) containing assembly complex of EcoR124I were performed. The main aim was to study the kinetics of the dissociation of the GST-HsdR(PrrI)-MTase (R_1-complex), characterise the energy landscape of this process and gain knowledge about the forces necessary to rupture bonds existing

between subunits. The DFS measurements were obtained with different retraction speeds of the AFM tip leading to different loading rates. k_{diss}, x_{diss} and $\tau(0)$ of the studied molecular complex were measured.

The force distance curves were recorded between mica surfaces coated with a uniform layer of MTase (Section 2.10.2.2) and Si_3N_4 AFM tips, amino functionalised (Section 2.10.3.4) and coupled to a PEG linker (Section 2.10.3.5). The maleimide (MAL) group at the other end of the linker was reacted with the thiol group in cysteine of glutathione (Figure 6.5).

The structure of glutathione is complementary to the glutathione *S*-transferase (GST; 26 kD) binding site. GST is an enzyme that catalyses nucleophilic attack by reduced glutathione (GSH) on non-polar compounds containing an electrophilic carbon, nitrogen, or sulphur atom (Hayes *et al.*, 2005). GST is widely used to form the GST gene fusion system, which is used to purify and detect proteins of interest, here HsdR(PrrI), *via* the high affinity for glutathione of the fusion derivative GST-HsdR(PrrI). This method of attachment, therefore, has been chosen for DFS measurements.

A thiol-mediated coupling is also used in commercially available glutathione beads and does not hinder the binding of GST. HsdR(PrrI) fused with GST could be easily attached to the AFM tip (functionalised with PEG), *via* the glutathione, to avoid steric effects.

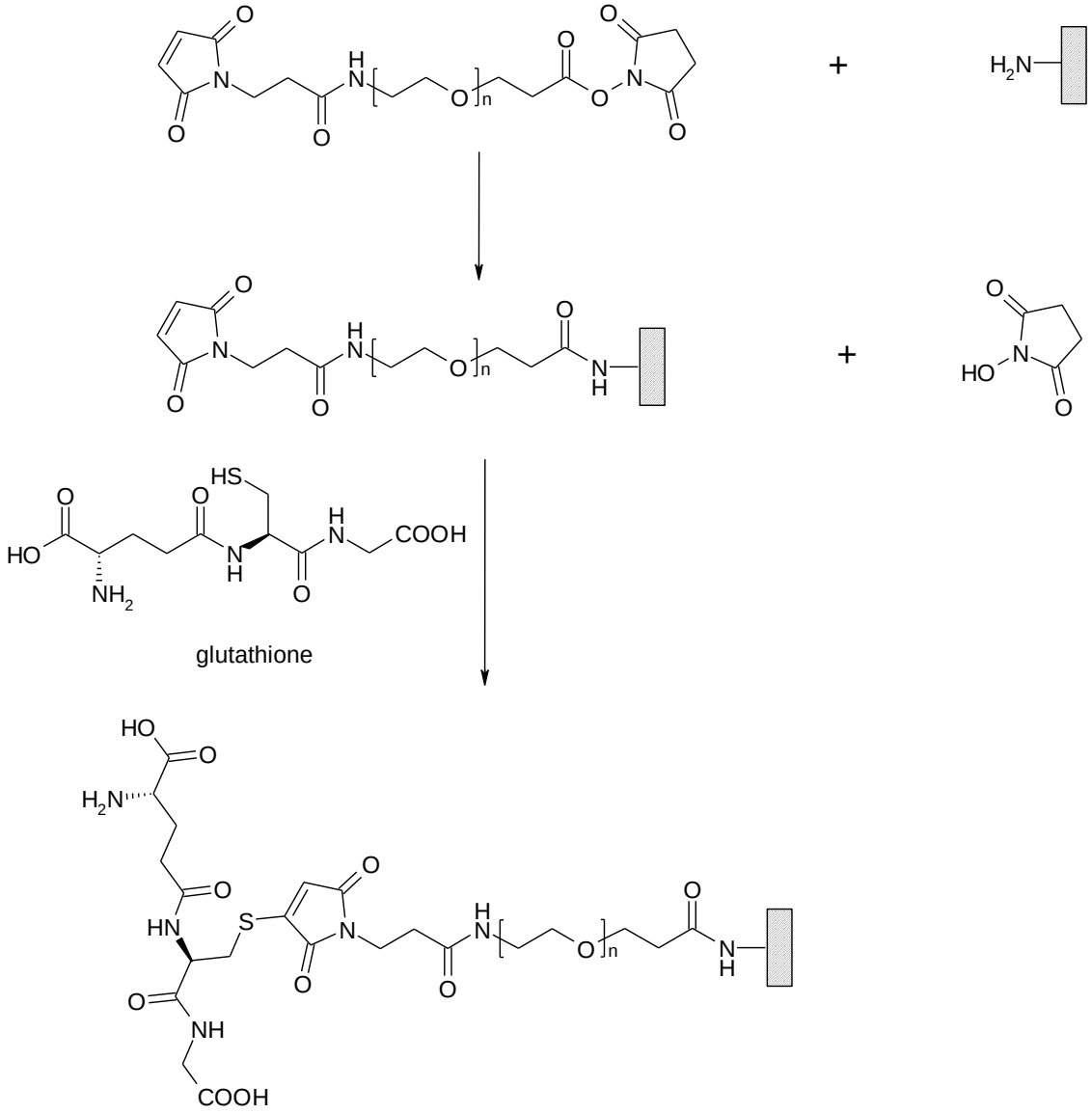

Figure 6.5. Coupling of glutathione to PEGylated, amino-functionalised Si_3N_4 AFM tip. n = 12.

6.2 Results and discussion

6.2.1 Deposition of MTase layer on mica

In a manner analogous to the previous chapter, the first experiments were aimed at producing a homogeneous layer of MTase on a mica surface to allow direct studies of GST-HsdR(PrrI)-MTase interactions.

6.2.1.1 AFM Tapping mode imaging in air

To investigate the formation of a complete layer of MTase on mica, pre-treated with PLL (Section 2.10.1.1), a series of AFM images were obtained from solutions of increasing MTase concentration (Figure 6.6).

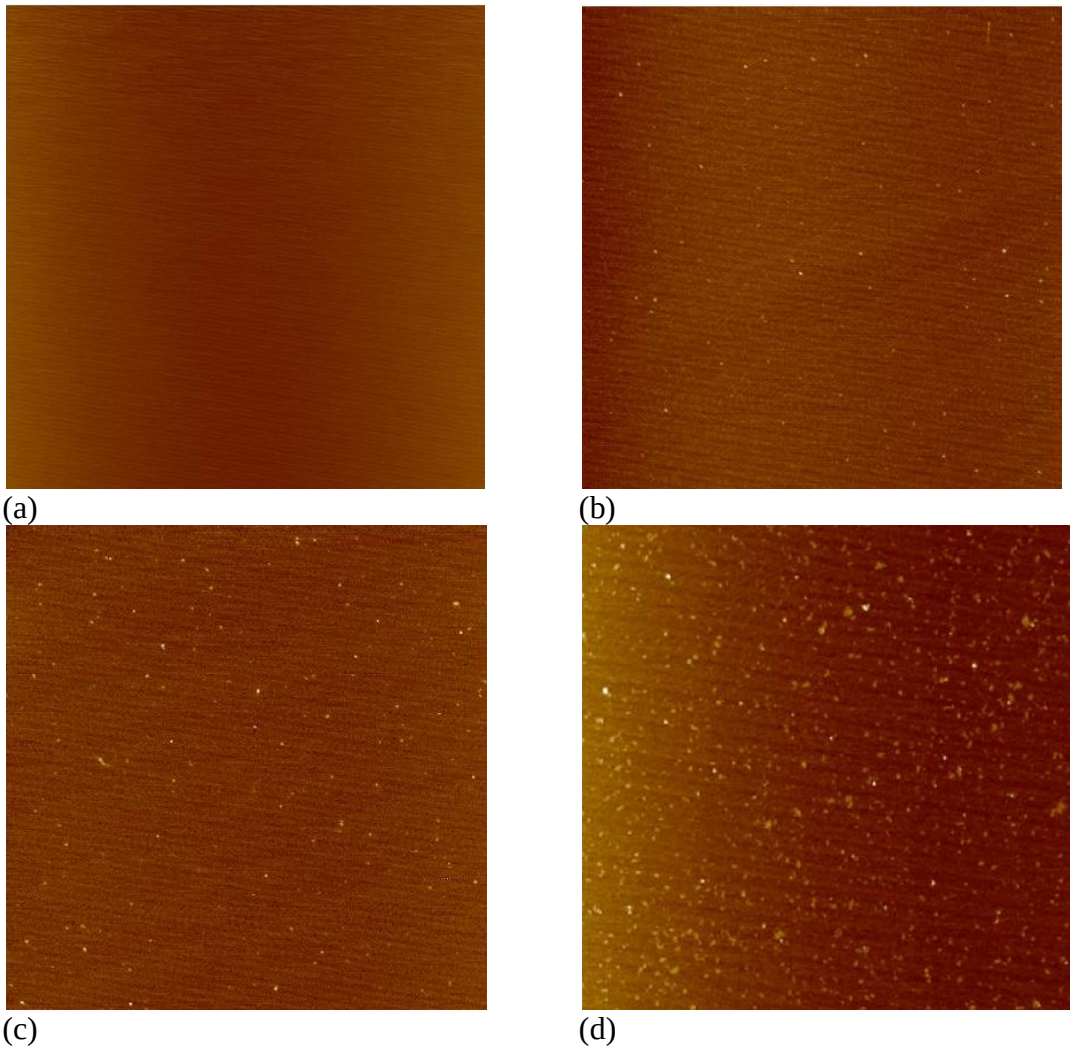

(a) (b)

(c) (d)

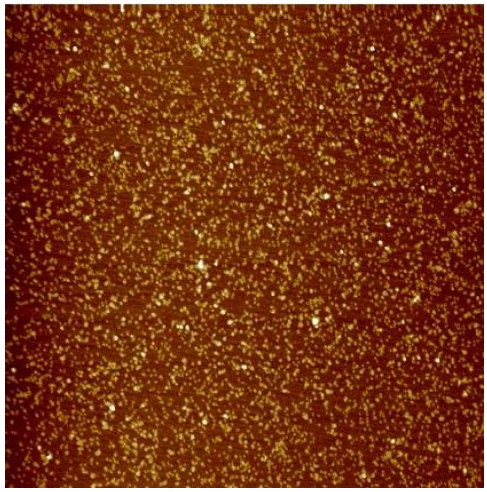
(e)

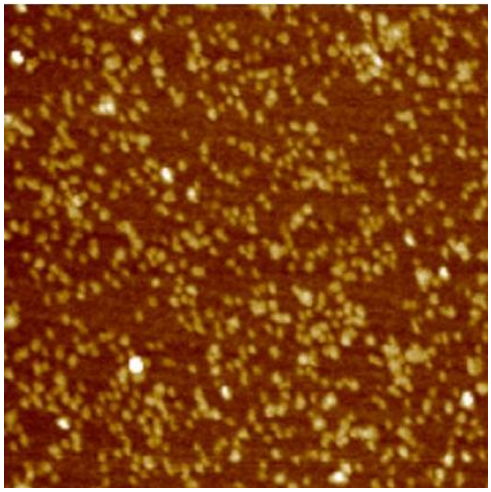
(e')


(f)

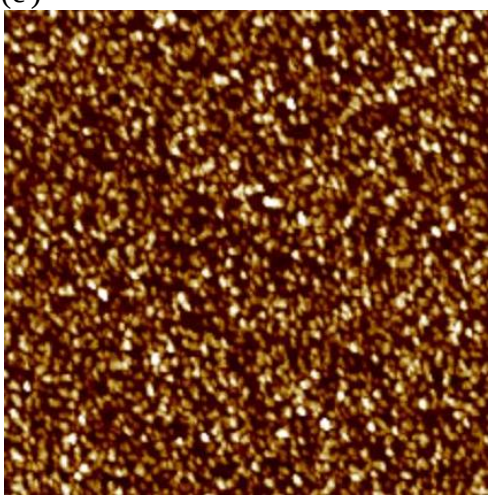
(f')


(g)

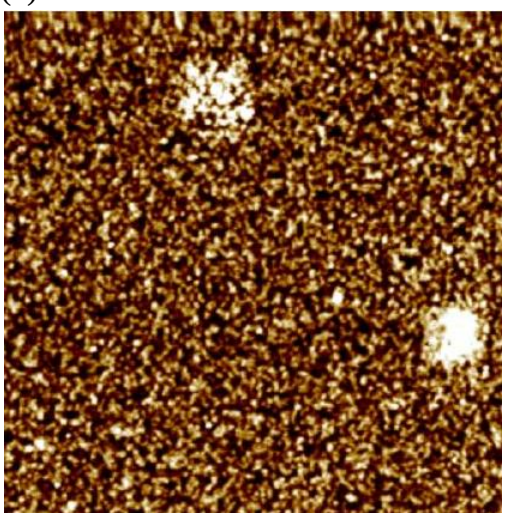
(g')

Figure 6.6. Tapping mode AFM image in air of (a) mica surface pre-treated with PLL (10 µm × 10 µm; z-scale 3 nm); (b-g) mica (pre-treated with PLL) covered with MTase (5 µm × 5 µm; z-scale 3 nm): (b) 1 nM, (c) 10 nM, (d) 50 nM, (e) 100 nM, (e') magnification of (e) (1.7 µm × 1.7 µm; z-scale 3 nm), (f) 200 nM, (f') magnification of

image (f) (2 µm × 2 µm; z-scale 3 nm), (g) 300 nM, (g') magnification of image (g) (2.5 µm × 2.5 µm; z-scale 3 nm).
Mica and mica pre-treated with PLL, used as controls, produced featureless images (Figure 6.6a). Increasing coverage by protein was observed on surfaces from 1 nM (Figure 6.6b) to 200 nM (Figure 6.6f), where, in the latter case, a homogeneous monolayer was produced. At higher concentrations (≥ 300 nM; Figure 6.6g), the presence of protein aggregates were observed.

6.2.1.2 Tapping mode imaging in liquid

To investigate whether the MTase layer, produced from the 200 nM concentration, would remain stable on the mica surface prior to further functionalisation, AFM imaging (Tapping mode®) was performed in PBS buffer (pH 7.4). The MTase monolayer was found to remain intact and, therefore, would be suitable for subsequent use (Figure 6.7).

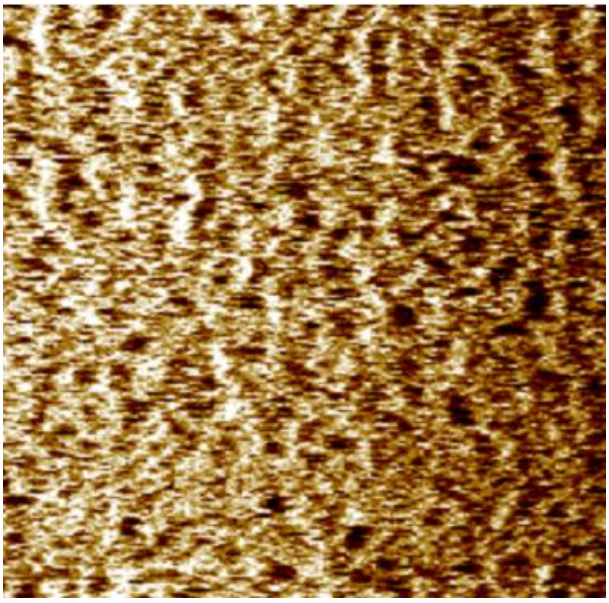

Figure 6.7. Typical AFM image (Tapping mode) of a MTase monolayer (PLL pre-treated mica exposed to 200 nM MTase) in PBS buffer (pH 7.4) (2.1 µm × 2.1 µm, z-scale 4 nm).

6.2.2 DFS measurements of HsdR-MTase complex using a PEG spacer

The next experiments were aimed at measuring adhesion forces between HsdR(PrrI), as the GST fusion protein and attached to an Si_3N_4 tip *via* a PEG linker (NHS-PEG_{12}-MAL; Section 2.10.4.5), to the MTase layer (200 nM) on mica (Section 6.2.1) in PBS buffer (pH 7.4).

For DFS studies, one thousand force curves (10 areas, each of an array of 10 × 10 force distance curves; lateral separation, 100 ± 5 nm, ramp size, 400 nm) obtained for each of 4 different tip retraction speeds (100, 250, 500 and 1000 nm s^{-1}; leading to different loading rates) were acquired.

6.2.2.1 Selecting force curves

Force-distance curves representing a specific single interaction peak were identified (Figure 6.8). These had a non-linear shape at the onset of retraction and before the first adhesion maximum, characteristic of PEG linker stretching, rather than a linear shape, as seen with 'hard' interactions. Approx. 7 % (for each retraction speed) fitted this criterion and were selected for the further analysis.

The challenge was the identification of specific interactions for the GST-HsdR(PrrI)-MTase complex, and therefore, a series of control experiments, each using a GST-HsdR(PrrI) modified tip, were studied. These involved a mica surface only, PLL pre-treated mica and in the third case, a blocking experiment where free GST-HsdR(PrrI) was added to block the MTase binding sites. The force distance curves obtained for these control experiments indicated mostly a lack of a rupture event. In the blocking

experiment, only 4 % of the retraction curves showed a specific interaction event, with a peak force at *ca.* 23 pN, which could probably be attributed to a decrease in the number of specific binding sites on the otherwise blocked MTase layer.

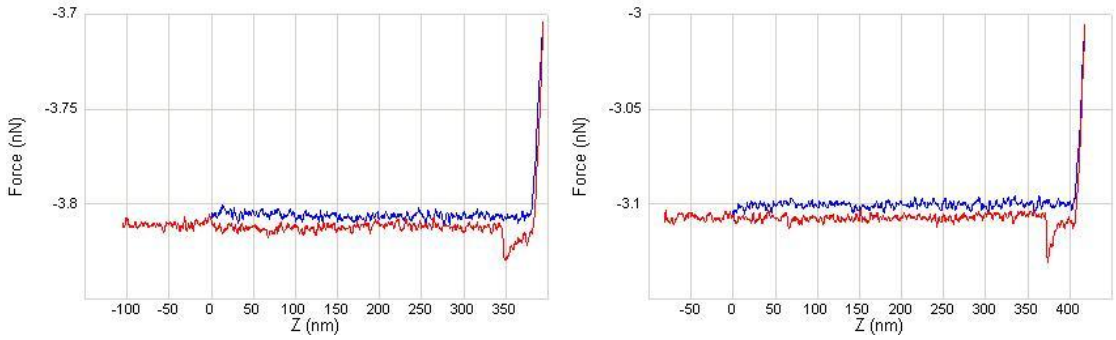

(a) (b)

Figure 6.8. Typical force-distance curves between GST-HsdR(PrrI) on an Si_3N_4 tip (amino functionalised, coupled *via* glutathione and a PEG linker) and MTase (attached to mica, pre-treated with PLL). A mean single adhesion peak is shown, which was used for further analysis. Blue trace = approach curve, red trace = retract curve (with adhesion event).

6.2.2.2 Rupture forces and rupture length analysis

The retraction part of each selected force-distance curve was analysed by measurement of f and rupture length l_r parameters corresponding to the height and the width of the adhesion event, respectively. k_s was determined for each selected force-distance curve from the slope of force f *vs.* rupture length l_r (see Figure 6.1) (Yuan *et al.*, 2000). The mean of the obtained k_s values was used for calculation of the loading rate for four different retraction speeds of AFM tip.

The force distribution histograms, each constructed of *ca.* 70 unbinding events, were obtained for each R_f and used to determine f^* (Figure 6.9a-d). For the largest R_f (2183 pN s^{-1}), f^* was calculated to be 26 ± 8 pN (Figure 6.14a). A decrease in f^* was observed

with decreasing R_f, as expected (Nevo *et al.*, 2003). Similarly, f^* was calculated to be 23 ± 8, 20 ± 8 and 18 ± 4 pN for R_f values corresponding to 936, 450 and 150 pN s^{-1}, respectively (Figures 6.9b-d).

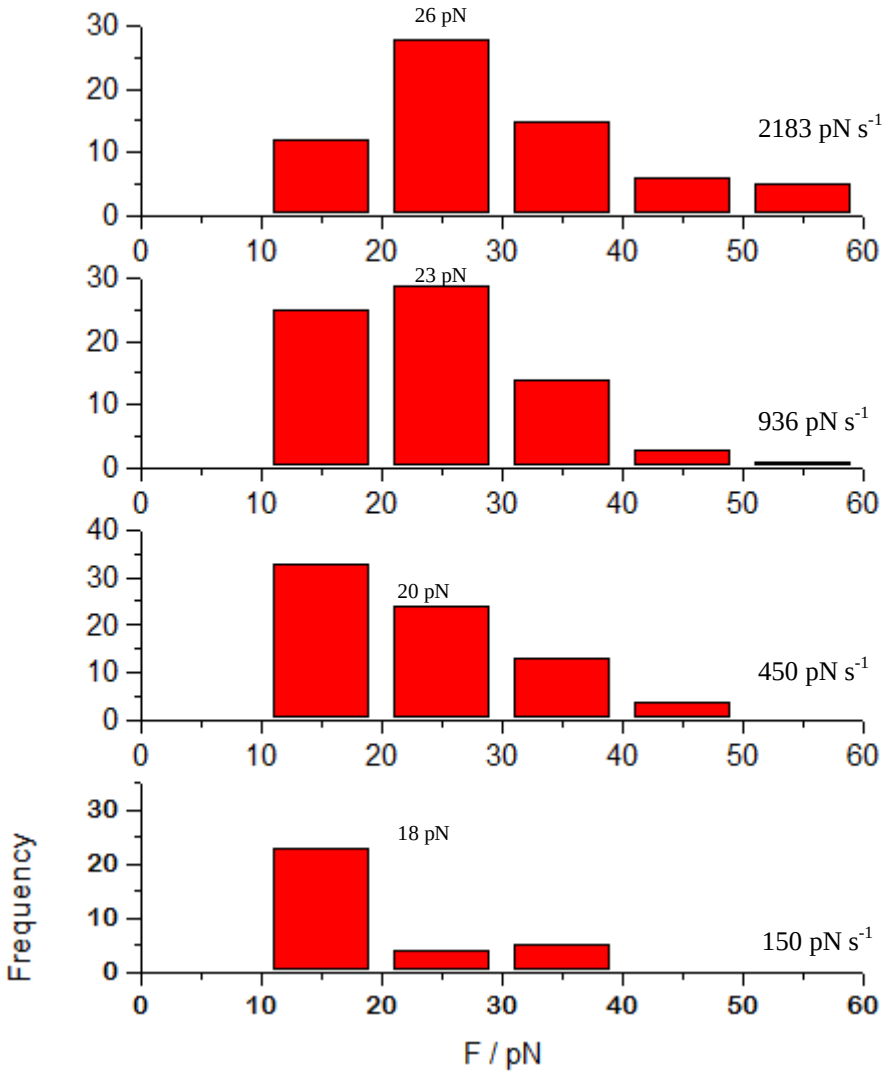

Figure 6.9. Rupture force distribution histograms of GST-HsdR(PrrI)-MTase system recorded for different values of R_f; top to bottom: R_f = 2183 pN s^{-1}, f^* = 26 ± 8 pN; R_f = 936 pN s^{-1}, f^* = 23 ± 8 pN; R_f = 450 pN s^{-1}, f^* = 20 ± 8 pN; R_f = 150 pN s^{-1}, f^* = 18 ± 4 pN. Bin size = 10 pN (*ca.* same value as the noise threshold of the cantilever).

These values represent the forces necessary to rupture bonds between MTase and GST-HsdR(PrrI). There is no available literature for this system in which to compare these forces. K_d values determined for the R_1-complex (10^{-9} M) (Janscak *et al.*, 1998) involved the presence of DNA which differs from protein-protein interactions in the present work and therefore the values cannot be compared.

The obtained forces of *ca.* 26 pN for the GST-HsdR(PrrI) are about half the value of those measured for a single biotin-avidin interaction (*ca.* 47 pN) (Chapter 5). The f^* of 18 ± 4 pN obtained at R_f =150 nm s^{-1} is close, although above, the lower limit of AFM resolution (due to thermal fluctuation) for the type of cantilevers used (6 – 10 pN).

A wide range distribution of unbinding forces was observed in repeats of the same experiment at the same AFM tip retraction speed (Figure 6.9). The average rupture force at any particular pulling velocity is not sufficient to characterise the strength of the molecular bond (Raible *et al.*, 2006).

Analysis of force-distance curves allow the determination of rupture length (l_r) in addition to the unbinding force (F). A Gaussian function fitted to the frequency distribution of l_r yields the most probable rupture length (l^*) (Figure 6.10). In this case, l^* = 14 ± 7 nm, which probably corresponds to the combined length of the PEG linker (MEL-dPEG$_{12}$-NHS length = 5.3 nm (manufacturer value; Section 2.11.4.5); L = 4.2 nm (Section 5.2.2)) plus the height of GST-HsdR(PrrI) (1.6 nm; Chapter 4). The difference is likely to be due to an error in the latter distance caused by dehydration of the protein.

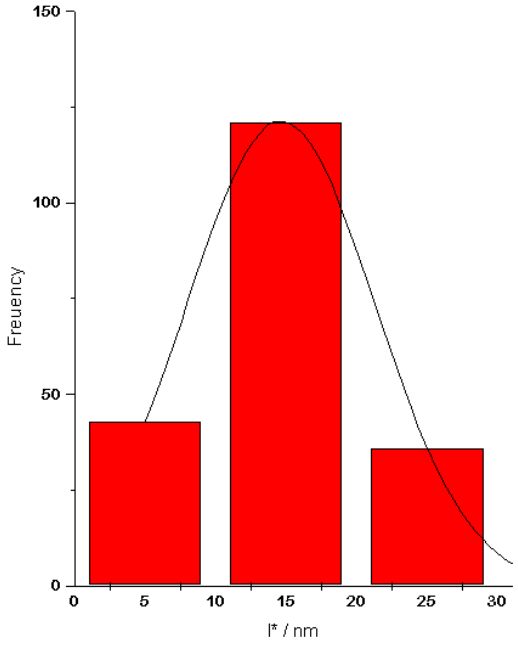

Figure 6.10. Histogram showing the distribution of l_r for the GST-HsdR(PrrI)-MTase complex; $l^* = 14 \pm 7$ nm.

6.2.2.3 Linear dependence between unbinding forces and loading rate

Values of f^* for the GST-HsdR(PrrI)-MTase complexes were plotted against the corresponding values of R_f on a half-logarithmic scale (Figure 6.11). A straight-line fit was observed, which is characteristic of the existence of a single energy barrier (Evans and Ritchie, 1997). Standard deviations (SD; from Gaussian fits to the force histograms) were not used for the experimental uncertainty estimation, since all the histograms were naturally broadened by thermal activation, even in the absence of experimental uncertainty (Evans and Ritchie, 1997).

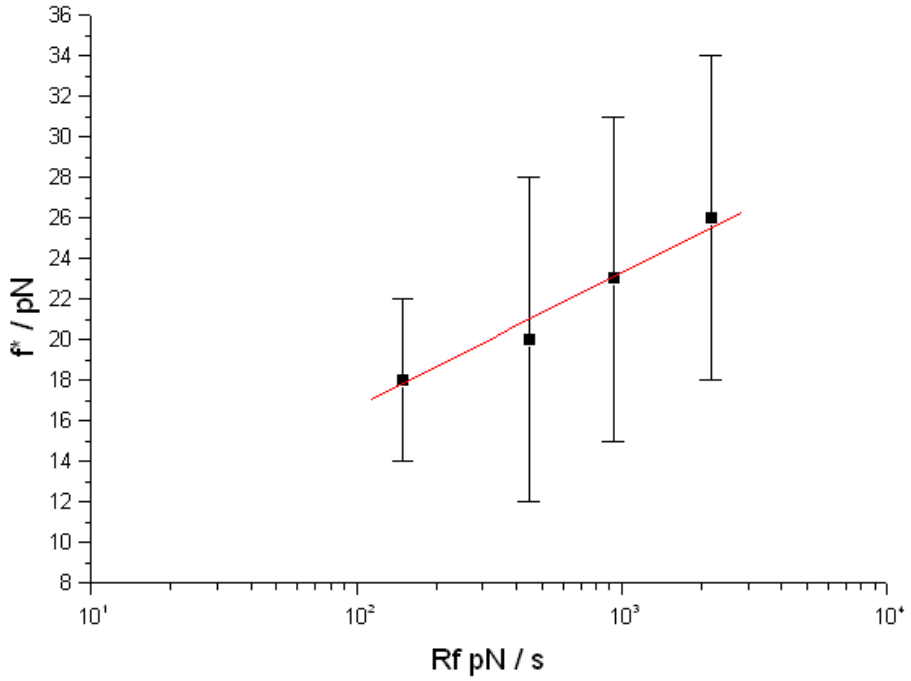

Figure 6.11. Linear dependence of *f** and R_f for the GST-HsdR(PrrI)-MTase complex.

The *f** values were plotted against corresponding values of ln(*Rf*). The Bell model parameters $k_{diss}(0)$ and x_{diss} were determined from linear regression. The slope *a* (3.03) and intercept *b* (2.3) (Figure 6.12) were obtained from Equations 6.13 and 6.14

$$a = \frac{n\sum x_i y_i - \sum x_i \sum y_i}{n\sum x_i^2 - (\sum x_i)^2} \qquad \text{(Equation 6.13)}$$

$$b = \frac{1}{n}(\sum y_i - a\sum x_i) \qquad \text{(Equation 6.14)}$$

where x_i and $y_i = f^*$ and R_f, respectively, and *n* = number of measurements. The *Δa* and *Δb* values correspond to the deviations from the values *a* and *b* obtained from the linear regression fit of *f** *vs.* ln(*Rf*). Errors for *a* (0.37) and *b* (2.47) values were determined using Equations 6.15 and 6.16:

$$\Delta a = \sqrt{\frac{n[\sum y_i^2 - a\sum x_i y_i - b\sum y_i\ ]}{(n-2)[n\sum x_i^2 - (\sum x_i)^2]}} \qquad \text{(Equation 6.15)}$$

$$\Delta b = \sqrt{\frac{1}{n}\Delta a^2 \sum x_i^2} \qquad \text{(Equation 6.16)}$$

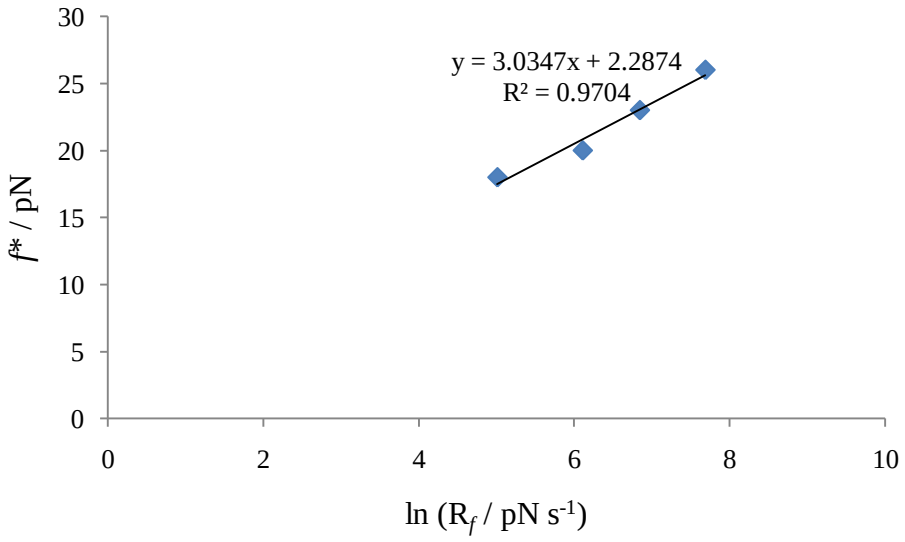

Figure 6.12. f^* *vs.* ln(R_f) plot showing values of a (gradient) and b (intercept). Errors Δa = 0.37; Δb = 2.47.

By fitting the Bell-Evans Equations (Equations 6.11 and 6.12), x_{diss} and k_{diss} for the GST-HsdR(PrrI)-MTase complex were calculated to be 1.35 nm (13.5 Å) and 0.16 s^{-1}, respectively. The lifetime $\tau(0)$ of the GST-HsdR(PrrI)-MTase bond was calculated to be 6.25 s.

Pairs of molecules forming complexes in solution may display different binding properties to those covalently anchored to the tip and substrate and give rise to steric hindrance and, hence, different dissociation rates. Therefore comparison of the values obtained statically may differ from results determined dynamically. For some pairs of

molecules with a single energy barrier, k_{diss} at F = 0 might agree with bulk measurements. A dissociation rate for the R_1-complex of 3×10^{-2} s^{-1} (Seidel *et al.*, 2005) has been estimated from the measured dissociation constant $K_{diss,R1}$ ~ 1 nM (Janscak *et al.*, 1998), although the interaction between the MTase and HsdR was made in the presence of DNA. It is likely that the presence of DNA in the sample will change the rate of thermodynamic equilibrium.

6.3 AFM tip functionalisation with GST antibodies

The forces between anti-GST antibody and GST were measured as an additional example of protein-protein interactions. Anti-GST antibodies were covalently attached to the Si_3N_4 tip using a PEG linker (Section 2.10.3.6). GST was attached to mica pre-treated with PLL (Section 2.10.1.1).

The time available toward the end of the project allowed only for initial experiments, the force-distance measurements were obtained between these two surfaces at a retraction speed of 1.5 μm s^{-1}. Three cantilevers (k_{nom} = 0.01 N m^{-1}) were used.

Forces obtained, excluding the hard interaction, were plotted as a histogram, and an f^* value of 43 ± 12 pN was determined from the distribution maximum (Figure 6.13). The wide distribution of detected forces may indicate multiple binding, which is highly probably due to the presence of two binding sites for the antigen.

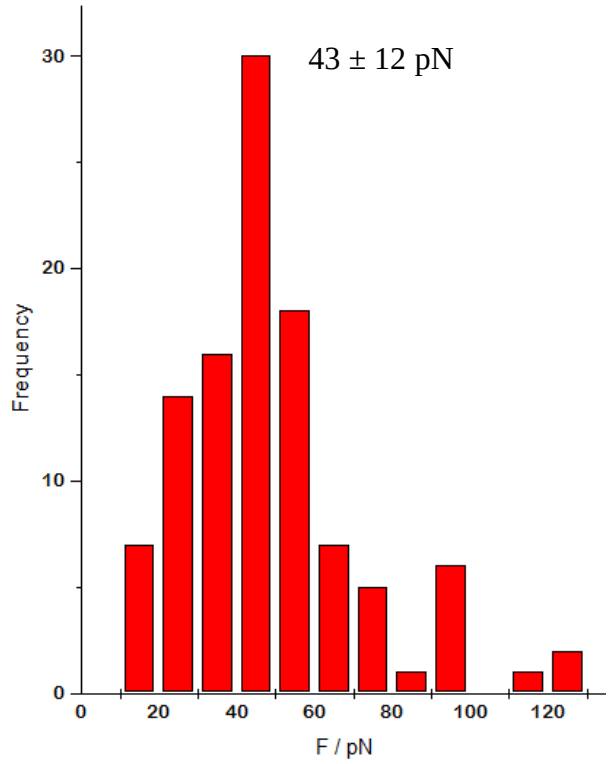

Figure 6.13. Histogram of unbinding forces obtained for the specific interactions between GST on the mica surface and antibodies attached to the Si_3N_4 tip.

In a further experiment, the same GST-antibody modified tips were used to measure the forces necessary to rupture bonds between the tip and HsdR(PrrI) fused with GST attached to the mica surface. The obtained values of unbinding forces (Figure 6.14) were found to be 39 ± 10 pN, which is similar to the results obtained for the GST anti-GST pair. The orientation of GST-HsdR(PrrI) attached to the mica was random; the GST could be in a position suitable for interactions with antibodies or hidden from them. In the latter case, antibodies would be able to interact in an unspecific manner with HsdR(PrrI) molecules. The forces measured in this experiment, however, were similar to the forces obtained between antibodies and GST (39 ± 10 pN and 43 ± 12 pN,

respectively). Therefore, the measured forces are specific to rupture bonds between GST and antibodies.

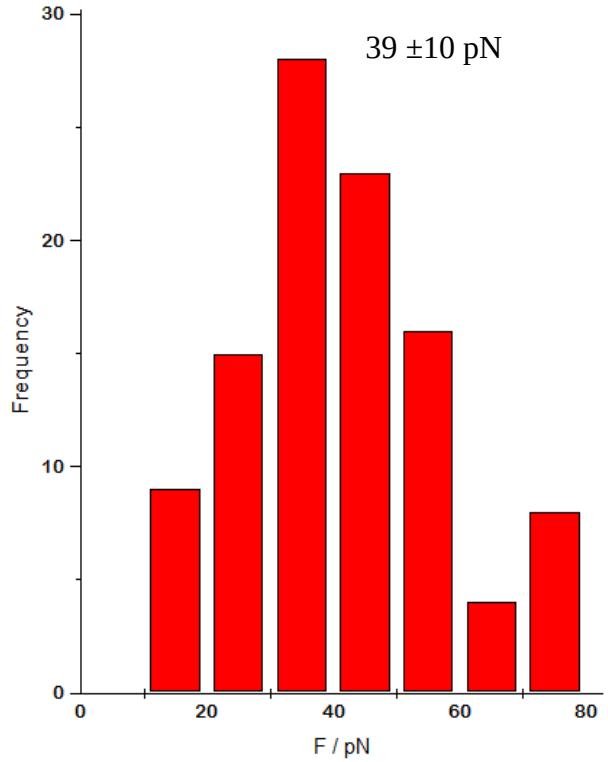

Figure 6.14. The unbinding forces measured between antibodies covalently attached to the AFM tip and GST- HsdR(PrrI) proteins on the mica surface.

The force distribution observed for GST and anti-GST experiments was wider when compared to the data for GST-HsdR(PrrI) attached to the mica surface. Higher forces recorded with the values of *ca.* 90 and 120 pN may be due to the simultaneous rupture of two or three bonds respectively.

The forces between glutathione and GST obtained by Yoshimura *et al.* (2006) at similar loading rate (2000 pN s^{-1}) were *ca.* 100 pN, suggesting that the binding at this stage of tip functionalisation was stronger and tighter than that between GST-HsdR(PrrI) and

MTase and therefore any possibility of HsdR detachment from the tip was assumed to be smaller. The rupture forces recorded for most of the protein-protein interactions range from 20 pN to 150 pN at a loading rate below 1000 pN s^{-1} (Evans *et al.*, 2001; Marshall *et al.*, 2005).

6.4 Conclusions

Force distance measurements were used for the first time to investigate GST-HsdR(PrrI)-MTase protein-protein interactions within a Type I R-M system, where the former subunit was attached to the AFM tip *via* a PEG linker and the MTase deposited on the mica surface. A dynamic approach has been used to obtain the kinetic information of this system. The major task was to adopt strong attachment of GST-HsdR(PrrI) to the Si_3N_4 tip using a linker to avoid steric hindrance and provide the best conditions for allowing the interaction of the subunits. The quality of the MTase layer on the mica was verified by imaging in air and liquid, and obtained by increasing concentration of MTase. Simple attachment of MTase *via* PLL was found to be reproducible, stable over time, temperature and in liquid therefore suitable for force-distance measurements. The simplicity of the steps used during surface modification eliminates factors that increase the possibility of additional nonspecific interactions.

Thousands of measurements obtained in DFS mode were necessary to allow classification and identification of the shape characteristic of the specific interaction between MTase and GST-HsdR(PrrI). Forces in the range of 18 – 26 pN were measured at four different retraction speeds (different loading rates) of the AFM tip. These values

were lower than those of the avidin-biotin system (*ca.* 47 pN), as expected, since the avidin-biotin complex is the strongest noncovalent bond between any pair of molecules.

Loading rate dependent measurements allowed the acquisition of useful information about the kinetic parameters of the R_1-complex. A linear dependence of f^* *vs.* $\ln(R_f)$ GST-HsdR(PrrI)-MTase revealed the existence of single energy barrier. The multiple energy barriers (three) reported for the avidin-biotin system may suggest that larger forces than in GST-HsdR(PrrI)-MTase, where only a single energy barrier is present, would be required to overcome these barriers. Kinetic parameters x_{diss} and k_{diss} for the GST-HsdR(PrrI)-MTase complex were calculated to be 1.35 nm (13.5 Å) and 0.16 s^{-1}, respectively, and the lifetime $\tau(0)$ of the GST-HsdR(PrrI)-MTase bond was calculated to be 6.25 s.

Additional force values obtained for the GST – anti-GST antibodies (43 ± 12 pN) and HsdR- anti-GST antibodies (39 ± 10 pN) were similar to each other and larger than those observed for GST-HsdR(PrrI)-MTase, suggesting that the 18 – 26 pN forces were realistic for the complex.

Chapter 7

Conclusions and further work

7.1 Summary

The work presented leads to a better understanding of single molecule interactions and forces within the type I R-M multisubunit and multifunctional enzyme using the force sensing tool, AFM. The main aim of the project was to investigate the intermolecular forces necessary to hold the subunits together as a holoenzyme. This would be important information for exploring the possibility of using EcoR124I as a nanoactuator for a toxicity biosensor.

Protein-surface and DNA-protein interactions were studied by a series of experiments including immobilisation of proteins on mica followed by visualisation. The first step towards DNA-EcoR124I interactions was obtained by immobilisation of DNA and proteins on the mica surface. The DNA fragments with a single recognition binding site for EcoR124I positioned in the middle or at 1/3 of the length of DNA, were used to the assemble the holoenzyme. DNA imaging in the presence of divalent cations (Mg^{2+}, Ca^{2+}, Ni^{2+}) was undertaken to establish conditions for reproducible DNA immobilisation so that protein-DNA interactions could be routinely investigated.

A salt layer ($MgCl_2$, $NiCl_2$ and $CaCl_2$) partially present on surfaces was problematic for obtaining reproducible height measurements necessary for molecular volume analysis.

A uniform layer was obtained using mica pre-treated with PLL prior DNA immobilisation. The contour length of the DNA molecules was measured to investigate the effect of PLL on DNA length, where experimental and theoretical values were in close agreement also supporting PLL to be useful mica pre-treatment prior to DNA-protein immobilisation.

Mg^{2+} present in the native environment of the EcoR124I and necessary for its activity was predicted to be the most suitable for DNA-protein investigations. The visualisation of DNA molecules in the presence of Mg^{2+} in liquid was only possible after mica pre-treatment with PLL. The accuracy of DNA width measurements, necessary for molecular volume calculations, was not improved by imaging in liquid; therefore visualisation of DNA-protein complexes were continued in air, an easier and more reproducible method.

The stable and reproducible images of the enzyme subunits and their complexes were obtained on PLL pre-treated mica. The EcoR124I holoenzyme was reconstituted *in vitro* by premixing purified MTase and HsdR (Janscak *et al.*, 1998). The presence of only one protein molecule bound to DNA was observed. Primers were designed to produce DNA fragments of known length and position of the target sequence for the enzyme. The specificity of binding was therefore confirmed from the contour length measurement of the DNA molecules and the position of attached proteins. The effect of cations present in the deposition buffer on DNA-protein complexes was also investigated. In the presence of Ca^{2+} and Ni^{2+}, a decrease in the number of DNA-protein complexes was observed. This may be attributed to stronger DNA binding to mica caused by Ni^{2+} or that the Ni^{2+} may affect the stability of the proteins and their binding to DNA. For Ca^{2+},

the decrease in the number of DNA-protein complexes may be due to the known decrease in activity of some enzymes acting with nucleic acids with these ions.

V_m of measured subunits or complexes were typically found to be lower than theoretical values, V_c.. The flattening of molecules and/or dehydration during the drying step in sample preparation were probably factors affecting the height measurements. Tip convolution, resulting in image broadening of features, was partly overcome using width measurements at half maximal height, as suggested by Schneider (1998). Only a few DNA-R_2 complexes, identified by V_m measurements, were observed, which could be explained by instability of above complex described by Janscak (1998). The dissociation of the R_2-complex into an R_1-complex and free HsdR and subsequently free MTase and HsdR has been suggested to control the opposing activities of restriction and modification *in vivo* (Firman *et al.*, 2000). The intermediate stage in the EcoR124I assembly pathway, DNA-R_1-complexes were mostly observed when HsdR(R124I) was involved in complex composition, which could be explained as this is the native subunit for the MTase. For GST-HsdR(PrrI) used in the assembly of the R_1-complex, an increase in V_m was detected due to the presence of an additional 26 kDa of the GST. In contrast, only a small number of complexes were observed for HsdR(PrrI) involved in the assembly of the R_1-complex, supporting unpublished evidence that complexes incorporating this hybrid subunit are less stable than those with the wild-type subunit. The effect of ATP analogues on the assembly and DNA binding of EcoR124I was also investigated. ATP-γ-S and AMP-pnp have been suggested to freeze the enzyme as an initiation complex and are involved in a slow dissociation of the HsdR subunit. The addition of ATP-γ-S in all cases showed a decrease in the number of imaged complexes, suggesting an influence on enzyme stability and induced dissociation of HsdR from the

complex. The majority of the complexes observed (assumed from V_m calculations) indicated the presence of MTase bound to DNA. The AMP-pnp also reduced the number of DNA-R_1-complexes, however a greater number were observed compared to the use of ATP-γ-S. This suggests a slower process of dissociation with AMP-pnp, which may involve the lack of hydrolysis. The structural difference between ATP-γ-S and AMP-pnp cofactors may have different effects on the protein-protein interactions and the final conformational state of the complex, therefore the mechanism of dissociation might be different. More R_1-complexes were observed for the HsdR(PrrI) subunit fused with GST than without fusion, suggesting an influence of GST on the stability of the protein.

The addition of ATP, although not novel, confirmed the enzyme activity by showing the ability of the enzyme to translocate. The dimerisation seen for EcoKI (Berge *et al.*, 2000; Nevies *et al.*, 2009), was not observed for EcoR124I, in agreement with magnetic tweezers work by van Noort *et al.* (2004) and Seidel *et al.* (2004). Seidel *et al.* (2005) suggested a difference in the EcoR124I dissociation pathway into R_1-complex and free HsdR in the presence and absence of ATP, where this molecule is involved in conformational changes of the initiation complex prior translocation. ATP may alter the subunit's stability, explaining the observation that ATP destabilises the R_2-complex of EcoR124I.

In Chapter 5, the interactions between the well-known biotin-avidin pair were investigated using two methods of tip functionalisation. When a glutaraldehyde was used for immobilisation, many multiple events were seen in the force curves, corresponding to many biotin-interactions. Analysis of the final "pull-off" event yielded

information on single-molecule or near single-molecule interactions. For instance, the smallest rupture force measured was 56 ± 13 pN, thought to be due to a single biotin-avidin rupture event (one bond) and was supported by literature values. A periodicity with two other maxima at 98 ± 15 and 161 ± 3 pN were also seen, which may correspond to two and three avidin-biotin interactions, respectively. A peak at 225 ± 9 pN was also observed. The use of a PEG linker allowed more sensitive measurements to be made, with a single biotin-avidin interaction at 47 ± 9.5 pN being detected and, again, a periodicity of between two further force maxima at 93 ± 7 and 143 ± 4 pN, corresponding to the rupture of two and three avidin-biotin bonds. The PEG and glutaraldehyde methods allowed the acquisition of similar force values corresponding to a single bond rupture. In the former method, however, single interactions were mostly detected (~ 70% of analysed force-distance curves), whereas for the latter method obtained forces represented mostly two interactions. This detailed study of the well-known biotin-avidin model system aided interpretation of the novel HsdR-MTase system.

Forces between a GST-HsdR(PrrI) motor subunit attached to an AFM tip using a PEG linker and MTase on PLL pre-treated mica were measured. The loading rate was varied over several orders of magnitude, in DFS mode, to provide information concerning the dissociation pathway of the bond and other kinetic parameters. Forces in the range of 18 -26 pN were measured at four retraction speeds (loading rates). A single barrier in the energy landscape of the complex was found in the dissociation pathway (x_{diss}) to be located 13.5 Å from the bound state. These values were lower than those of the avidin-biotin system (*ca.* 47 pN), as expected, since the avidin-biotin complex is the strongest noncovalent bond between any pair of molecules and three energy barriers need to be

overcome. The value k_{diss} for the GST-HsdR(PrrI)-MTase complex were calculated to be 0.16 s^{-1} and the lifetime $\tau(0)$ of the GST-HsdR(PrrI)-MTase bond was calculated to be 6.25 s.

Additionally, the intermolecular interactions were investigated at a single retract rate between GST – anti GST antibodies (43 ± 12 pN) and HsdR- anti-GST antibodies (39 ± 10 pN). The obtained force values were similar to each other and larger than those observed for GST-HsdR(PrrI)-MTase, which may suggest that forces were realistic for above complex.

7.2 Further work

Future investigations of the loading rate dependence upon the dissociation of GST-HsdR(PrrI)-MTase should be extended over more orders of magnitude, not permitted with the current AFM setup. Furthermore, the force volume measurements should be investigated by precise deposition of MTase proteins *via* DNA. This would allow specific HsdR-MTase and nonspecific HsdR-DNA interactions to be clearly distinguished by comparing forces at particular image positions. Nanolithography methods should be also employed for accurate deposition of proteins on the surface and attachment to the different surfaces also requires further investigation.

The imaging of translocating EcoR124I in liquid would not be possible with "conventional" AFM due to the short time of the process (*ca.* 1 – 2 s for 1 kB DNA; Seidel *et al.*, 2004). Further investigations, could be carried out using fast-scan (< 20 ms) AFM (Humphris *et al.*, 2005).

Complementary quartz crystal microbalance (QCM) investigations, using different HsdR/MTase concentrations, should also allow k_{ass} and hence k_D values to be determined for comparison with the AFM data.

The elucidation of the crystal structure of HsdR using ATP analogues would provide an improved understanding of the regions involved in protein-protein interactions.

Magnetic Tweezer studies combined with fluorescent labelled ATP could be employed for investigation of the initiation of the translocation process in the presence of motor subunit mutants.

The possible inhibition of the translocation process by DNA-binding drugs should be investigated, if the motor is to be used in drug-target screening.

Sensitivity of the motor to the presence of hydrophobic compounds, which are probable environmental pollutants, could be additionally carried out to study contamination at the single molecule level.

References

Abadjieva, A., Patel, J., Zinkevich, V., Firman, K. (1994). Deletions within the DNA recognition subunit of M.*Eco*R124I that identify a region involved in protein protein interactions between HsdS and HsdM. *J. Mol. Biol.* 241, 35-43.

Aggarwal, A.K. (1995). Structure and function of restriction endonucleases. *Curr. Opin. Struct. Biol.* 5, 11-19.

Akiyama Y., Otsuka, Y. Nagasaki, Kato, M., Katoaka K. (2000). Selective synthesis of heterobifunctional poly(ethylene glycol) derivatives containing both mercapto and acetal termianals, *Bioconjug. Chem.* 11, 947-950.

Albrecht, T.R., Akamine, S., Carver, T.E., Quate, C.F. (1990). Microfabrication of cantilever styli for the atomic force microscope. *J. Vac. Sci. Technol.* A8, 3386-3396.

Alexander, S. (1977). Adsorption of chain molecules with a polar head. *J. Phys.* 38, 983-987.

Allen, M.J., Hud, N.V., Balooch, M., Tench, R.J., Siekhaus, W.J., Balhorn, R. (1992). Tip-radius-induced artifacts in AFM images of protamine-complexed DNA. *Fibers Ultramicrosc.* 42, 1095-1100.

Allen, S., Davies, J., Dawkes, A.C., Davies, M.C., Edwards, J.C., Parker, M.C., Roberts, C.J., Sefton, J., Tendler, S.J.B., Williams, P.M. (1996). In situ observation of

streptavidin–biotin binding on an immunoassay well surface using an atomic force microscope. *FEBS Lett* 390, 161–164.

Allen, S., Chen, X., Davies, Davies, M.C., Dawkes, A.C., Edwards, J.C., Roberts, C.J., Sefton, J., Tendler, S.J.B., Williams, P.M. (1997). Detection of antigen-antibody binding events with the atomic force microscope. *Biochemistry* 36, 7457-7463.

Ashkin, A., Schutze, K., Dziedzic, J.M., Euteneuer, U., Schliwa, M. (1990). Force generation of organelle transport measured *in vivo* by an infrared laser trap. *Nature* 348, 346-348.

Aso, C., Aito, Y. (1962). Intramolecular-intermolecular polymerization of glutaraldehyde. *Bull. Chem. Soc. Japan* 35,1426.

Bailey, S.W. (1984). Micas. Mineralogical Society of America, Washington, DC. *Rev. Mineral.* 13, 573-584.

Beech, I.B., Smith, J.R., Steele, A.A., Penegar, I., Campbell, S.A. (2002). The use of atomic force microscopy for studying interactions of bacterial biofilms with surfaces. *Journal of Colloids and Surfaces B: Biointerfaces* 23, 231-247.

Bell, G.I. (1978). Models for the specific adhesion of cells to cells. *Science* 200, 618-627.

Bennink, M.L., Nikova, D.N., van der Werf, K.O., Greve, J. (2003). Dynamic imaging of single DNA-protein interactions using atomic force microscopy. *Anal. Chim. Acta* 479, 3-15.

Berg, O., Winter, R.B., von Hippel., P.H. (1981). Diffusion-driven mechanism of protein translocation on nucleic acids. 1. Models and theory. *Biochem.* 20, 6929-6948.

Berge, T., Ellis, D. J., Dryden, D.T., Edwardson, J. M., Henderson, R.M.(2000).Translocation-independent dimerization of the EcoKI endonuclease visualized by atomic force microscopy *Biophys J*. 1, 479-484.

Berquand, A., Xia, N., Castner, D.G., Clare, B.H., Abbott, N.L., Dupres, V., Adriaensen, Y., Dufrene, Y.F. (2005). Antigen binding forces of single anti-lysozyme Fv fragments explored by atomic force microscopy. *Langmuir* 21, 5517-5523.

Bezanilla, M., Drake, B., Nudler, E., Kashlev, M., Hansma, P.K., Hansma, H.G. (1994). Motion and enzymatic degradation of DNA in the atomic force microscope. *Biophys. J.* 67, 2454-2459.

Bezanilla, M., Manne, S., Laney, D.E., Lyubchenko, Y.L., Hansma, H.G. (1995). Adsorption of DNA to mica, silylated mica and minerals: characterization by atomic force microscopy. *Langmuir* 11, 655- 659.

Bickle, T.A. (1987). DNA restriction and modification systems. In *Escherichia coli* and *Salmonella typhimurium. Cellular and Molecular Biology* (Ingraham, J.L., Low, K.B.,

Magasanik, B., Neidhardt, F.C., Schaechter, M., Umbarger, H.E., Eds.), 692-696. American Society for Microbiology, Washington DC.

Bickle, T.A., Kruger, D.H. (1993). Biology of DNA restriction. *Microbiol Rev.* 57, 434-450.

Binnig, G., Garcia, N., Rohrer, H. Conductivity sensitivity of inelastic scanning tunneling microscopy. (1985). *Phys. Rev. B Condens. Matter* 32, 1336-1338.

Binnig, G., Rohrer, H., Gerber, C. Weibel, E.(1982). Surface studies by Scanning Tunneling Microscopy. Physical Review Letters 49,57-61.

Binnig, G., Quate, C.F., Gerber, C. (1986). Atomic force microscope. *Phys. Rev. Lett.* 56, 930-933.

Bloomfield, V.A. (1997). DNA condensation by multivalent cations. *Biopolymers* 44, 269-282.

Bowen, W.R., Lovitt, R.W., Wright, C.J. (2001). Atomic force microscopy study of the adhesion of Saccharomyces cerevisiae. *J. Colloid Interface Sci.* 237, 54-61.

Broun, G., Selegny, E., Avrameas, S., Thomas. D. (1969). Enzymatically active membranes: some properties of cellophane membranes supporting cross-linked enzymes. *Biochim. Biophys. Acta* 185, 260-262.

Buhler, R., Yuan, R. (1978). Characterization of a restriction enzyme from *Escherichia coli* K carrying a mutation in the modification subunit. *J. Biol. Chem.* 253, 6756-6760.

Burnham, N.A., Colton, R.J., Pollock, H.M. (1993). Interpretation of force curves in force microscopy. *Nanotechnology* 4, 64-80.

Bussiek, M., Mucke, N., Langowski, J. (2003). Polylysine-coated mica can be used to observe systematic changes in the supercoiled DNA conformation by scanning force microscopy in solution. *Nucleic Acids Res.* 31, 137e.

Bustamante, C., Rivetti, C. (1996). Visualizing protein-nucleic acid interactions on a large scale with the scanning force microscope. *Annu. Rev. Biophys. Biomol. Struct.* 25, 395-429.

Bustamante, C., Rivetti, C., Keller, D.J. (1997). Scanning force microscopy under aqueous solutions. *Curr. Opin. Struct. Biol.* 7, 709-716.

Bustamante, C., Vesenka, J., Tang, C.L., Rees, W., Guthold, M., Keller, R. (1992). Circular DNA molecules imaged in air by scanning force microscopy. *Biochemistry* 31, 22-26.

Butt, H.-J, Siedle, P., Seifert, K., Seeger, T., Fendler, K., Bamberg, E., Goldie, K., Engel, A. (1993). Scan speed limit in atomic force microscopy. *J. Microscopy* 169, 75-84.

Carneiro, M.J., Zhang, W., Ioannou, C., Scott, D.J., Allen, S., Roberts, C.J., Soultanas, P. (2006). The DNA-remodelling activity of DnaD is the sum of oligomerization and DNA-binding activities on separate domains. *Mol. Microbiol.* 60, 917-924.

Calisto, B.M., Pich, O.Q., Pinol, J., Fita, I., Querol, E., Carpena, X. (2005). Crystal structure of a putative type I restriction-modification S subunit from mycoplasma genitalium. *J. Mol. Biol.* 351, 749-762.

Cammas, S., Nagasaki, Y., Kataoka, K. (1995). Heterobifunctionalpoly(ethylene oxide): synthesis of alpha-methoxy-omega amino and alpha-hydroxy-omega-amino PEOs with the same molecular weights. *Bioconjug. Chem.* 6, 226-230.

Campbell, S.A., Smith, J.R., Jungblut, H., Lewerenz, H.J. (2007). Protein imaging on a semiconducting substrate: A scanning tunnelling microscopy investigation. *J. Electroanal. Chem.* 599, 313-322.

Chilkoti, A., Boland, T., Ratner, B.D., Stayton, P.S., (1995). The relationship between ligand-binding thermodynamics and protein-ligand interaction forces measured by atomic force microscopy. *Biophys. J.* 69, 2125-2130.

Claesson, P.M., Herder, P., Stenius, P., Eriksson. J.C., Pashley, R.M. (1986). An ESCA and AES study of ion-exchange on the basal plane of mica. *J. Colloid Interface Sci.* 109, 31-39.

Clausen-Schaumann, H., Seitz, M., Krautbauer, R., Gaub, H.E. (2000). Force spectroscopy with single bio-molecules. *Curr. Opin. Chem. Biol.* 4, 524-530.

Cleveland, J. P., Manne, S., Bocek, D., Hansma, P.K. (1993). A nondestructive method for determining the spring constant of cantilevers for scanning force microscopy. *Rev. Sci. Instrum.* 64**,** 403-405.

Clifford, C.A., Seah, M.P. (2005). The determination of atomic force microscope cantilever spring constants via dimensional methods for nanomechanical analysis. *Nanotechnology* 16, 1666-1680.

Colton, R.J., Baselt, D.R., Dufrêne, Y.F., Green, J.B., Lee, G.U. (1997). Scanning probe microscopy. *Curr. Opin. Chem. Biol.* 1, 370-377.

Cowan, G. M., Daniel, A.S., Gann, A.A.F., Kelleher, J.E., Murray, N. E. (1988). Defining domains in type-I restriction and modification enzymes. *Gene* 74, 239-241.

Czajkowsky, D.M., Iwamoto, H., Shao, Z. (2000). Atomic force microscopy in structural biology: from the subcellular to the submolecular. *J. Electron Microsc. (Tokyo)* 49, 395- 406.

Dai, P., Wang, S., Taub, H., Buckley, J.E., Ehrlich, S.N., Larese, J.Z., Binnig, G., Smith, D.P. (1993). X-ray-diffraction and scanning-tunneling-microscopy studies of a liquid-crystal film adsorbed on single-crystal graphite. *Phys. Rev. B Condens. Matter* 47, 7401-7407.

Dame, R.T., Wyman, C., Goosen, N. (2003). Insights into the regulation of transcription by scanning force microscopy. *J. Microsc.* 212, 244-253.

Dammer, U., Hegner, M., Anselmetti, D., Wagner, P., Dreier, M., Huber, W., Güntherodt, H.J. (1996). Specific antigen/antibody interactions measured by force microscopy. *Biophys J* 70, 2437–2424.

Deniz, A.A., Mukhopadhyay, S., Lemke, E.A. (2007). Single-molecule biophysics: at the interface of biology, physics and chemistry. *J. Royal Soc. Interface* 5, 15-45.

Dowd, D.R., Lloyd, R.S. (1990). Biological significance of facilitated diffusion in protein-DNA interactions. *J. Biol. Chem.* 265, 3424-3431.

Drake, B., Prater, C.B., Weisenhorn, A.L., Gould, S.A., Albrecht, T.R., Quate, C.F., Cannell, D.S., Hansma, H.G., Hansma, P.K. (1989). Imaging crystals, polymers, and processes in water with the atomic force microscope. *Science* 243, 1586-1589.

Dryden, D.T.F., Cooper, L.P., Murray, N.E. (1993). Purification and characterisation of the methyltransferase from the type I restriction and modification system of Escherichia coli K12. *J. Biol. Chem.* 268, 13228-13236.

Dryden, D.T.F., Cooper, L.P., Thorpe, P.H., Byron, O. (1997). The *in vitro* assembly of the *Eco*KI type I DNA restriction/modification enzyme and its *in vivo* implications. Biochemistry 36, 1065-1076.

Dryden, D.T.F., Murray, N.E., Rao, D.N. (2001). Nucleside triphosphate-dependent restriction enzymes. Nucleic Acids Res. 29, 3728-3741.

Dupres, V., Menozzi, F.D., Locht, C., Clare, B.H., Abbott, N.L., Cuenot, S., Bompard, C., Raze, D., Dufrene, Y.F. (2005). Nanoscale mapping and functional analysis of individual adhesins on living bacteria. *Nature Methods* 2, 515-520.

Dupres, V., Verbelen, C., Dufrene, Y.F. (2007). Probing molecular recognition sites on biosurfaces using AFM. *Biomaterials* 28, 2393-402.

Eaton, P., and West, P. (2010). Atomic Force Microscopy. Oxford University Press, Oxford.

Ebner, A., Hinterdorfer, P., Gruber, H.J. (2007a). Comparison of different aminofunctionalization strategies for attachment of single antibodies to AFM cantilevers. *Ultramicroscopy* 107, 922-927.

Ebner, A., Wildling, L., Kamruzzahan, A.S., Rankl, C., Wruss, J., Hahn, C.D., Hölzl, M., Zhu, R., Kienberger, F., Blaas, D., Hinterdorfer, P., Gruber, H.J. (2007b). A new, simple method for linking of antibodies to atomic force microscopy tips. *Bioconjug. Chem.* 18, 1176-1184.

Edstrom, R.D., Meinke, M.H., Yang, X.R., Yang, R., Elings, V., Evans, D.F. (1990). Direct visualization of phosphorylase-phosphorylase kinase complexes by scanning tunneling and atomic force microscopy. *Biophys J.* 58, 1437-1448.

Eisenberg-Domovich, Y., Hytonen, V.P., Kulomaa, M.S., Wilchek, M., Bayer, E.A., Livnah, O. (2005). Crystal structure of an avidin-related protein: insight into high-affinity biotin binding and protein stability. *J. Biol. Chem.* 61, 528-538.

Ellis, D.J., Dryden, D.T.F., Berge, T., Edwardson, J.M., Henderson,R.M. (1999). Direct observation of DNA translocation and cleavage by the EcoKI endonuclease using atomic force microscopy. *Nature Struct. Biol.* 6, 15-17.

Engel, A., Lyubchenko, Y., Muller, D. (1999). Atomic force microscopy: a powerful tool to observe biomolecules at work. *Trends Cell Biol.* 9, 77-80.

Engel, A., Schoenenberger, C.A., Muller, D.J.(1997). High resolution imaging of native biological sample surfaces using scanning probe microscopy. *Curr. Opin. Struct. Biol*. 7, 279-284.

Erie, D.A., Yang, G., Schultz, H.C., Bustamante, C. (1994). DNA bending by Cro protein in specific and nonspecific complexes: implications for protein site recognition and specificity. *Science* 266, 1562-1566.

Evans, E. (1998). Energy landscapes of biomolecular adhesion and receptor anchoring at interfaces explored with dynamic force spectroscopy. *Faraday Discuss.* 111, 1-16.

Evans, E. (1999). Looking inside molecular bonds at biological interfaces with dynamic force spectroscopy. *Biophys. Chem.* 82, 83-97.

Evans, E. (2001). Probing the relation between force-lifetime and chemistry in single molecular bonds. *Annu. Rev. Biophys. Biomol. Str.* 30, 105-128.

Evans, E., Leung, A., Hammer, D., Simon, S. (2001). Chemically distinct transition states govern rapid dissociation of single L-selectin bonds under force. *Proc. Natl. Acad. Sci. USA* 98, 3784-3789.

Evans, E., Ritchie, K. (1997). Dynamic strength of molecular adhesion bonds. *Biophys. J.* 72, 1541-1555.

Evans, E., Ritchie, K., Merkel, R. (1995). Sensitive force technique to probe molecular adhesion and structural linkages at biological interfaces. *Biophys. J.* 68, 2580-2587.

Eve, J.K., Patel, N., Luk, S.Y., Ebbens, S.J., Roberts, C.J. (2002). A study of single drug particle adhesion interactions using atomic force microscopy. *Int. J. Pharm.* 238, 17-27.

Finn, F.M., Titus, G., Montibeller, J.A., Hofmann, K. (1980). Hormone-receptor studies with avidin and biotinylinsulin-avidin complexes. *J. Biol. Chem.* 255, 5742-5746.

Finn, F.M., Titus, G., Hofmann, K. (1984). Ligands for insulin receptor isolation. *Biochem.* 23, 2554-2558.

Firman, K., Dutta, C., Weiserova, M., Janscak, P. (2000). The role of subunit assembly in the functional control of type I restriction-modification enzymes. *Mol. Biol. Today* 1, 1-8.

Firman, K., Szczelkun, M.D. (2000). Measuring motion on DNA by the type I restriction endonuclease EcoR1241 using triplex displacement. *EMBO J.* 19, 2094-2102.

Florin, E.L., Moy, V.T., Gaub, H.E. (1994). Adhesion forces between individual ligand-receptor pairs. *Science* 264, 415-417.

Freitag, S., Le Trong, I., Klumb, L., Stayton, P.S., Stenkamp, R.E. (1997). Structural studies of the streptavidin binding loop. *Protein Sci.* 6, 1157-1166.

Fried, M., Crothers, D.M. (1981). Equilibria and kinetics of lac repressor-operator interactions by polyacrylamide gel electrophoresis. *Nucleic Acids Res*. 9, 6505-6525.

Friedsam, C., Del Campo Becares, A., Jonas, U., Gaub, H.E., Seitz, M. (2004). Polymer functionalized AFM tips for long-term measurements in single-molecule force spectroscopy. *Chem. Phys. Chem.* 5, 388-393.

Freifelder, D. (1987). *Molecular Biology*, 2nd Ed., Jones and Bartlett, Boston, 160-163.

Fritz, J., Katopodis, A.G., Kolbinger, F., Anselmetti, D. (1998). Force-mediated kinetics of single P-selectinyligand complexes observed by atomic force microscopy. *Proc. Natl. Acad. Sci. USA* 95, 12283-12288.

Gaboriaud, F., Dufrene, Y.F. (2007). Atomic force microscopy of microbial cells: Application to nanomechanical properties, surface forces and molecular recognition forces. *Colloids Surf. B Biointerfaces* 54, 10-19.

Gaines, G.L. (1957). The ion-exchange properties of muscovite mica. *J. Phys. Chem.* 61, 1408-1413.

Galburt, E.A., Stoddard, B.L. (2002). Catalytic mechanisms of restriction and homing endonucleases. *Biochemistry* 41, 13851-13860.

Garner, M.M., Revzin, A. (1981). A gel electrophoresis method for quantifying the binding of proteins to specific DNA regions: application to components of the Escherichia coli lactose operon regulatory system. *Nucleic Acids Res*. 9, 3047-3060.

Gennes, P.G. (1980). Conformations of polymers attached to an interface. *Macromolecules* 13, 1069-1075.

Gibson,C. T., Watson, G.S., Myhra, S. (1996). Determination of the spring constants of probes for force microscopy/spectroscopy. Nanotechnology 7, 259–262.

Grandbois, M., Beyer, M., Rief, M., Clausen-Schumann, H., Gaub, H. E. (1999). How strong is a covalent bond? *Science* 283, 1727-1730.

Green, N.M. (1975). Avidin. In *Adv. Protein Chem.*, Academic Press,, New York (Anfinsen, C.B., Edsall, J.T., Richard, F.M., Eds.), 29, 85-133.

Green, N.M., Konieczny, L., Toms, E.J., Valentine, R.C. (1971). The use of bifunctional biotinyl compounds to determine the arrangement of subunits in avidin. *Biochem. J.* 25, 781-791.

Grubmuller, H., Heymann, B., Tavan, P.(1996). Ligand binding: molecular mechanics calculation of the streptavidin-biotin rupture force. *Science.* 271, 997-999.

Guo, S., Ray, C., Kirkpatrick, A., Lad, N., Akhremitchev, B.B. (2008). Effects of multiple-bond ruptures on kinetic parameters extracted from force spectroscopy measurements: revisiting biotin-streptavidin interactions. *Biophys. J.* 95, 3964-3976.

Guthold, M., Bezanilla, M., Erie, D.A. Jenkins, B., Hansma, H.G., Bustamante, C. (1994). Following the assembly of RNA polymerase-DNA complexes in aqueous solutions with the scanning force microscope. *Proc. Natl. Acad. Sci. USA.* 91, 12927-12931.

Hackl, E.V., Kornilova, S.V., Blagoi, Y.P. (2005). DNA structural transitions induced by divalent metal ions in aqueous solutions. *Int. J. Biol. Macromol*. 35, 175-191.

Hansma, H.G., Laney, D.E. (1996). DNA binding to mica correlates with cationic radius: assay by atomic force microscopy *Biophys. J.* 70, 1933-1939.

Hansma, H.G. (1995). Atomic force microscopy of biomolecules. *J. Vac. Sci. Technol. B.* 14, 1390-1395.

Hansma, H.G., Bezanilla, M., Zenhausern, F., Adrian, M., Sinsheimer, R.L. (1993). Atomic force microscopy of DNA in aqueous solutions. *Nucleic Acids Res.* 21, 505-512.

Hansma, H.G., Golan, R., Hsieh, W., Lollo, C.P., Mullen-Ley, P., Kwoh, D. (1998). DNA condensation for gene therapy as monitored by atomic force microscopy. *Nucleic Acids Res.* 26, 2481-2487.

Hansma, H.G., Vesenka, J., Siegerist, C., Kelderman, G., Morrett, H., Sinsheimer, R.L., Elings, V., Bustamante, C., Hansma, P.K. (1992). Reproducible imaging and dissection of plasmid DNA under liquid with the atomic force microscope. *Science* 256, 1180-1184.

Hansma, H.G., Laney, D.E., Bezanilla, M., Sinsheimer, R.L., Hansma, P.K. (1995). Applications for atomic force microscopy of DNA. *Biophys. J.* 68, 1672-1677.

Hansma, H.G., Revenko, I., Kim, K., Laney, D.E. (1996). Atomic force microscopy of long and short double-stranded, single-stranded and triple-stranded nucleic acids. *Nucleic Acids Res.* 24, 713-720.

Hansma, H.G., Browne, K.A., Bezanilla, M., Bruice, T.C. (1994). Bending and straightening of DNA induced by the same ligand: characterization with the atomic force microscope. *Biochemistry* 33, 8436-8441.

Hazel, L.L., Tsukruk, V.V. (1999). Spring contants of composite ceramic/gold cantilevers for scanning probe microscopy. *Thin Solid Films* 339, 249-257.

Hayes J.D., Flanagan J.U., Jowsey, I.R. (2005). Glutathione transferases. *Annu. Rev. Pharmacol. Toxicol*. 45, 51-88.

Hedges, R.W., Datta, N.(1972). R124, an fiR factor of a new compatibility class. *J. Gener. Microbiol.* 71, 403-405.

Heinz, W.F., Hoh, J.H. (1999). Spatially resolved force spectroscopy of biological surfaces using the atomic force microscope. *Trends Biotechnol.* 17, 143-150.

Helm, C.A., Knoll, W., Israelachvili, J.N. (1991). Measurement of ligand-receptor interactions. *Proc. Natl. Acad. Sci. USA.* 88, 8169-8173.

Hendrickson, W.A., Pahler, A., Smith, J.L., Satow, Y., Merritt, E.A., Phizackerley, R.P. (1989). Crystal structure of core streptavidin determined from multiwavelength anomalous diffraction of synchrotron radiation. *Proc. Natl. Acad. Sci. USA* 86, 2190-2194.

Heney, G., Orr, G.A. (1981). The purification of avidin and its derivatives on 2-iminobiotin-6-aminohexyl-Sepharose 4B. *Anal Biochem*. 114, 92-96.

Heuser, J. (1989). Protocol for 3-D visualization of molecules on mica *via* the quick-freeze, deep-etch technique. *J. Electron Microsc. Tech.* 13, 244-263.

Hinterdorfer, P., Baumgartner, W., Gruber, H.J., Schilcher, K., Schindler, H. (1996). Detection and localization of individual antibody-antigen recognition events by atomic force microscopy. *Proc. Natl. Acad. Sci. USA*. 93, 3477-3481.

Hinterdorfer, P., Dufrene, Y.F. (2006). Detection and localization of single molecular recognition events using atomic force microscopy. *Nature Methods* 3, 347-355.

Hinterdorfer, P., Schilcher, K., Baumgartner, W., Gruber, H.J., Schindler, H. (1998). A mechanistic study of the dissociation of individual antibody-antigen pairs by atomic force microscopy. *Nanobiol.* 4, 39-50.

Hinterdorfer, P., Schutz, G., Kienberger, F., Schindler, H. (2001). Detection and characterization of single biomolecules at surfaces. *J. Biotechnol.* 82, 25-35.

Hofmeier, H., Pahnke, J., Weidl, C.H., Schubert, U.S. (2004). Combined biotin-terpyridine systems: a new versatile bridge between biology, polymer science and metallo-supramolecular chemistry. *Biomacromol. 5*, 2055-2064.

Humphris, A.D.L., Miles, M. J., Hobbs J. K. (2005). A mechanical microscope: High-speed atomic force microscopy. *Applied Physics letters* 86, 034106-1-3.

Hutter, J. L., Bechhoefer, J. (1993). Calibration of atomic-force microscope tips. *Rev. Sci. Instrum*. 64, 1868-1873.

Israelachvili, J.N. (1992). Intermolecular and Surface Forces, *Academic Press*, Second Edition, San Diego.

Janscak, P., Bickle, T.A. (1998). The DNA recognition subunit of the Type IB restriction-modification enzyme *Eco*AI tolerates circular permutations of its polypeptide chain. *J. Mol. Biol*. 284, 937-948.

Janscak, P., Bickle, T.A. (2000). DNA supercoiling during ATP-dependent DNA translocation by the Type I restriction enzyme *Eco*AI. *J. Mol. Biol.* 295, 1089-1099.

Janscak, P., Dryden, D.T., Firman, K. (1998). Analysis of the subunit assembly of the type IC restriction-modification enzyme EcoR124I. *Nucleic Acids Res.* 26, 4439-4445.

Janscak, P., MacWilliams, M.P., Sandmeier, U., Nagaraja, V., Bickle, T.A. (1999). DNA translocation blockage, a general mechanism of cleavage site selection by type I restriction enzymes. *Eur. Mol. Biol. Org. J.* 18, 2638-2647.

Jaschke, M., Butt, H.J., Bamberg, E., Hasemann, O.F., Krimphove, E.K., Manne, W.S. Gaub, H.E. (1996). The atomic force microscope as a tool to study and manipulate local surface properties. *Biosens. Bioelectonics* 11, 601-612.

Janshoff, A., Neitzert, M., Oberdorfer, Y., Fuchs, H. (2000). Force Spectroscopy of Molecular Systems-Single Molecule Spectroscopy of Polymers and Biomolecules. *Angew Chem Int* Ed Engl 39, 3212-3237.

Jansen, E.F., Tomimatsu, Y., Olson. A.C. (1971). Cross-linking of α-chymotrypsin and other proteins by reaction with glutaraldehyde. *Arch. Biochem. Biophys*. 144, 394-400.

Jeppesen, C., Wong, J.Y., Kuhl, T.L., Israelachvili, J.N., Mullah, N., Zalipsky, S., Marques, C.M. (2001). Impact of polymer tether length on multiple ligand-receptor bond formation. *Science* 293, 465-468.

Jing, G., Ma, J., Yu, D. (2007). Calibration of the spring constant of AFM cantilever. J. *Electron. Microsc.* 56, 21-25.

Johnson, W.T. (2008). Imaging DNA in Solution with the AFM. Application Note. Agilent Techonogies.

Jung, Y.J., Hong, B.J., Zhang, W., Tendler, S.J., Williams, P.M., Allen, S., Park, J.W. (2007). Dendron arrays for the force-based detection of DNA hybridization events. *J. Am. Chem. Soc*. 129, 9349-9355.

Kaasgaard, T., Mouritsen, O.G., Jorgensen, K. (2001). Screening effect of PEG on avidin binding to liposome surface receptors. *Int. J. Pharm.* 214, 63-65.

Kada, G., Blayney, G., Jeyakumar, L.H., Kienberger, F., Pastushenko, V.P., Fleischer, S., Schindler, H., Lai, F.A., Hinterdorfer, P. (2001). Recognition force microscopy/spectroscopy of ion channels: applications to the skeletal Ca2+ release channel (RYR1). *Ultramicroscopy* 86, 129-137.

Kaelin, W.G. Jr, Krek, W., Sellers, W.R., DeCaprio, J.A., Ajchenbaum, F., Fuchs, C.S., Chittenden, T., Li, Y., Farnham, P.J., Blanar, M.A. (1992). Expression cloning of a cDNA encoding a retinoblastoma-binding protein with E2F-like properties. *Cell* 70, 351-364.

Kaiser, K., Marek, M., Haselgruebler, T., Schindler, H., Gruber, H.J. (1997). Basic studies on heterobifunctional biotin-PEG conjugates with a 3-(4 pyridyldithio)propionyl marker on the second terminus. *Bioconjug. Chem. 8*, 545-551.

Kamruzzahan, A.S.M., Ebner, A., Wildling, L., Kienberger, F., Riener, C.K., Hahn, C.D., Pollheimer, P.D., Winklehner, P., Hölzl, M., Lackner, B., Schörkl, D.M., Hinterdorfer, P., Gruber, H.J. (2006). Antibody linking to atomic force microscpe tips via dulfide bond formation. *Bioconjug. Chem.* 17, 1473-1481.

Kannan, P., Cowan, G.M., Daniel, A.S., Gann, A.A.F., Murray, N.E. (1989). Conservation of organisation in the specificity polypeptides of two families of type I restriction enzymes. *J. Mol. Biol.* 209, 335-344.

Kasas, S., Thomson, N.H., Smith, B.L., Hansma, H.G., Zhu, X., Guthold, M., Bustamante, C., Kool, E.T., Kashlev, M., Hansma, P.K. (1997). Escherichia coli RNA polymerase activity observed using atomic force microscopy. *Biochemistry* 36, 461-468.

Kawahara, J,. Ohmori, T., Ohkubo, T., Hattori, S., Kawamura, M. (1992). The structure of glutaraldehyde in aqueous solution determined by ultraviolet absorption and light scattering. *Anal. Biochem*. 201, 94-98.

Ke, S., Wright, J.C., Kwon, G.S. (2007). Intermolecular interaction of avidin and PEGylated biotin. *Bioconjug. Chem.* 18, 2109-2114.

Kellermayer, M.S., Smith, S.B., Granzier, H.L., Bustamante, C. (1997). Folding-unfolding transitions in single titin molecules characterized with laser tweezers. *Science* 276, 1112-1116. Erratum in: *Science* (1997), 277, 1117.

Kienberger, F., Pastushenko, V.P., Kada, G., Gruber, H.J., Riener, C.K., Schindler, H., Hinterdorfer, P. (2000). Static and dynamic properties of single poly(ethylene glycol) molecules investigated by force microscopy. *Single Mol.* 1, 123-128.

Kienberger, F., Ebner, A., Gruber, H.J., Hinterdorfer, P.(2006). Molecular recognition imaging and force spectroscopy of single biomolecules. *Acc Chem Res.* 39, 29-36.

Kim, J.S., DeGiovanni, A., Jancarik, J., Adams, P.D., Yokota, H., Kim, R., Kim, S.H. (2005). Crystal structure of DNA sequence specificity subunit of a type I restriction-modification enzyme and its functional implications. *PNAS* 102, 3248-3253.

Kim, M.-S., Chio, J.-H., Kim, J.-H., Parkm Y.-K. (2010). Accurate determination of spring constant of atomic force microscope cantilevers and comparison with other methods. *Measurement* 43, 520-526.

Kishino, A., Yanagida, T. (1988). Force measurements by micromanipulation of a single actin filament by glass needles. *Nature* 334, 74-76.

Klein, D.C., Stroh, C.M., Jensenius, H., van Es, M., Kamruzzahan, A.S., Stamouli, A., Gruber, H.J., Oosterkamp, T.H., Hinterdorfer, P. (2003). Covalent immobilization of single proteins on mica for molecular recognition force microscopy. *Chem. Phys. Chem*. 4, 1367-1371.

Kneale, G.G. (1994). A symmetrical model for the domain structure of type I DNA methyltransferases. *Mol Biol*. 243, 1-5.

Kojima, H., Muto, E., Higuchi, H., Yanagida, T. (1997). Mechanics of single kinesin molecules measured by optical trapping nanometry. *Biophys. J.* 73, 2012-2022.

Koppelman, M.H., Dillard, J.G. (1977). A study of the adsorption of Ni(II) and Cu(II) by clay minerals: *Clays Clay Miner.* 25, 457-462.

Kurzban, G.P., Bayer, E.A., Wilchek, M., Horowitz, P.M. (1991). The quaternary structure of streptavidin in urea. *J. Biol. Chem.* 266, 14470-14477.

Kusiak, M., Price, C., Rice, D., Hornby, D.P. (1992). The HsdS polypeptide of the type IC restriction enzyme *Eco*R124 is a sequence-specific DNA-binding protein. *Mol. Microbiol.* 21, 3251-3256.

Laemmli, U.K., (1970). Cleavage of structural proteins during the assembly of the head of bacteriophage T4. *Nature* 227, 680-685.

Lal, R., John, S.A. (1994). Biological applications of atomic force microscopy. *Am. J. Physiol.* 266, 1-21.

Lamprou, D.A., Smith, J.R., Nevell, T.G., Barbu, E., Willis, C.R., Tsibouklis, J. (2010). Self-assembled structures of alkanethiols on gold-coated cantilever tips and substrates for atomic force microscopy: molecular organisation and conditions for reproducible deposition. *Appl. Surf. Sci.* 256, 1961-1968.

Lapkouski, M., Panjikar, S., Smatanova, I.K, Csefalvay, E. (2007). Purification, crystallization and preliminary X-ray analysis of the HsdR subunit of the EcoR124I endonuclease from Escherichia coli. *Acta Crystallogr.* 63, 582-585.

Lapkouski, M., Panjikar, S., Janscak, P., Smatanova, I.K., Carey, J., Ettrich, R., Csefalvay, E. (2009). Structure of the motor subunit of type I restriction-modification complex EcoR124I. *Nature Struct. Mol. Biol.* 16, 94-99.

Leckband, D.E., Schmitt, F.J., Israelachvili, J.N., Knoll, W. (1994). Direct force measurements of specific and nonspecific protein interactions. *Biochemistry* 33, 4611-4624.

Leckband, D., Israelachvili, J. (2001). Intermolecular forces in biology, *Quaterly Reviews of Biophysics* 34, 105 – 267.

Lee, C.K., Wang, Y.M., Huang, L.S., Lin, S. (2007). Atomic force microscopy: determination of unbinding force, off rate and energy barrier for protein-ligand interaction. *Micron* 38, 446-461.

Lee, G.U., Kidwell, D.A., Colton, R.J., (1994a). Sensing discrete streptavidin-biotin interactions with atomic force microscopy. *Langmuir* 10, 354-357.

Lee, G.U., Chris, L.A., Colton, R.J. (1994). Direct measurement of the forces between complementary strands of DNA. *Science* 266, 771-773.

Lee, I., Marchant, R.E. (2003). Molecular interaction studies of hemostasis: fibrinogen ligand-human receptor interactions. *Ultramicroscopy* 97, 341-352.

Leger, J.F., Romano, G., Sarkar, A., Robert, J., Bourdieu, L., Chatenay, D., Marko, J.F. (1999). Structural transitions of a twisted and stretched DNA molecule. *Phys. Rev. Lett*. 83, 1066-1069.

Li, J., Bai, C., Wang, C., Zhu, C., Lin, Z., Li, Q., Cao, E. (1998). A convenient method of aligning large DNA molecules on bare mica surfaces for atomic force microscopy. *Nucleic Acid Res*. 26, 4785-4786.

Lim, K., Herron, J.N. (1992). Molecular simulation of protein-PEG interaction. In *Poly(ethylene glycol) Chemistry: Biotechnical and Biomedical Applications* (Harris, J. M., Ed.) 29-56, Plenum Press, New York.

Lindsay, S.M., Lyubchenko, Y.L., Gall, A.A., Shlyakhtenko, L.S., Harrington, R.E. (1992). Imaging DNA molecules chemically bound to a mica surface. *Proc. SPIE*, *Scanning Probe Microscopies* 1639, 84-90 (Srinivas Manne Ed).

Liu, Z., Li, Z., Zhou, H., Wei, G., Song, Y., Wang, L. (2005). Imaging DNA molecules on mica surface by atomic force microscopy in air and in liquid. *Microsc. Res. Tech.* 66, 179-185.

Livnah, O., Bayer, E.A., Wilchek, M., Sussman, J.L. (1993a). Three-dimensional structure of avidin and the avidin-biotin complex. *Proc. Natl. Acad. Sci. USA*. 90, 5076-5080.

Livnah, O., Bayer, E.A., Wilchek, M., Sussman, J.L. (1993b).The structure of the complex between avidin and the dye, 2-(4-hydroxyazobenzene) benzoic acid (HABA). *FEBS Lett.* 328, 165-168.

Lo, Y.-S., Zhu, Y.-J., Beebe, T.P. Jr (2001). Loading-rate dependence of individual ligand-receptor bond-rupture forces studied by atomic force microscopy. *Langmuir* 17, 3741-3748.

Luckham, P.F., Smith, K. (1998). Direct measurement of recognition forces between proteins and membrane receptors. Faraday Discuss. 111, 307-320.

Lyubchenko, Y., Shlyakhtenko, L., Harrington, R., Oden, P., Lindsay, S. (1993a). Atomic force microscopy of long DNA: imaging in air and under water. *Proc. Natl. Acad. Sci. USA* 90, 2137-2140.

Lyubchenko, Y.L., Gall, A.A., Shlyakhtenko, L.S, Harrington, R.E., Jacobs, B.L., Oden, P.I., Lindsay, S.M. (1992). Atomic force microscopy imaging of double stranded DNA and RNA. *J. Biomol. Struct. Dyn.* 10, 589-606.

Lyubchenko, Y.L., Gall, A.A., Shlyakhtenko, L.S. (2001). Atomic force microscopy of DNA and protein-DNA complexes using functionalized mica substrates. *Methods Mol. Biol*. 148, 569-578.

Lyubchenko, Y.L., Jacobs, B.L., Lindsay, S.M., Stasiak, A. (1995). Atomic force microscopy of nucleoprotein complexes. *Scanning Microsc.* 9, 705-725.

Lyubchenko, Y.L., Oden, P.I., Lampner, D., Lindsay, S.M., Dunker, K.A. (1993b). Atomic force microscopy of DNA and bacteriophage in air, water and propanol: the role of adhesion forces. *Nucleic Acids Res.* 21, 1117-11123.

Lyubchenko, Y.L., Shlyakhtenko, L.S. (2009). AFM for analysis of structure and dynamics of DNA and protein-DNA complexes. Methods 47, 206-213.

Maniatis, T., Fritsch, E.F., Sambrook, J. (1982). *Molecular cloning. A laboratory manual*. Cold Spring Harbor Laboratory, New York.

Mann, A., Richa, R., Ganguli, M. (2008). DNA condensation by poly-L-lysine at the single molecule level: Role of DNA concentration and polymer length**.** *J. Controlled Rel.* 125, 252-262.

Marek, M., Kaiser, K., Gruber, H.J. (1997). Biotin-pyrene conjugates with poly(ethylene glycol) spacers are convenient fluorescent probes for avidin and streptavidin. *Bioconjug. Chem. 8*, 560-566.

Marshall, B.T., Sarangapani, K.K., Lou, J., McEver, R.P. and Zhu, C. (2005). Force history dependence of receptor-ligand dissociation. *Biophys. J.* 88, 1458-1466.

Merkel, R. (2001). Force spectroscopy on single passive biomolecules and single biomolecular bonds. *Phys. Reports* 346**,** 343-385.

Merkel, R., Nassoy, P., Leung, A., Ritchie, K., Evans, E. (1999). Energy landscapes of receptor-ligand bonds explored with dynamic force spectroscopy. *Nature* 397, 50-53.

Meselson, M., Yuan, R. (1968). DNA restriction enzyme from E. coli. *Nature* 217, 1110-1114.

Metzger, S.W., Natesan, M., Yanavich, C., Schneider, J., Lee, G.U. (1999). Development and characterization of surface chemistries for microfabricated biosensors. *J. Vac. Sci. Technol. A* 17, 2623-2628.

Michaelis, J., Muschielok, A., Andrecka, J., Kugel, W., Moffitt, J. R. (2009). DNA based molecular motors. *Phys. Life Rev.* 6, 250-266.

Miles, M.J., McMaster, T., Carr, H.J., Tatham, A.S., Shewry, P.R., Field, J.M., Belton, P.S., Jeenes, D., Hanley, B., Whittam, M., Cairns, P., Morris, V.J., Lambert, N. (1990). Scanning tunneling microscopy of biomolecules. *J. Vac. Sci. Technol., A* 8, 698-702.

Modesti, M., Ristic, D., van der Heijden, T., Dekker, C., van Mameren, J., Peterman, E.J., Wuite, G.J., Kanaar, R., Wyman, C. (2007). Fluorescent human RAD51 reveals multiple nucleation sites and filament segments tightly associated along a single DNA molecule. *Structure* 15, 599-609.

Moore, N.W., Kuhl, T.L. (2006). The role of flexible tethers in multiple ligand-receptor bond formation between curved surfaces. *Biophys. J.* 91, 1675-1687.

Moreno-Herrero, F., Colchero, J., Baro, A.M. (2003). DNA height in scanning force microscopy. *Ultramicroscopy* 96, 167-174.

Moy, V.T., Florin, E.-L., Gaub, H.E. (1994a). Adhesive forces between ligand and receptor measured by AFM. *Colloid Surf. A* 93, 343-334.

Moy, V.T., Florin, E.-L., Gaub, H.E. (1994b). Intermolecular forces and energies between ligands and receptors. *Science* 266, 257-259.

Muller, D.J., Amrein, M., Engel, A.(1997). Adsorption of biological molecules to a solid support for scanning probe microscopy. *J. Struct. Biol.* 119, 172-188.

Muller, D.J., Engel, A. (1997). The height of biomolecules measured with the atomic force microscope depends on electrostatic interactions *Biophys. J.* 73, 1633-1644.

Muller, D.J., Heymann, J.B., Oesterhelt, F., Moller, C., Gaub, H., Buldt, G., Engel, A. (2000). Atomic force microscopy of native purple membrane. *Biochim. Biophys. Acta* 1460, 27-38.

Murray, N.E. (2000). Type I restriction systems: sophisticated molecular machines (a legacy of Bertani and Weigle). *Microbiol. Mol. Biol. Rev.* 64, 412-434.

Murray, N.E. (2002). Immigration control of DNA in bacteria: self versus non-self. *Microbiol.* 148, 3-20.

Nagasaki, Y., Kutsuna, T., Iijima, M., Kato, M., Kataoka, K., Kitano, S., Kadoma, Y. (1995). Formyl-ended heterobifunctional poly(ethylene oxide): synthesis of

poly(ethylene oxide) with a formyl group at one end and a hydroxyl group at the other end. *Bioconjug. Chem*. 6, 231-233.

Neaves, K.J., Cooper, L.P., White, J.H., Carnally, S.M., Dryden, D.T.F., Edwardson, J.M., Henderson, R.M. (2009). Atomic force microscopy of the EcoKI Type I DNA restriction enzyme bound to DNA shows enzyme dimerization and DNA looping. *Nucleic Acids Res.* 37, 2053-2063.

Neish, C.S., Martin, I.L., Henderson, R.M., Edwardson, J.M. (2002). Direct visualization of ligand-protein interactions using atomic force microscopy. *Br J Pharmacol.* 135, 1943-1950.

Neuman, K.C., Nagy, A. (2008). Single-molecule force spectroscopy: optical tweezers, magnetic tweezers and atomic force microscopy. *Nature Methods* 5, 491-505.

Nevo, R., Stroh, C., Kienberger, F., Kaftan, D., Brumfld, V., Elbaum, M., Reich, Z., Hinterdorfer, P., (2003). A molecular switch between alternative conformational states in the complex of Ran and importin b1. *Nature Struct. Biol.* 10, 553-557.

Newman, M., Lunnen, K., Wilson, G., Greci, J., Schildkraut, I., Phillips, S.E.V. (1998). Crystal structure of restriction endonuclease BglI bound to its interrupted DNA recognition sequence. *EMBO J.* 17, 5466-5476.

Nishimura, S., Scales, P.J., Tateyama, H., Tsunematsu, K., Healy, T.W. (1995). Cationic modification of muscovite mica: an electrokinetic study. *Langmuir* 11, 291-295.

Noppl-Simson, D.A., Needham, D. (1996). Avidin-biotin interactions at vesicle surfaces: adsorption and binding, crossbridge formation, and lateral interactions. *Biophys. J.* 70, 1391-1401.

Obarska, A., Blundell, A., Feder, M., Vejsadová, Š., Šišáková, E., Weiserová, M., Bujnicki, J.M., Firman, K. (2006). Structural model for the multisubunit type IC restriction-modification DNA methyltransferase M.EcoR124I in complex with DNA. *Nucleic Acids Res.* 34, 1992-2005.

Obarska-Kosinska, A., Taylor, J.E., Callow, P., Orlowski, J., Bujnicki J.M., Kneale, G. G. (2008). HsdR subunit of the type I restriction-modification enzyme ecor124i: biophysical characterisation and structural modelling. *J. Mol. Biol.* 376, 438-452.

Oberhauser, A.F., Carrion-Vazquez, M. (2008). Mechanical biochemistry of proteins one molecule at a time. *Biol. Chem*. 283, 6617-6621.

Ohshiro, T., Maeda, M. (2010). Single-molecule imaging of DNA duplexes immobilized on surfaces with a scanning tunneling microscope. *Chem Commun*. 46, 2581-2583.

Pashley, R.M. (1981). Hydration forces between mica surfaces in Li+, Na+, and Cs+ electrolyte solutions: a correlation of double layer and hydration forces with surface cation exchange properties. *J. Colloid Interface Sci.* 83, 531-546.

Pashley, R.M., McGuiggan, P.M., Ninham, B.W., Evans, D.F. (1985). Attractive forces between uncharged hydrophobic surfaces: direct measurements in aqueous solution. *Science* 229, 1088-1089.

Pastre, D., Hamon, L., Landousy, F., Sorel, I., David, M.O., Zozime, A., Le Cam, E., Pietrement, O. (2006). Anionic polyelectrolyte adsorption on mica mediated by multivalent cations: a solution to DNA imaging by atomic force microscopy under high ionic strengths. *Langmui*r 22, 6651-6660.

Pastre, D., Hamon, L., Mechulam, A., Sorel, I., Baconnais, S., Curmi, P.A., Le Cam, E., Pietrement, O. (2007). Atomic force microscopy imaging of dna under macromolecular crowding conditions. *Biomacromol.* 8, 3712-3717.

Pastre, D., Hamon, L., Sorel, I., Le Cam, E., Curmi, P.A., Piétrement, O. (2009). Specific DNA-protein interactions on mica investigated by atomic force microscopy. *Langmuir* 26, 2618-2623.

Pastre, D., Pietrement, O., Fusil, S., Landousy, F., Jeusset, J., David, M.O., Hamon, L., Le Cam, E., Zozime, A. (2003). Adsorption of DNA to mica mediated by divalent counterions: a theoretical and experimental study. *Biophys. J.* 85, 2507-2518.

Patel, J., Taylor, I., Dutta, C.F., Kneale, G.G., Firman, K. (1992). High-level expression of the cloned genes encoding the subunits of and the intact DNA methyltransferase, M.*Eco*R124. *Gene* 112, 21-27.

Piekarowicz, A., Goguen, J.D. (1986). The DNA sequence recognized by the *Eco*DXXI restriction endonuclease. *Eur. J. Biochem.* 154, 295-298.

Piramowicz, M. de O., Czuba, P., Targosz, M., Burda, K., Szymonski, M. (2006). Dynamic force measurements of avidin-biotin and streptavadin-biotin interactions using AFM. *Acta Biochim. Polonica*. 53, 93-100.

Prakash-Cheng, A., Junichi, R. (1993). Delayed expression of *in vivo* restriction activity following conjugal transfer of *Escherichia coli hsd*K (restriction-modification) genes. *J. Bacteriol.* 175, 4905-4906.

Price, C., Shepherd, J.C.W., Bickle, T.A. (1987). DNA recognition by a new family of type I restriction enzymes: a unique relationship between two different DNA specificities. *Eur. Mol. Biol. Organ. J.* 6, 1493-1498.

Pugliese, L., Coda, A., Malcovati, M., Bolognesim, M. (1993). Three-dimensional structure of the tetragonal crystal form of egg-white avidin in its functional complex with biotin at 2.7 Å resolution. *J. Mol. Biol.* 231, 698-710.

Raab, A., Han, W., Badt, D., Smith-Gill, S.J., Lindsay, S.M., Schindler, H., Hinterdorfer, P. (1999). Antibody recognition imaging by force microscopy. *Nature Biotechnol.* 17, 901-905.

Radmacher, M., Fritz, M., Hansma, H. G., Hansma, P. K. (1994). Direct observation of enzyme activity with the atomic force microscope. *Science* 265, 1577-1579.

Raible, M., Evstigneev, M., Bartels, F.W., Eckel, R., Nguyen-Duong, M., Merkel, R., Ros R., Anselmetti, D., Reimann, P. (2006). Theoretical analysis of single-molecule force spectroscopy experiments: heterogeneity of chemical bonds. *Biophys. J.* 90, 3851-3864.

Ramirez-Aguilar, K.A., Rowlen, K.L. (1998). Tip characterization from afm images of nanometric spherical particles. *Langmuir* 14, 2562-2566.

Ratcliff, G.C., Erie, D.A. (2001). A novel single-molecule study to determine protein--protein association constants. *J. Am. Chem. Soc.* 123, 5632-5635.

Rief, M., Clausen-Schaumann, H., Gaub, H.E. (1999a). Sequence dependent mechanics of single DNA-molecules. *Nature Struct. Biol.* 6, 346-349.

Rief, M., Gautel, M., Oesterhelt, F., Fernandez, J.M., Gaub, H.E. (1997). Reversible unfolding of individual titin immunoglobulin domains by AFM. *Science* 276, 1109-1112.

Rief, M., Pascual, J., Saraste, M., Gaub, H.E. (1999b). Single molecule force spectroscopy of spectrin repeats: low unfolding forces in helix bundles. *J. Mol. Biol.* 286, 553-561.

Riener, C.K., Stroh, C.M., Ebner, A., Klampfl, C., Gall, A.A., Romanin, C., Lyubchenko, Y.L., Hinterdorfer, P., Gruber, H.J. (2003). Simple test system for single molecule recognition force microscopy. *Anal. Chim. Acta* 479, 59-75.

Rippe, K., Guthold, M., von Hippel, P.H., Bustamante, C. (1997). Transcriptional activation via DNAlooping: visualization of intermediates in the activation pathway of E. coli RNA polymerase x sigma 54 holoenzyme by scanning force microscopy. *J. Mol. Biol.* 270, 125-138.

Roberts, M.J., Bentley, M.D., Harris, J.M. (2002). Chemistry for peptide and protein PEGylation. *Adv. Drug Deliv. Rev.* 54, 459-476.

Roberts, R.J., Belfort, M., Bestor, T., Bhagwat, A.S., Bickle, T.A., Bitinaite, J., Blumenthal, R.M., Degtyarev, S.K., Dryden, D.T.F., Dybvig, K., Firman, K., Gromova, E.S., Gumport, R.I., Halford, S.E., Hattman, S., Heitman, J., Hornby, D.P., Janulaitis, A., Jeltsch, A., Josephsen, J., Kiss, A., Klaenhammer, T.R., Kobayashi, I., Kong, H., Krüger, D.H., Lacks, S., Marinus, M.G., Miyahara, M., Morgan, R.D., Murray, N.E., Nagaraja, V., Piekarowicz, A., Pingoud, A., Raleigh, E., Rao, D.N., Reich, N., Repin, V.E., Selker, E.U., Shaw, P.C., Stein, D.C., Stoddard, B.L., Szybalski, W., Trautner, T.A., Van Etten, J.L., Vitor, J.M., Wilson, G.G., Xu, S.Y. (2003). A nomenclature for

restriction enzymes, DNA methyltransferases, homing endonucleases and their genes. *Nucleic Acids Res*. 31, 1805-1812.

Sader, J.E., Chon, J.W.M., Mulvaney, P. (1999). Calibration of rectangular atomic force microscope cantilevers. *Rev. Sci. Instrum*. 70, 3967-3969.

Sader, J. E., White, L. (1993). Theoretical analysis of the static deflection of plates for atomic force microscope applications. *J. Appl. Phys*. 74, 1-9.

Sader, J. E. (1995). Parallel beam approximation for V- shaped atomic force microscope cantilevers. *Rev. Sci. Instrum.* 66, 4583-4587.

Schneider, S.W., Larmer, J., Henderson, R.M., Oberleithner, H. (1998). Molecular weights of individual proteins correlate with molecular volumes measured by atomic force microscopy. *Pflugers Arch-Eur. J. Physiol.* 435, 362-367.

Schulz, A., Mucke, N., Langowski, J., Rippe, K. (1998). Scanning force microscopy of Escherichia coli RNA polymerase sigma54 holoenzyme complexes with DNA in buffer and in air. *J. Mol. Biol.* 283, 821-836.

Schwesinger, F., Ros, R., Strunz, T., Anselmetti, D., Guntherodt, H. J., Honegger, A., Jermutus, L., Tiefenauer, L., and Plückthun, A. (2000). Unbinding forces of single antibody-antigen complexes correlate with their thermal dissociation rates. *Proc. Nat. Acad. Sci. USA* 97, 9972-9977.

Senden, T., Ducker, W. (1994). Experimental Determination of Spring Constants in Atomic Force Microscopy. *Langmuir* 10, 1003-1004.

Seidel, R., Bloom, J.G.P., van Noort, J., Dutta, C.F, Dekker, N.H., Firman, K., Szczelkun, M.D., Dekker, C. (2005). Dynamics of initiation, termination and reinitiation of DNA translocation by the motor protein EcoR124I. *EMBO J.* 24, 4188-4197.

Seidel, R., van Noort, J., van der Scheer, C., Bloom, J. G. P., Dekker, N. H., Dutta, C. F., Blundell, A., Robinson, T., Firman, K., Dekker, C. (2004). Real-time observation of DNA translocation by the type i restriction-modification enzyme EcoR124I. *Nature Struct. Mol. Biol.* 11, 838-843..

Shao, Z., Yang, J., Somlyo, A.P. (1995). Biological atomic force microscopy: from microns to nanometers and beyond. *Annu. Rev. Cell Dev. Biol.* 11, 241-265.

Shlyakhtenko, L.S., Gall, A.A., Filonov, A., Cerovac, Z., Lushnikov, A., Lyubchenko, Y.L. (2003). Silatrane-based surface chemistry for immobilization of DNA, protein-DNA complexes and other biological materials. *Ultramicroscopy* 97, 279-287.

Shlyakhtenko, L.S., Potaman, V.N., Sinden, R.R., Gall, A.A., Lyubchenko, Y.L. (2000). Structure and dynamics of three-way DNA junctions: atomic force microscopy studies. *Nucleic Acids Res.* 28, 3472-3477.

Siedlecki, C.A., Marchant, R.E. (1998). Atomic force microscopy for characterization of the biomaterial interface. *Biomaterials.* 19, 441-454.

Sistla, S., Rao, D.N. (2004). S-Adenosyl-L-methionine-dependent restriction enzymes. *Crit. Rev. Biochem. Mol. Biol*. 39, 1-19.

Smith, D.E., Tans, S.J., Smith, S.B., Grimes, S., Anderson, D.L., Bustamante, C. (2001). The bacteriophage phi29 portal motor can package DNA against a large internal force. *Nature* 413, 748-752.

Smith, J.D., Arber, W., Kuhnlein, U. (1972). Host specificity of DNA produced by *Escherichia coli*. XIV. The role of nucleotide methylation in *in vivo* B-specific modification. *J. Mol. Biol.* 63, 1-8.

Smith, S.B., Finzi, L., Bustamante, C. (1992). Direct mechanical measurements of the elasticity of single DNA molecules by using magnetic beads. *Science* 258, 1122-1126.

Smith, D.B., Johnson, K.S.(1988). Single step purification of polypeptides expressed in Echerichia Coli as fusions with glutathione S-transferase. *Gene* 67, 31-40.

Song, Y., Li, Z., Liu, Z., Wei, G., Wang, L., Sun, L. (2005). Immobilization of DNA on 11-mercaptoundecanoic acid-modified gold (111) surface for atomic force microscopy imaging. *Microsc Res Tech*. 68, 59-64.

Strunz, T., Oroszlan, K., Schafer, R., Guntherodt, H.J. (1999). Dynamic force spectroscopy of single DNA molecules. *Proc. Natl. Acad. Sci. USA* 96, 11277-11282.

Studier, F.W., Bandyopadhyay, P.K. (1988). Model for how type I restriction enzymes select cleavage sites in DNA. *Proc. Natl. Acad. Sci. USA* 85, 4677-4681.

Studier, F.W., Moffatt, B.A. (1986). Use of bacteriophage T7 RNA polymerase to direct selective high-level expression of cloned genes. *J. Mol. Biol.* 189, 113-130.

Suri, B., Shepherd, J.C.W., Bickle, T.A. (1984). The *Eco*A restriction and modification system of *Escherichia coli* 15T-: enzyme structure and DNA recognition sequence. *Cold Spring Harbor Symp. Quant. Biol.* 43, 1217-1221.

Sushko, L., Shluger, A. L., Rivetti, C. (2006). Simple model for DNA adsorption onto a mica surface in 1:1 and 2:1 electrolyte solutions. *Langmuir, 22*, 7678-7688.

Svoboda, K., Block, S.M. (1994). Force and velocity measured for single kinesin molecules. *Cell* 77, 773-784.

Szczelkun, M.D., Dillingham, M.S., Janscak, P., Firman, K., Halford, S.E. (1996). Repercussions of DNA tracking by the type IC restriction endonuclease *Eco*R124I on linear, circular and catenated substrates. *EMBO J.* 15, 6335-6347.

Szczelkun, M.D.,Janscak, P., Firman, K., Halford, S.E. (1997). Selection of non-specific DNA cleavage sites by the type IC restriction endonuclease *Eco*R124I. *J. Mol.Biol* .271, 112-123.

Takusagawa, F., Fujioka, M., Spies, A., Schowen, R.L. (1998). S-Adenosylmethionine (AdoMet)-dependent methyltransferases. In: *Comprehensive Biological Catalysis: A Mechanistic Reference,* 1, 1-30. M. Sinnott, Ed., Academic Press.

Taylor, I., Patel, J., Firman, K., Kneale, G.G. (1992). Purification and biochemical characterisation of the *Eco*R124 modification methylase. *Nucleic Acids Res.* 20, 179-186.

Taylor, I., Watts, D., Kneale, G. (1993). Substrate recognition and selectivity in the type IC DNA modification methylase M.*Eco*R124I. *Nucleic Acids Res.* 21, 4929-4935.

Taylor, I. A., Davis, K. G., Watts, D., Kneale, G. G. (1994). DNA binding induces a major structural transition in a type I methyltransferase. *Eur. Mol. Biol. Org. J.* 13, 5772-5778.

Tessmer, I., Moore, T., Lloyd, R.G., Wilson, A., Erie, D.A., Allen, S., Tendler, S.J. (2005). AFM studies on the role of the protein RdgC in bacterial DNA recombination. *J Mol Biol.* 350, 254-262.

Thielking, V., Selent, U., Kohler, E., Landgraf, Z., Wolfes, H., Alves, J., Pingoud, A. (1992). Mg^{2+} confers DNA binding specificity to the EcoRV restriction endonuclease. *Biochemistry* 31, 3727-3732.

Thomson, N.H., Kasas, S. Smith, B., Hansma, H.G., Hansma, P.K. (1996). Reversible binding of DNA to mica for AFM imaging. *Langmuir*, 12, 5905-5908.

Thundat, T., Allison, D.P., Warmack, R.J., Brown, G.M., Jacobson, K.B., Schrick, J.J., Ferrell, T.L., 1992. Atomic force microscopy of DNA on mica and chemically modified mica. *Scanning Microsc.* 6, 911-918.

Tiner, W.J., Sr., Potaman, V.N., Sinden, R.R., Lyubchenko, Y.L. (2001). The structure of intramolecular triplex DNA: atomic force microscopy study. *J. Mol. Biol.* 314, 353-357.

Titheradge, A.J.B., Ternent, D., Murray, N.E. (1996). A third family of allelic *hsd* genes in *Salmonella enterica*: sequence comparisons with related proteins identify conserved regions implicated in restriction of DNA. *Mol. Microbiol*. 22, 437-447.

Torii, A., Sasaki, M., Hane, K., Okuma, S. (1996). A method for determining the spring constant of cantilevers for atomic force microscopy.*Meas. Sci. Technol*. 7, 179–184.

Tskhovrebova, L., Trinick, J., Sleep, J.A., Simmons, R.M. (1997). Elasticity and unfolding of single molecules of the giant muscle protein titin. *Nature* 387, 308-312.

Tyndall, C., Meister, J., Bickle, T.A. (1994). The *Escherichia coli prr* region encodes a functional type IC DNA restriction system closely integrated with an anticodon nuclease gene. *J. Mol. Biol.* 237, 266-274.

van der Linden, E., Sanchez, H., Kinoshita, E., Kanaar, R., Wyman, C. (2009). RAD50 and NBS1 form a stable complex functional in DNA binding and tethering. *Nucleic Acids Res.* 37, 1580-1588.

van Noort, J., van der Heijden, T., Dutta, C.F., Firman, K., Dekker, C. (2004). Initiation of translocation by Type I restriction-modification enzymes is associated with a short DNA extrusion. *Nucleic Acids Res.* 32, 6540-6547.

Veigel, C., Bartoo, M.L., White, D.C., Sparrow, J.C., Molloy, J.E. (1998). The stiffness of rabbit skeletal actomyosin cross-bridges determined with an optical tweezers transducer. *Biophys. J.* 75, 1424-1438.

Vesenka, J., Guthold, M., Keller, C.L.T ang, D., Delaine, E., Bustamante, C. (1992). Substrate preparation for reliable imaging of DNA molecules with the scanning force microscope. *Ultramicroscopy* 42, 1243-1249.

Vesenka, J., Miller, R., Henderson, E. (1994). Three-dimensional probe reconstruction for atomic force microscopy. *Rev. Sci. Instrum.* 65, 1-3.

Viani, M.B. Schaffer, T.E., Chand, A., Rief, M., Gaub, H.E., Hansma, P.K. (1999). Small cantilevers for force spectroscopy of single molecules. *J. Appl. Phys.* 86, 2258-2262.

Vipond, I.B., Halford, S.E. (1995). Specific DNA recognition by EcoRV restriction endonuclease induced by calcium ions. *Biochemistry* 34, 1113-1119.

Wang, M.D., Schnitzer, M.J., Landick, R., Gelles, J., Block, S.M. (1998). Force and velocity measured for single molecules of RNA polymerase. *Science* 282, 897-901.

Watson, J.D., Hopkins, N.H., Roberts, J.W., Seitz, J.A., Weiner, A.M. (1988). *Molecular Biology of the Gene*, Benjamin/Cummings, Menlo Park, CA, 249.

Watson, J.D., Crick, F.H.C. (1953). Molecular structure of nucleic acids. Structure for deoxyribose nucleic acid. *Nature* 171, 737-738.

Weber, P.C., Ohlendorf, D.H., Wendoloski, J.J., Salemme, F.R. (1989). Structural origins of high-affinity biotin binding to streptavidin. *Science* 243, 85-88.

Weber, P.C., Wendoloski, J.J., Pantoliano, M.W., Salemme, F.R. (1992). Crystallographic and thermodynamic comparison of natural and synthetic ligands bound to streptavidin. *J. Am. Chem. Soc.* 114, 31197-31200.

Weiner, M.P., Anderson, C., Jerpseth, B., Wells, S., Johnson-Bown, B., Vaillancourt, P. (19945). Studier pET system vectors and hosts. *Strategies* 7, 41-43.

Weisendanger, R. (1994). *Scanning Probe Microscopy and Spectroscopy*. Cambridge University Press, Cambridge.

Weiserova, M., Dutta, C.F., Firman, K. (2000). A novel mutant of the type I restriction-modification enzyme *Eco*R124I is altered at a key stage in the subunit assembly pathway. *J. Mol. Biol.* 304, 301-310.

Weiserova, M., Firman, K. (1998). Isolation of a non-classical mutant of the DNA recognition subunit of the type I restriction endonuclease R.*Eco*R124I. *Biol. Chem.* 379, 585-589.

Widom, J., Baldwin, R. L. (1980). Cation-induced toroidal condensation of DNA studies with $Co3^{+}(NH_3)_6$. *J. Mol. Biol.* 144, 431–453.

Wilchek, M., Bayer, E.A., Livnah, O. (2006). Essentials of biorecognition: the (strept)avidin-biotin system as a model for protein-protein and protein-ligand interaction. *Immunol Lett.* 103,27-32.

Wilson, G.G., Murray, N.E. (1991). Restriction and modification systems. *Annu. Rev. Genetics* 25, 585-627.

Wong, J., Chilkoti, A. and Moy, V.T. (1999). Direct force measurements of the streptavidin-biotin interaction. *Biomol. Eng.* 16, 45-55.

Wyman, C., Grottkopp, E., Bustamante, C., Nelson H.C.M. (1995). Determination of heat-shock transcription factor 2 stoichiometry at looped DNA complexes using scanning force microscopy. *EMBO J.* 14, 117-123.

Wyman, C., Rombel, I., North, A.K., Bustamante, C., Kustu, S. (1997). Unusual oligomerization required for activity of NtrC, a bacterial enhancer-binding protein. *Science* 275, 1658-1661.

Yang, W., Lee, J., Nowotny, M. (2006). Making and breaking nucleic acids: two-Mg^{2+}-ion catalysis and substrate specificity. *Mol. Cell* 22, 5-13.

Yanish-Perron, C., Vieira, J., Messing, J. (1985). Improved M13 phage cloning vectors and host strains: nucleotide sequence of the M13mp18 and pUC19 vectors. Gene 33, 103-119

Ye, J.Y., Umemura, K., Ishikawa, M., Kuroda, R. (2000). Atomic force microscopy of DNA molecules stretched by spin-coating technique. *Anal. Biochem.* 281, 21-25.

Yu, J., Zhang, Z., Cao, K., Huang, X. (2008). Visualization of alkali-denatured supercoiled plasmid DNA by atomic force microscopy. *Biochem. Biophys. Res. Commun.* 374, 415-418.

Yokoyama, M., Okano, T., Sakurai, Y., Kikuchi, A., Ohsako, N., Nagasaki, Y., Kataoka, K. (1992). Synthesis of poly(ethylene oxide) with heterobifunctional reactive groups at its terminals by an anionic initiator, *Bioconjug. Chem.* 3, 275-276.

Yoshimura, S.H., Takahashi, H., Otsuka, S., Takeyasu, K. (2006). Development of glutathione-coupled cantilever for the single-molecule force measurement by scanning force microscopy. *FEBS Lett.* 580, 3961-3965.

Yuan, C., Chen, A., Kolb, P. and Moy, V.T. (2000). Energy landscape of streptavidin-biotin complexes measured by atomic force microscopy. *Biochemistry* 39, 10219-10223.

Yuan, R., Bickle, T.A., Ebbers, W., Brack, C. (1975). Multiple steps in DNA recognition by restriction endonuclease from E. coli K. *Nature* 256, 556-560.

Yuan, R., Hamilton, D.L., Burckhardt, J. (1980). DNA translocation by the restriction enzyme from *E.Coli*.K. *Cell* 20, 237-244.

Yuan, R., Meselson, M. (1970). A specific complex between a restriction endonuclease and its DNA substrate. *Proc. Natl. Acad. Sci. USA* 65, 357-362.

Yunchang, G., Xingfei., Z., Jielin, S., Minqian, L., Jun, H. (2004). Height measurement of DNA molecules with lift mode AFM. *Chin. Sci. Bulletin*. 49, 1574-1577.

Zhang, X,. Wójcikiewicz, E., Moy, V.T. (2002). Force spectroscopy of the leukocyte function - associated antigen -1/intercellular adhesion molecule-1 interaction. *Biophys. J.* 83, 2270-2279.

Zhong, Q., Inniss, D., Kjoller, K., Elings, V.B. (1993). Fractured polymer/silica fiber surface studied by tapping mode atomic force microscopy. *Surf. Sci. Lett.* 290, L668-L692.

Zinkevich, V., Popova, L., Kryukov, V., Abadjieva, A., Bogdarina, I., Janscák, P., Firman, K. (1997). The HsdR subunit of R.*Eco*R124II: cloning and over-expression of the gene and unexpected properties of the subunit. *Nucleic Acids Res.* 25, 503-510.

Zlatanova, J., Leuba, S.H., Yang, G., Bustamante, C., van Holde, K. (1994). Linker DNA accessibility in chromatin fibers of different conformations: a reevaluation. *Proc. Natl. Acad. Sci. USA* 91, 5277-5280.

Zlatanova, J., Lindsay, S.M., Leuba, S.H. (2000). Single molecule force spectroscopy in biology using the atomic force microscope. *Prog. Biophys. Mol. Biol.* 74, 37-61.

http://afmhelp.com/index.php?option=com_content&view=article&id=65%3Aconvolution&Itemid=64

http://www.pasteur.ac.ir/ researchDepartment/GeneBank/Plasmid.htm.

www.ism.cnr.it/english/linee/MD.P06.006.php